STRUCTURE AND PROPERTIES OF CdSe HETEROJUNCTIONS

Thesis submitted for the degree of
Doctor of Philosophy

by

FAKKIRAPPA HANUMAPPA GEJJI

Department of Metallurgy
Imperial College of Science and Technology
University of London

August 1976

TO MY PARENTS

ABSTRACT

Films of CdSe were grown by focussed electron beam evaporation in high vacuum on the three singular faces of Ge. On (100) and (111) oriented substrates epitaxy was obtained throughout the range of substrate temperatures from 350°C to 450°C. On (110) oriented substrates the epitaxial growth range of substrate temperatures was 300°C to 450°C.

CdSe epitaxial films grown on (100) oriented Ge substrates had the cubic sphalerite structure in parallel alignment with the Ge. The diffraction pattern of these films contained no satellite spots but <111> streaks were present. When these films were tilted to the (110) orientation the <111> streaks ran continuously in the plane of the (110) diffraction pattern. Well defined square arrays of parallel moire double diffraction spots from areas of heterojunction of Ge and CdSe were observed in the (100) electron diffraction patterns of all the observed devices. Hence parallel moire fringes were observed invariably showing the parallel alignment of the film and the substrate at the interface.

Epitaxial films of CdSe grown on (110) oriented Ge substrates again had basically the cubic sphalerite structure in parallel alignment with the Ge. These films grown throughout the epitaxial range contained domain-form transformed faulted structures. Streaks but no satellite spots were observed in the electron diffraction patterns of these films.

When tilted to (112) orientation one of the <111> streaks ran parallel to the plane of the (112) diffraction

pattern and contained intensity maxima. Parallel moire fringes were observed in the micrographs of these specimens, showing again the parallel alignment of the film and the substrate at the interface.

Annealing studies of these specimens, showed that the faults in the domain-form structure could be eliminated leaving behind antiphase domain boundaries.

CdSe epitaxial films grown on (111) Ge substrates again had the cubic sphalerite structure. Streaks but no satellite spots were observed in the diffraction patterns of these films. Well defined rosettes of moire double diffraction spots from areas of heterojunction where Ge and CdSe were of comparable thicknesses, were always observed in all the devices, but the double diffraction spots were rotated from the parallel alignment positions. Hence "nearly-parallel rotation" moire fringes were observed in the micrographs of all these devices. The new phenomenon of "nearly-parallel rotation epitaxy" was found at the interfaces of these devices for the first time.

Evidence for the occurrence of 60^{o} misfit dislocations was found for the first time in these epitaxial heterojunctions.

In the second phase of this work studies of current-voltage characteristics of p-n Ge/CdSe heterojunctions were carried out. The current-voltage characteristics showed the good rectifying properties of these p-n Ge/CdSe heterojunctions. The forward log I versus V characteristics revealed that the charge transport mechanism across the hetero-

junction was predominantly by recombination-tunnelling. The reverse bias log $\frac{I}{V}$ versus $V^{-\frac{1}{2}}$ characteristics showed that the transport mechanism in the reverse direction was predominantly by Zener tunnelling at higher voltages in these devices.

CONTENTS Page No.

ABSTRACT 3

PART I: STRUCTURAL PROPERTIES OF CdSe EVAPORATED IN VACUUM ONTO Ge 10

CHAPTER I: 11

1.1 INTRODUCTION 11

1.2 THE CRYSTAL STRUCTURE OF II-VI COMPOUNDS 16

1.3 DESCRIPTION OF SPHALERITE AND WURTZITE STRUCTURES ON THE BASIS OF STACKING OF LAYERS 21

1.4 POLAR CHARACTER OF II-VI COMPOUNDS 23

CHAPTER II: LITERATURE REVIEW 27

2.1 EPITAXY 27

2.1.1 Some Parameters that Affect the Growth of Epitaxial Films 28

2.1.2 Substrate Temperature 28

2.1.3 Deposition Rate 30

2.1.4 Effect of Contamination 32

2.1.5 Substrate Orientation 34

2.2 VAPOUR GROWTH OF II-VI COMPOUNDS 37

2.3 REVIEW OF THE EPITAXIAL GROWTH OF CdSe 40

2.4 REVIEW OF THE EPITAXIAL GROWTH OF II-VI COMPOUNDS 45

2.5 NUCLEATION AND GROWTH OF EPITAXIAL FILMS 48

2.6 MISFIT AND MISFIT DISLOCATIONS 53

2.7 ANNEALING OF II-VI EPITAXIAL FILMS 58

Page No.

CHAPTER III: EXPERIMENTAL APPARATUS AND PROCEDURE FOR GROWING EPITAXIAL FILMS 61

3.1 APPARATUS 61

3.1.1 The Vacuum System 61

3.1.2 The Electron Beam Evaporator 63

2.1.3 The Substrate Holder and Heater Assembly 65

3.2 PREPARATION OF Ge SUBSTRATES 67

3.3 PREPARATION OF CdSe EPITAXIAL FILMS 70

3.4 THE SUBSTRATE THINNING PROCESS 72

3.5 MEASUREMENT OF CdSe FILM THICKNESS 74

CHAPTER IV: ANALYSIS OF THE EXPERIMENTAL RESULTS 77

4.1 EPITAXIAL GROWTH RANGES OF SUBSTRATE TEMPERATURE 77

4.2 STRUCTURE OF CdSe FILMS DEPOSITED ON (100) Ge SUBSTRATES 82

4.2.1 Moire Patterns and Fringes 86

4.2.2 Identification of {111} Planar Defects Present in (100) CdSe Films 90

4.3 STRUCTURE OF CdSe FILMS GROWN ON (110) Ge SUBSTRATES 100

4.4 STRUCTURE OF CdSe FILMS GROWN ON (111) Ge SUBSTRATES 111

4.4.1 Tilting of CdSe/$Ge_{(111)}$ Specimens from the (111) Orientation to the (110) Orientation. 118

4.4.2 To deduce Formulae for Azimuthal Angular Rotation and "Nearly-Parallel Rotation" Moire Fringe spacings. 121

Page No.

4.4.3 Observation of "Nearly-Parallel Rotation" Moire Fringes 129

4.4.4 Observation of Misfit Dislocations in CdSe/Ge (111) Heterojunctions 137

CHAPTER V: ANNEALING OF CdSe EPITAXIAL FILMS 147

CHAPTER VI: DISCUSSION OF THE EXPERIMENTAL RESULTS 167

6.1 EPITAXIAL GROWTH RANGES OF SUBSTRATE TEMPERATURE 167

6.2 COMPARISON TO PREVIOUS WORK 170

6.3 STRUCTURAL PERFECTION OF THE CdSe FILMS 172

PART II: ELECTRICAL PROPERTIES OF CdSe/Ge HETEROJUNCTIONS 174

CHAPTER VII: THEORY OF HETEROJUNCTIONS 175

7.1 INTRODUCTION 175

7.2 THEORY OF HETEROJUNCTIONS 176

7.2.1 The Energy-Band Diagram and Diffusion Model of Anderson 177

7.2.2 The Emission Model of Perlman and Feucht 181

7.2.3 Tunnelling Model 183

7.2.4 Tunnelling-Recombination Model 184

7.2.5 Emission-Recombination Model 187

7.3 THE SYNTHESIS OF TRANSPORT MODELS 189

Page No.

CHAPTER VIII: POSSIBLE CURRENT CONDUCTION MECHANISMS 193

8.1 SINGLE CARRIER SPACE CHARGE LIMITED CURRENT 193

8.2 TWO CARRIER SPACE CHARGE LIMITED CURRENTS 196

8.3 TUNNELLING EFFECT 200

CHAPTER IX: EXPERIMENTAL RESULTS AND DISCUSSION 203

9.1 PREPARATION OF CdSe/Ge HETEROJUNCTIONS 203

9.2 METAL CONTACTS TO CdSe 205

9.3 THE EXPERIMENTAL SETUP 209

9.4 EXPERIMENTAL I-V CHARACTERISTICS 213

9.5 THE EQUILIBRIUM ENERGY-BAND DIAGRAM FOR THE Ge/CdSe $_{p-n}$ HETEROJUNCTION 216

9.6 FORWARD LOG I-V CHARACTERISTICS 221

9.7 REVERSE BIAS I-V CHARACTERISTICS. 233

CHAPTER X: CONCLUSIONS AND PROPOSALS FOR FUTURE WORK 240

REFERENCES 245

ACKNOWLEDGEMENTS 259

PART I

"STRUCTURAL PROPERTIES OF CdSe EVAPORATED IN VACUUM ONTO Ge"

CHAPTER 1

1.1 INTRODUCTION

The II-VI compounds are formed from equal numbers of atoms of an element from the IIB column of the periodic table and of an element from the VIB column. These are particularly the selenides, sulphides and tellurides of mercury, zinc and cadmium (Aven&Prenner 1967). The II-VI compounds have related physical and chemical properties. These compounds are believed to be direct band gap materials (Segall 1967). The forbidden energy gaps of these materials range from the minimum value of 0.02 eV for HgTe to the maximum of 3.7 eV for ZnS (Bube 1960). The bonding in the compounds is a mixture of ionic and covalent. A review of the properties of II-VI compounds is given by Aven and Prenner (1967).

A great deal of work has been done on thin films of II-VI compounds. The information regarding the technologically valuable polycrystalline films has been reviewed by Vecht (1966) and Cusano (1967). Over the last decade a substantial body of work has been published on epitaxial films of these compounds. This has now reached the stage at which not only does it provide a valuable contribution to the development of II-VI compounds as semiconducting device materials, but also constitutes a significant body of new information regarding epitaxy. It is desirable to produce the II-VI compounds as bulk crystals and as thin films of high perfection and purity with controlled doping and stoichiometry. Then it should be possible to make heterojunctions of

reproducible and predictable properties and new types of II-VI solid state devices might become commercially viable. In any case however, the availability of such epitaxial single crystalline materials is a necessary condition for the quantitative study of the semiconductor properties of these II-VI compounds and their heterojunctions.

For over a decade the epitaxy of II-VI compounds has been the subject of extensive research in this laboratory (Holt 1974). In the studies of the vacuum growth of these compounds on various substrate materials, it has been found that certain experimental parameters greatly affect the epitaxial growth. These experimental parameters include the vacuum conditions, method of evaporation, deposition rate, substrate structure and surface as well as the substrate temperature. The knowledge of epitaxial growth in our laboratory has to a large extent been due to experiments carried out in high vacua in the range 10^{-5} to 10^{-6} torr. In practice it has been found that the substrate temperature has indeed a great effect on the epitaxial growth. The effect of this parameter is such that below a certain substrate temperature epitaxy does not occur and above that critical temperature epitaxy does occur.

In the earlier work on epitaxy ionic substrates were used for the epitaxial growth of ZnTe (Holt 1966a, 1969a), ZnS (Woodcock and Holt 1969, Holt and Woodcock, 1970) and CdS (Wilcox and Holt 1969, Holt and Wilcox, 1971). Recently

research studies of epitaxy of II-VI compounds have concentrated on growth on elemental Ge and Si semiconducting substrates. These concerned the epitaxial growth of ZnTe on Ge (Mufti and Holt 1972), CdS on Ge (Abdalla et al. 1973), CdTe on Ge (Abdalla and Holt 1973) and CdTe on Si (Holt and Abdalla 1974). Ge and Si have been used as substrates in these studies because of their great technological value as solid state electronic materials and also they are the most extensively studied elemental semiconductors. Indeed the main objective of using these Ge, and Si substrates is to fabricate epitaxial heterojunctions with II-VI compounds, to study the structural, electrical and optical properties of these heterojunctions and to investigate their possible device applications.

As a result of systematic continued investigations on the epitaxial growth and structure of II-VI compounds on ionic and elemental semiconductors in this laboratory and elsewhere, certain general laws of epitaxy have emerged. These include the general occurrence of either the parallel epitaxial orientation or the quasi-parallel epitaxial orientation. The parallel epitaxial orientation between sphalerite structure II-VI films and substrates with cubic system crystal structures is (hkl) film parallel to (hkl) substrate with [uvw] film parallel to [uvw] substrate, where [uvw] is a direction in the (hkl) plane. Whether the substrate surface is (100), (110) or (111) this parallel epitaxial orientation

always occurs. In the case of the quasi-parallel epitaxial orientation the film has the Wurtzite structure on a substrate with cubic structure. This orientation relation is (0001) film parallel to (111) substrate with $[11\bar{2}0]$ film parallel to $[1\bar{1}0]$ substrate.

Thus the important fact is that sphalerite structure II-VI compound films grown on cubic substrates always have the parallel orientation and wurtzite structure II-VI compound films grown on cubic crystal structure substrates always have the quasi-parallel orientation. No other epitaxial orientation relations have been reported in the literature so far.

From the above mentioned epitaxial studies of II-VI compounds and the semiconductor literature, it is evident that CdSe is the least exploited material among II-VI compounds in spite of the widespread interest in it as a photoconductor material.

Hence the first objective of this work was to investigate for the first time whether CdSe could be grown epitaxially on the three faces of Ge and to test whether the general laws of epitaxy mentioned above apply in this case also. Secondly, it was intended to study the electrical properties of CdSe/Ge heterojunctions.

All the structural analysis of the CdSe/Ge devices in the three (100), (110) and (111) orientations was done with the help of electron diffraction and transmission electron

microscopy, since this technique is capable of great resolution at high magnification. The associated technique of high resolution dark field electron microscopy also was used to remove any ambiguities in the interpretation of bright field images. The transmission electron microscopes used for this programme of structural investigations were an AEI EM 6G 100 kV electron microscope, a Philips EM 301 100 kV electron microscope and an AEI EM7 1000 kV electron microscope.

The work presented here is reported in two parts. The first part deals with the structural properties of CdSe/Ge heterojunctions. Part I contains six chapters. Chapters I and II are concerned with the most relevent literature. Chapter III is a description of the apparatus and the experimental techniques for the growth of thin films. Chapters IV, V and VI contain the analysis and discussion of the experimental results respectively. The second part deals with the electrical properties of CdSe/Ge (111) heterojunctions and contains three chapters. Chapter VII deals with the theory of heterojunctions. Chapter VIII is a survey of the literature on carrier conduction mechanisms. Chapter IX deals with the analysis and discussion of the experimental results.

Finally a short chapter deals with conclusions and proposals for further work.

The present work is another step forward in the programme of study of the epitaxy of II-VI compounds which has gone on in this laboratory for the past ten years.

1.2 THE CRYSTAL STRUCTURE OF II-VI COMPOUNDS

The crystal structures of the II-VI compounds resemble the diamond structure. The diamond structure is a result of covalent bonding. The basic structural unit of the diamond structure is the tetrahedron. In this structure each atom is tetrahedrally co-ordinated by the four nearest neighbouring identical atoms, as shown in fig. 1.1(a). By interconnecting other tetrahedra to one another in a particular way the diamond structure can be formed. It has a cubic symmetry. The unit cell of the diamond structure is shown in fig. 1.1(b). It is a face centred cubic cell with four extra atoms inside the unit cell. The elements silicon, germanium, carbon and grey tin crystallise in the diamond structure.

The crystal structures of the II-VI compounds, with the atoms tetrahedrally co-ordinated as in the diamond structure are referred to as "adamantine" structures.

The principal of these structures are sphalerite and wurtzite. The adamantine structures have a basis of two different types of atoms associated with each lattice point. The basic feature of these adamantine structures is that each atom of one kind is tetrahedrally co-ordinated by four atoms of the other kind. This is the basic difference between the diamond structure and the sphalerite and wurtzite structures.

Fig. 1.2(b) shows the unit cell of the sphalerite (zinc blende) structure. The sphalerite structure has the

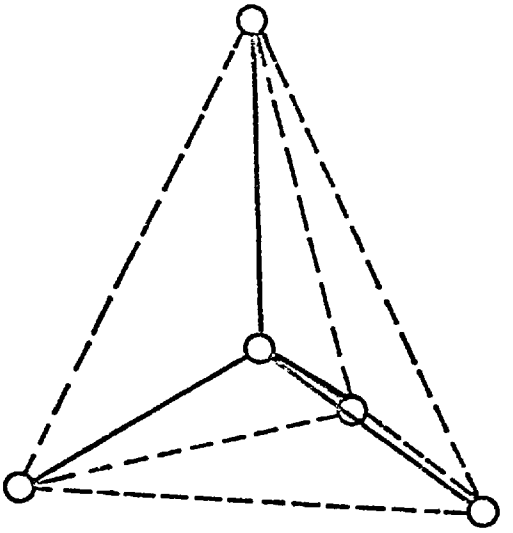


Fig. 1.1(a) The tetrahedral co-ordination of one atom by its four neighbouring atoms.

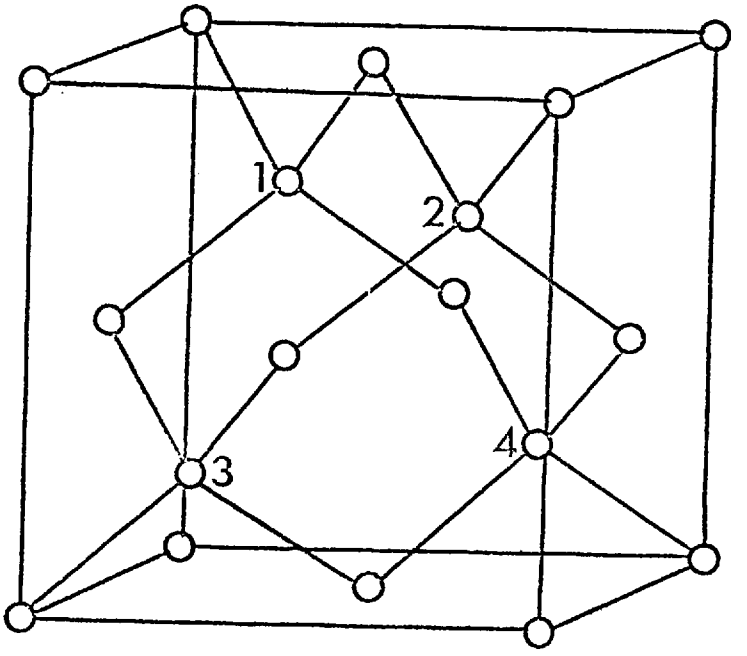
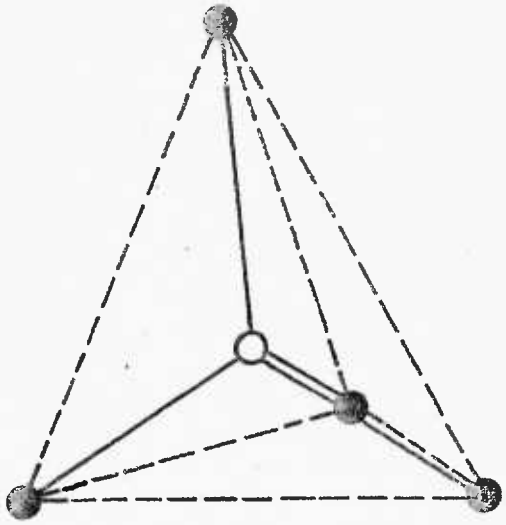
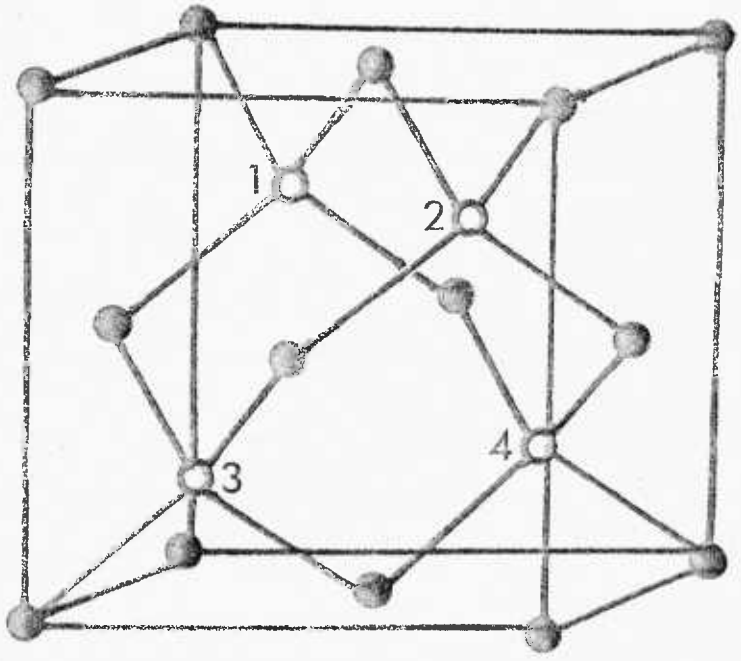


Fig. 1.1(b) The unit cell of the diamond structure. Atoms 1, 2, 3 and 4 all lie inside the unit cell. The rest of the atoms occupy the f.c.c. positions.



(a)

Fig. 1.2(a) The tetrahedral co-ordination of one atom by its four neighbours.



(b)

Fig. 1.2(b) The unit cell of the sphalerite structure. Open circles represent Se atoms and solid circles represent Cd atoms.

same atomic positions as in the diamond structure. Hence the sphalerite structure also has cubic symmetry. It has the face centred cubic space lattice with four extra atoms inside the unit cell. Each Cd atom is tetrahedrally co-ordinated by four Se atoms and vice versa as shown in Fig. 1.2(a). The sphalerite structure has a basis of two atoms of different kind with co-ordinates (0,0,0) and $(\frac{1}{4},\frac{1}{4},\frac{1}{4})$ associated with each lattice point. The f.c.c. sublattices of atoms of the two kinds are displaced from each other by a quarter of a body diagonal. The unit cell contains four molecules of CdSe or four atoms of Cd and four atoms of Se. Following Roth (1967) these occupy the positions with the following co-ordinates:

Cd at $(0,0,0)(0,\frac{1}{2},\frac{1}{2})(\frac{1}{2},0,\frac{1}{2})(\frac{1}{2},\frac{1}{2},0)$

and

Se at $(\frac{1}{4},\frac{1}{4},\frac{1}{4})(\frac{1}{4},\frac{3}{4},\frac{3}{4})(\frac{3}{4},\frac{1}{4},\frac{3}{4})(\frac{3}{4},\frac{3}{4},\frac{1}{4})$.

Unlike the diamond structure the sphalerite structure has no centre of symmetry. That is the (111) plane is not equivalent to the $(\bar{1}\bar{1}\bar{1})$ plane. These planes have different physical and chemical properties. The polar character of II-VI compounds is discussed in section 1.4.

The wurtzite structure is illustrated in fig. 1.3. This has the hexagonal space lattice and hexagonal symmetry. In the wurtzite structure unit cell there are two CdSe molecules, with Cd atoms at (0,0,0) and $(\frac{1}{3},\frac{2}{3},\frac{1}{2})$ and two Se atoms

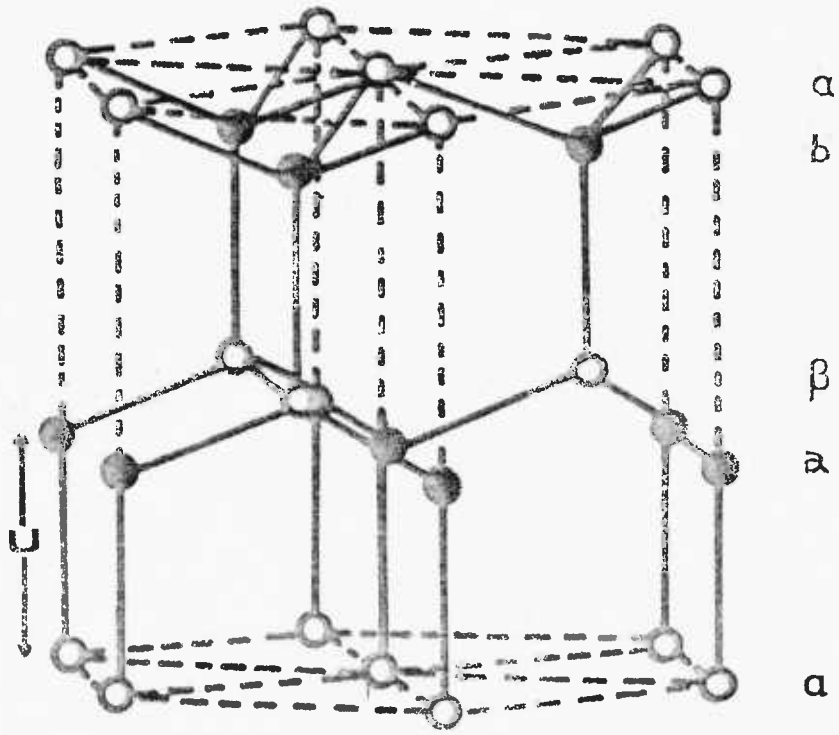


Fig. 1.3 The unit cell of the wurtzite structure.

Open circles represent Se atoms and solid circles represent Cd atoms. Roman letters indicate layers of Cd atoms and Greek letters indicate layers of Se atoms. The interatomic spacing of atoms of different types is denoted by u.

at (0,0,u) and $(\frac{1}{3},\frac{2}{3},\frac{1}{2}+u)$, where $u = \frac{3}{8}$ for the crystal of ideal $\frac{c}{a} = 1.633$.

If $\frac{c}{a} = 1.633$ and $u = \frac{3}{8}$, then the wurtzite structure corresponds to tetrahedral co-ordination (Roth 1967). In the case of the II-VI compounds, the values of $\frac{c}{a}$ are as follows: For CdSe, $\frac{c}{a} = 1.632$, for ZnSe, $\frac{c}{a} = 1.658$, for CdTe, $\frac{c}{a} = 1.637$, for ZnTe, $\frac{c}{a} = 1.645$ and for CdS, $\frac{c}{a} = 1.620$ (taken from Holt 1969a).

1.3 DESCRIPTION OF SPHALERITE AND WURTZITE STRUCTURES ON THE BASIS OF STACKING OF LAYERS

The sphalerite and wurtzite structures can be described in terms of double layer stacking sequences based on the close packing of atoms as in the cases of the face centred cubic structure and the hexagonal close packed structure respectively. Fig. 1.4 and 1.5 show the double layer stacking of atoms. The atom in one sublayer rests on the top of the atom of the other sublayer.

The sphalerite structure can be described by the stacking sequence aαbβcγaαbβcγ ... etc., as shown in fig. 1.4 where the Roman letters represent planes of group IIB type atoms and the Greek letters represent planes of group VIB type atoms. In this case the stacking sequence repeats itself after three double layers. These layers are {111} double atom planes of the sphalerite structure.

The wurtzite structure can be described by the stacking sequence aαbβaαbβ ..... etc. as shown in fig. 1.5.

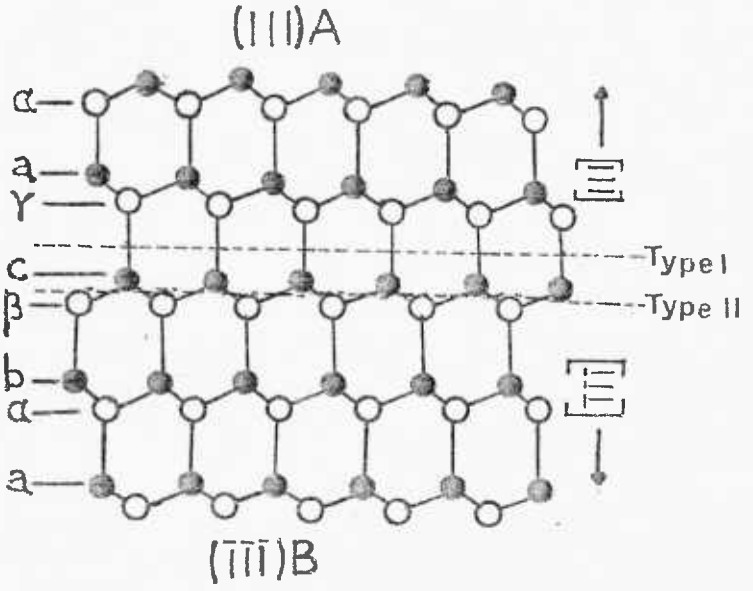


Fig. 1.4 The stacking sequence of the {111} planes of the sphalerite structure.

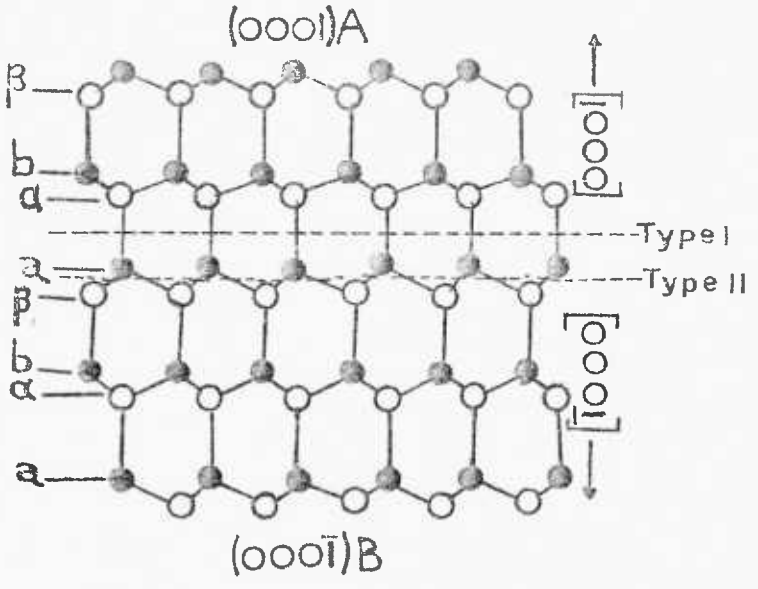


Fig. 1.5 The stacking sequence of the {0001} planes of the wurtzite structure.

Where the Roman letters stand for the layers of group IIB type atoms and the Greek letters stand for the layers of group VIB type atoms. In this case the stacking sequence repeats itself after two double layers. These layers are the {0001} double atom planes of the wurtzite structure.

Bonding between one layer of atoms and its two adjacent layers is not equal. Between α and a, β and b, γ and c layers, there is only one bond per atom. Between α and b, β and c, and γ and a layers there are three bonds per atom. Hence slip or cleavage usually occurs between the former pairs of planes and not between the latter pairs of planes.

1.4 POLAR CHARACTER OF II-VI COMPOUNDS

II-VI compounds crystallise in the sphalerite and wurtzite structures. Descriptions of the sphalerite and wurtzite structures are given in the previous sections 1.2 and 1.3.

The sphalerite and wurtzite structures lack a centre of symmetry. Fig. 1.4 and 1.5 show the sphalerite and wurtzite structures, drawn to show the stacking sequences of {111} and {0001} atomic planes respectively. In the sphalerite structure a definite order of occurrence of the (111) planes of atoms of the two chemical species constituting the compound can be seen. Similarly in the wurtzite structure a definite order of occurrence of the (0001) planes of atoms of the two chemical species constituting the compound can be seen. Since these structures are non-centrosymmetric, it is seen from Figs.

1.4 and 1.5 that the opposite faces of {111} and {0001} slices of II-VI materials with the sphalerite and wurtzite structures are surfaced with IIB atoms at one side and VIB atoms at the other side. This means that the opposite sides of {111} slices and {0001} slices of materials with sphalerite and wurtzite structures are physically and chemically distinguishable (Warekois et al. 1962, Barber and Heasell 1965, and Gatos and Lavine 1965).

In the figures 1.4 and 1.5 the faces in which the surface atoms are of the IIB element are referred to as (111)A faces, and those in which surface atoms are of the VIB element as $(\bar{1}\bar{1}\bar{1})$B faces. There is also polarity in the bulk of these crystals, because the order of appearance of the atoms connected by <111> bonds in the sphalerite structure, and <0001> bonds in the wurtzite structure reverses when the direction reverses. That is, in the $[111]_a$ direction the sequence is IIB-VIB. Here the subscript a, on a [111] direction indicates the sense along a covalent bond from the atom of the element from the IIB column of the periodic table to the atom of the VIB element. Similarly in the $[\bar{1}\bar{1}\bar{1}]_b$ direction the sequence is VIB-IIB.

Similarly there exists bulk or volume polarity in the $[0001]_a$ and $[000\bar{1}]_b$ directions, in the wurtzite structure.

From Fig. 1.4 it is seen that there are type I and type II (111) planes in the sphalerite structure. Across the type I (111) plane there is only one bond per atom,

whereas across the type II (111) planes there are three bonds per atom. Therefore it is very probable that the sphalerite structure materials part or cleave or generally terminate along type I (111) planes, and not along type II (111) planes. This means that opposite sides of a (111) slice should be (111)A and $(\bar{1}\bar{1}\bar{1})$B faces. That is a (111)A surface is a free surface terminating in IIB atoms each triply bonded to the interior and a $(\bar{1}\bar{1}\bar{1})$B surface is the opposite side free surface terminating in VIB atoms each triply bonded to the interior. A similar argument applies to the wurtzite structure.

Both surface and bulk polarity seem to influence the epitaxial growth of II-VI compounds. Weinstein et al. (1965, 1967) and Cardona et al. (1965) deposited CdS by chemical vapour phase methods on the (111) Ga faces of GaAs, and GaP substrates. They found that the CdS films had the wurtzite structure. However when the CdS was grown on the $(\bar{1}\bar{1}\bar{1})$P face of GaP and the $(\bar{1}\bar{1}\bar{1})$ As face of GaAs the films had the sphalerite structure. This showed that changing the polarity of the substrate surface changed the film structure.

That this is notalways the case was shown in the following works. Holloway and Wilkes (1968) deposited CdS on InSb. They found that films of CdS evaporated onto both the (111) In and the $(\bar{1}\bar{1}\bar{1})$ Sb faces of InSb had the sphalerite structure. Yim and Stofko (1974) grew CdSe epitaxial films on (0001) and $(000\bar{1})$ faces of CdS. It was found that the CdSe films had the hexagonal wurtzite structure on both the faces of CdS.

Igarashi(1971) deposited CdS on one face of each of CdTe and GaP, two faces of InAS and the six faces: (001), (110), (112)A, (21$\bar{1}$)B (221)A and (22$\bar{1}$)B, of GaAs. This work established that there is a pronounced tendency for the directional polarity of substrates to be continued in the polarity of the II-VI epitaxial films deposited on them. That is, the [0001]a direction in the CdS films was almost always aligned with one of the [111]a directions in the substrate..

The polarity of sphalerite and wurtzite structure II-VI films grown on diamond structure Si and Ge substrates cannot be determined by the polarity of the substrate since the diamond structure is non-polar (centrosymmetric). In only one case, that of vacuum evaporated ZnSe onto Ge (111), a polarity determination has been reported by Deasley et al (1970). In this case ZnSe grew with the ($\bar{1}\bar{1}\bar{1}$) Se face outward.

The possibility that antiphase domains might occur in these structures has been considered in chapter V. Fig. 5.1 (chapter V) shows how polarity reversed domains can be surfaced when the occupation of the sublattice sites by the two atomic species is changed. The boundary between two antiphase domains is called an antiphase domain boundary (APB). A more detailed account of APBs is given in chapter V.

CHAPTER II

LITERATURE REVIEW

2.1 EPITAXY

Epitaxy is a term used to express the phenomenon of a crystal growth of one material on the crystal surface of another, so that there is a simple orientation relationship between the two crystals. The oriented overgrowth of a substance over itself is called "auto epitaxy" and on another substance is called "hetero epitaxy". Epitaxial growth of a solid film over a liquid surface of another substance is called "rheo epitaxy".

Royer (1928) suggested that a small misfit (less than 15%) is necessary for the occurrence of epitaxy. The misfit parameter is defined as the percentage difference between the lattice spacings of the two crystals along a particular crystallographic direction, and can be expressed as $\frac{a-b}{a} \times 100$, where a and b are the lattice spacings of the substrate and the overgrowth respectively. Schulz (1951 and 1952) showed that the Royer hypothesis was not obeyed by many substrate overgrowth systems. In fact in the latter work it was shown that percentage misfit as large as 90 in the case of CsI/LiF, 105 in the case of RbBr/Ag, 101 in the case of Sn/Ag, -36 in the case of Cu/NaCl and -31 in the case of Ag/PbS still permitted epitaxy. This does not mean that misfit is not an important parameter (see sections 2.5 and 2.6). It is

expected to be the key parameter in the understanding of epitaxy in terms of the relative positioning of the atoms.

The experimental and theoretical aspects of thin film epitaxy have been reviewed by Pashley (1956, 1965), Holt (1974) and Matthews (1975A and B).

However some of the more important parameters such as (1) substrate temperature, (2) deposition rate (3) effect of contamination and (4) substrate orientations that affect epitaxy are given below.

2.1.1 Some Parameters that Affect the Growth of Epitaxial Films

2.1.2 Substrate Temperature

It is well known in the literature that to achieve epitaxial growth of a deposit, it is necessary to heat a substrate to a suitable temperature. (F.C.C. metals on NaCl by Brück 1936, Ge on CaF_2 by Sloope and Tiller 1962, 1965, CdTe on Mica by Suito and Shiojiri 1963, Ge on Ge by Krikorian 1964, Ge on CaF_2 by Schalla et al. 1964, GaAS on NaCl by Evans and Noreika 1966, ZnTe on ionic substrates by Holt 1966, face centred cubic metals on ionic substrates by Ino et al. 1964 and by Sella and Trillat 1964, ZnS on NaCl by Woodcock and Holt 1969, ZnTe on Mica by Dhere and Goswami 1969).

Sequences of electron diffraction patterns showing the orientation behaviour of CdSe films with Ge substrate temperature are shown in Fig.4(sec.4·1). At low substrate temperatures films grew with randomly oriented fine grained structures.

These films gave ring electron diffraction patterns. These are assigned the degree of orientation values R = 0. With increase in the substrate temperature, the films grew with an increased fraction of their volume in epitaxial orientation. These films, gave rise to mixed ring and spot patterns. Such films are given the values R = 25, R = 50 or R = 75, depending upon the relative intensities of the ring and spot components of the diffraction patterns. In a certain range of substrate temperatures the films grew well oriented by giving rise to spot diffraction patterns. These films are given the value R = 100 indicating epitaxy. The range of substrate temperatures for which films grow epitaxially is called the "epitaxial growth range" of substrate temperatures. Thus heating of the substrate during the growth of a film provides an increase in the migratory capacity of the condensed atoms or molecules, and facilitates the formation of oriented crystals. As the substrate temperature is increased it is found that the film growth changes from the polycrystalline to a well oriented single crystal state.

In the present work (and in the previous works, Holt 1974) before films were deposited, the Ge substrates were heated to 600^{o}C and then cooled to the deposition temperature. It is thought that this removed any adsorbed material from the substrate surface and provided one of the optimum conditions for reproducible epitaxial film growth.

Substrate temperature not only plays an important role in epitaxial film growth but also it determines the

upper cut off temperature at which films cease to deposit. For details see chapter IV, section 4.1 and chapter VI, section 6.1.

2.1.3 Deposition Rate

Woodcock and Holt (1969) made a systematic study of the influence of the growth conditions such as substrate temperatures, vacuum pressure, contamination and deposition rate on ZnS films deposited on NaCl. They found that deposition rates of 1Å /sec, 10Å /sec and 100Å /sec had no effect on the structure of the films. On the other hand films grown at 250 Å/sec and 300 Å/sec deposition rates were found to contain included wurtzite structure grains, which might be explained on the basis of the non-stoichiometric deposition of ZnS. Similar effects were found in CdS films deposited on ionic substrates by Wilcox and Holt (1969). The effect of increasing the deposition rate was to decrease the structural perfection of the films considerably. Comparison was made between the diffraction patterns of films deposited under similar conditions except for an order of magnitude difference in deposition rates. They found that the slowly deposited films had a diffraction pattern containing no satellite spots whereas rapidly deposited films had a diffraction pattern containing satellite spots.

These extra spots were attributed to the presence of included grains. Mufti A.R. (1972) while working on ZnTe on Ge tried different deposition rates. It was found that

the films grown at very high deposition rates had polycrystalline structures.

Aberdam et al. (1969) deposited CdSe on $YMnO_3$ (yttrium manganite) in ultra high vacuum. Films were deposited in the substrate temperature ranges from 180°C to 250°C. The degree of orientation was found to be dependent on the rate of deposition. A deposition rate of 3 Å/sec. gave fully epitaxial CdSe films, the substrate temperature being 210°C. CdSe films were disoriented when the deposition rate was 25Å /sec, the substrate temperature being 250°C.

It appears in general, that rapid deposition rates affect the epitaxial growth of II-VI films and reduce the structural perfection of the films.

On the other hand Booker and Unvala (1965) while studying Si on Si found that a high deposition rate was necessary for getting Si films free from stacking faults.

Matthews (1959) found that the structural quality of Au, Ag and Cu epitaxial films deteriorated when the deposition rate onto NaCl substrates was too slow. He found that under these conditions, the nucleation density was low and each nucleus attained an appreciable size before coalescence began. As a result due to large diffusion distances reorientation and recrystallisation of grains in random orientations was more difficult. This means that rapid deposition rates and hence high nucleation densities and high substrate temperatures were the preferable conditions for good epitaxial growth at

least for metals like Au, Ag and Cu.

2.1.4 Effect of Contamination

In the literature it is found that studies of the effect of contamination of substrate surfaces on epitaxial growth of thin films of various materials are mostly concerned with ionic substrates like NaCl. No similar work on the diamond structure Ge and Si has been published except in one case that the effect of vacuum carbon contamination on Si autoepitaxy has been in fact reported by Ogden et al (1974). Many epitaxial thin films are prepared by vacuum evaporation in oil-pumped systems generally operating at pressures of 10^{-5} torr. At this pressure the hydrocarbons and water vapour adsorbed on the substrate surface and nearby surfaces of the substrate holder might cause hindrance to the epitaxial film growth. The effect of oil and water vapour contamination on NaCl (100) substrates upon the epitaxial growth of ZnS was investigated by Unvala et al. (1968). They found that the cleanliness of the substrate surface and the use of an ultra high vacuum widened the epitaxial growth range of temperature and improved the crystalline perfection as well. Woodcock and Holt (1969) while studying the influence of vacuum contamination on the structure of ZnS films evaporated onto NaCl, found that changing from an electron beam evaporator to a radiant tantalum evaporator deteriorated the structure of the films. This was attributed to the presence of Ta in the films, which was responsible for the occurrence of

included grains in the ZnS films.

Thus it has been observed by some workers that contamination of the vacuum system can be reduced by reducing the pressure in the working chamber. That is, changing from high vacuum to ultra high vacuum leads to good quality epitaxial films (Spinnulescu-Caránaru (1969), Unvala et al. (1969) and Calow et al. (1972)).

On the other hand, Woodcock and Holt (1969) while studying ZnS epitaxy on NaCl found that it was not the ultra high vacuum, but the method of evaporation by focussed electron beam evaporator that was mainly responsible for the widest epitaxial growth range of substrate temperatures, and structurally most perfect films.

Matthews and Grunbaum (1964, 1965) found that the best quality Au films grown on NaCl were obtained if the substrate was exposed to air prior to film deposition. On the contrary, Woodcock and Holt found that the epitaxial range of ZnS on vacuum cleaved NaCl was wider than that on air cleaved NaCl substrates.

Matthews (1965) observed that even though the orientation of the initial nuclei was better in films grown on vacuum cleaved substrates than it was on substrates exposed to air before deposition, the nucleation density on the contaminated substrates was much greater. The latter was responsible for earlier coalescence which had already been shown to promote epitaxy (Matthews 1959).

In our present work on CdSe on Ge, to get reproducible epitaxy, outgassing of substrate, substrate heater assembly and even source material was a must. This reduced the contamination and provided the optimum growth condition.

However the effect of contamination of the substrate surface on the growth of thin films seems to be not clear or certain.

2.1.5 Substrate Orientation

Substrate parameters like substrate orientation, substrate temperature and substrate polarity are some of the important factors determining the structure and orientation of epitaxial films in general and II-VI epitaxial films in particular. The effect of substrate temperature is dealt with in the section 2.1.2. In the literature, the substrate orientations that are extensively used for epitaxial investigations are (100), (110) and (111) (Holt 1974, Francombe and Sato 1964, Pashley 1956,1965, Chopra 1969, and Matthews 1975 A and B). As a result of continued and extensive systematic research on the epitaxial growth and structure of Zn and Cd chalcogenides on ionic and covalent substrates, the natural laws of epitaxy have emerged. The II-VI compounds always grow at low temperatures with the cubic sphalerite structure in (100) and (110) orientations, when grown on (100) and (110) ionic or diamond structure substrates. This is ascribed to the impossibility of matching the symmetry of (100) planes and (110) planes exactly by any planes in the

hexagonal structure. This means that in these orientations there must always be a large fraction of non-coincident lattice sites in the interface. The number of these sites is reduced if the compounds grow with the cubic sphalerite structure in parallel alignment. Secondly, the II-VI compounds always grow either with the cubic sphalerite structure in (111) orientation or with the hexagonal wurtzite structure in (0001) orientation on (111) oriented ionic or diamond structure substrates. (111) surfaces are normal to a three-fold rotational symmetry axis which can be matched by either the (111) plane in the sphalerite structure or the (0001) plane in the wurtzite structure and high density coincidence lattice networks can be formed in both the cases. It has also been found that when II-VI compounds grew with the sphalerite structure on (100),(110) and (111) surfaces the epitaxial growth orientation was always parallel. When they grew with the hexagonal wurtzite structure the epitaxial growth orientation was found to be quasi-parallel. These were the generally observed phenomena of the epitaxial growth orientation and structure of II-VI films. For the first time in research on the epitaxy of II-VI compounds, however, we have found another epitaxial orientation in the CdSe/Ge (111) heterojunction. This is called the nearly-parallel rotation epitaxial orientation relationship (Gejji and Holt 1975; chapter IV). This nearly-parallel orientation was found to be present in all the CdSe/Ge (111) heterojunctions prepared throughout the epitaxial range of temperatures.

This deviation from exact parallelism is substrate orientation dependent; i.e. it occurs only on (111) Ge substrates.

Chopra and Khan (1967) studied the epitaxial growth of CdS on (100) surfaces of NaCl at temperatures down to 20°C. The CdS films grown at the lowest epitaxial temperatures had the wurtzite structure. In contrast, Wilcox and Holt (1969) while studying the epitaxial growth and structure of CdS films on (100) surfaces of NaCl found that the CdS films had the sphalerite structure in agreement with the general rule quoted above, the epitaxial temperature range being 150°C to 300°C. Van Dijk (1967) grew CdS on (110) faces of Ge and found that the CdS films had a polycrystalline wurtzite structure.

Weinstein et al. (1965 and 1967) deposited CdS on the (111) Ga faces of GaAs and GaP substrates and on the $(\bar{1}\bar{1}\bar{1})$P faces of GaP and the $(\bar{1}\bar{1}\bar{1})$ As faces of GaAs. They found that the CdS films deposited on the (111) Ga faces of GaAs and GaP had the hexagonal wurtzite structure but the films deposited on the $(\bar{1}\bar{1}\bar{1})$ As and $(\bar{1}\bar{1}\bar{1})$P faces of GaAs and GaP respectively, had the sphalerite structure. On the other hand, Holloway and Wilkes (1968) found that CdS films deposited on both the (111) In and the $(\bar{1}\bar{1}\bar{1})$ Sb faces of InSb had the cubic sphalerite structure. This means that changing the polarity of the substrate surface does not always change the film structure. Aven and Garwacki (1963) have observed the growth of CdS films on the (111) faces of ZnTe. Epitaxial

films were grown on the (111) faces containing Zn atoms whereas polycrystalline films resulted on the Te faces.

2.2 VAPOUR GROWTH OF II-VI COMPOUNDS

When II-VI compounds are grown in vacuum on single crystal substrates two important physical processes are involved. These are (1) the evaporation of a II-VI compound into its constituent elements and , (2) condensation of the constituent elements on the substrate surface to form the film of the compound.

Goldfinger and Jeunehomme (1963) found that vapours of the metals from group II always exist in monoatomic form and vapours of the non-metals from group VI consist mainly of diatomic molecules. CdSe, like other II-VI compounds dissociates during evaporation according to the reaction,

$$CdSe_{(solid)} \rightleftarrows Cd_{(gas)} + \tfrac{1}{2} Se_{2(gas)}$$

This reaction indicates that CdSe is dissociated to its constituent elements. Therefore the vapour arriving at the substrate surface is a mixture of Cd and Se_2 in the stoichiometric proportion. Since the vapour pressures of the two constituent elements is many order of magnitude greater than that of the compound at the same temperature, no enrichment of the source occurs.

The equilibrium composition of the II-VI compounds is a function of the partial pressures of the two constituent

elements and the temperature during the crystal growth (Goldfinger and Jeunehomme 1963). Any deficiency in one or the other constituent elements is generally accommodated by vacancies on the appropriate sublattice site in the crystal structure, and it can also be compensated for by incorporating the extra atoms of the excess elements as interstitials within the crystal structure. Conversely, the relative vapour pressures of the constituent elements over a crystal are functions of the crystal growth temperature. Therefore, in a crystal growing system in which the source and substrate temperatures are different and where, for example, the vapours are carried along by an inert gas, the composition of the growing crystal will differ from that of the source as the excess of one of the two elements is carried away by the transport gas.

It is possible to supress evaporation of the solid by increasing the relative pressure of either of the gaseous components (Somorjai 1962, Somorjai and Jepsen 1964, Somorjai and Stemple 1964, Somorjai and Lester 1965 and Kroger 1964). This is achieved in closed systems by ensuring that the starting material is of the required composition. In open systems using vapour transport methods, the vapour pressure can be controlled directly and continuously. This can also be achieved during vacuum evaporation of the thin films by evaporating the compound together with an excess of the appropriate element.

Fischer (1966) pointed out that II-VI compounds grown at higher temperatures contain cation and anion vacancies. When the crystal cools down, some of the vacancies will be frozen in the lattice. IIB metal (cation) vacancies are of acceptor type whereas VIB nonmetal (anion) vacancies are of donor type. The fact that the IIB-VIB compounds with the exception of CdTe have either n or p-type conductivities was explained by Fischer (1966) in terms of the ratio $\frac{r_c}{r_a}$; where r_c and r_a are the radii of the cation and anion respectively. He calculated the ratios for CdO $\frac{r_c}{r_a} = 2.2$, ZnO $\frac{r_c}{r_a} = 1.98$, CdS $\frac{r_c}{r_a} = 1.42$, CdSe $\frac{r_c}{r_a} = 1.30$, ZnS $\frac{r_c}{r_a} = 1.26$, ZnSe $\frac{r_c}{r_a} = 1.15$, CdTe $\frac{r_c}{r_a} = 1.12$ and ZnTe $\frac{r_c}{r_a} = 0.99$.

Fischer showed that the compounds having larger r_c tend to be n-type whereas a compound having larger r_a tends to be p-type.
Accordingly ZnTe always tends to be p-type. CdTe is found to be the only material among IIB and VIB compounds which can be prepared with either type of conductivity, whereas CdS and CdSe always tend to be n-type.

Somorjai and Jepsen (1964) found that CdS crystals, heat treated at the higher temperature (1200^{o}C) and pressure (20 atmospheres) in sulphur vapour remained n-type. They pointed out that sulphur vacancies are always present in the bulk of the CdS crystals in larger concentrations than cadmium vacancies. Heat treatment of CdS in sulphur or cadmium vapour changes only the magnitude of the excess sulphur

vacancy concentration relative to its concentration in the unannealed crystals.

Burmeister and Stevenson (1967) prepared wurtzite structure CdSe crystals. The as-grown CdSe crystals were n-type. The CdSe crystals annealed at 900^{o}C for a period of 7 days under saturated cadmium or sulphur pressure were found to remain n-type.

Ludke (1971) showed that the heat treatment of CdTe crystals in Cd, Ga or In vapour converted the CdTe from p-type to n-type. Whereas the CdTe films annealed in Te vapours were p-type.

2.3 REVIEW OF THE EPITAXIAL GROWTH OF CdSe

Ratcheva et al (1973) evaporated CdSe on (0001) oriented sapphire (Al_2O_3) substrates, in a pressure of 5×10^{-5} torr. A structure change was observed for the substrate temperature range from 400^{o} to 620^{o}C. From 400^{o}C to 460^{o}C CdSe layers were polycrystalline; from 460 to 530^{o}C CdSe layers were fine textured with a low extent of preferred orientation; from 530^{o} to 570^{o} C, layers were well textured with a high extent of preferred orientation. In the narrow substrate temperature range 570^{o} to 620^{o}C, the condition for formation of monocrystalline structure was achieved, varying in extent of perfection according to the temperature and the growth rate. The best monocrystalline structure was obtained at the substrate temperature 585^{o}C and an electron back reflection pattern was obtained to assess the wurtzite structure

monocrystallinity.

Gashin and Simashkevich (1973) obtained by gas-transport epitaxy of CdSe on (110) faces of zinc telluride (ZnTe) single crystalline substrates. In the substrate temperature range from 450° to 700°C, single crystalline CdSe films of cubic modification were grown. Current-voltage and capacitance-voltage characteristics of the heterojunctions were measured. In the forward bias upto 1.2V, the current increased exponentially with voltage. They found that the interface states do not appreciably influence the heterojunction properties. Anderson's model was used for the calculation of the heterojunction parameters and the construction of the band diagram.

Sergeyeva et al (1972) grew CdSe (and other II-VI compounds CdS, ZnS, ZnSe) by the method of vacuum evaporation and condensation in a vacuum of 10^{-4}-10^{-5} torr on mica (001) plane. The growth range of films having wurtzite and sphalerite modifications versus evaporation temperature and epitaxial temperature for CdSe were investigated. Their best CdSe films had mixed or a sphalerite structure for substrate temperatures below 400°C and the wurtzite structure above 400°C to 550°C. The resistivity of the CdSe was found to be 10^6 Ω cm. The electron mobility was found to be 100-450cm^2/Vsec.

Ratcheva et al (1972) grew CdS and CdSe on (111) Ge and (111) CaF_2 substrates by a vapour phase transport method.

The CdSe layers were (0001) oriented. The epitaxial growth ranges for CdSe were: for Ge (111) substrates — temperatures from 540°C to 600°C; for Ca F_2 (111) substrates— temperatures from 660°C to 720°C and, for Si (111) substrates — temperatures from 640°C to 740°C. On Si (111) oriented substrates very small local growth islands were realised with (0001) orientation. CdS was found to be epitaxial on (111) faces of Ge and CaF_2 in the substrates temperature ranges of 540° to 650°C. Electron back-reflection patterns were obtained to assess the single crystallinity.

Al'taman et al (1968) deposited CdSe films on (111) faces of CaF_2 in a vacuum of 10^{-6} torr. Substrates were heated to 600°C prior to deposition. Epitaxial growth of CdSe was found to depend on the substrate temperature and rate of deposition. Films were deposited in the substrate temperatures range of 25°C to 500°C. Films were polycrystalline upto 300°C. Single crystal CdSe containing various microstructures was produced from 440°C to 460°C. Above 480°C the CdSe films had again a partial orientation. The resistivity of the films grown under optimum conditions ranged from $10^8 \Omega$ cm to $5 \times 10^6 \Omega$ cm. The electron mobility was 70 - 120 $cm^2/Vsec$.

Kalinkin et al (1962) evaporated CdSe on to the (111) surfaces of NaCl, KCl and KBr. The CdSe films deposited at substrate temperatures from 20°C to 250°C were found to be polycrystalline and partially oriented with hexagonal symmetry. Their diffraction patterns contained irrational reflections.

The CdSe films grown at substrate temperatures above 250°C (to 350°C) were found to be monocrystalline with wurtzite structure in (0001) orientation. They showed that the quality of the films did not depend upon whether the deposition took place on a carefully or poorly polished substrate.

Kalinkin et al (1963) evaporated CdSe onto the (100) and (110) faces of NaCl. They investigated the dependence of the structural quality of the films upon the treatment of the substrate crystal, such as polishing, etching and annealing. They grew CdSe on these faces at room temperature. It was found that the structure of the CdSe film was polycrystalline with hexagonal symmetry. CdSe was deposited on (100) faces of NaCl, which were thermally cleaned prior to deposition and maintained at 250°C. The CdSe layer grown was found to contain mixed cubic and hexagonal phases. Increasing the substrate temperature up to 350°C, resulted in failure to produce structurally improved films. Upon chemically etching the NaCl substrates, prior to film deposition, these mixed phases disappeared completely and the CdSe films were found to be of single cubic phase.

Aberdam et al. (1969) deposited CdSe on (0001) surfaces of $YMnO_3$ (Yttrium manganite) in ultra high vacuum of 10^{-9} torr. Substrates were heated to 1200°C, for 30 minutes heat treatment, prior to the CdSe deposition. Then the substrates were cooled to deposition temperature. Films were deposited in the range of substrate temperatures from 180°C to 250°C. The degree of orientation was found to be

dependent on the rate of deposition. A deposition rate of 3Å /sec gave fully epitaxial CdSe films, the substrate temperature being 210°C. CdSe films were found to be disoriented, when the deposition rate was 25Å /sec, the substrate temperature being 250°C.

Epitaxial CdSe single crystal films of about 1.8 cm diameter, were grown on freshely cleaved mica by Brunnschwiler (1966). The growth of the CdSe film took place in two stages. In the first stage the substrate temperature was held steady at 200°C so that initial nucleation would take place. Evaporation was continued until the film reflectivity was increased by about 20 per cent. The evaporation was interrupted and the substrate temperature was raised to 400°C, and then the evaporation was completed. Transmission electron diffraction patterns obtained from the films showed that the whole area of the CdSe film was single crystal.

CdSe was evaporated on to step-free and step-rich air-cleaved NaCl substrates by Yukio Yasuda (1968). The substrate temperature at which oriented overgrowth occurred was found to be about 130°C lower on step-rich areas than on step-free areas of the cleavage surface. The films grown on (001) faces were characterised by the presence of twinned cubic and hexagonal structures. The CdSe films grown on (111) faces of NaCl at temperatures from 20°C to 100°C had polycrystalline structures with both hexagonal and cubic phases present. Films grown at substrate temperatures from

200°C to 320°C had mixed cubic and hexagonal structures, whereas the CdSe films grown at temperatures from 330°C to 370°C had the hexagonal wurtzite structure.

Yim and Stofko (1974) deposited CdSe on (0001) faces of sapphire and cadmium sulphide by a chemical vapour deposition method. CdSe was found to grow with the wurtzite structure on (0001) faces of sapphire and on (0001) and (000$\bar{1}$) faces of cadmium sulphide. The epitaxial growth range of temperatures was 550° to 750°C.

Manasevit and Simpson (1971) studied the epitaxy of II-VI compounds by an oraganometallic chemical vapour deposition process. They showed that CdSe films grown on (0001) Al_2O_3 (sapphire) at 600°C had the hexagonal wurtzite structure.

2.4 REVIEW OF THE EPITAXIAL GROWTH OF II-VI COMPOUNDS

Holt (1966a) evaporated ZnTe on to freshly cleaved surfaces of CaF_2, BaF_2, NaF, NaCl and LiF in vacuum. The substrate temperature was varied in each case and the other experimental parameters were held constant. Films were examined by transmission electron microscopy. He found that the grain sizes of the films increased monotonically with substrate temperature, but in the case of ZnTe/NaF films the size remained constant. Secondly, as the substrate temperature rose the structures changed from randomly oriented polycrystalline films, through fibre structures and a series of mixed structures to well oriented epitaxial films, but just

before the ZnTe ceased to deposit the films of ZnTe reverted to a randomly oriented polycrystalline structure. Film structure irreproducibility occurred in the cases of NaF, NaCl and LiF substrates even at the optimum substrate temperature.

Woodcock and Holt (1969) deposited ZnS on NaCl by evaporation in an ultra high vacuum. They studied the influence of the growth conditions on the structure of the films. They found that the most important single parameter in producing the widest range of epitaxial substrate temperatures and the most perfect films was the use of a focussed electron beam evaporator. Contamination raised the minimum substrate temperature for epitaxial growth and also resulted in the incorporation of doubly positioned wurtzite structure grains in the sphalerite structure films. Co-evaporation of either Zn or S with ZnS produced sphalerite structure films containing singly positioned wurtzite grains.

Holt and Woodcock (1970) studied the defect structures of epitaxial films of ZnS grown on vacuum cleaved NaCl in an ultra high vacuum. The ZnS films were found to be free from both microtwins and included grains of wurtzite material. However the diffraction patterns were streaked in <111> directions due to planar defects. These planar defects did not disappear when the films were annealed in vacuum or in H_2S.

Wilcox and Holt (1969) deposited CdS films on the (100) cleavage faces and cut and polished (110) and (111) faces of

NaCl and also on the (111) cleavage faces of BaF_2 in vacuum. They studied the effect of substrate orientation on the structure of the epitaxial films. The CdS films grown on the (111) faces of these substrates had the hexagonal wurtzite structure with great structural perfection. They grew epitaxially over a wide range of substrate temperatures. The films of CdS grown on (100) and (110) faces of NaCl substrates had the cubic sphalerite structure. These films were found to be free from included grains.

CdS epitaxial films were grown on (100), (110) and (111) faces of Ge in vacuum by Abdalla et al (1973). Films grown on the (111) faces of Ge had the hexagonal wurtzite structure with high structural perfection. Films grown on the (100) faces of Ge had the cubic sphalerite structure. These films contained a high density of {111} planar defects. CdS films grown on the (110) faces of Ge, below $370^{o}C$, had the cubic sphalerite structure and the films grown above $370^{o}C$ had the domain-form transformed structure.

Mufti and Holt (1972) grew ZnTe epitaxial films on the (100) and (111) faces of Ge in vacuum. These ZnTe films had the cubic sphalerite structure. ZnTe films grown on (111) faces of Ge in the upper epitaxial range of temperatures were found to contain twins.

Abdalla and Holt (1973) evaporated CdTe films onto the (100), (110) and (111) faces of Ge. On the (111) faces of Ge the films had the hexagonal wurtzite structure with high

structural perfection. Films grown on (100) faces of Ge had the cubic sphalerite structure and these films contained a high density of {111} planar defects. CdTe grown on (110) faces of Ge had the cubic sphalerite structure and these contained the domain-form transformed structure.

Holt and Abdalla (1974) evaporated CdTe films on to (111) faces of Si in high vacuum. They found that CdTe could be grown epitaxially on Si. The CdTe films had the hexagonal wurtzite structure with high structural perfection.

2.5 NUCLEATION AND GROWTH OF EPITAXIAL FILMS

According to nucleation theory (by Walton 1962a,b, Hirth and Pound 1963, Halpern 1967, Lewis and Campbell 1967) evaporated atoms arrive at the substrate surface in the form of isolated atoms. These atoms will prefer to reside at positions of minimum energy, namely at atomic sites. When there is an appreciable number of adsorbed atoms on the substrate surface, those which collide (interact) can become temporarily bound together. As soon as a cluster of atoms reaches a certain critical size it becomes stable. These critical clusters or nuclei contain a small number of atoms. This seems to be below 10 atoms (Walton 1962a,b, Walton et al. 1963 and Yang et al. 1954). Growth then proceeds from these centres. These nuclei grow further in size until they coalesce and the film becomes continuous.

Without going deeply into the nucleation theory and becoming committed to any particular model the three epitaxial

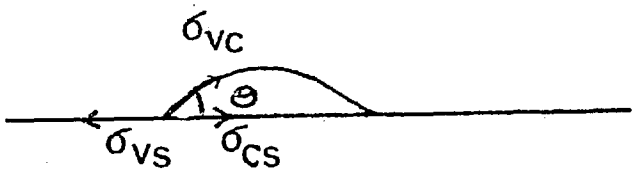


Fig. 2.1 The contact angle of a spherical cap-shaped nucleus is determined by the equilibrium between the surface tensions σ_{VS} of the vapour-substrate surface, σ_{VC} of of the vapour-condensate surface and σ_{CS} of the condensate-substrate interface.

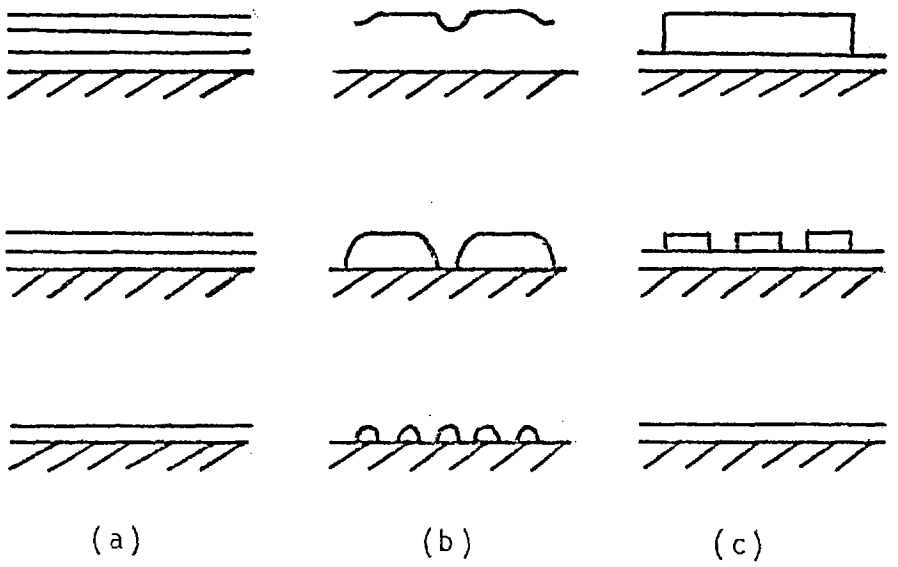


Fig. 2.2 Three modes of epitaxial growth: (a) layer-by-layer growth; (b) formation and growth from discrete nuclei; (c) initial formation of a tightly bound layer (or layers) followed by nucleation and growth.

growth processes (a) layer-by-layer growth, (b) formation and growth from discrete nuclei or (c) initial formation of a tightly bound layer followed by nucleation and growth which have been discussed in the literature (Bauer, 1958) could be understood as follows:

The mode of nucleation and initial growth of epitaxial films is governed strongly by the bonding between deposit and substrate (Stowell 1975). Consider such a cap-shaped hemispherical nucleus as shown in fig. 2.1. For equilibrium contact angle θ, $\sigma_{VS} = \sigma_{CS} + \sigma_{VC} \cos \theta$ (Hirth and Pound 1963), where σ_{VS}, σ_{VC} and σ_{CS} are the surface tensions of the vapour-substrate surface, vapour-condensate surface and condensate-substrate interface respectively.

The deposit "wets" the substrate surface when $\theta = 0$. That is $\sigma_{VS} = \sigma_{CS} + \sigma_{VC}$. In this case it is to be expected that growth will occur in layer-by-layer manner (fig. 2.2a; Frank and Van der Merve 1949, Van der Merve 1950, 1973, and 1974). $\sigma_{CS} = 0$ is the condition for ideal auto-epitaxy. When $\sigma_{CS} + \sigma_{VC} > \sigma_{VS}$, θ is finite and the deposit forms by nucleation of discrete particles that grow three dimensionally (Fig. 2.2b) and eventually agglomerate into a continuous film. As θ

increases, the bonding between substrate and deposit becomes progressively weaker than the cohesive binding in the deposit particles. The third case corresponds to $\sigma_{CS} + \sigma_{VC} < \sigma_{VS}$. In this case the deposit-substrate binding is stronger than that within the deposit. This means, initially the deposit grows as strongly bound layers on top of which discrete nuclei may form at a latter stage as shown in Fig. 2.2c. This account gives general classification which indicates at least qualitatively the dependence of the initial stages of thin film growth on binding forces.

In all these three cases, it is possible for the initial deposit to be elastically strained to match the substrate lattice. This is referred to as "pseudomorphic" growth , (Matthews, 1961, 1963, 1964, 1966, 1967; Jesser and Matthews 1967, 1968, 1969; Matthews and Jesser 1967; Yagi et al. 1971.). The predominant condition for this to occur is that the strain necessary to ensure coherency at the substrate-deposit interface should be small ($\lesssim$ 12%). Initially the overgrowth is strained elastically, but as the overgrowth thickens the strain energy exceeds that at which it is energetically favourable to introduce misfit dislocations at the interface, thereby loosing coherency. The defect content and crystallography of the substrate play an important part in determining the types of misfit dislocations that are generated (see for details the above references). This summarises the layer-by-layer mode of growth.

It has been pointed out above that the nucleation mode of thin film formation occurs in the moderate to weak condensate-substrate binding situation ($\theta>0$). In this case the deposited atoms (or molecules) are initially equilibrated thermally with the substrate. They diffuse and interact to form polyatomic clusters (nuclei). The nuclei continue to grow. Because of their nonuniform spatial distribution on the substrate, they grow together and agglomerate. Such deposit-substrate systems have been studied in detail with the aid of in situ transmission electron microscopy (Pashley et al., 1964; Basset, 1964; Pocza, 1967; Cooper-smith et al., 1966; Sato et al., 1969; Yagi et al., 1969; Stowell, 1972.). Agglomerating deposit islands can change shape in a way that has been referred to as "liquidlike" (Basset 1960; Pashley and Stowell 1962). This description was given because of the similarity of this process to that of the running together of liquid droplets. A neck is formed between the two coalescing islands. Then the necks are thickened as the two coalescing islands grow together. Analysis of the rates at which the necks between the coalescing islands are filled in has shown this to be due to mass transfer by surface self-diffusion of the deposit atoms (Pashley et al., 1964; Pashley and Stowell, 1966; Stowell, 1969). As the size of the islands increases, the deposit takes on a lace-like appearance with long narrow channels of deposit-free substrate. The channels and holes later fill in to give a complete film.

There is no evidence known to the author that thin films have grown according to the third mode of growth.

2.6 MISFIT AND MISFIT DISLOCATIONS

A misfit will exist at an interface where two perfect single crystals of different materials with different lattice parameters meet. Since the two materials have different lattice parameters in any crystallographic direction, a disregistry exists. The term "misfit" therefore refers to the natural disregistry of the atoms in the two atomic planes which define the interface. If a and b are lattice parameters of the two crystals on either side of the interface then the misfit is given by $\delta = \frac{a-b}{\frac{a+b}{2}}$. This is the natural way of expressing the misfit; the ratio of the difference in lattice parameters to the average of the lattices of the two crystals defining the interface. Generally the misfit is expressed in percentage. The expression can also be deduced as follows (Brooks 1952): Let the two lattice parameters of the two cubic system crystals in parallel alignment be represented by

$$a = c(1 + \frac{\delta}{2})$$

$$b = c(1 - \frac{\delta}{2})$$

where δ is a small fraction and c may be described as the lattice parameter of the reference lattice.

$$\therefore \quad \frac{a}{b} = \frac{2 + \delta}{2 - \delta}$$

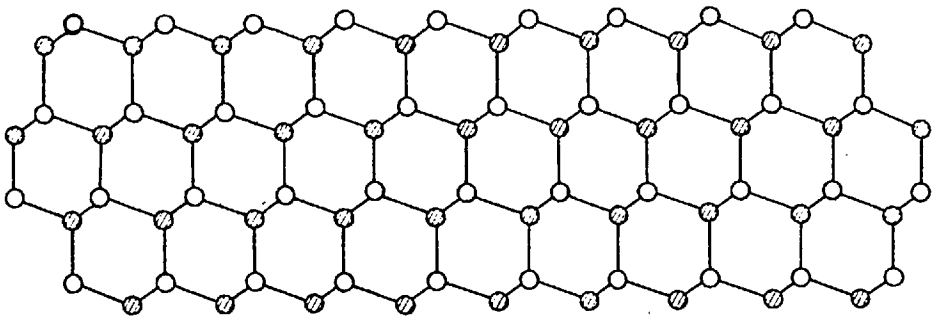
$$\text{i.e.} \qquad \delta = \frac{a - b}{\frac{a + b}{2}}$$

Generally the single crystal substrate is thick and the epitaxial layer grown on it is a thin film in comparison. Hence accommodation of the misfit at the interface can be explained as follows: In the previous section three modes of initial nucleation and growth of epitaxial films have been considered. In these cases (Stowell 1975) the initial growth was found to be pseudomorphic, in the sense that the initial deposit was experimentally found to be elastically strained to match the substrate. This shows that in the initial growth stage, the misfit between the deposit and the substrate is accommodated by elastic strain. As the overgrowth thickens, the strain energy exceeds that at which it becomes energetically favorable to introduce misfit dislocations at the interface, thereby loosing complete coherency. Hence the misfit is accommodated by the generation of misfit dislocations at the interface. Without committing to any model, Figs. 2.3 and 2.4 show how the misfit at the interface is accommodated by the generation of misfit dislocations as the film thickens. From the figures it is evident that $p = na = (n+1)b$;

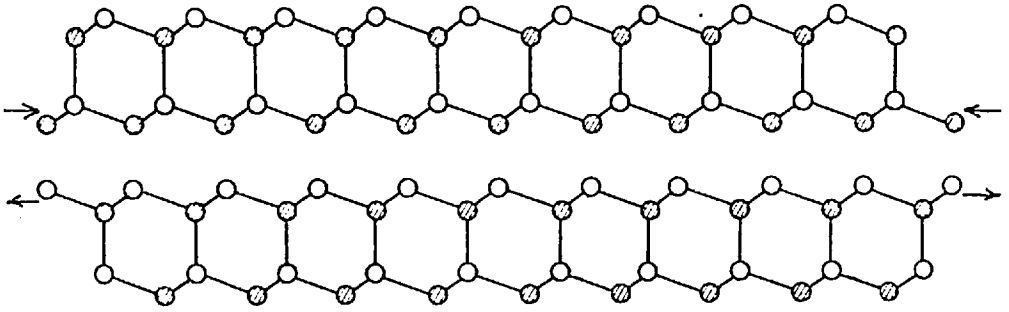
where p is the misfit dislocation spacing, n is any integer and a and b are the lattice repeat distances in the two crystals along a single crystallographic direction.

$$na = (n+1)b \quad \text{i.e.} \quad n = \frac{b}{a-b}$$

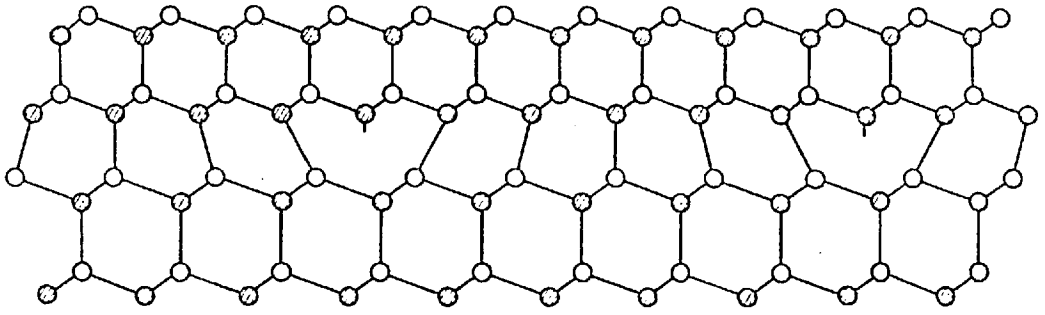
$$\therefore \qquad p = \frac{ab}{a-b} \quad \text{(Van der Merwe 1964 and Holt 1966b)}$$



(a)



(b)



(c)

Fig. 2.3 This ball-and-wire model, is considered to be produced by cutting a crystal along the (111) plane and increasin the lattice parameter on one side and decreasing it on the other to the values of the two materials concerned as shown in (a) and (b). The figure (c) illustrates the junction on (111) plane of misfitting sphalerite structures showing the misfit dislocations, for the case in which p = 5a = (5+1)b. A dangling bond occurring at a spacing p marks the positions of successive misfit dislocations (After Holt 1966b).

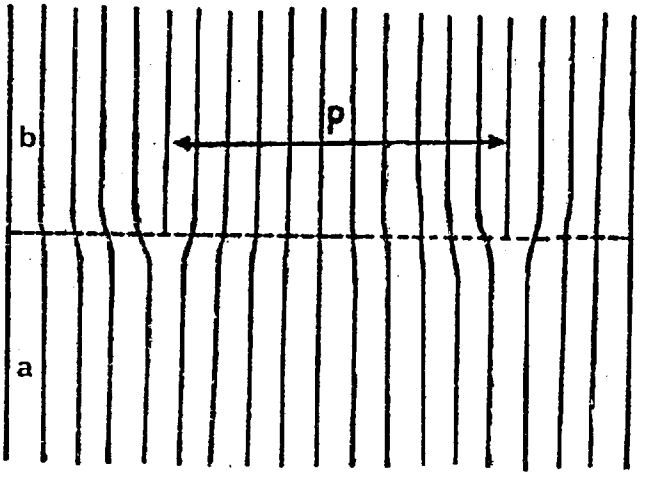


Fig. 2.4 Illustration of the dislocation concept of a misfitting interface.

One of the important features that the two figures exhibit is that after the coherency break down, the interface is divided into regions of good register separated from one another by regions where register is bad. The regions of bad register or bad fit resemble crystal dislocations and because of this, these are called interfacial or misfit dislocations. And these will be regularly spaced according to the above formula. It is to be noted that the generation of misfit dislocation occurs in the crystal of smaller lattice parameter. The dislocations shown in the figures are edge type dislocations.

Matthews (1961) observed edge type misfit dislocations in $PbSe/PbS_{(100)}$ parallel epitaxial bicrystal systems. It was found that 96% of the misfit was accommodated by the misfit dislocations and only 4% by elastic strain. The spacing of the dislocations was found to be according to the prediction of the above formula.

The dislocations shown in fig. 2.4 resembled those envisaged by Frank and Van der Merwe (1949) in that they were in edge orientation and had Burgers vectors parallel to the interface plane. Similar misfit dislocations in edge orientation and with Burgers vectors parallel to the interface have been observed in epitaxial combination of lead selenide on lead sulphide (Matthews, 1961, 1971; Yagi et al., 1971), in copper on nickel (Matthews and Crawford, 1970) in gold on palladium (Matthews 1964, 1966) and palladium on gold (Cherns and Stowell, 1973).

In our present work we have observed misfit dislocations which probably have their Burgers vectors parallel to the interface plane; but these seem to be of mixed edge and screw type. The edge component seems to accommodate the dilatational misfit whereas the screw component seems to be responsible for the observed rotation of the film through 2^{o} 24' relative to the substrate (section 4.4.4). This type of misfit dislocation occurrence in heterojunctions is the first of its kind to be reported in research on epitaxial heterojunctions of II-VI compounds/IV elements.

2.7 ANNEALING OF II-VI EPITAXIAL FILMS

Annealing has many effects on as-grown epitaxial films of II-VI compounds.

Newbury and Kirk (1974) investigated the effects of annealing on ZnSe grown on (100) surfaces of Ge. ZnSe epitaxial films were grown at a Ge substrate temperature of 430^{o}C. The transmission electron diffraction patterns of the ZnSe films were found to contain strong <111> streaks, due to a high density (more than $10^{13}/cm^{2}$) of planar defects, and satellite spots due to twins. The ZnSe/Ge heterojunctions were placed in quartz ampoules together with small lumps of ZnSe. Then the ampoules were evacuated and sealed. These were annealed at 900^{o}C for 2 hours. The transmission electron diffraction patterns of these annealed films were found to be free from <111> streaks, and twin satellite spots. Sharply

defined kickuchi patterns were found to be present due to the high structural perfection of the films. The stacking faults and dislocations in the micrographs were well resolved and stacking fault density was estimated to be of the order of $10^7/cm^2$. This showed that the structural quality of the films was high and that the defect density was reduced considerably on annealing.

Holt and Abdalla (1975) studied the annealing effect at relatively low temperatures on CdTe epitaxial films grown on (100) and (111) faces of Ge. The diffraction patterns of as-grown (100) CdTe films were streaked in the <111> directions, indicating the presence of high densities of {111} planar defects. These films were annealed at 400°C for 6 to 9 hours. The diffraction patterns of the annealed films contained no <111> streaks, showing that the {111} planar defects were reduced substantially. Moreover kickuchi bands appeared as a result presumably of a decrease in the point defect density in the material. (0001) oriented CdTe films grown at 370°C on (111) Ge substrates, did not show any structural changes on annealing at 440°C for 6 hours. However the moire fringes in the (0001) CdTe/Ge (111) heterojunctions disappeared after annealing, and widely spaced lines were observed. Following Vermaak and Van der Merwe (1964), they interpreted these as interdiffusion misfit dislocations.

In the present work CdSe films grown on (110) faces of Ge were annealed. As-grown CdSe films on (110) faces of

Ge were found to contain the domain-form transformed structure (Section 4.3). Films grown at 380°C, were annealed at 500°C for 50 minutes. It was found that the characteristic domains disappeared because the faults were annealed out, leaving behind domain boundaries (Chapter V). These domain boundaries were found to be antiphase boundaries (Holt et al 1976). This is the first time that antiphase domain boundaries were shown to occur in II-VI epitaxial films.

Wilcox and Holt (1976) investigated the Lath-form transformed structure in (110) CdS films annealed at 450°C for 30 minutes. The films were originally grown on (110) NaCl substrates at 300°C. These were removed from the substrates and transmission electron diffraction studies showed them to be in the (110) orientation with the sphalerite structure and to be free of second phase grain and twins. Some of these films were annealed while supported on coarse 100 mesh gold grids. These films were found to have the domain-form structure. When similar films were annealed while supported on fine 400 mesh gold grids, the Lath-form transformed structure was found in the films. The lath-form tranformed structure gave transmission electron diffraction pattern which indicated that the unit cell height in the transformed laths was twice the height of the original sphalerite structure unit cell. This they attributed to an ordered structure involving one or more point defects per two sphalerite structure unit cells.

CHAPTER III

EXPERIMENTAL APPARATUS AND PROCEDURE FOR GROWING EPITAXIAL FILMS

3.1 APPARATUS

3.1.1 The Vacuum Systems

A schematic diagram of the vacuum system used in this experiment is shown in Fig. 3.1. The vacuum system consisted of an evaporation chamber; that is a 12" bell jar placed on a steel base plate. This evaporation chamber was evacuated to high vacuum in the range between 10^{-5} to 10^{-6} torr by an Edwards 2" diffusion pump model E02, backed by an Edwards rotary oil pump model ES75 with a capacity of 82 litres per minute. A liquid nitrogen trap was fixed to the diffusion pump. It was always filled with liquid nitrogen during experiments for growing CdSe films by evaporation on to Ge substrates. The pumping speed of the diffusion pump was 75 litres per second using a silicone oil of type M.S.704. The pressure in the chamber was measured using a BIRVAC penning gauge model T1001. The vacuum system was provided with an air-admittance valve to let air into the chamber. The vacuum system was also provided with a baffle valve between the vacuum chamber and the diffusion pump to isolate the diffusion pump from the vacuum chamber when the chamber was let up to atmospheric pressure.

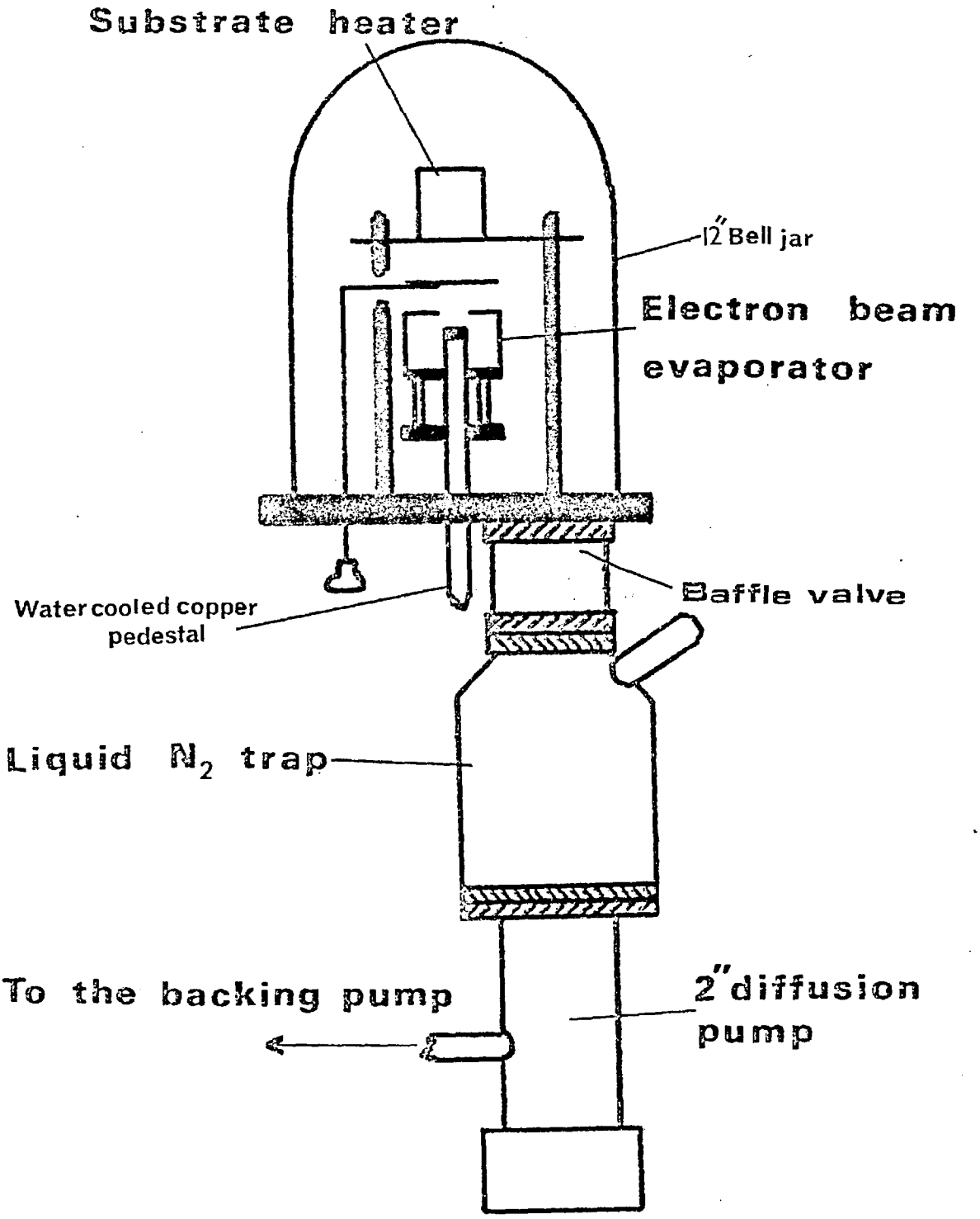


Fig. 3.1 The Vacuum System

3.1.2 The Electron Beam Evaporator

The source material, CdSe, was evaporated by heating it, using a focussed electron beam evaporator of the type developed by Unvala (1963). The electron beam evaporator assembly is shown in Fig. 3.2. In this method of evaporation of the source material both the source material and substrate were out of line of sight of the tungsten filament.

The source CdSe was contained in a stainless steel crucible held in a water cooled copper pedestal which was surrounded by the tungsten filament and a focussing electrode. This assembly was so constructed that it was possible to focus the electron beam spot on the source material surface at its centre, well away from the walls of the crucible and not producing any heating effect on the walls of the crucible. This minimised the contamination arising from crucible wall heating. The focussing electrode was made of wire mesh. The focussing electrode and the tungsten filament holder were mounted on a stage of three insulating pillars which could be moved up and down by a lever arrangement. During the evaporation of CdSe the height of the focussing electrode was always adjusted to produce a hot spot of about 2mm diameter for the required input power. This standardized the growth rate of the epitaxial CdSe. The power input to the source was determined by the product of emission current and the accelerating voltage. The input power could be varied either by changing the emmission current or the accelerating voltage. In the case of CdSe, adjustment of both simultaneously was found to be more practicable.

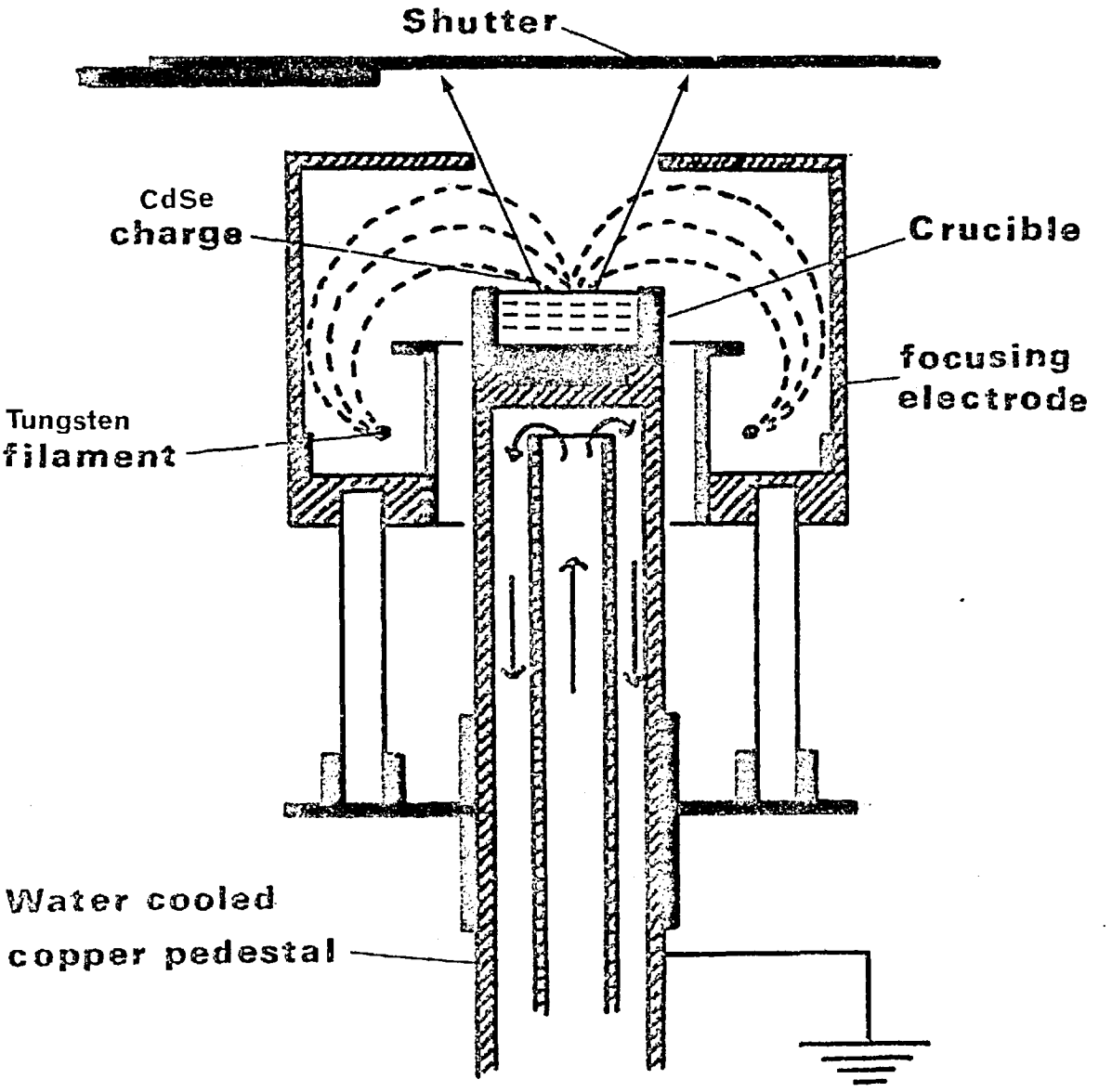


Fig. 3.2 The Electron Beam Evaporator

A shutter was provided between the evaporator and the substrate heater. The shutter was kept closed during the outgassing of the CdSe to keep away the outgassed vapour from the substrate. This also prevented the contamination of the source during the thermal cleaning of the substrate and the substrate heater assembly. The shutter was moved to one side to let the CdSe vapour deposit on the substrate for a required length of film-growing time and then closed.

3.1.3 The Substrate Holder and Heater Assembly

The substrate heater assembly is shown in Fig. 3.3. It consisted of a tantalum heater coil, molybdenum inner heat **shield** , molybdenum outer heat shield, and molybdenum substrate holder. The substrate heater assembly was mounted on a circular stainless steel insulated base plate, with a central hole to let the CdSe vapour deposit on the substrate. The substrate holder was mounted by means of two stainless steel screw rods which were fixed rigidly to the base plate and insulated from it. The substrate holder was provided with two or four holes to hold substrates of 3 mm diameter. The substrates were heated by the radiation from the tantalum heater coil which was provided with a power supply with a voltage variable upto 25 volts. The substrate holder with substrates was screened from the heated tantalum coil by inner heat **shield** . The outer heat shield prevented the radiation from the heater coil from radiating out. This arrangement provided approximately black body conditions

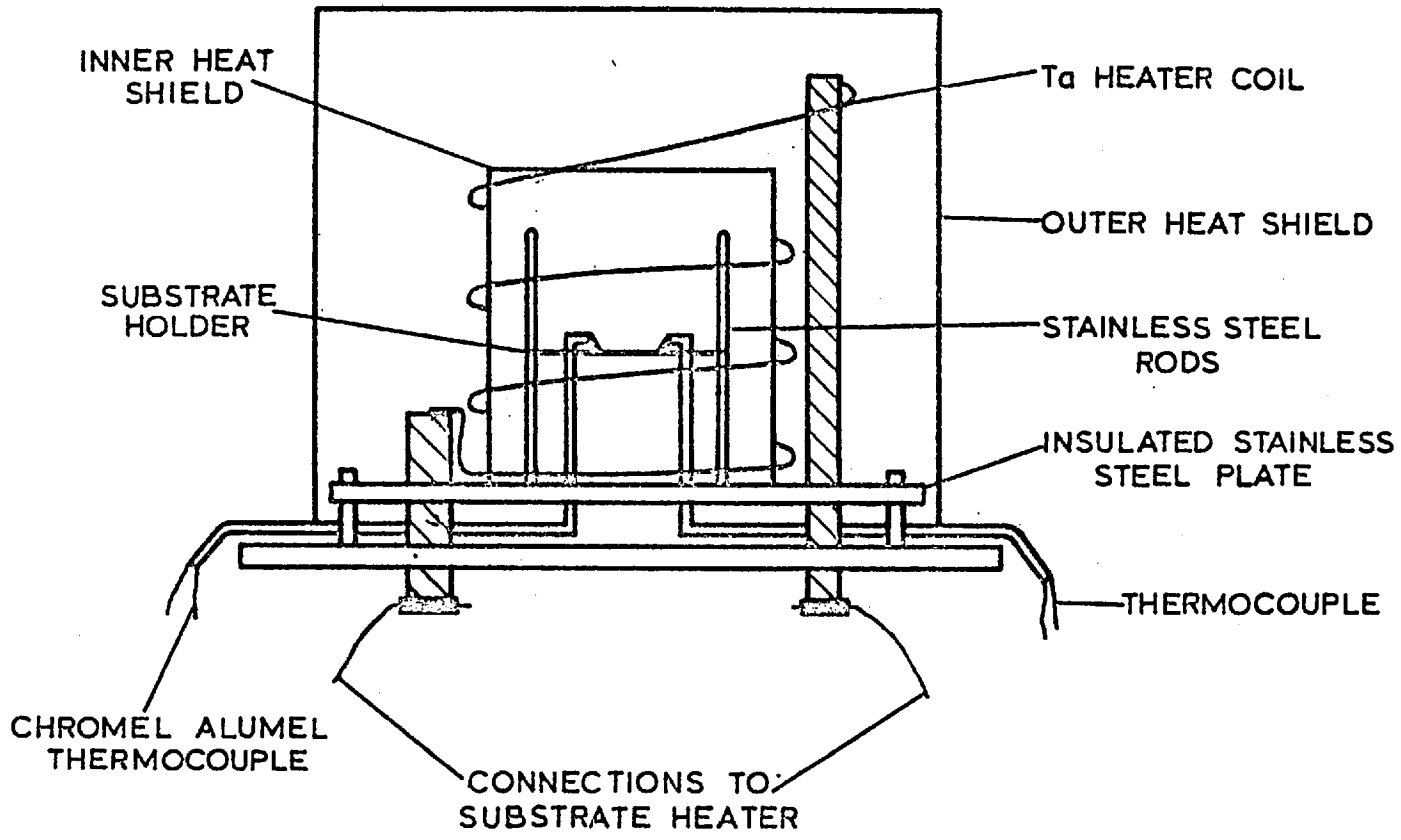


Fig. 3.3 The Substrate Heater Assembly

inside the heater so that uniform distribution of temperature in the substrate holder region could be attained rapidly. The substrate temperature was measured using two chromel-alumel thermocouples placed beneath the substrate. These thermocouples were led into the substrate heater region by means of silica tubing.

With this arrangement it was possible to raise the temperature upto 900^{o}C for the thermal cleaning of the substrate holder and heater assembly in vacuum. This was found to be essential to outgas the substrate heater assembly between successive growth runs. This prevented the danger of contamination of the substrate surface by materials deposited in the previous evaporations. It was one of the important conditions for the reproducible growth of good quality epitaxial films in this work. The effect of contamination has been dealt with in section 2.1.4. The height of the substrate holder above the surface of CdSe was kept constant at about 7 cms. Changing the tantalum heater coil to a tungsten heater coil had no effect on the reproducibility or quality of epitaxial films in this work.

3.2 PREPARATION OF Ge SUBSTRATES

As a result of previous work in this laboratory it was known that the quality of the polished substrate surface had a great effect on the degree of epitaxy. Hence efforts were made to prepare flat, smooth and scratch-and etch-pit-free

substrate surfaces by carefully polishing them first mechanically and then chemically.

Germanium substrates in the form of circular slices 2 cms in diameter and 0.5 mm thick or in the form of oval shaped slices 0.4 mm thick were obtained from the electronics materials unit of the Royal Radar Establishment. These single crystal Ge slices were already cut parallel to the (111), (110) or (100) planes and were p-type.

The slices were mechanically polished on a rotating wheel polisher using silicon carbide to remove the initial damaged surface of Ge. The depth of damage of the germanium surfaces was further reduced by additional polishing using 2 μm diameter alumina powder. Ge slices were cleaned carefully with distilled water first and then trichloroethylene to remove any traces of the silicon carbide or alumina. Further polishing on 1 μm diamond paste reduced the depth of damage to about 1 μm and gave a mirror like surface. Then the slices were cleaned in trichloroethylene and in distilled water and finally in an ultrasonic bath.

The Ge slices were mounted on a glass slide using picene wax so that the polished surface was dipped in the wax. They were ultrasonically cut into discs of 3 mm diameter to fit into the AEI EM6G (100kV),Philips Em301(100kV) and AEI EM7 (1000kV) transmission electron microscope specimen holders. The Ge discs were separated from the picene wax by dipping the glass slides in boiling trichloroethylene. The separated discs were washed successively in fresh trichloroethylene

a number of times to ensure that all traces of wax were completely removed. Finally they were rinsed in distilled water and then in methyl alcohol.

The damaged layer left by the mechanical polishing process on the surfaces of the discs was removed by chemical polishing. The chemical polishing solution consisted of

50 cc of 70% nitric acid
30 cc of 99% glacial acetic acid
30 cc of 40% hydrofluoric acid

and a drop of 79.92% bromine.

The solution was heated to about $60^{o}C$ in a PTFE beaker. The discs were dropped into the solution and the beaker was gently shaken for about 45 seconds. The discs were immediately removed from the solution and held under a stream of distilled water for about 10 minutes to ensure that the chemical solution was washed away. Finally the discs were rinsed in methyl alcohol. The polished surface of the Ge discs were examined under a travelling microscope to check their suitability for film growth.

A very interesting effect of the nature of the substrate surface was found in this work. The (100), (110) and (111) oriented Ge substrates were prepared by this same method. The (110) surfaces were found to be free from etch-pits, scratches or other roughness in the sense that these could not be seen in the low power microscope. On the other hand

(100) and (111) surfaces did contain etch pits which could be detected in the low power microscope. As a result it was found that the minimum epitaxial growth temperature for (110) Ge surfaces was lower by 50^{o}C than for (100) and (111) Ge surfaces. Since all the other growth conditions were the same, this can be attributed to the differences in the smoothness of the surfaces of the substrates at different orientations.

3.3 PREPARATION OF CdSe EPITAXIAL FILMS

The CdSe used in this work was supplied by Koch-light Laboratories and stated by them to be of 99.999% purity. The CdSe was in the form of a fine powder. It was loaded into the stainless steel crucible. The Ge substrates after polishing were placed in the grooves of the substrate holder with their polished surfaces down facing the CdSe source.

The vacuum chamber was pumped down to 2 x 10^{-6} torr. When a pressure of about 2 x 10^{-6} torr was attained the source CdSe was outgassed. This was done by switching on the emission current and accelerating voltage and then defocussing the electron beam furnace so that whole volume of CdSe charge was heated. Completion of this process could be detected by monitoring the pressure in the vacuum chamber. The emission current and accelerating voltage were switched off. Immediately the substrate heater current was switched on to 15 amps and the substrate was heated to 600^{o}C for thermal cleaning of the substrate surface and also to outgas the

heater assembly. The substrate heater current was immediately reduced to zero to allow the substrate to cool down to the deposition temperature. As the substrate cooled down from 600^{o}C, the emission current and accelerating voltage of the source were switched on to required power for evaporation. The electron beam furnace was raised so that the electron beam was well focussed on the CdSe surface giving a hot spot of about 2 mm diameter at the centre.

When this adjustment was complete power was reduced to a minimum to keep the source warm until it was to be evaporated for film growth. When the substrate temperature fell to the deposition temperature this was maintained constant. The input power to the source was raised to the required value for evaporation and the shutter was moved to one side. The deposition time was 1½ minutes. The substrate temperature was monitored during the deposition by the alumel-chromel thermocouples. After 1½ minutes the shutter was closed and the power supplies were switched off. During deposition the pressure was below 10^{-5} torr. Specimens were removed from the chamber when they had cooled down below 50^{o}C for electrochemical thinning of the Ge substrates.

With the same growth procedure films were grown for different times of deposition to get films of different thicknesses. For chemical etching the films were grown from 3 - 5 minutes, and for electrical measurement films were grown for 15 - 20 minutes on 5 mm diameter substrates. In all these cases the films were found to be reproducibly epitaxial.

3.4 THE SUBSTRATE THINNING PROCESS

After the CdSe film deposition the Ge substrates were to be thinned. The process of thinning the germanium involved the removal of a portion of the germanium as far as possible completely from the CdSe film, so that the exposed portion of the film could be examined under transmission electron microscopy for its structural properties.

The apparatus used for thinning the germanium was of the type developed by Blankenbergs and Wheeler (1963-64). A line diagram of the apparatus is shown in Fig. 3.4. Similar apparatus was used by Booker and Stickler (1962) and Wilcox and Holt (1970). The chemical solution used for thinning germanium consisted of 25 gm of KOH and 12 gm of NH_4Cl dissolved in 2000 cc of distilled water.

The germanium substrates were held firmly in the central hole of a copper disc fixed to specimen holder using lacomit solution. Lacomit was resistent to the thinning solution and light could not pass through into the specimen holder. The copper disc was covered with lacomit at all places where the jet-solution might reach. An area of substrate of about 2 mm diameter was always free from lacomit.

The chemical solution from a reservoir was allowed to flow through a perspex jet and through the 1 mm diameter stainless steel nozzle on the germanium substrate. A beam of light from an electric lamp was collimated through the transparent perspex jet and through a 1 mm diameter stainless steel nozzle on to the Ge substrate. During thinning

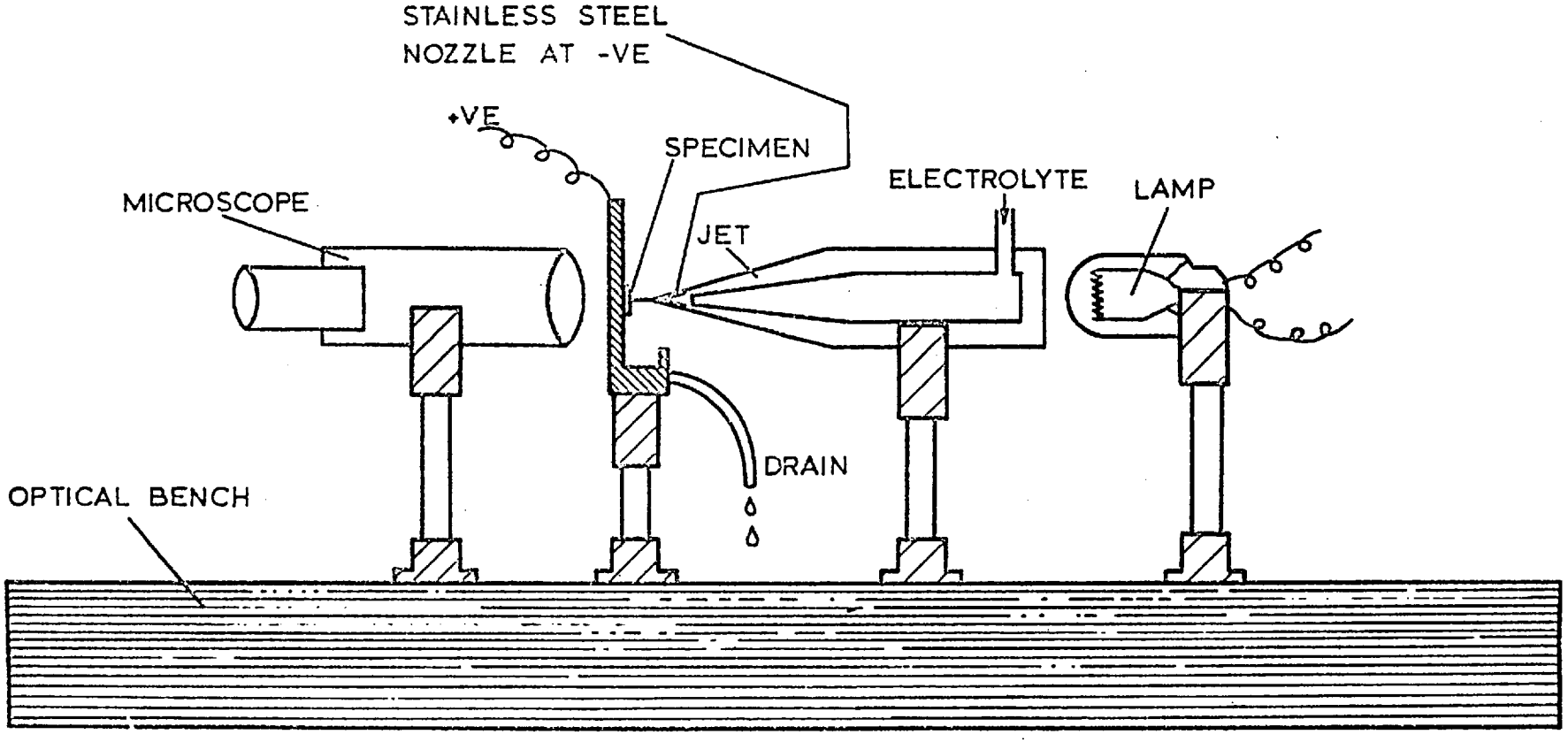


Fig. 3.4 The Electrochemical Jet-Thinner

germanium the stainless steel nozzle was held at a -ve potential and the copper disc at a +ve potential. The current drawn was 20 mA. The time in which Ge thinned through was about 8 minutes. Thinning through the germanium was evidenced by observing transmitted light in the travelling microscope (which was focussed on the film). The D.C. power supply and the flow of chemical solution were switched off simultaneously as soon as the transmitted light was observed in the travelling microscope. Otherwise the CdSe film could be broken due to the pressure exerted by the solution. With this strength of KOH solution a current of 14 to 20 mA was sufficient to polish the Ge side in the well defined polishing plateau (Hirsch et al. 1965).

3.5 MEASUREMENT OF CdSe FILM THICKNESS

CdSe film thickness was determined using a Nomarski interferometer on a "MeF" Reichert microscope. The Nomarski interferometer depends in its operation on the splitting of reflected light from the specimen by a Wollaston prism. Monochromatic light of wave length λ = 5890Å was used. It was incident normally on the CdSe film at the edge where there was a stepdown to the Ge substrate. The interference fringes had the form shown in Fig. 3.5. The straightness of interference fringes is evidence of the flatness of the CdSe film surfaces. The fringes are laterally displaced on crossing the edge by a distance which is a measure of the step height

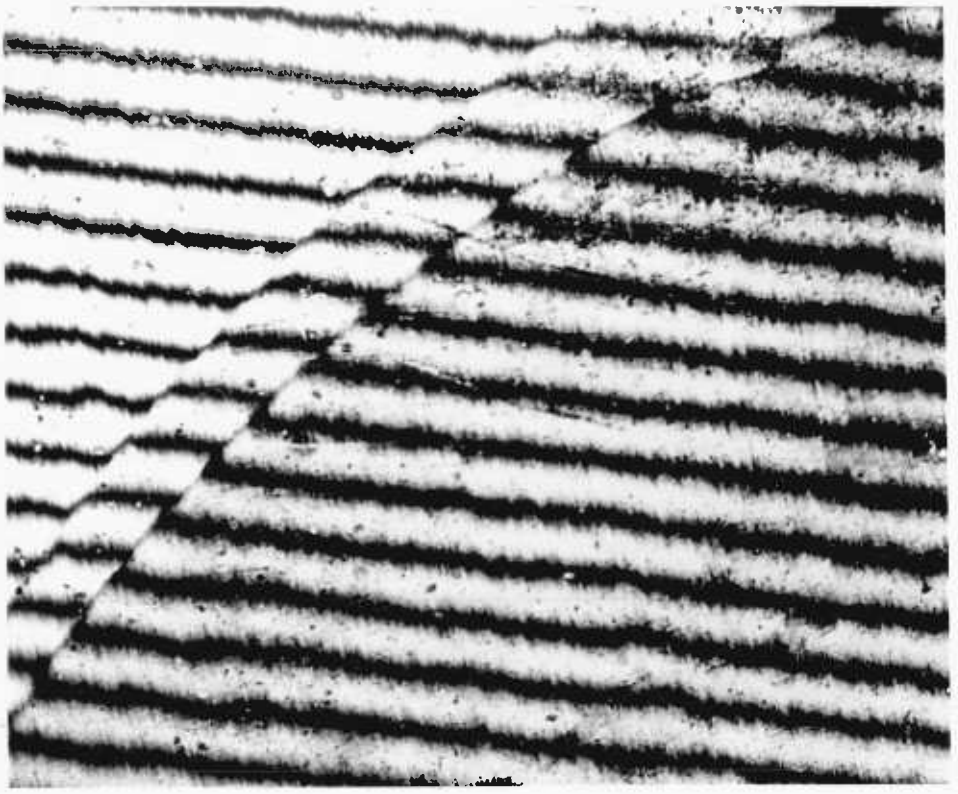


Fig. 3.5 Interferogram of a CdSe/Ge heterojunction taken near the edge of the CdSe film with a Nomarski Interferometry arrangement. The CdSe was grown on (111) Ge at 400°C for 1½ minutes.

of the CdSe film. The film thickness was calculated using the formula $t = \frac{\lambda}{2n}$, where λ is the wavelength of incident light and n is the ratio of the fringe spacing to the lat-eral shift of the fringe at the step. Thin film thickness measurement by the Nomarski interference method does not involve the refractive index of the material because the light producing the fringes does not penetrate into the film.

The film thicknesses as measured by the Nomarski interferometer method were found to be 1200Å to 2000Å, for films grown under conditions intended to produce approximately constant film thickness. The time of film growth was $1\frac{1}{2}$ minute. Hence the combined effect of any variations in evaporation rate and sticking co-efficient was a variation of only ± 25% in film thickness.

CHAPTER IV

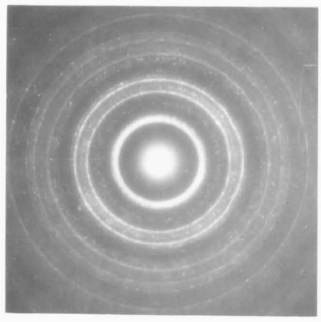
ANALYSIS OF THE EXPERIMENTAL RESULTS

4.1 EPITAXIAL GROWTH RANGES OF SUBSTRATE TEMPERATURE

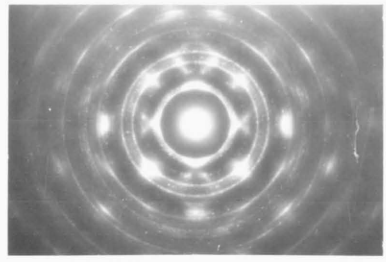
Films of CdSe were deposited in vacua in the 10^{-5} to 10^{-6} torr range, on Ge substrates with (100), (110) and (111) orientations. Attempts were made to grow CdSe films at Ge substrate temperatures from 200°C to 500°C. The experimental results were represented by a graph of the R-parameter versus substrate temperature ($T^{o}c$), as shown in figs. 4.1, 4.2, 4.3. The R-parameter stands for the degree of relative orientation of the films. This was introduced by Ino et al (1964) in studies of epitaxy of metal films and by Holt (1966a) in studies of epitaxy of ZnTe on ionic substrates.

The degree of relative orientation was determined from the selected area transmission electron diffraction patterns of the CdSe films, obtained from the AEI EM6G, 100 kV, transmission electron microscope. For example Fig. 4 shows observations of diffraction patterns of CdSe films grown on (100) faces of Ge, to show the variation in relative degree of orientation or structure with substrate temperature.

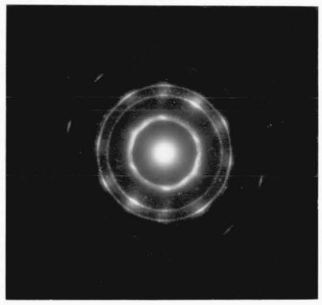
The value R = 100 was assigned to the epitaxial films, giving rise to spot diffraction patterns. This showed that in certain ranges of growth substrate temperature the CdSe films grew in a single orientation relationship with the substrate.



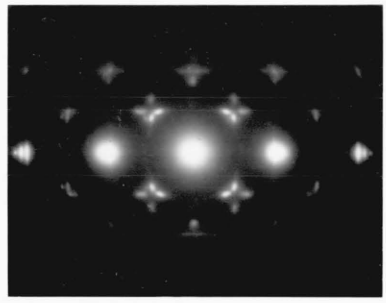
R = 0
T = 270°C



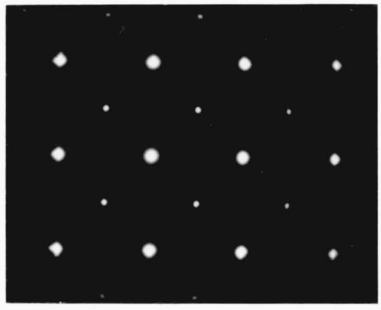
R = 50
T = 320°C



R = 25
T = 300°C



R = 75
T = 330°C



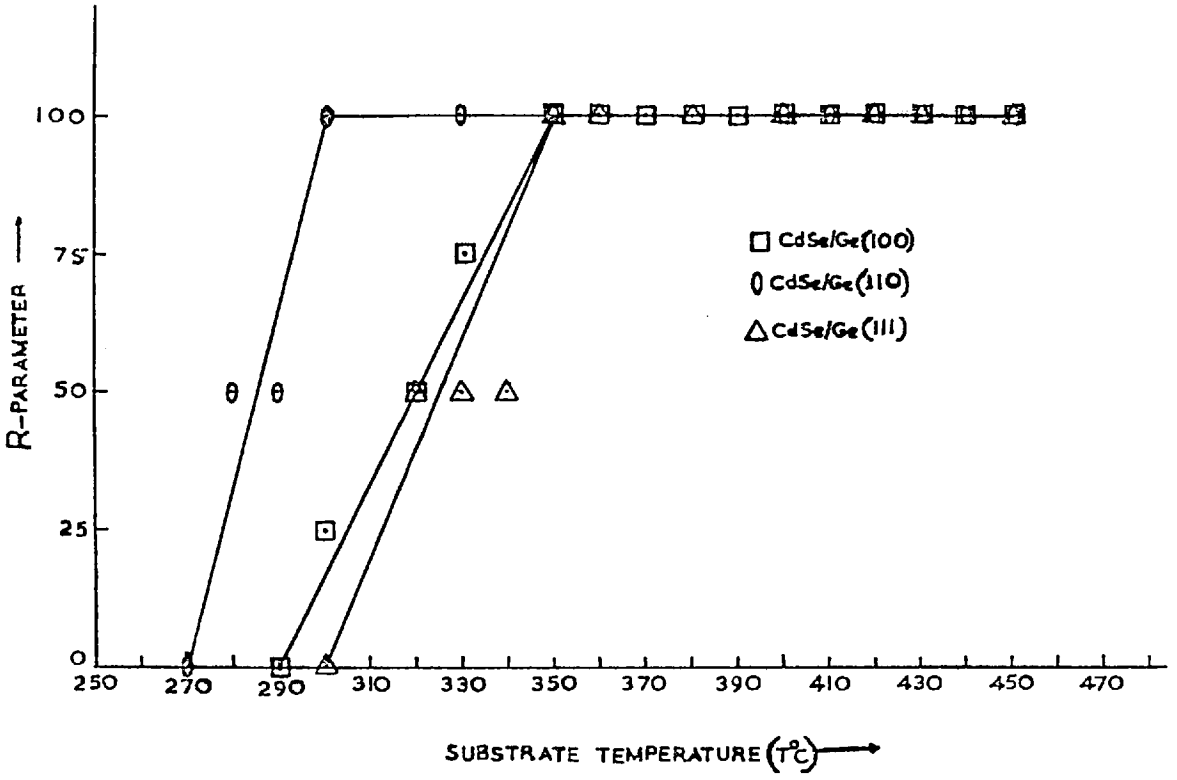
R = 100
T = 370°C

Fig. 4 THE FIVE R-PARAMETER VALUES. FROM R = 0 TO R = 100. Diffraction patterns of films of CdSe, grown on (100) faces of Ge.

The value R = 0 was assigned to the films giving rise to ring electron diffraction patterns. This showed that at low substrate temperatures the CdSe films grew in randomly oriented, fine grain polycrystalline structures.

Over a relatively narrow range of substrate temperatures, the structure of the CdSe films changed systematically from polycrystalline to epitaxial monocrystalline through a series of intermediate partially oriented structures. The intermediate values R = 25, R = 50, and R = 75, were assigned to the films giving rise to mixed spot and ring transmission electron diffraction patterns. The values 25, 50 and 75 were assigned for diffraction patterns, in which the ring pattern is stronger than, equal to and weaker than the spot pattern respectively. This interpretation for the intermediate values cannot be made quantitative because the intensities of transmission electron diffraction spots and rings can not be related to simple structure factor considerations. This is because of the occurrence of multiple and incoherent (inelastic) diffraction processes. Hence the intermediate values of R, are ill-defined.

However, the use of the graph of R-parameter versus substrate temperature makes it compact and convenient to present the results of large numbers of transmission electron diffraction observations. Hence Figs. 4.1, 4.2 and 4.3 summarise the observations on the variation of the degree of orientation of CdSe films with growth ranges of Ge substrate temperature. It also indicates that the minimum



Figs. 4.1 CdSe/Ge (100)

4.2 CdSe/Ge (110)

4.3 CdSe/Ge (111)

The variation with substrate temperature of the degree of orientation R of films of CdSe evaporated on to Ge surfaces. R = 100 indicates epitaxy □: (100), ○: (110) and △: (111) oriented substrates.

epitaxial growth temperature was 350°C for CdSe films deposited on (100) and (111) faces of Ge and 300°C for the CdSe films grown on (110) faces of Ge.

Figs. 4.1 and 4.3 indicate that epitaxial growth was invariably obtained for all substrate temperatures from 350°C to 450°C on (100) and (111) oriented surfaces of Ge. From fig. 4.2 it is evident that epitaxial growth was reproducibly obtained for all substrate temperatures from 300°C to 450°C on (110) surfaces of Ge and the minimum epitaxial growth temperature was 50°C lower than on the other two singular surfaces.

These graphs indicate that the maximum epitaxial growth cut off temperature was 450°C on all the three surfaces of Ge. Above this temperature, CdSe films could not deposit on any of the three surfacesof Ge, due to the onset of a vapour phase chemical attack reaction. Ge substrates, which were held at temperatures above 450°C, while CdSe was evaporated had always etch pitted surfaces.

The form of these graphs is similar to those previously obtained for CdS deposited on (111) Ge (Wilcox 1970), CdS evaporated on to (100), (110) and (111) faces of Ge (Abdalla et al. 1973), CdTe deposited on (100), (110) and (111) faces of Ge (Abdalla and Holt 1973) and CdTe grown on (111) Si (Holt and Abdalla 1974). This is partly because, in the present case and in these cases, the epitaxial upper cut off temperatures, above which II-VI films could not be deposited on

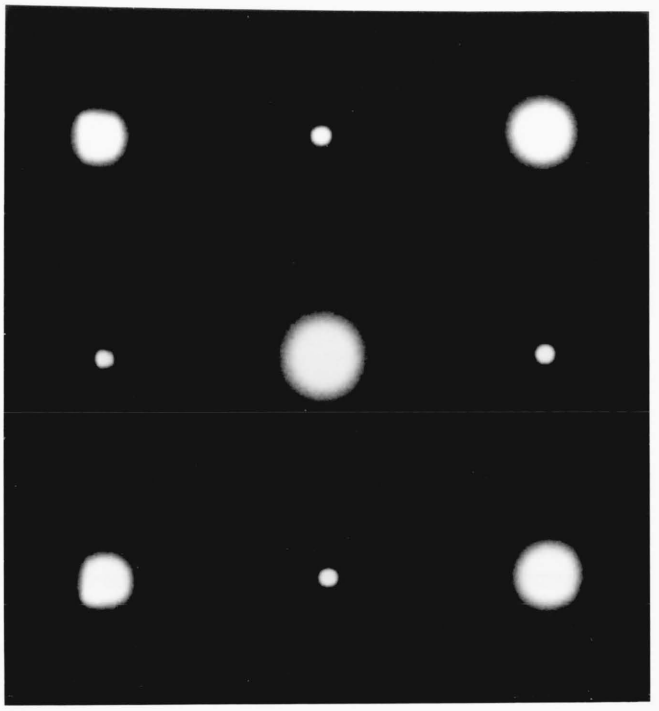
Ge and Si substrates due to the onset of vapour phase chemical attack reactions were well defined. A similar upper cut off temperature was found in the case of ZnSe deposited on Ge by Calow et al (1968).

The form of these graphs is not similar to those previously obtained for ZnTe on (100) and (111) faces of Ge (Mufti and Holt 1972) for ZnS on NaCl (Woodcock and Holt 1969) and for CdS on ionic substrates (Wilcox and Holt 1969). In all these cases, above the upper epitaxial growth temperatures, the degree of orientation of the films fell, just before the films ceased to deposit. In the case of ionic substrates this was due to the onset of the sublimation of the substrate material. More about the upper cut off temperature is given in chapter VI, section 6.1.

4.2 STRUCTURE OF CdSe FILMS DEPOSITED ON (100) Ge SUBSTRATES

Fig. 4.4(a) shows a typical transmission electron diffraction pattern of a CdSe film epitaxially grown on a (100) face of Ge. The indexing of this and similar diffraction patterns of CdSe films is shown in Fig. 4.4(b). This showed that the CdSe films grew epitaxially with the cubic sphalerite structure in (100) orientation, at all temperatures in the epitaxial growth range 350°C - 450°C. The CdSe/Ge epitaxial growth orientation relationship was (100) CdSe||(100) Ge, with $[0\bar{1}1]$ CdSe||$[0\bar{1}1]$ Ge. This parallel epitaxial orientation relationship between the CdSe films and Ge substrates

(a)



(b)

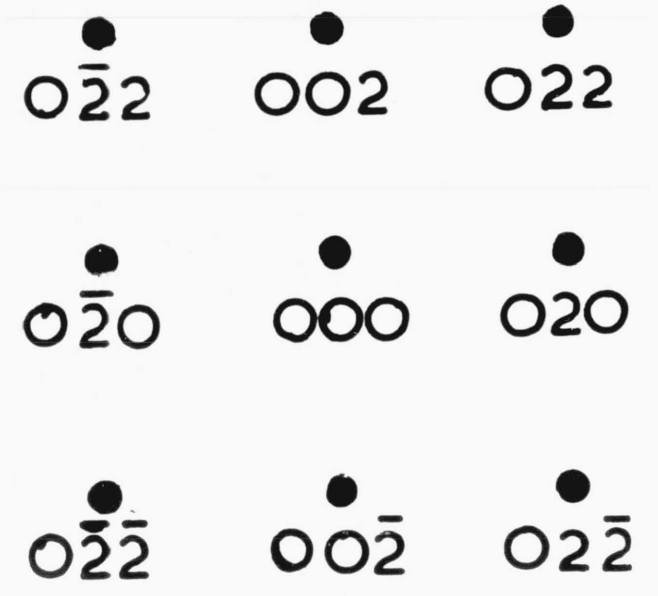
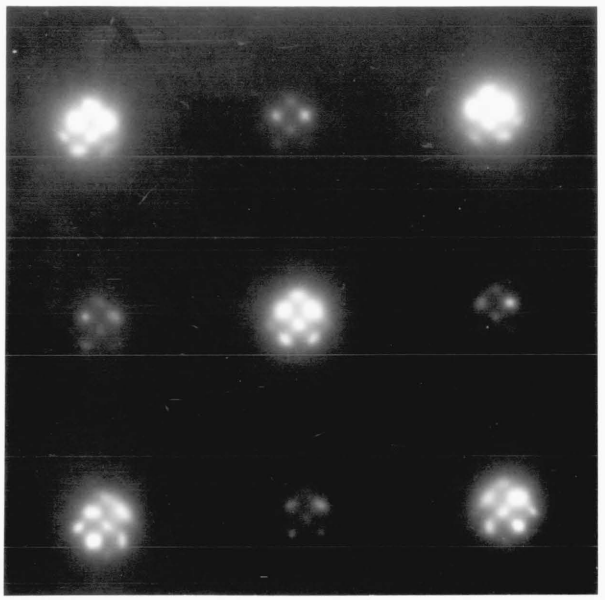


Fig. 4.4 (a) Selected area transmission electron diffraction pattern from a film of CdSe grown on a (100) surface of Ge at 390°C. The pattern was recorded with the incident electron beam in the exact [100] direction.

(b) Indexed plot of the diffraction pattern shown in (a).

(a)



(b)

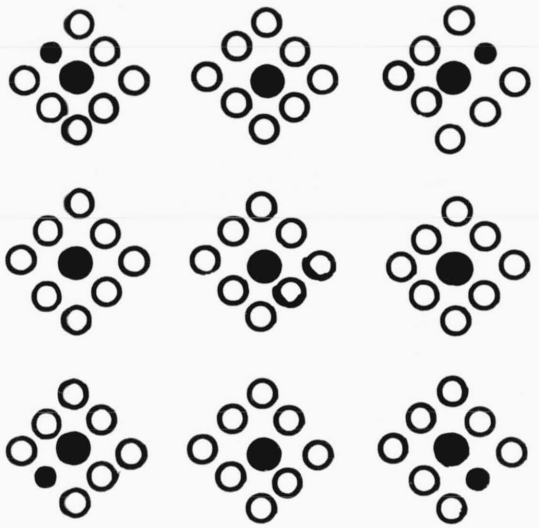


Fig. 4.5 (a) Transmission electron double diffraction pattern from an area in which the CdSe and Ge were of comparable thickness. The CdSe was epitaxially grown at 370°C on (100) Ge.

(b) The complete arrays of double diffraction moire spots (open circles) about the CdSe spots (large solid circles) and Ge spots (small solid circles) in the (100) reciprocal lattice plane. This is the explanation of the experimental transmission electron diffraction pattern shown in Fig. 4.5(a).

was determined as follows. In very thin regions of the specimens in which Ge was completely thinned through and hence only CdSe was present, the diffraction patterns observed were like that shown in fig. 4.4(a). In thick regions the diffraction pattern was almost entirely due to Ge and was similar and parallel to that for the CdSe. This fact was confirmed by further observations in the regions where the CdSe film and Ge substrates overlapped and they were of comparable thickness as shown in fig. 4.5(a). In such regions diffraction spots due to CdSe and Ge were observed together with arrays of double diffraction spots. The plot of this moire electron diffraction pattern is shown in fig. 4.5(b). From figs. 4.5(a) and 4.5(b) it is seen that each 002 type CdSe spot is surrounded by square "moire arrays" of eight double diffraction spots and each 022 type CdSe spot is surrounded by eight diffraction spots; seven of them are due to double diffraction, but one of them is the corresponding Ge 022 spot. This is because 002 type reflections (superlattice reflections) are not allowed reflections in the cubic diamond structure Ge (Cullity 1956) according to structure factor considerations, but 002 type superlattice reflections are allowed reflections in the cubic sphalerite structure according to structure factor considerations. It is also seen that the 022 type CdSe spot and the 022 type Ge spot lie exactly along the same [011] direction. This shows that the Bragg reflecting planes in the overlapped crystals were in parallel alignment. Hence it is experimentally

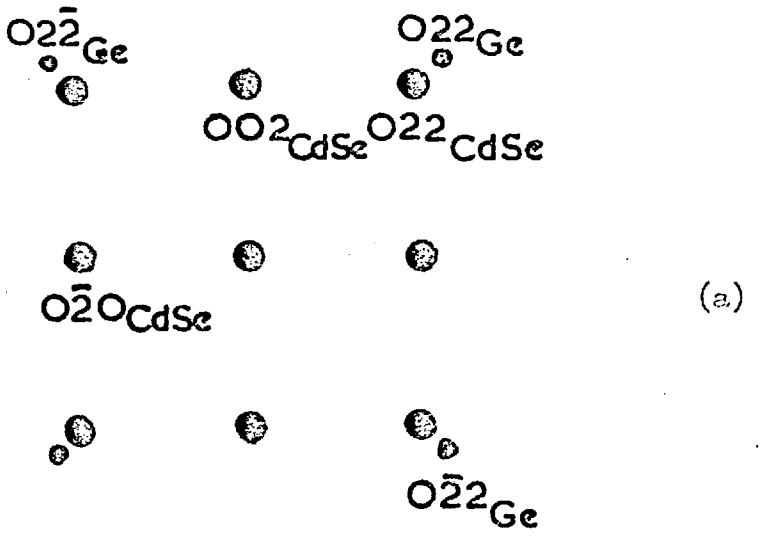
confirmed that the CdSe/Ge epitaxial growth orientation relationship was that (100) CdSe//(100)Ge with [011] CdSe// [011]Ge.

Thus the best method to determine the epitaxial orientation relationship between the films and substrates was to observe the superimposed diffraction patterns that arise in areas of specimen in which both CdSe and Ge were present in comparable thicknesses.

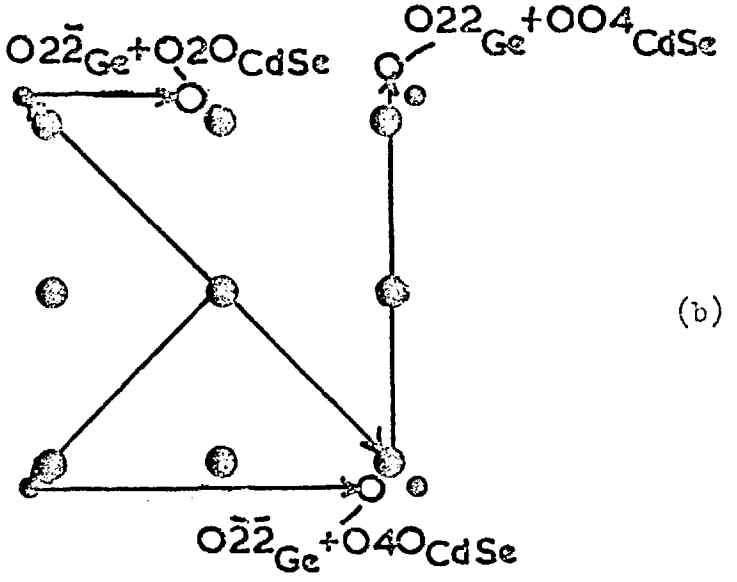
4.2.1 Moire Patterns and Fringes

The diffraction patterns like that shown in fig. 4.5(a), arising in overlapping CdSe and Ge will be referred to as moire patterns since they arise from the diffraction effects which give rise to moire fringes in the transmission electron micrographs.

The interpretation of the occurrence of square "moire arrays" or moire patterns like that shown in fig. 4.5(a) and (b), in the reciprocal lattice space is given in fig. 4.6 . This shows the indexed plot of the superposed (100) CdSe and (100) Ge diffraction patterns, in reciprocal lattice space for parallel alignment of the two crystals as shown in figs. 4.5(a) and (b). The way in which the neighbouring pairs of spots arising from 022 type reflections in CdSe and Ge, as shown in fig. 4.6(a) gives rise to additional spots by double diffraction is indicated in fig. 4.6(b). Thus the result of double diffraction replication of the 022 Ge spots round each of the CdSe spot is the square "moire



(a)



(b)

Fig. 4.6 (a) Indexed patterns of (100) CdSe and Ge in parallel alignment.

(b) Illustration of the way in which double diffraction first in the Ge and then in CdSe indicated by two successive vectors produces additional moire spots indicated by open circles and indexed with the two reflections concerned.

arrays" of spots shown in figs. 4.5(a) and (b). The diffraction vectors involved in producing these moire diffraction patterns, as can be seen in fig. 4.6(b), lie in the (100) plane in reciprocal space. These diffraction conditions therefore are exactly satisfied without taking the effects of the buckling of the specimen into account and these arrays are readily obtained. This is the explanation of the experimental transmission electron moire diffraction patterns like that shown in fig. 4.5(a).

When the electron beam was incident on an area of specimen with comparable thicknesses of CdSe and Ge moire fringes were always observed as shown in fig. 4.7. The moire fringes resulting from the overlapping of crystals of differing lattice parameter but in parallel alignment are known as parallel moire fringes. Their spacing is given (Hirsch et al. 1965) by

$$D_{parallel} = \frac{d_1 \, d_2}{d_1 - d_2}$$

where d_1 and d_2 are the spacings of the Bragg reflecting planes in the two crystals which give rise to the interfering beams. The moire fringes seen in fig. 4.7 are the result of the interference between 022 reflections of CdSe and Ge. The spacings of the Bragg reflecting 022 planes in CdSe and Ge are calculated, using the expression $d_{hkl} = \frac{a}{(\sqrt{h^2+k^2+l^2})}$ where a is the lattice parameter and hkl are the Miller indices of the reflecting planes. For CdSe a = 6.077Å (x-ray powder

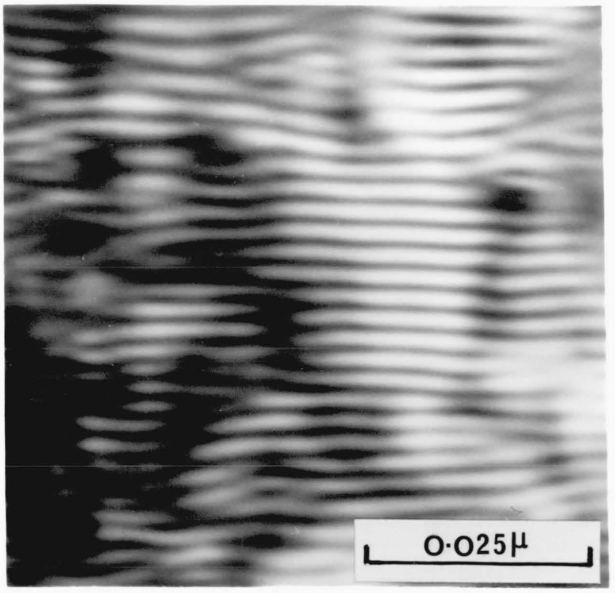


Fig. 4.7 Typical bright field transmission electron micrograph showing the parallel moire fringes of CdSe/Ge (100) heterojunction. The CdSe was epitaxially grown at 400°C on (100) Ge.

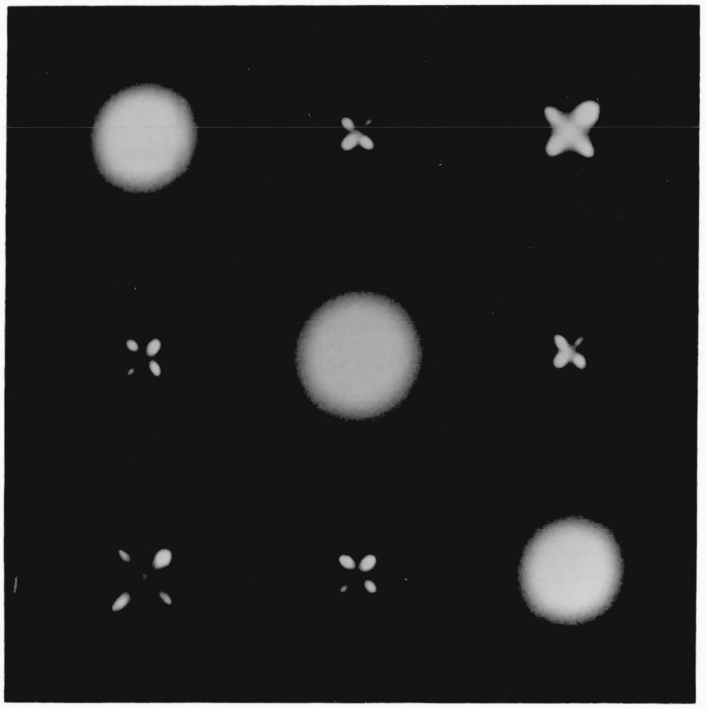


Fig. 4.8 Diffraction pattern of the same film as shown in Fig. 4.4(a) but now tilted slightly off the exact [100] beam direction.

data file No. 19-191) and for Ge a = 5.6576Å (Swanson and Tatge 1951); substituting these values in the above expression for the moire fringe spacing the calculated value of $D_{parallel}$ = 29.1Å . The experimentally measured value for the moire fringe spacings in (100) CdSe/(100)Ge heterojunctions was 29.2Å . This excellent agreement confirms the interpretation given above for the diffraction patterns of the form shown in fig. 4.5(a). A more detailed interpretation of moire patterns and fringes, is given in sections 4.4.2 and 4.4.3.

4.2.2 Identification of {111} Planar Defects Present in (100) CdSe Films

When the electron beam incident on (100) oriented CdSe films was exactly parallel to the [100] film normal, the diffraction patterns always obtained were of the type shown in fig. 4.4(a). No satellite spots due to three dimensional defects were ever observed in the diffraction patterns of epitaxial CdSe films. This was evidenced that the (100) CdSe epitaxial films were free from three dimensional defects such as twins or included grains of second phase material with wurtzite structure (Holt 1969a).

But when the epitaxial (100) CdSe films were tilted slightly away from the exact (100) orientation in the electron microscope, the diffraction pattern changed to the form shown in fig. 4.8. The diffraction patterns were always found to be streaked in <111> directions. This was evidence that numerous {111} planar defects were present in the (100) CdSe

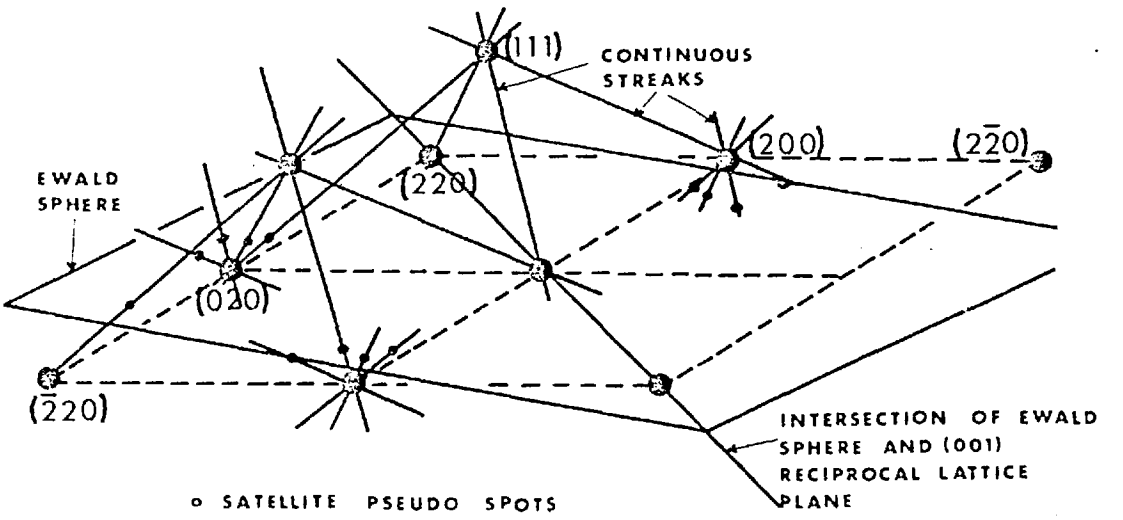


Fig. 4.9 Origin of the satellite pseudo-spots shown in Fig. 4.8 due to the cutting of <111> streaks in reciprocal space by the Ewald sphere of reflection. (After Holt and Woodcock 1970).

epitaxial films. Similar patterns have been observed in other cases of II-VI films grown on (100) surfaces of cubic system crystal substrates, and analysed in case of the films grown on ionic substrates (Holt and Woodcock 1970) and Holt and Wilcox 1971). The analysis of the films grown on Ge (100) surfaces is given below.

It is clear from fig. 4.8 that sets of four intensity maxima occur around the positions of the CdSe matrix spots. This happens when the Ewald sphere of reflection intersects four continuous <111> streaks in reciprocal lattice space. The correct interpretation of this situation was given by Holt and Woodcock (1970) as shown in fig. 4.9.

The <111> streaks are perpendicular to the {111} planes in which planar defects lie. The (100) diffraction pattern does not contain any <111> directions. Therefore these continuous <111> streaks instead of running in the plane of (100) reciprocal lattice space, must be inclined to it, and when these streaks cut the nearly planar Ewald sphere of reflection, this forms the sets of four intensity maxima around the CdSe matrix spots. These intensity maxima are known as satellite pseudo-spots. They move in and out relative to the main matrix spot as and when the CdSe film is tilted in the electron microscope. Therefore the distances of these pseudo-spots from the matrix spots depend upon the amount of the film tilt from [100] film normal. It is seen from fig. 4.8 that the pseudo-spots have a characteristic elliptical form. This arises due to the intersection of

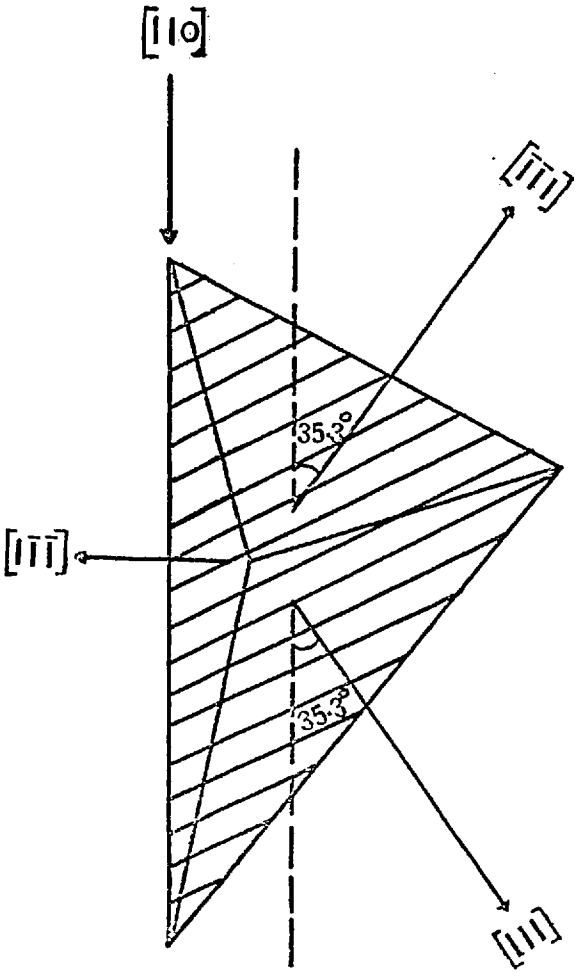


Fig. 4.10(a) Thompson's tetrahedron showing the orientation of the four {111} planes of the sphalerite structure, when the electron beam is incident on the CdSe film in [1$\bar{1}$0] direction. Two of the planes are parallel to the beam and the other two planes are inclined 35.3^0 to the [1$\bar{1}$0] beam direction. The cross-hatched rear face normal is [$\bar{1}\bar{1}\bar{1}$].

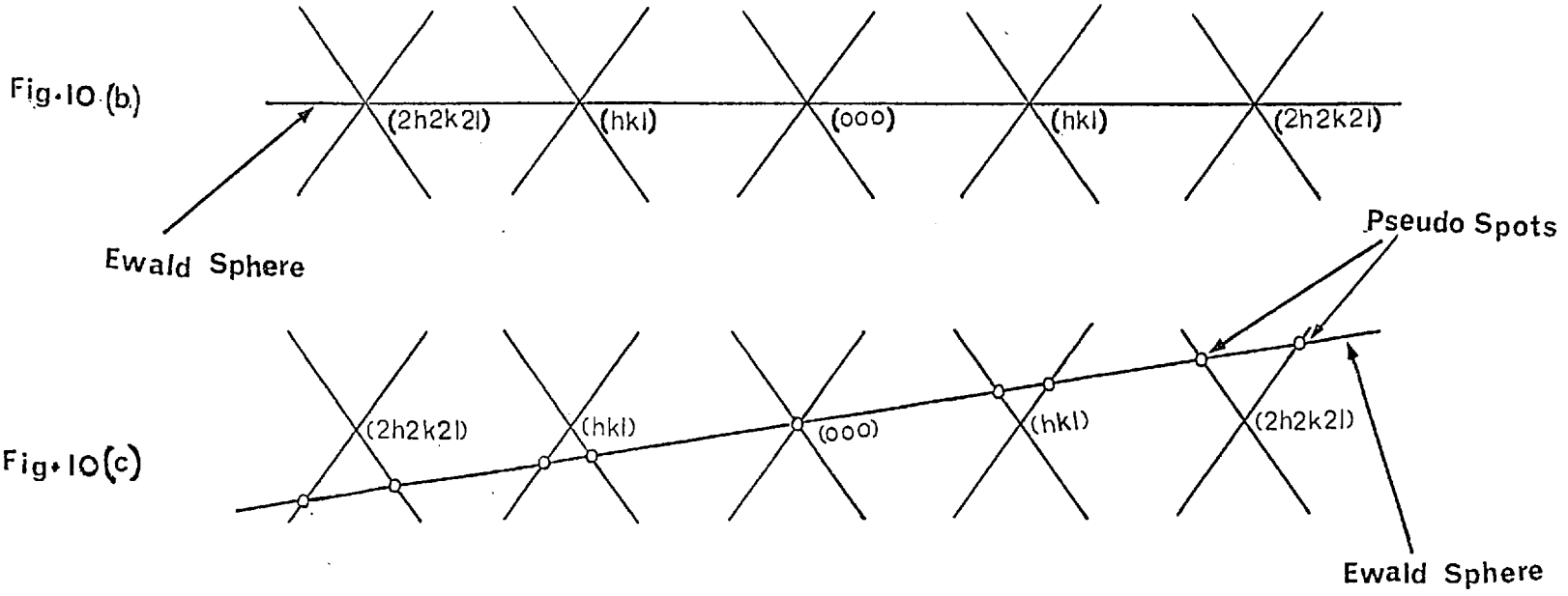


Fig. 4.10(b) The two $[\bar{1}\bar{1}1]$ and $[11\bar{1}]$ streaks intersect the sphere of reflection at matrix spots in the reciprocal lattice space, when the film is tilted to exact (110) orientation.

Fig. 4.10(c) The two $[\bar{1}\bar{1}1]$ and $[11\bar{1}]$ streaks intersect the sphere of reflection in the reciprocal lattice space, giving rise to two pseudospots when the film is tilted slightly away from the exact (110) orientation.

the approximately planar Ewald sphere with right-circular-cylindrical <111> streaks. This suggested that the observed intensity maxima were due to {111} planar defects, but not due to three dimensional defects such as twins or included grains of second phase material of wurtzite structure. This is because real satellite spots due to three dimensional defects appear and disappear always at the same point with slight tilting of the specimen in electron microscopy.

Further confirmation that the observed intensity maxima arose due to the four sets of {111} planar defects was confirmed in high voltage microscopy using an AEI EM7. In this microscopy specimens can be tilted about 60^{o}, about the two perpendicular directions in a horizontal plane.

From an indexed diffraction pattern of (110) oriented epitaxial CdSe films as shown in figs. 4.15(a) and 4.15(b), (Sec.4.3) it is evident that the (110) diffraction pattern contains the $1\bar{1}\bar{1}$ and $\bar{1}1\bar{1}$ diffraction spots. That is the (110) diffraction pattern contains two of the four <111> directions, namely $[1\bar{1}\bar{1}]$ and $[\bar{1}1\bar{1}]$. Therefore the $(1\bar{1}\bar{1})$ and $(\bar{1}1\bar{1})$ planes are parallel to the [110] direction and the other two $(\bar{1}\bar{1}1)$ and (111) planes are inclined at 35.3^{o} to the [110] direction as indicated by the Thompsons tetrahedron as shown in fig. 4.10(a).

Fig. 4.11 shows a typical selected area (110) diffraction pattern of a CdSe epitaxial film, when the film was tilted from the (100) orientation to the (110) orientation in the high voltage microscope. The angle between the continuous streaks is 70^{o} 30", which is the angle between the $(1\bar{1}\bar{1})$ and

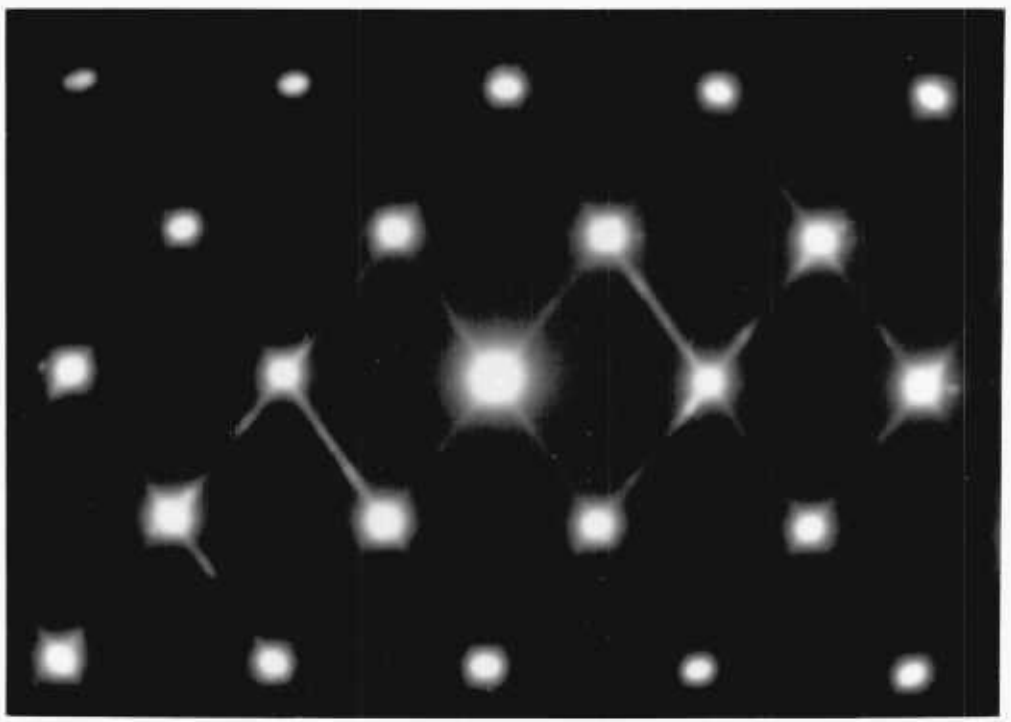


Fig. 4.11 Selected area diffraction pattern of a CdSe film tilted from (100) orientation to exact (110) orientation through 45°. The two $[1\bar{1}\bar{1}]$ and $[\bar{1}1\bar{1}]$ streaks are seen running continuously in the plane of the (110) diffraction pattern. No intensity maxima are seen. The CdSe was grown epitaxially on (100) Ge at 400°C.

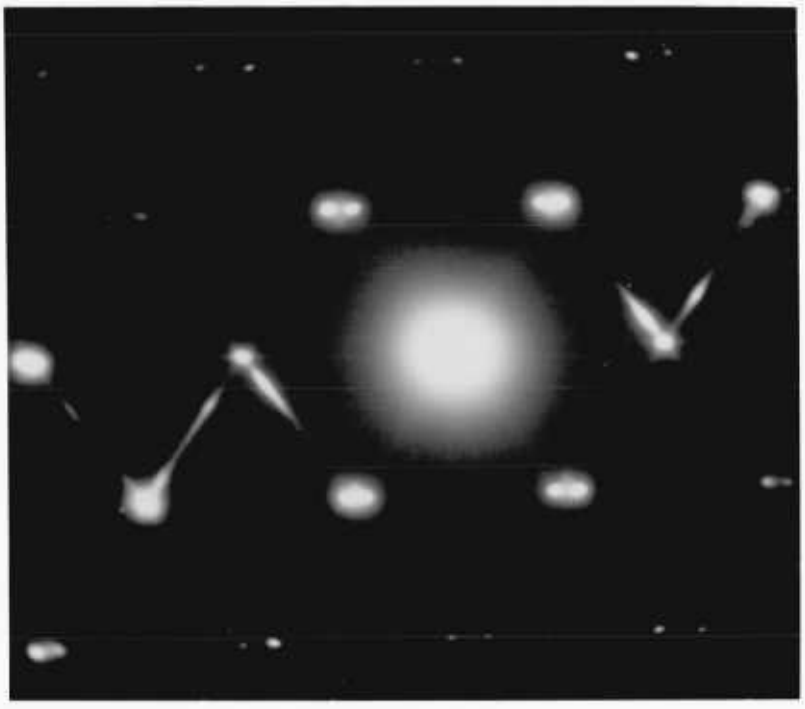


Fig. 4.12 Selected area diffraction pattern of the same area of the same CdSe film as shown in Fig. 4.11 but now tilted slightly off the exact (110) orientation in AEI EM7 million volt transmission electron microscope. Pseudo spots and extended streaks can be seen.

$(\bar{1}1\bar{1})$ planes.

The other two streaks perpendicular to the $(\bar{1}\bar{1}1)$ and (111) defect planes do not lie in the plane of the (110) diffraction pattern i.e. they intersect the sphere of reflection at the main matrix spots in the (110) reciprocal lattice plane as shown in fig. 4.10(b). It is also noticeable that the continuous streaks had a uniform intensity which showed that the planar defects were random.

When the CdSe film was tilted slightly away from (110) orientation the diffraction pattern changed to the form shown in fig. 4.12. The two <111> streaks perpendicular to the $(1\bar{1}\bar{1})$ and (111) planes intersect the Ewald sphere of reflection giving rise to the pseudo-spots spaced a variable distance apart in the [002] direction as shown in fig. 4.10 (c), whereas the other two <111> streaks perpendicular to the $(1\bar{1}\bar{1})$ and $(\bar{1}1\bar{1})$ planes appear extended in the (110) reciprocal lattice space. These observations confirm that the pseudo-spots or the intensity maxima observed in (100) diffraction patterns of (100) oriented CdSe films grown on (100) faces of Ge, arose due to the {111} planar defects. The appearance of pseudo-spots corresponded to the presence of high density of planar defects of the order of 10^{12} to $10^{13}/cm^2$ (Holt and Woodcock 1970).

Fig. 4.13 shows a typical bright field micrograph of a (100) oriented CdSe film grown on a (100) oriented Ge



Fig. 4.13 Typical bright field micrograph of a (100) CdSe film grown at 400°C. The fine scale fringe and dot contrast is characteristic of films with type of structure corresponding to Fig. 4.8.

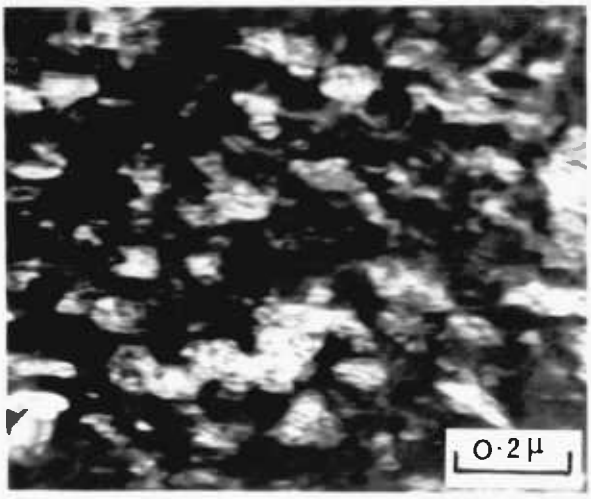


Fig. 4.14 High resolution dark field micrograph of the same film as shown in Fig. 4.13. This micrograph was recorded using one of the pseudo spots as shown in Fig. 4.7 for imaging.

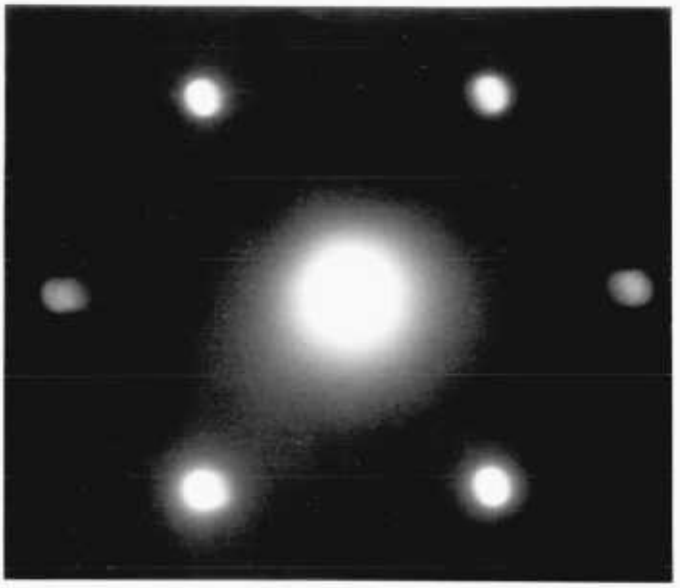
substrate. The dominant and characteristic feature of this bright field micrograph is the fine scale fringe and dot contrast. The interference of the main transmitted beam with the beams corresponding to pseudo-satellite beams gives rise to these contrast effects.

A high resolution dark field micrograph of one of the pseudo spots, used for imaging is shown in fig. 4.14. Triangular features of irregular size and shape can be seen. The dimensions of larger features were found to vary from about 1500Å to 2100Å, which is approximately equal to the thicknesses; 1200Å to 2000Å of the CdSe films.

4.3 STRUCTURE OF CdSe FILMS GROWN ON (110) Ge SUBSTRATES

Fig. 4.15(a) shows a typical electron diffraction pattern obtained from an area of CdSe film, from which the Ge had been removed completely, and when the electron beam was exactly parallel to the [110] film normal. Indexing of this and similar diffraction patterns of CdSe films grown on (110) Ge substrates is shown in fig. 4.15(b). This showed that the films had the cubic sphalerite structure in (110) orientation. When the films were tilted slightly off the exact (110) orientation, the diffraction pattern changed to the form shown in fig. 4.16. The diffraction spots always appeared split into pairs of pseudo-spots and separated along the <002> directions as shown in the fig. 4.16. This splitting of diffraction spots in pairs of pseudo-spots was observed

(a)



(b)

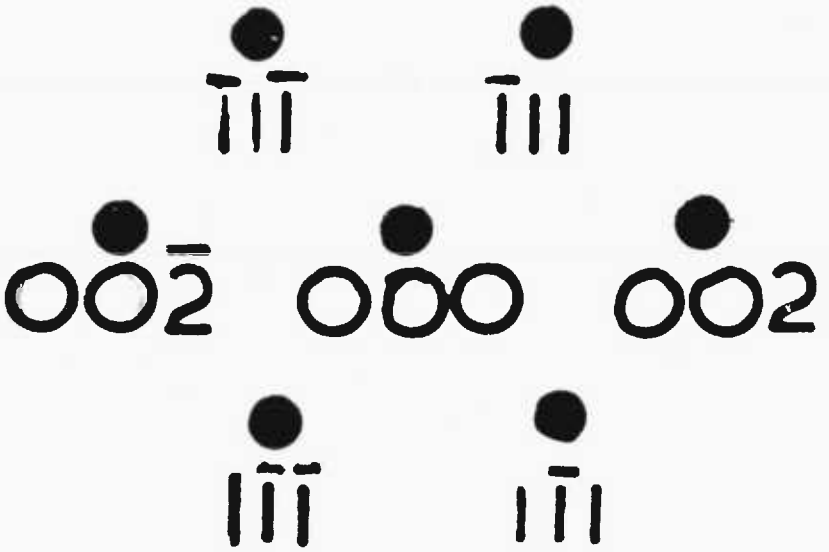


Fig. 4.15 (a) Selected area diffraction pattern of a CdSe film grown on (110) Ge at 440°C. This is the pattern obtained with the electron beam incident on the film in the exact [110] direction.

(b) The pattern in (a) is that of the sphalerite structure and indexes as shown.



Fig. 4.16

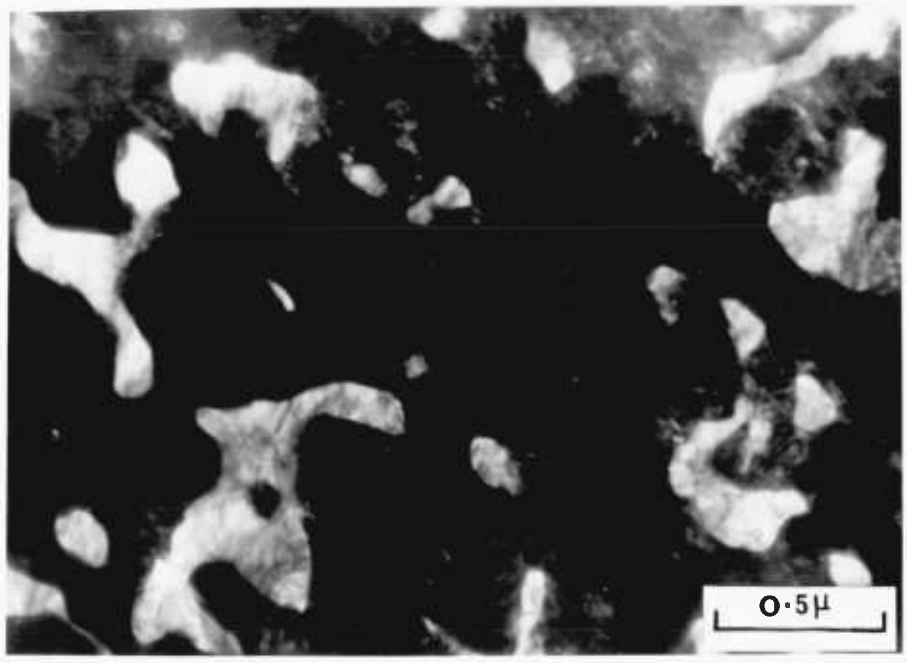


Fig. 4.17

Fig. 4.16 Diffraction pattern of the same film of CdSe as shown in Fig. 4.15(a) but now the film is tilted slightly off the exact (110) orientation.

Fig. 4.17 Bright field transmission electron micrograph of the same film.

in all the CdSe films grown at all temperatures in the epitaxial range: $300^{o}C$ to $450^{o}C$.

The characteristic appearance of the micrographs of the (110) CdSe epitaxial films is shown in fig. 4.17. This form of contrast in bright and dark areas of jig-saw-puzzle-piece shape arises from the domain-form transformed structure. This type of structure arises from faulting on the $(\bar{1}\bar{1}1)$ and (111) planes in (110) oriented CdSe films of sphalerite structure. One type of domain faults or transforms on the one {111} plane and the second type of domain faults or transforms on the other {111} plane. Thus the two {111} faulted planes give rise to streaks in the reciprocal lattice space in the <111> directions normal to the fault planes. The two types of streak run through every point in reciprocal lattice space giving rise to the pairs of split pseudo-spots, where they cut the sphere of reflection as shown in fig. 4.16.

The interpretation of the occurrence of the pseudo-spots in the (110) diffraction patterns of the films, tilted slightly off (110) orientation is given below.

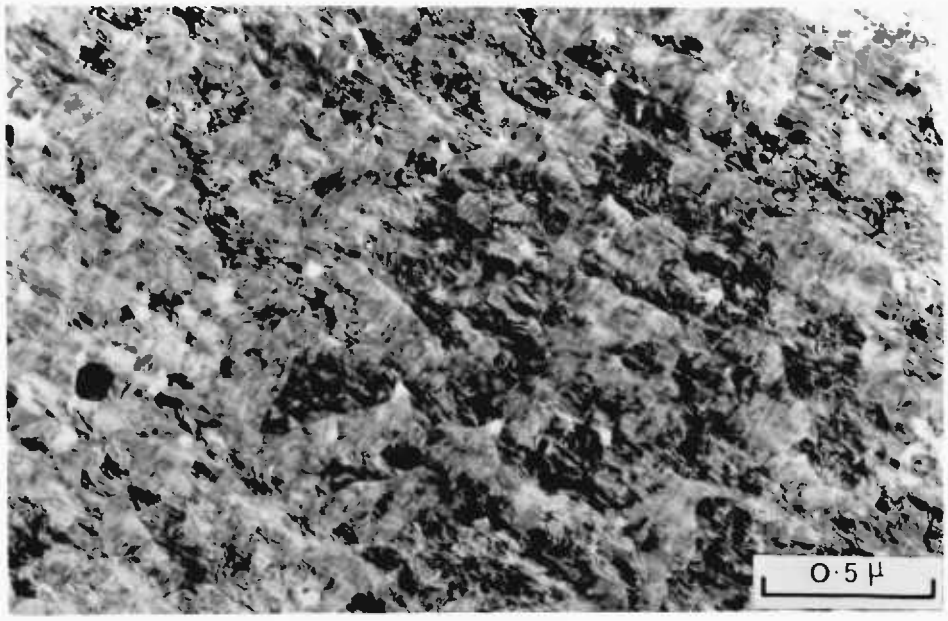
Fig. 4.10(a) (Sec. 4.2) shows the Thompsons tetrahedron, whose four faces represent the four {111} planes in the (110) oriented sphalerite structure film, when the electron beam is exactly parallel to [110] film normal. Fig. 4.15(a) shows the (110) diffraction pattern of the CdSe film when the electron beam was exactly parallel to [110] direction.

Thus from fig. 4.10(a) and fig. 4.15(a) it is clear that the $(1\bar{1}\bar{1})$ and $(\bar{1}1\bar{1})$ planes parallel to [110] direction

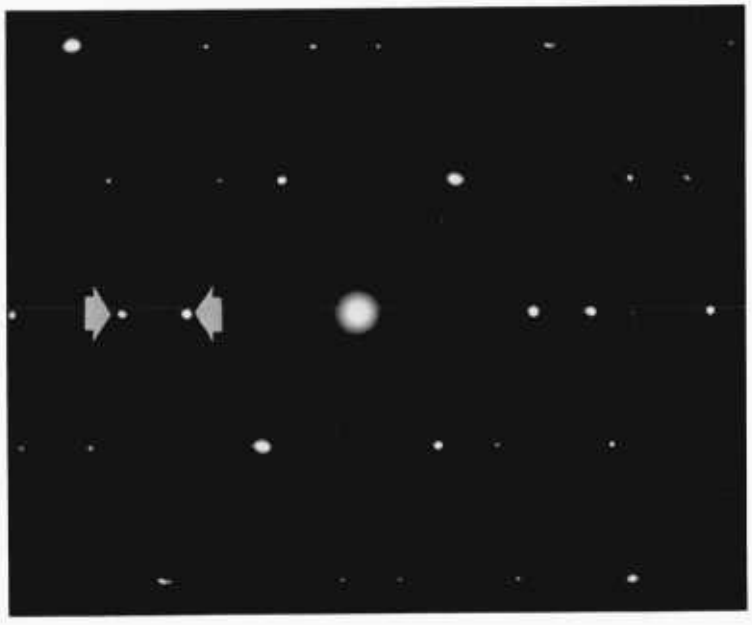
are not faulted and no streaks normal to $(1\bar{1}\bar{1})$ and $(\bar{1}1\bar{1})$ planes are observed. This can be verified by comparing the (110) diffraction pattern shown in fig. 4.15(a) with (110) diffraction pattern shown in fig. 4.11. Also fig. 4.10(b) shows how the two <111> streaks arising from the other two $(\bar{1}\bar{1}1)$ and (111) faulted planes and normal to them intersect the sphere of reflection at all the reciprocal lattice points in the plane of the (110) diffraction pattern.

However when the films were tilted slightly away from the (110) orientation the diffraction pattern changed to the form shown in fig. 4.16. And fig. 4.10(c) shows how the streaks normal to the $(\bar{1}\bar{1}1)$ and (111) faulted planes intersect the Ewald sphere of reflection forming the two pseudo-spots on either side of matrix spots in the reciprocal lattice. The separation of these pseudo-spots in the <002> direction depends upon the tilt of the film from the (110) orientation and hence on the positions at which the nearly planar sphere of reflection intersects the <111> streaks in reciprocal space as shown in fig. 4.16 and fig. 4.10(c). These pseudo-spots do in fact move in and out from the position of the CdSe main matrix spots with variation in the film tilt and are never observed to appear and disappear at fixed positions in the microscope observations. Thus these tilting observations established the correctness of the above interpretation.

That the one type of domain faulted or transformed on the $(\bar{1}\bar{1}1)$ plane diffracting into one pseudo-spot and the other domain faulted on the other (111) plane diffracting into the



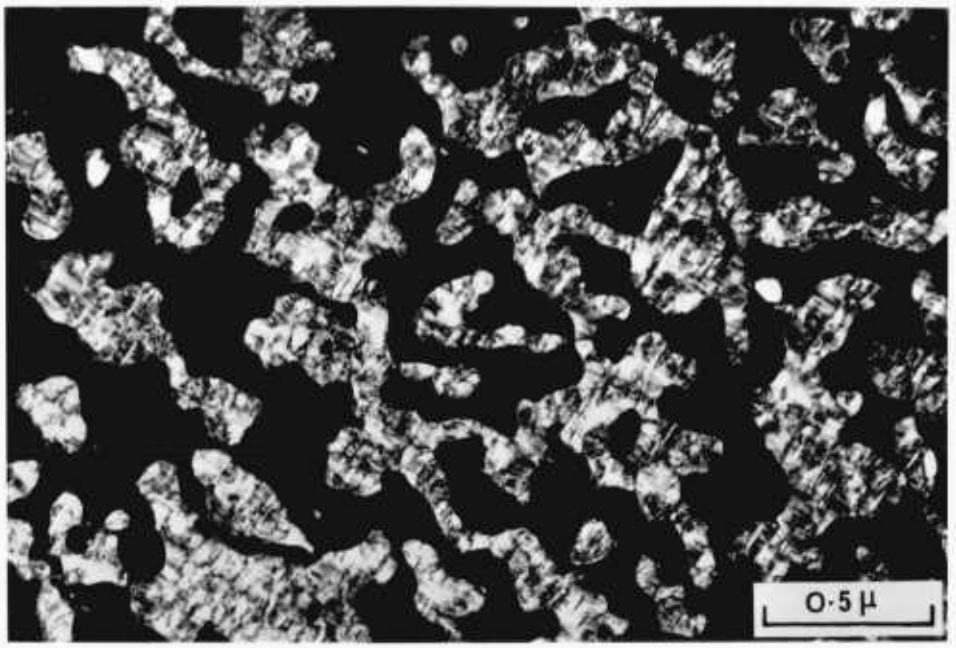
(a)



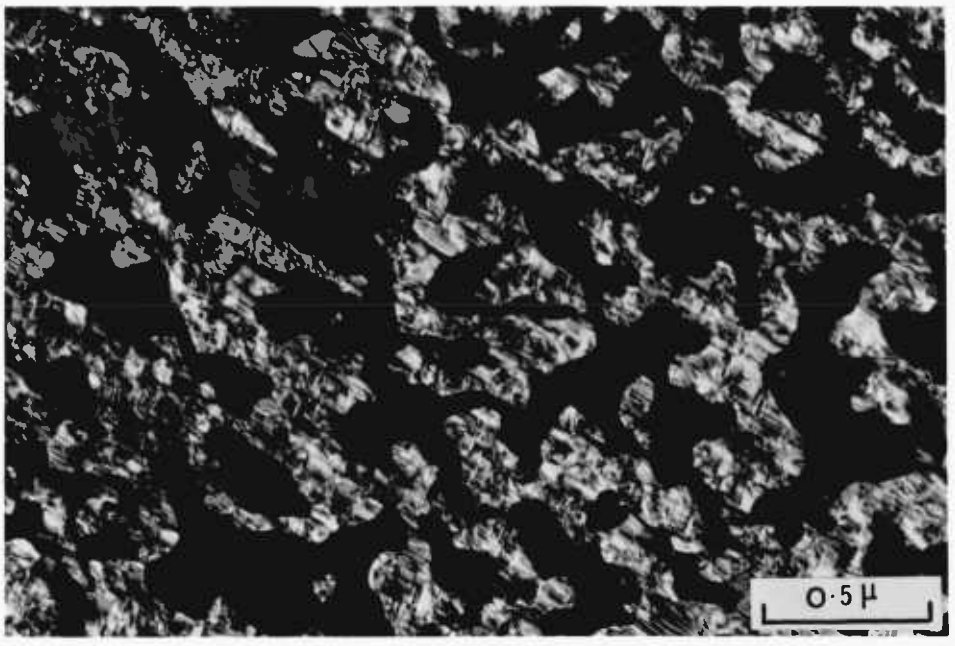
(b)

Fig. 4.18 (a) Bright field micrograph of the (110) CdSe film grown on (110) Ge at 400°C.

(b) Corresponding selected area transmission electron diffraction pattern.



(c)



(d)

Fig. 4.18 (c) High resolution dark field micrograph of the same CdSe film recorded when one of the pseudo spots indicated by an arrow was used for imaging.

(d) High resolution dark field micrograph of the same area of the film recorded when the pseudo-spot indicated by the other arrow was used for imaging.

other pseudo spot of each pair was confirmed by high resolution dark field microscopy. Fig. 4.18(a) and (b) are a bright field micrograph and the corresponding diffraction pattern of a CdSe film grown at 400°C on (110) Ge substrate. Fig. 4.18(c) and (d) are dark field images recorded when the pseudo-spots at the 002 matrix spot position were used individually for imaging. In these micrographs one type of domain faulted or transformed on one {111} plane appears bright and other type of domain faulted on the other plane appears dark.

The satellite pseudo-spots observed in the cases of (100) CdSe films grown epitaxially on (100) Ge substrates and of (110) CdSe film grown epitaxially on (110) Ge substrates as discussed above show that faults occurred on all the four {111} planes in the (100) oriented CdSe films, whereas in the (110) oriented CdSe films faults occurred only on the two {111} planes inclined at 35.3° to the [110] direction. Thus the {111} planar defects in sphalerite structure films in different orientations can be identified by diffraction streak studies.

The theory of diffraction streaks due to stacking faults in f.c.c. crystals has been given by Patterson (1952) and Whelan and Hirsch (1957). Thomas et al. (1965) have discussed the occurrence of streaks by planar defects and precipitates.

To establish experimentally the nature of the {111} planar defects in the domains, the (110) CdSe films were tilted from the (110) orientation to the (112) orientation through

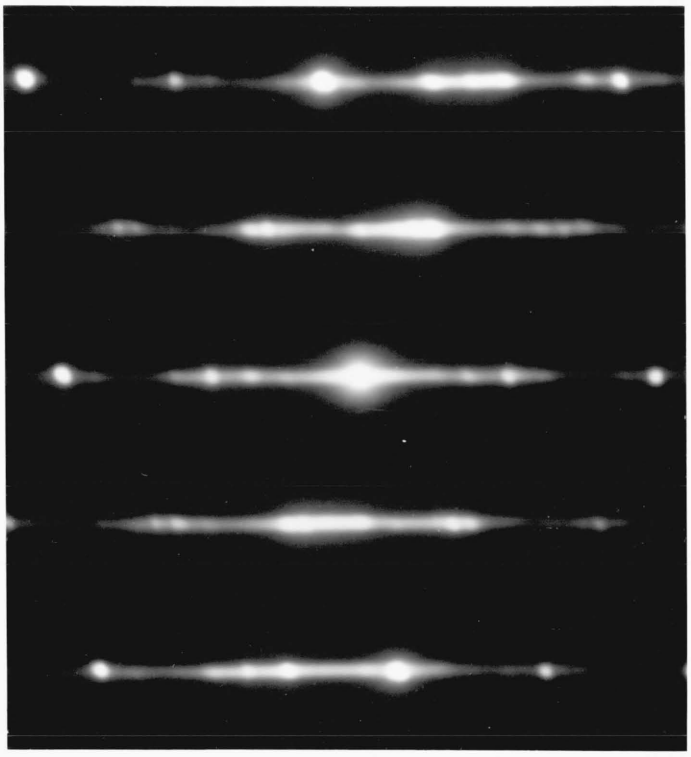


Fig. 4.19 Transmission electron diffraction pattern of a CdSe film grown at 400°C on (110) Ge substrate. This diffraction pattern was recorded when the CdSe film was tilted from (110) orientation to (112) orientation through 54.7°, in AEI EM7 million volt electron microscope.

54.7° in the AEI EM7 million volt transmission electron microscope. This brought the (112) plane containing one of the two <111> streaks normal to the electron beam so that it could be recorded with the result shown in fig.4.19. Along this <111> streak intensity maxima were seen. This showed that the domains faulted in a partially random and partially regular manner. The other <111> streak could not be brought into the plane of observation because the electron beam used to be cut off by the specimen stage due to the large tilt.

The domain-form transformed structures so far investigated in this laboratory, in (110) oriented CdS, CdTe and now in CdSe, were found to be different in nature. In CdS (Abdalla et al. 1973) faulting was regular, in CdTe (Abdalla and Holt 1973) faulting was random and in the present work on CdSe faulting was partially random and partially regular.

The analysis of the domain form structure in (110) oriented CdSe films involved the study of (1) the nature of the domains in as-grown films and (2) the nature of the domains in annealed films. Part one was dealt with above and part two is dealt with in chapter V on annealed CdSe epitaxial films.

So far it has been shown that the domain-form transformed structure films consist of two types of domains which appear in strong dark and bright contrast with irregular, interlocking, jig-saw-puzzle-piece shapes. This form is very similar to that of the double positioning twin "domains"



Fig. 4.20 Bright field micrograph of an epitaxial film of CdSe grown on (110) Ge at 400°C. Moire fringes can be seen running across the domain boundaries which contain a few fringe terminations.

observed in epitaxial films of f.c.c. metals by Dickson and Pashley (1962) and Pashley and Stowell (1963) and in ZnTe films by Holt (1969a). Hence the description of this structure found in the (110) oriented II-VI films as "domain form".

Fig. 4.20 is a typical bright field micrograph showing moire fringes due to the interference of beams diffracted in the Ge and the CdSe. The spacing of the moire fringes is found to be about 29.3Å and the calculated value of the parallel moire fringe spacing for 220 type reflections is 29.1Å (section 4.2.1). This showed that the CdSe and Ge were in parallel alignment.

4.4 STRUCTURE OF CdSe FILMS GROWN ON (111) Ge SUBSTRATES

Fig. (4.21(a) shows a typical transmission electron diffraction pattern of a CdSe film alone, after the Ge has been removed completely. The indexing of this and similar diffraction patterns is shown in fig. 4.21(b). This showed that the CdSe films again had the cubic sphalerite structure, in (111) orientation. To confirm this and to determine the epitaxial growth orientation relationship of the CdSe films grown on (111) oriented Ge substrates, the diffraction patterns of areas of the specimens where the CdSe film and the Ge had comparable thicknesses, were observed and recorded. Typical of such moire electron diffraction patterns is that shown in fig. 4.22(a). The plot of the moire electron diffraction pattern or electron double diffraction pattern is shown in fig. 4.22(b). It is seen that each CdSe spot is surrounded by a hexagonal rosette of six spots, five of them being

(a)



(b)

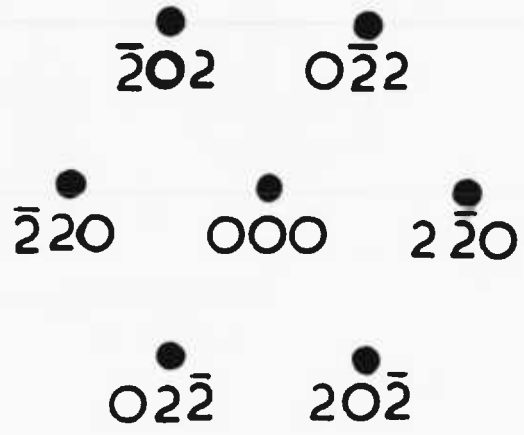
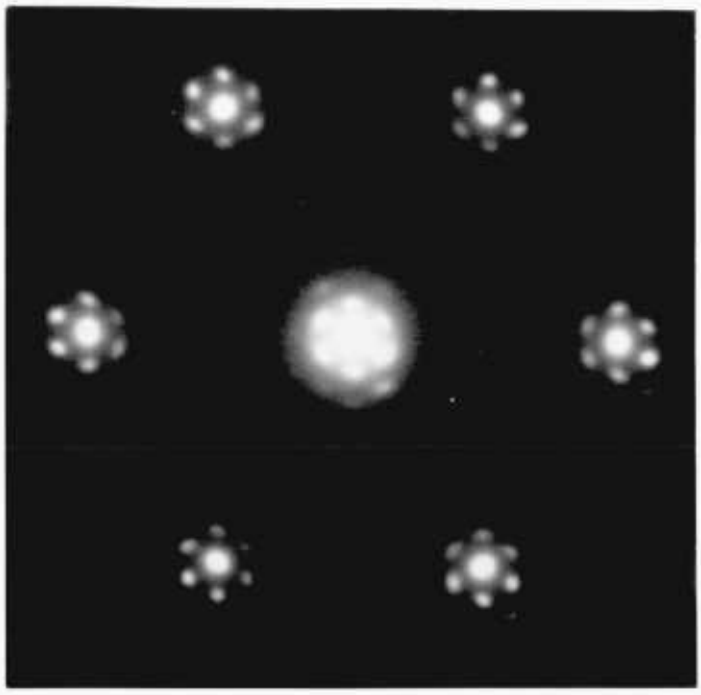


Fig. 4.21 (a) Selected area transmission electron diffraction pattern of a CdSe film grown on (111) Ge at 420°C.

(b) Indexed plot of the diffraction pattern shown in (a).

(a)



(b)

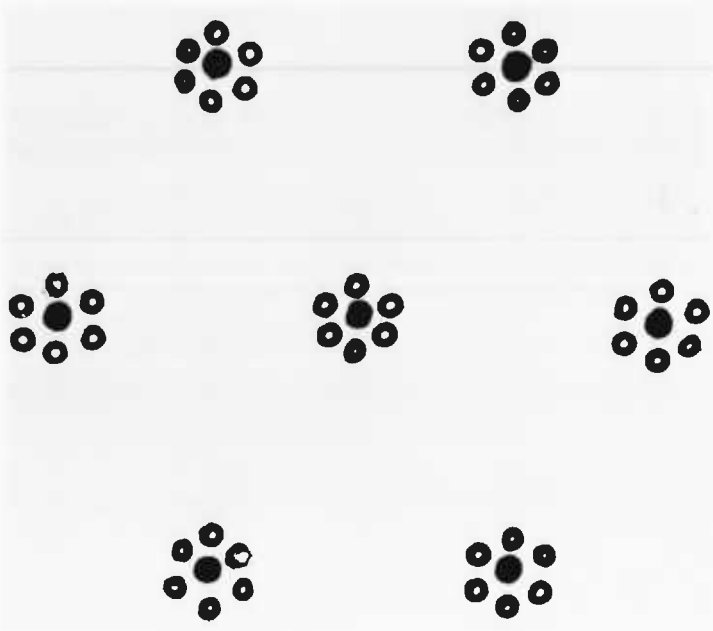


Fig. 4.22 (a) Transmission electron double diffraction pattern from an area in which the CdSe and Ge were of comparable thickness. The CdSe was epitaxially grown on (111) Ge at 400°C.

(b) Plot of the double diffraction moire pattern shown in (a). Large solid circles are CdSe $2\bar{2}0$ type spots and open circles are double diffraction spots one of them being Ge $2\bar{2}0$ type spot.

double diffraction spots and one of them being the Ge spot. This confirmed that the CdSe had the cubic sphalerite structure in (111) orientation. From figs. 4.22(a) and (b) it is evident that the hexagonal arrays of double diffraction spots and Ge spots have been rotated from the positions they would occupy for the parallel epitaxial orientation relationship: (111) CdSe parallel to (111) Ge with $[0\bar{1}1]$ parallel to $[0\bar{1}1]$ Ge. This can be clearly seen by comparison with the parallel orientation moire pattern for ZnTe grown on (111) Ge described below.

Fig. 4.23(a) is the plot interpreting the double diffraction parallel moire pattern of ZnTe/Ge (111) overlapping epitaxial crystals. It is seen that $2\bar{2}0$ type ZnTe spot is surrounded by hexagonal arrays of moire spots one of them being $2\bar{2}0$ Ge spot, and that the $2\bar{2}0$ spots of ZnTe and Ge lie along the same $[1\bar{1}0]$ direction. This confirmed that ZnTe had the cubic sphalerite structure and that the epitaxial orientation relationship was (111) ZnTe parallel to (111) Ge with $[1\bar{1}0]$ ZnTe parallel to $[1\bar{1}0]$ Ge. (Mufti A.R. 1972).

The plot interpreting the double diffraction moire pattern of CdTe/Ge (111) heterojunctions is shown in fig. 4.23(b). It can be seen that $11\bar{2}0$ CdTe and $2\bar{2}0$ Ge spots fall close to each other and as a result double diffraction occurs giving rise to hexagonal arrays of moire spots round each $2\bar{2}0$ Ge spot. This type of pattern shows that CdTe had the hexagonal wurtzite structure in (0001) orientation. The epitaxial orientation relationship was (0001) CdTe parallel

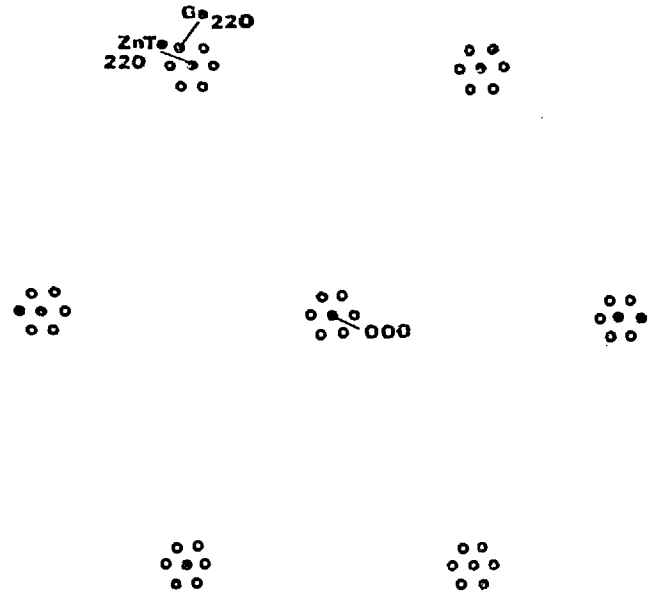


Fig. 4.23(a) Plot interpreting double diffraction parallel moire pattern of ZnTe/Ge overlapping epitaxial crystals. Central solid circles are ZnTe diffraction spots, outer solid circles are Ge diffraction spots and open circles are double diffraction spots (Taken from **Mufti** 1972).

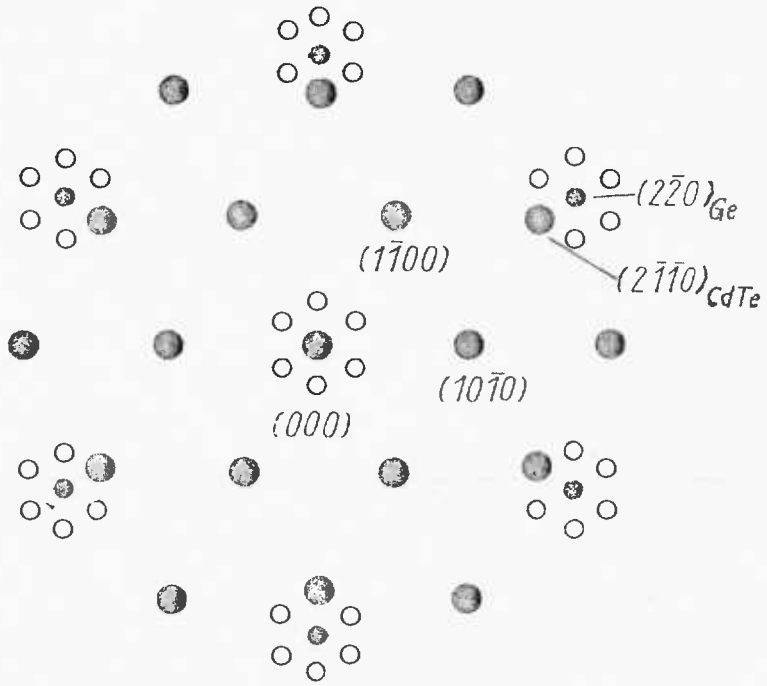


Fig. 4.23(b) Plot interpreting double diffraction quasi-parallel moire pattern of a CdTe/Ge(111) heterojunction. Large solid circles are CdTe spots, small solid circles are Ge spots and open circles are double diffraction spots (Taken from Abadalla, 1973).

to (111) Ge with $[11\bar{2}0]$ CdTe parallel to $[1\bar{1}0]$ Ge (Abdalla I.M. 1973). This is referred to as the "quasi parallel" orientation relationship. The $10\bar{1}0$ type CdTe spots do not occur near any spot in the Ge (111) diffraction pattern. Therefore these $10\bar{1}0$ type CdTe spots appear isolated. This situation is not found in figs. 4.22(a) and (b). Thus it is evident that CdSe did not grow with the wurtzite structure on (111) Ge and did not have the quasi-parallel epitaxial orientation relationship.

Rotation moire diffraction patterns similar to fig. 4.22(a) were observed in rotated overlapping Au crystals in (111) orientation by Basset et al. (1958). In this case the two (111) Au crystals were put one on top of the other after these had been prepared. This similarity of the diffraction patterns confirms that the rotation diffraction moire pattern observed in the present work were due to relative azimuthal rotation of the two crystals about the [111] interface normal.

The rotation of hexagonal arrays of moire spots through 30^{o}, from their position in parallel alignment was found to be due to the rotation of the overlapping CdSe crystals relative to the Ge, through a small azimuthal angle about 2^{o} 24', about the [111] normal to the substrate surface. The reciprocal lattice vector theory to deduce this azimuthal angular rotation (α) is given in the section 4.4.2. On the basis of the experimental results interpreted in this way, a new epitaxial growth orientation relationship emerged and it

will be referred as "nearly-parallel rotation" epitaxy. More details on this "nearly-parallel rotation" epitaxy are given in next sections 4.4.2 to 4.4.4.

Irrational satellite spots (Holt 1966a) were never observed in the diffraction patterns of CdSe films grown on (111) faces of Ge. Hence the (111) CdSe films were free from three dimensional defects such as microtwins, double positioning twins and included grains with the wurtzite structure.

No splitting of the diffracton spots was ever observed in the diffraction patterns of (111) CdSe films, when they were tilted off the exact (111) orientation in transmission electron microscopy observations. That is "pseudo-spots" although observed in the (100) and (110) CdSe films were never observed in the (111) diffraction patterns of CdSe films.

This was evidence that the CdSe films grown on (111) faces of Ge, were free from two dimensional planar defects at least in the densities above about 10^{12} cm^{-2} required to produce streaks in diffraction patterns.

4.4.1 Tilting of CdSe/Ge (111) Specimens from the (111) Orientation to the (110) Orientation

The fact that CdSe had grown on (111) Ge surfaces with the cubic sphalerite structure was established in the previous section 4.4. Further experimental evidence to demonstrate this is given below.

(a) (b) (c)

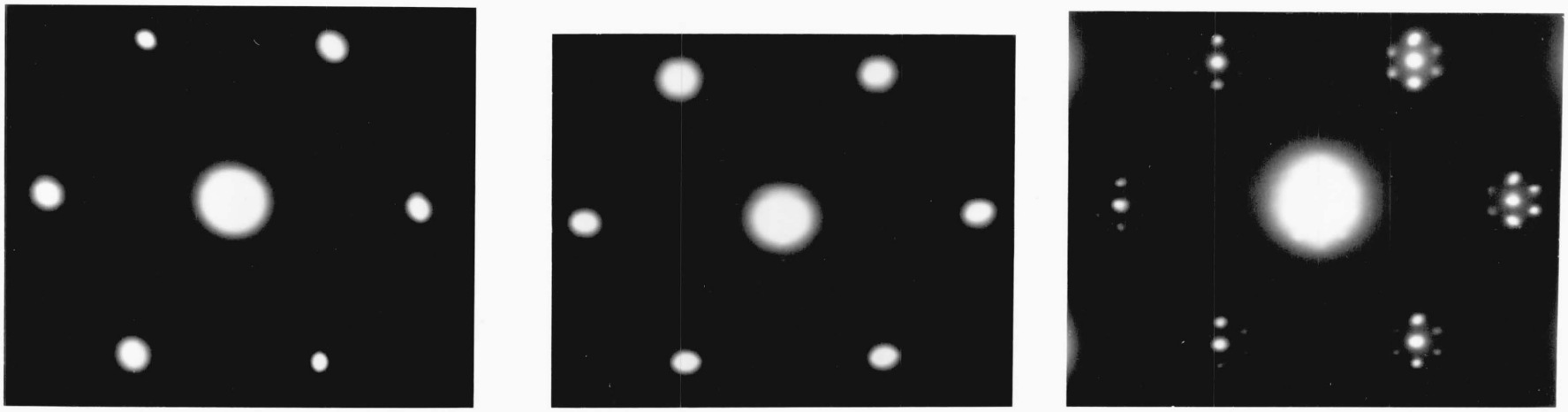


Fig. 4.24 (a) Selected area transmission electron diffraction pattern of a CdSe film grown on (111) Ge at 400°C.

(b) Selected area diffraction pattern of the same area of the CdSe film when tilted from (111) orientation to (110) orientation in an AEI EM7 million volt electron microscope.

(c) Transmission electron double diffraction moire pattern from an area of the same CdSe/Ge specimen, in which CdSe and Ge were of comparable thickness. This was recorded when the specimen was tilted to (110) orientation in an AEI EM7 million volt electron microscope.

It is well known that the diffraction patterns of the diamond structure Ge and the sphalerite structure CdSe film in the (111) orientation contain the same set of allowed reflections. Therefore the pairs of diffraction spots with the same indices arising from the two overlapping crystals are closely spaced. Then double diffraction occurs with the production of hexagonal arrays of moire spots at each allowed reflection site. From fig. 4.22(a) and (b) it is clear that each $2\bar{2}0$ type CdSe spot is surrounded by hexagonal arrays of moire spots one of them being the corresponding $2\bar{2}0$ Ge spot, and that the hexagonal arrays of moire spots are rotated from their position in parallel alignment through 30^{o}.

Fig. 4.24(a) shows the selected area transmission electron (111) diffraction pattern of a (111) CdSe film alone, when the electron beam in the high voltage AEI EM7 microscope was parallel to the [111] direction. Then the specimen was tilted 35.3^{o}, by the help of the high tilting stage of the microscope. That is the specimen was tilted from (111) orientation to the (110) orientation so that the electron beam was parallel to the [110] direction. Fig. 4.24(b) shows the (110) diffraction pattern of the same CdSe film alone. If the CdSe film had not grown with the cubic sphalerite structure, on tilting through 35.3^{o} it would not have given the (110) diffraction pattern as shown in fig. 4.24(b). When the specimen was tilted to the (110) orientation and the electron beam parallel to the [110] direction was made incident on the overlapping heterojunction system, where the CdSe and Ge were of comparable

thicknesses the double diffraction pattern was obtained from the same specimen as shown in fig. 4.24(c). It can be seen from fig. 4.24(c) that (110) CdSe was parallel to (110) Ge and that the CdSe had the cubic sphalerite structure.

This showed that the CdSe films had grown certainly with cubic sphalerite structure in (111) orientation on the (111) face of Ge.

4.4.2 To Deduce Formulae for Azimuthal Angular Rotation and "Nearly-Parallel Rotation" Moire Fringe Spacings

The double diffraction pattern typical of that shown in fig. 4.22(a), observed in CdSe/Ge (111) epitaxial studies is a new phenomenon. Therefore it is considered worth while to derive related formulae for the rotation moire fringe spacings and the azimuthal angle of rotation of two (111) crystals about the [111] interface normal.

For example fig. 4.25 shows the hexagonal arrays of moire spots round a CdSe spot for parallel epitaxial orientation. Here the CdSe and Ge spots lie in the same $[0\bar{1}1]$ direction in the reciprocal lattice. The reciprocal lattice vector is the distance from the centre spot to any particular diffraction spot. If $\underset{\sim}{g}_1$ and $\underset{\sim}{g}_2$ are the lattice vectors for the CdSe and Ge spots and d_1 and d_2 are the spacings of the Bragg reflecting planes in the CdSe and Ge crystals respectively, then by definition,

$$|\underset{\sim}{g}_1| = \frac{1}{d_1} \quad \text{and} \quad |\underset{\sim}{g}_2| = \frac{1}{d_2} . \qquad 4(1)$$

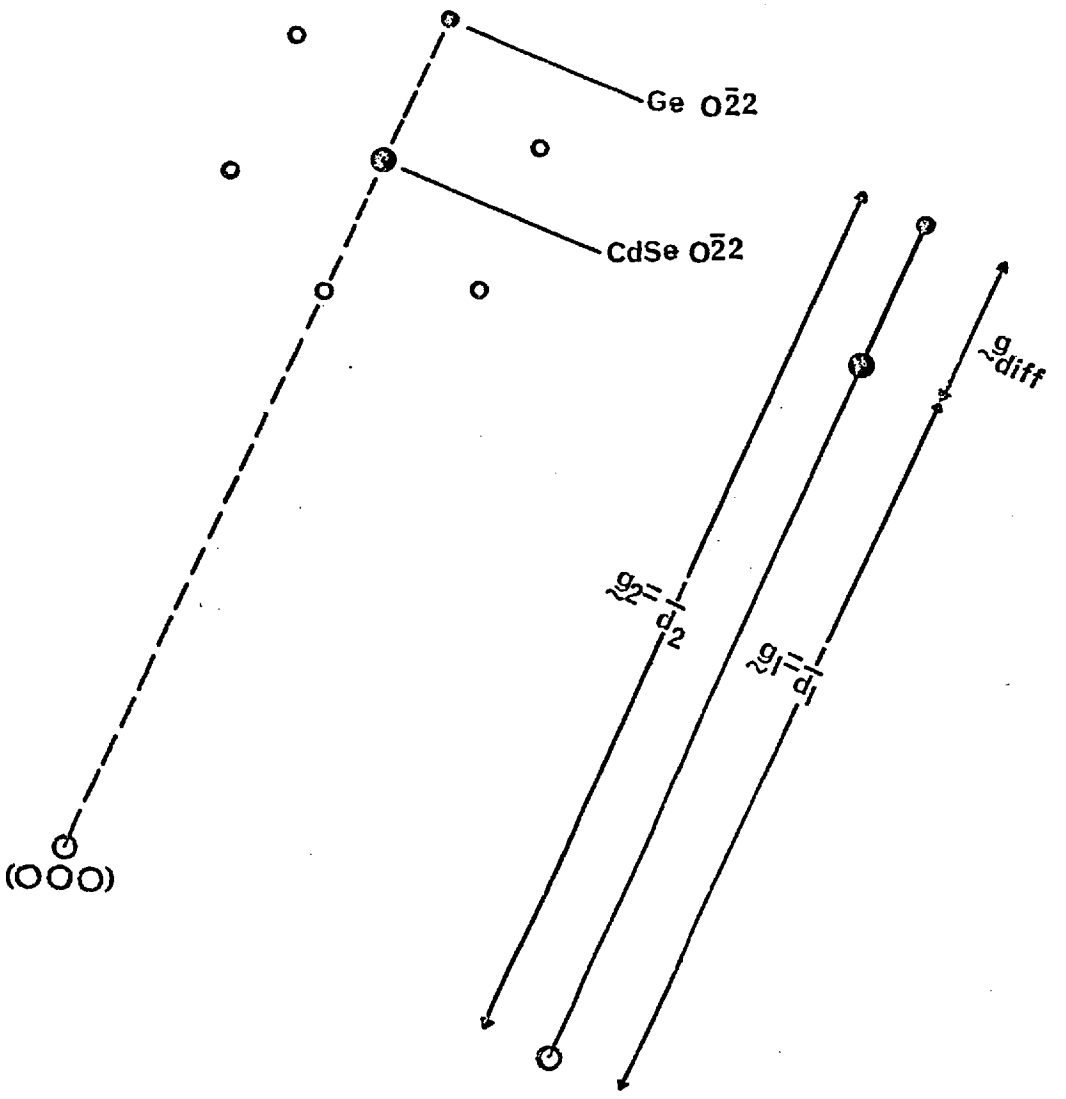


Fig. 4.25 Plot interpreting the hexagonal arrays of parallel moire double diffraction pattern. The reciprocal lattice vectors for Ge $0\bar{2}2$, and CdSe $0\bar{2}2$ diffraction spots are denoted by $\underset{\sim}{g}_1$ and $\underset{\sim}{g}_2$ respectively. The difference between the $\underset{\sim}{g}_1$ and $\underset{\sim}{g}_2$ is denoted by $\underset{\sim}{g}_{diff}$.

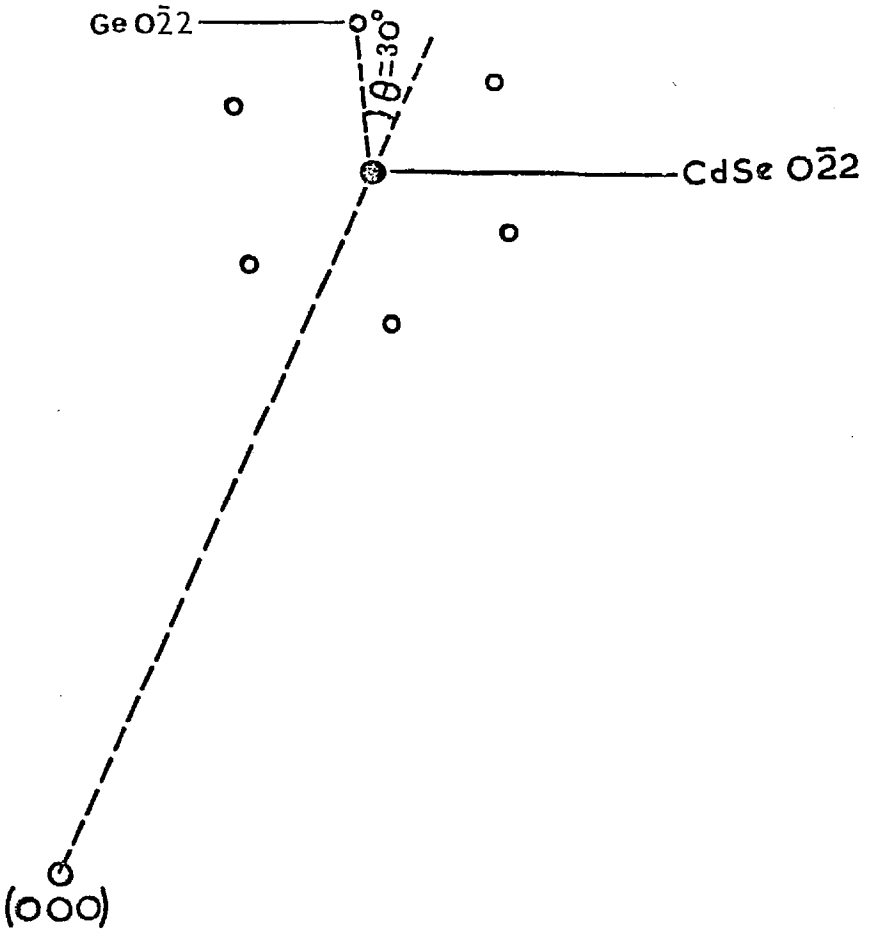


Fig. 4.26 Plot interpreting the hexagonal arrays of "nearly-parallel rotation" moire double diffraction pattern. It is seen that moire spots have rotated 30° from the position in the parallel alignment.

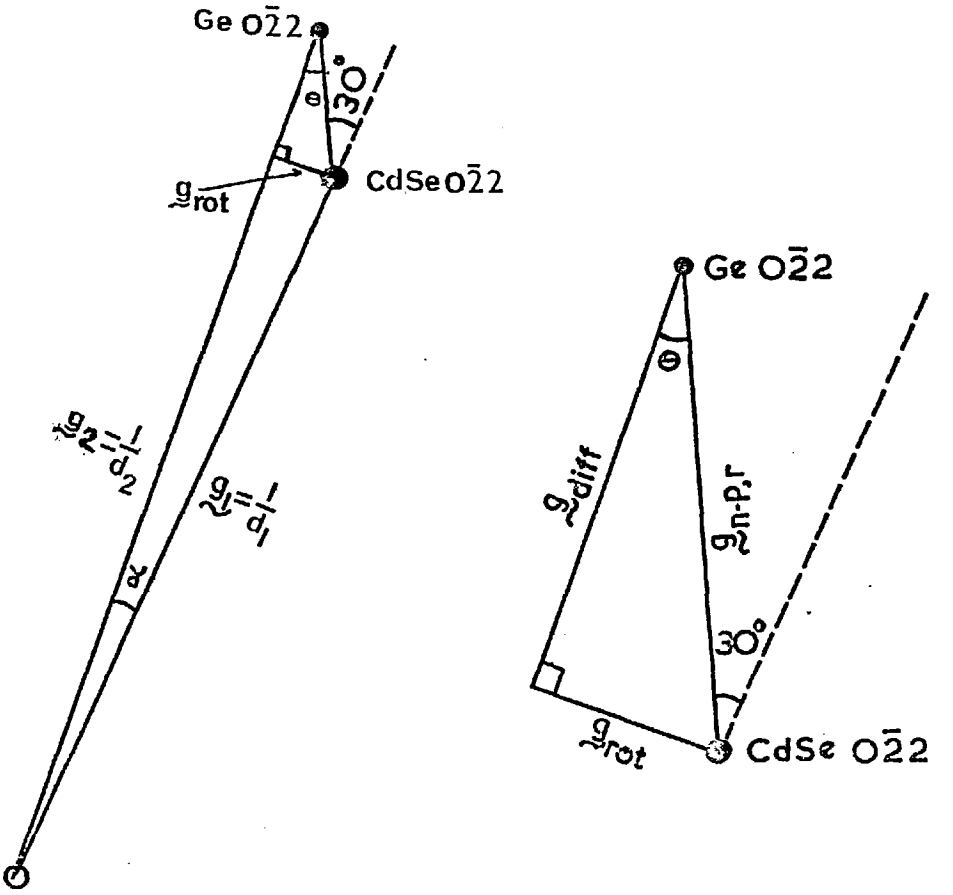


Fig. 4.27 In the "nearly-parallel rotation" moire double diffraction pattern the 0$\bar{2}$2 diffraction vectors for CdSe and Ge differ in direction by an angle α. The enlarged drawing shows the triangle, two of the apices of which are the CdSe and Ge 0$\bar{2}$2 diffraction spots.

From fig. 4.25 the difference in the two reciprocal lattice vectors is,

$$|g_{diff}| = |\underset{\sim}{g}_2| - |\underset{\sim}{g}_1| \qquad 4(2)$$

$$= \frac{1}{d_2} - \frac{1}{d_1} = \frac{d_1 - d_2}{d_1\ d_2} \qquad 4(3)$$

$\therefore$ The parallel moire fringe spacing is given by definition,

$$D_p = \frac{1}{|g_{diff}|} = \frac{d_1\ d_2}{d_1 - d_2} \qquad 4(4)$$

which is a well-known (Basset et al. 1958 and Hirsch et al. 1965) formula.

If the two overlapping crystals of different lattice parameter e.g. CdSe and Ge are rotated through a small azimuthal angle α, about the [111] interface normal, then hexagonal arrays of moire spots rotate through an angle θ from the position in parallel alignment. This is shown in figs. 4.26 and 4.27.

From fig. 4.27

$$\sin\alpha = \frac{|\underset{\sim}{g}_{rot}|}{\frac{1}{d_1}} \qquad \therefore\ \underset{\sim}{g}_{rot} = \frac{\sin\alpha}{d_1} \qquad 4(5)$$

and

$$|\underset{\sim}{g}_{diff}| \simeq \frac{1}{d_2} - \frac{1}{d_1} = \frac{d_1 - d_2}{d_1\ d_2} \qquad 4(6)$$

$$|\underset{\sim}{g}_{n-p,r}|^2 = |\underset{\sim}{g}_{diff}|^2 + |\underset{\sim}{g}_{rot}|^2 \qquad 4(7)$$

Here we make an important assumption that leads to the concept of "nearly-parallel rotation". This makes that the angle

of rotation α very small, so that $\sin\alpha = \alpha$. Then

$$|\underset{\sim}{g}_{rot}| = \frac{\sin\alpha}{d_1} \simeq \frac{\sin\alpha}{d_2}$$

simplifies to

$$|\underset{\sim}{g}_{rot}| \simeq \frac{\alpha}{d_1} \simeq \frac{\alpha}{d_2} \qquad 4(8)$$

$$\therefore \quad |\underset{\sim}{g}_{n-p,r}|^2 = \left(\frac{d_1 - d_2}{d_1\ d_2}\right)^2 + \frac{\alpha}{d_1} \times \frac{\alpha}{d_2}$$

$$= \frac{(d_1-d_2)^2 + \alpha^2\ d_1\ d_2}{d_1^2\ d_2^2}$$

$$|\underset{\sim}{g}_{n-p,r}| = \frac{\left[(d_1-d_2)^2 + \alpha^2\ d_1\ d_2\right]^{\frac{1}{2}}}{d_1\ d_2} \qquad 4(9)$$

By definition the moire fringe spacings is given by

$$D_{n-p,r} = \frac{1}{|\underset{\sim}{g}_{n-p,r}|} = \frac{d_1\ d_2}{\left[(d_1-d_2)^2 + \alpha^2\ d_1\ d_2\right]^{\frac{1}{2}}} \qquad 4(10)$$

(Gejji and Holt 1975)

Using this formula rotation moire fringe spacings can be calculated.

This formula derived on the concept of "nearly parallel rotation" is the same as that given in "Electron microscopy of Thin Crystals" by Hirsch et al. (1965), page 358, but differs from the expression originally quoted by Basset et al. (1958) (see section 4.4.3).

From fig. 4.27, $$\tan\Theta = \frac{|\underset{\sim}{g}_{rot}|}{|\underset{\sim}{g}_{diff}|} \qquad 4(11)$$

and $\tan\theta \approx \tan 30^{o}$

Now $$|\underset{\sim}{g}_{rot}| = \tan\theta \times |\underset{\sim}{g}_{diff}| \qquad 4(12)$$

substituting for $|\underset{\sim}{g}_{rot}| = \frac{\sin\alpha}{d_1}$ and $|\underset{\sim}{g}_{diff}| = \frac{d_1 - d_2}{d_1 d_2}$ in the above equation 4(12) reduces to

$$\frac{\sin\alpha}{d_1} = \frac{d_1 - d_2}{d_1 d_2} \tan\theta$$

i.e.

$$\sin\alpha = \frac{d_1 - d_2}{d_2} \tan\theta \qquad 4(13)$$

But $\frac{\sin\alpha}{d_1} \approx \frac{\sin\alpha}{d_2}$, for small azimuthal rotations, therefore, also

$$\sin\alpha = \frac{d_1 - d_2}{d_1} \tan\theta \qquad \text{(Gejji and Holt 1975).}$$

From these formulae the azimuthal angle of rotation of one crystal over the other can be calculated from the known values of d_1, d_2 and θ.

In the present case, within the experimental error, $\theta = 30^{o}$ and d_1 and d_2 are the spacings of the Bragg reflecting $2\bar{2}0$ type planes in CdSe and Ge. The values of d_1 and d_2 can be calculated using the formula,

$$d_{hkl} = \frac{a}{(h^2 + k^2 + l^2)^{\frac{1}{2}}} \qquad 4(14)$$

in cubic system crystal structures.

$$\therefore \quad d_1 = \frac{6.077}{(2^2 + 2^2 + 0)^{\frac{1}{2}}} \qquad \because \text{ for CdSe lattice parameter } a = 6.077\text{Å and } hkl \equiv 0\bar{2}2$$

$$\text{and} \quad d_2 = \frac{5.6576}{(2^2 + 2^2 + 0)^{\frac{1}{2}}} \qquad \because \text{ for Ge lattice parameter } a = 5.6576\text{Å and } hkl \equiv 0\bar{2}2$$

substituting for θ, d_1 and d_2 in the above formula 4(13) and simplifying, we get

$$\sin\alpha = \sin 2^{\circ}\ 24'$$

$$\therefore \qquad \underline{\alpha = 2^{\circ}\ 24'} \qquad 4(15)$$

Hence the (111) CdSe grew in an orientation rotated about the [111] interface normal relative to the (111) Ge, through an azimuthal angle of $2^{\circ}\ 24'$.

Now the azimuthal angle of rotation $\alpha = 2^{\circ}\ 24'$ shows that $0\bar{2}2$ type planes in CdSe and Ge overlapping crystals have rotated from parallel alignment through this angle. Hence it was thought interesting to calculate the direction [hkl] in Ge, to which the $[0\bar{2}2]$ direction in CdSe is parallel.

The angle between directions $h_1\ k_1\ l_1$ and $h_2\ k_2\ l_2$ in cubic system crystals is given by

$$\cos\phi = \frac{h_1 h_2 + k_1 k_2 + l_1 l_2}{\left[(h_1^2 + k_1^2 + l_1^2)(h_2^2 + k_2^2 + l_2^2)\right]^{\frac{1}{2}}} \qquad 4(16)$$

By lengthy trial and error calculations it was found that the indices of the direction in Ge which was rotated 2^{o} 24' from the $[0\bar{1}1]$ direction would have to be as high as [11, 10, 0]. Thus the angle $\alpha = 2^{o}$ 24' does not appear to have any simple crystallographic significance, despite the crystallographic appearance of the 30^{o} angle of rotation of the moire spot arrays from their positions in a parallel epitaxial alignment pattern.

4.4.3 Observation of "Nearly-Parallel Rotation" Moire Fringes

In transmission electron microscopy an image of a specimen can be formed by the undeviated beam. This is called the bright field image of the specimen. Images can also be formed by a single electron diffracted beam. These are called dark field images. By allowing two coherent beams, i.e. the undeviated transmitted beam and one diffracted beam from the same area of a specimen to pass through the objective aperture, a periodic image can be formed. These periodic images in the form of fringes can be considered as a direct resolution of planes of atoms in the crystal. This direct resolution of crystal lattices in the form of periodic images, was first obtained by Menter (1956), in the case of specimens of metal organic compounds such as copper and platinum phthalocyanine with lattice spacings of 10-12 Å. The spacings of these periodic images was equal to the spacings between the crystal planes, giving rise to the diffracted beam. Further, the arrays of fringes formed were perpendicular

to the reciprocal lattice vector and hence parallel to the crystal planes resolved. Details of the observation of periodic images of crystal lattices are given by Menter (1957 and 1958).

Periodic images can also be observed in transmission electron microscopy when the electron beam is incident on overlapping crystal systems. This process of formation of crystal lattice periodic images does not depend upon the resolution limit of the microscope, unlike the process of direct resolution of crystal lattices. Therefore this process is called indirect lattice resolution, and the periodic images are called moire fringes. Such moire fringes were first observed by Mitsuishi et al (1951) in specimens of graphite.

In the direct resolution of crystal lattices, the image of the crystal lattice is formed by interference between the directly transmitted beam and the first order diffracted beam, whereas in the indirect resolution of crystal lattices, the image is formed due to the interference between the directly transmitted beam and the beam diffracted once by each of the superimposed lattices in succession. (Dowell et al 1956, 1957; Pashley et al 1957, Basset et al 1958, and Hashimoto and Uyeda, 1957).

Dowell et al. (1956, 1957) observed rotation moire fringes in fortuitously overlapping crystals of molybdenum trioxide (MoO_3), which were rotated about the interface normal. They gave a formula for the rotation moire fringe spacings,

$$D = \frac{d_1\ d_2}{\sqrt{d_1^2\ \alpha^2 + (d_2 - d_1)^2}} \qquad 4(17)$$

where α is the angle of rotation, and d_1 and d_2 are the spacings of Bragg reflecting planes.

Basset et al, (1958) observed rotation moire fringes, in (111) Au by placing one crystal on top of other. They gave a formula for the rotation moire fringe spacing,

$$D = \frac{d_1\ d_2}{(d_1^2 + d_2^2 - 2d_1\ d_2\ \cos\alpha)^{\frac{1}{2}}} \qquad 4(18)$$

which is different from the formula given by Dowell et al (1956).

Rotation moire fringes have not been observed hitherto in vacuum evaporated epitaxial films. In the present work rotation moire diffraction patterns and nearly-parallel rotation moire fringes have been observed for the first time. By treating the reciprocal lattice vectors, the formula for the nearly-parallel rotation moire fringe spacings was derived in the previous section and the formula is,

$$d_{n-p,r} = \frac{d_1\ d_2}{\left((d_1 - d_2)^2 + \alpha^2\ d_1\ d_2\right)^{\frac{1}{2}}} \qquad 4(10)$$

(Gejji and Holt 1975)

which is different from the above two formulae, but is that quoted by Hirsch et al (1965). Here d_1 and d_2 are the

spacings of the Bragg reflecting planes in CdSe and Ge respectively and α is the azimuth angle of rotation about the [111] heterojunction normal. $\alpha = 2^{o}\ 24'$ was obtained from the moire diffraction patterns using the formula $\sin\alpha = \frac{d_1 - d_2}{d_2} \tan\theta$ derived in the previous section.

The plane spacings d_1 and d_2 are calculated using the wellknown formula for cubic system crystal structures.

$$d = \frac{a}{(h^2 + k^2 + l^2)^{\frac{1}{2}}}$$ where a is the lattice parameter

and hkl are the miller-indices of the Bragg reflecting planes.

$$\therefore \quad d_1 = \frac{6.077}{(2^2 + 2^2 + 0)^{\frac{1}{2}}} \qquad \because \text{ for CdSe } a = 6.077\ \text{Å}, \quad hkl \equiv 0\bar{2}2$$

$$\text{and} \quad d_2 = \frac{5.6576}{(2^2 + 2^2 + 0)^{\frac{1}{2}}} \qquad \because \text{ for Ge } a = 5.657\ \text{Å}, \quad hkl \equiv 0\bar{2}2$$

Now $\alpha = 2^{o}\ 24' = 0.0419$ radian.

Substituting these values in the formula 4(10), "the nearly-parallel rotation" moire fringe spacing is calculated to be

$$D_{n-p,r} = 25.01\ \text{Å} . \qquad 4(19)$$

Figs. 4.28 and 4.29 show a typical transmission electron micrographs of CdSe/Ge (111) heterojunctions containing nearly-parallel rotation moire fringes. Such moire patterns and fringes were observed and recorded when the electron beam was incident on areas where the CdSe and the Ge had comparable



Fig. 4.28 Typical bright field transmission electron micrograph showing the nearly-parallel rotation moire fringes of CdSe/Ge (111) heterojunction. The CdSe was epitaxially grown on (111) Ge at 400°C.

Fig. 4.29

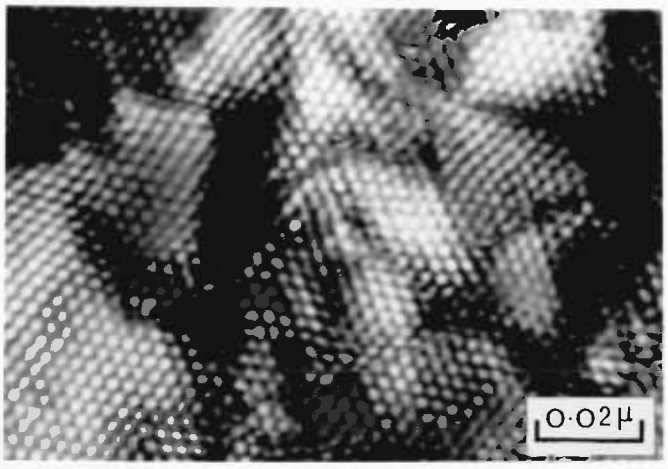


Fig. 4.30

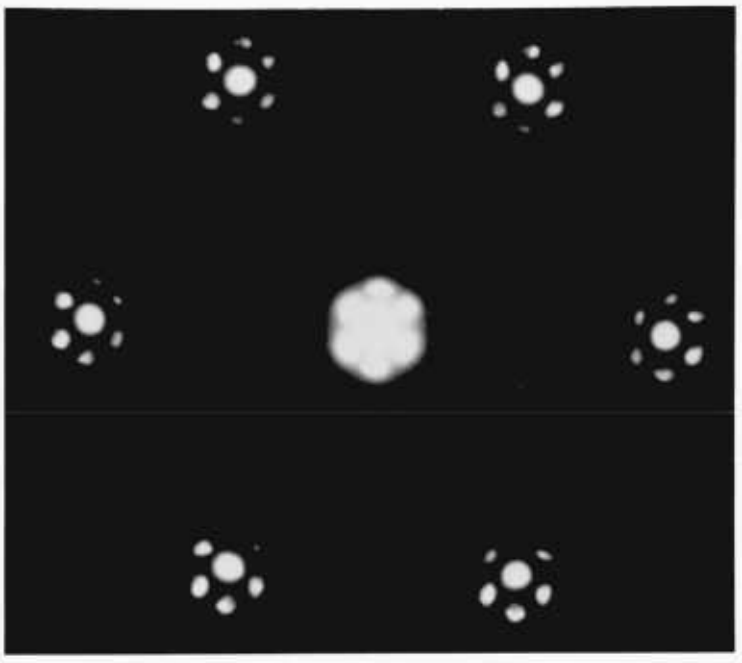


Fig. 4.29 Bright field micrograph of a CdSe/Ge (111) heterojunction showing all the three $2\bar{2}0$ type moire fringes. The CdSe was grown epitaxially on (111) Ge at 400°C.

Fig. 4.30 Nearly parallel rotation moire double diffraction pattern of a CdSe/Ge (111) heterojunction. The CdSe was epitaxially grown on (111) Ge at 400°C for 5 minutes.

thicknesses. A lengthy investigation was carried out to find the effect of film thickness on the azimuthal angular rotation ($\alpha = 2^{o}\ 24'$) and hence the moire fringe spacings. CdSe films were deposited on (111) Ge substrates, varying the time of deposition in steps of 15 seconds and holding the substrate temperature constant at $400^{o}C$, with all other growth parameters constant. The minimum deposition time was 15 seconds and maximum time of deposition was 5 minutes. In all these cases, the moire fringes were observed readily and the spacings were measured and found to be the same, about 25 ± 1 Å within the experimental errors. Thus the theoretically calculated, with $\alpha = 2^{o}\ 24'$, and experimentally measured spacings of moire fringes were in good agreement. The most significant observation was that the hexagonal arrays of moire diffraction spots were always found to be rotated through 30^{o}, from their positions in parallel alignment as shown in fig. 4.30. These experimental facts established that the CdSe and Ge crystals were rotated relatively about the [111] heterojunction normal though $2^{o}\ 24'$, from parallel alignment.

The densities of dislocations in all the films grown at different deposition times, were determined by counting the number of extra half moire fringes in the micrographs and are listed in the following table 4.1. It is seen that the density of dislocations is the same within experimental error in all cases and is about $1.5 \times 10^{11}/cm^{2}$. In gold and palladium superposed epitaxial films, the density of dislocation

Table 4.1

T.E.M. Plate No.	Time of Film Growth	Substrate Temp.	Density of Dislocation
2885	45 seconds	400°C	$1.533 \times 10^{11}/cm^2$
3924	1 minute	400°C	$1.561 \times 10^{11}/cm^2$
3951	1½ minutes	400°C	$1.590 \times 10^{11}/cm^2$
3584	1¾ minutes	400°C	$1.572 \times 10^{11}/cm^2$

was about 10^{11} (Basset et al 1958).

The calculation of the misfit δ between CdSe and Ge is given below.

$$\delta = \frac{2(a-b)}{a+b} \qquad \text{(Sec. 2·6; Chapter II)}$$

where a and b are the lattice parameters of CdSe and Ge respectively.

$$\therefore \quad \delta = \frac{2(6.077 - 5.6576)}{6.077 + 5.6576} \qquad \because \quad a = 6.077\ A^{o}.$$

$$= \frac{0.4194}{5.8673} \qquad \text{and} \quad b = 5.6576$$

$$\therefore \quad \delta = 0.0715$$

$$= 7.15\%$$

4.4.4 Observation of Misfit Dislocations in CdSe/Ge (111) Heterojunctions

The epitaxial CdSe films were grown on (111) faces of Ge for 3 minutes, which was double the deposition time for epitaxial studies reported in previous sections. The idea of growing the thicker films was to etch the CdSe films to a suitable thickness for resolving crystal defects.

The chemical etchant consisted of potassium permanganate ($KMnO_4$) dissolved in concentrated sulphuric acid (H_2SO_4). Potassium permanganate was added to sulphuric acid until the colour of the chemical solution became dark green. This

chemical reagent was used for etching CdS, ZnS and ZnSe by Rowe and Forman (1968). One advantage of this chemical reagent was that it needed no heating for reaction to take place and this etchant did not chemically attack or etch Ge.

CdSe/Ge (111) heteroepitaxial specimens were dipped in the chemical solution contained in a beaker. The time of etching was 8 seconds. Immediately the specimens were transferred to a second beaker containing concentrated H_2SO_4 to rinse and then they were transferred to third beaker containing distilled water for a final wash.

Immediately the specimens were transferred to and firmly held by Lacomit in the groove of the electro-chemical jet thinning specimen holder. The germanium side was thinned through as explained in section 3.4, chapter III.

The characteristic feature of bright field micrographs like that shown in fig. 4.31 were the equilateral triangular etch pits. The form of these etch pits was consistent with the symmetry of the (111) orientation of the cubic sphalerite structure of the films. Fig. 4.32 shows a (111) diffraction pattern of the same CdSe film. The observation of misfit dislocations in these CdSe/Ge(111) heterojunctions is given below.

Misfit dislocations were observed in CdSe/Ge(111) nearly-parallel rotation heteroepitaxial interfaces. Fig. 4.33 is a bright field transmission electron micrograph. One set of misfit dislocations with their lines parallel can be seen. The spacings of the misfit dislocations was measured to be about 50 ± 5 Å. These misfit dislocations were the first to be observed in nearly-parallel rotation epitaxial inter-

Fig. 4.31

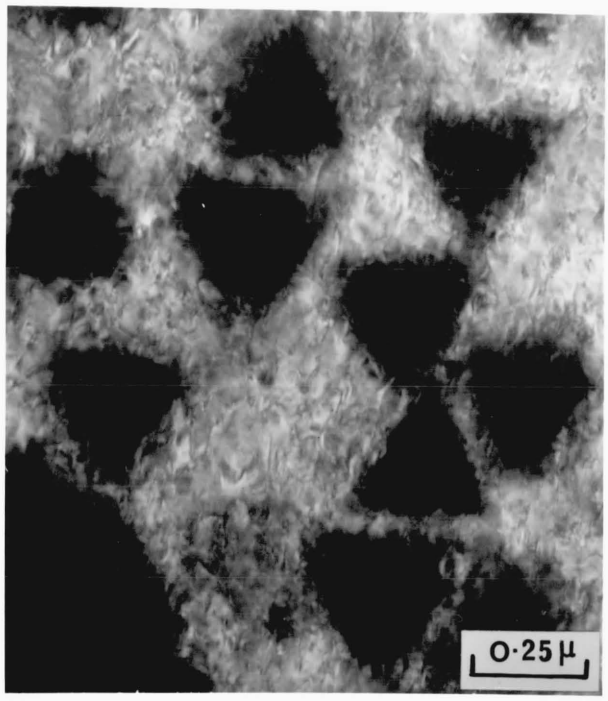


Fig. 4.32



Fig. 4.31 Typical bright field micrograph of a CdSe film grown on (111) Ge at 400°C for 3 minutes and chemically polished for 8 seconds. Triangular etch pits can be seen.

Fig. 4.32 Corresponding selected area transmission electron (111) diffraction pattern of the same CdSe film.

Fig.
4.33

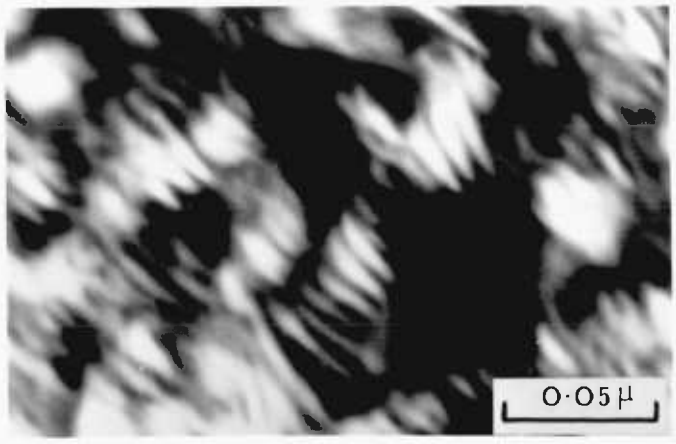


Fig.
4.34



Fig. 4.33 Bright field micrograph of a CdSe/Ge (111) heterojunction. The CdSe was grown on (111) Ge at 400°C. for 3 minutes and then chemically polished for 5 seconds. A set of parallel 60° dislocations can be seen.

Fig. 4.34 Bright field micrograph of a CdSe/Ge (111) heterojunction. The CdSe was grown on (111) Ge at 400°C. 60° misfit dislocations are indicated by arrows. It is seen that 60° misfit dislocations are parallel to $2\bar{2}0$ type moire fringes.

faces and the first to be observed in heterojunctions of II-VI films on IV substrates. Misfit dislocations were observed for the first time in semiconductors in PbS/PbSe epitaxial interfaces by Matthews (1961). Such misfit dislocations were also observed in gold on palladium by Matthews (1964, 1966), in copper on nickel by Matthews and Crawford (1970), in PbSe on PbS, Matthews (1971) and Yagi et al. (1971) and in palladium on gold by Cherns and Stowell (1973). In all these cases there was a parallel alignment between the film and the substrate.

The spacings of the nearly-parallel rotation moire fringes were measured and found to be about 25 Å (sections 4.4.2 and 4.4.3). These moire fringes were formed by the interference between the undeviated beam and a beam which had undergone two diffractions of the $2\bar{2}0$ type in the overlapping CdSe and Ge crystals. Hence the spacing of the nearly-parallel rotation interfacial misfit dislocations was found to be twice the nearly-parallel $2\bar{2}0$ type moire fringes.

This is as if the misfit dislocations shown in figs. 4.34 and 4.33 were moire fringes formed by interference between $1\bar{1}0$ type electron beams diffracted by $1\bar{1}0$ Bragg diffracting planes in CdSe and Ge overlapping crystals. But $1\bar{1}0$ type reflections are not allowed in diamond structure Ge or in sphalerite structure CdSe crystals by the structure factor. Fig. 4.34 is a bright field micrograph containing both misfit dislocations and moire fringes. It is clear from the figure that the spacing of the misfit dislocations is twice the spacing of the $2\bar{2}0$ type moire fringes and the misfit dis-

locations are found to be parallel to $2\bar{2}0$ type moire fringes. These facts established that the observed lines shown in figs. 4.33 and 4.34 were not moire fringes.

The misfit dislocations run in the (111) interface plane and their lines along one of the three $\langle 1\bar{1}0\rangle$ directions in the (111) plane between the CdSe and Ge crystals. The Burgers vectors are presumably of the form $\frac{a}{2}\langle 1\bar{1}0\rangle$, also lying in the (111) interface plane. Hence the two most likely possibilities are that the Burgers vector is parallel to the dislocation line direction and the misfit dislocations are pure screw or if the Burgers vector makes a 60^{o} angle with the $[1\bar{1}0]$ line direction the misfit dislocations are mixed screw-edge type. As a change in lattice parameter in parallel orientation results in edge type misfit dislocations, whereas screw dislocations are involved in a twist boundary; the 60^{o} misfit dislocation case seems to be more reasonable and is discussed below.

The lattice parameter of the deposited CdSe (6.077 Å) is greater than that of the substrate Ge (5.6576 Å). Hence it is expected that the CdSe lattice should be compressed. This is because the CdSe film is very thin in comparison. However the accomodation of the misfit by lattice strain does not seem to be significant because the spacings of the observed and calculated (section 4.4.3) nearly-parallel rotation moire fringes is about the same 25 Å. Hence the accommodation of the misfit between the CdSe film and the Ge substrate seems to be by means of misfit dislocations which also rotated the

CdSe through $2^{o}24'$ to produce an interfacial energy minimum in that nearly-parallel rotation orientation. That this could be the case is shown below.

Consider a 60^{o} dislocation as shown in fig. 4.35. The edge component of the Burgers vector is equal to $\underline{b}\sin 60^{o}$. Where $\underline{b}$ is the Burgers vector.

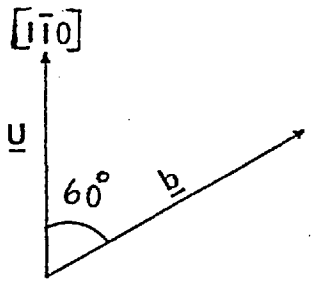


Fig. 4.35 Showing the 60^{o} misfit dislocation.

When coherency is completely lost the spacing p of the dislocations is given by the Brooks (1952) formula

$$p = \frac{|\underline{b}|}{\delta} \qquad \text{--------4(20)}$$

where $\underline{b}$ is the Burgers vector of the edge oriented dislocations and δ the misfit in an interface in parallel alignment.

Let us assume that the spacings of the mixed 60^{o} misfit dislocations can be given by an extension of the Brooks formula. This may be defined as the ratio of the edge component of the Burgers vector to the misfit in an interface.

Then the spacings of the mixed misfit dislocation is given by

$$p = \frac{|\underline{b}|\sin 60}{\delta} = \frac{|\underline{b}|\sin 60}{\dfrac{2(d_1-d_2)}{(d_1+d_2)}}$$

or

$$p = \frac{|\underline{b}|\sin 60}{2(d_1-d_2)} \times (d_1+d_2) \qquad 4(21)$$

where the misfit

$$\delta = \frac{2(d_1-d_2)}{(d_1+d_2)}$$

and d_1 and d_2 are the lattice repeat distances in the two crystals along crystallographic directions in the interface.

The rotation produced by the screw dislocations in a twist boundary is given by

$$\alpha = 2 \sin \frac{\alpha}{2} = \frac{|\underline{b}|}{p} \quad \text{(Read 1953)}$$

for small values of α.

or
$$p = \frac{|\underline{b}|}{2 \sin \frac{\alpha}{2}} \qquad 4(22)$$

The assumed 60^0 mixed dislocation has a screw component of Burgers vector equal to $\underline{b} \cos 60^0$. Let us assume that the spacings of the mixed 60^0 misfit dislocations can be given by an extension of Read's formula. On this assumption the spacings of the misfit dislocations is given by

$$p = \frac{|\underline{b}| \cos 60}{2 \sin \frac{\alpha}{2}} \qquad 4(23)$$

if α is small, which is the case for any nearly-parallel rotation orientation relation (section 4.4.2).

$\therefore$ From 4(21) and 4(23)

$$|\underline{b}| \sin 60 \, \frac{(d_1+d_2)}{2(d_1-d_2)} = \frac{|\underline{b}| \cos 60}{2 \sin \frac{\alpha}{2}}$$

$$\therefore \quad \text{Sin } \frac{\alpha}{2} = \frac{\cos 60^{o}}{\sin 60^{o}} \times \frac{d_1 - d_2}{d_1 + d_2}$$

$$\sin \frac{\alpha}{2} = \frac{d_1 - d_2}{d_1 + d_2} \cot 60^{o} \qquad 4(24)$$

For small angles, $\sin \frac{\alpha}{2} \simeq \frac{\alpha}{2}$ and

$$\frac{\alpha}{2} = \frac{d_1 - d_2}{d_1 + d_2} \cot 60^{o} \qquad 4(25)$$

$$\alpha = \frac{2(d_1 - d_2)}{d_1 + d_2} \cot 60^{o}$$

$$\underline{\alpha = \delta \cot 60^{o}} \qquad 4(26)$$

The lattice parameter misfit was calculated to be (section 4.4.3) $\delta = 0.0715$ and $\cot 60^{o} = \frac{1}{\sqrt{3}}$.

Substituting these in expression 4(26) we get

$$\alpha = 0.0419 \text{ radian}$$

$$\therefore \quad \alpha = 2^{o}\ 24'$$

which is the azimuthal angle of rotation of the (111) CdSe relative to the (111) Ge about the [111] heterojunction normal. The value of α calculated here on the 60^{o} dislocation model agrees well with the value of α derived on a reciprocal lattice treatment (section 4.4.2) from the experimental moire diffraction patterns (4.4).

For CdSe, $d_1 = \frac{6.077}{\sqrt{2}}$ where $hkl \equiv 0\bar{1}1$

and for Ge, $d_2 = \frac{5.6576}{\sqrt{2}}$ where $hkl \equiv 0\bar{1}1$

and assuming for $\underline{b} = \frac{a}{2}\langle 110\rangle = \frac{a}{\sqrt{2}} = \frac{6.077}{\sqrt{2}} \simeq \frac{5.6576}{\sqrt{2}}$

substituting these in formula 4(21) gives $p = 50.21$ Å . This is in good agreement with the observed spacings. This suggests that the dilatational misfit at the CdSe/Ge(111) heterojunction was essentially all accommodated by edge component of the 60° dislocations.

From expression 4(23)and the experimental value of $\alpha = 2^{\circ}\ 24'$ the average spacing for the screw components of the misfit dislocations is calculated to be about $p = \frac{\underline{b} \cos 60^{\circ}}{2 \sin \frac{\alpha}{2}} =$ 49.6 Å .

This suggests that the screw component of the 60° dislocation was responsible for the rotation of the CdSe film on (111) face of Ge through $2^{\circ}\ 24'$.

Thus the 60° dislocation model explains all the experimentally observed nearly-parallel rotation phenomena.

CHAPTER V

ANNEALING OF CdSe EPITAXIAL FILMS

Epitaxial films of CdSe were grown by focussed electron beam evaporation in vacua in the 10^{-6} torr range on the three singular faces of Ge as reported previously by Gejji and Holt (1975) and as described in chapter III, section 3.3. The CdSe material used in this work was the same as that used for the earlier structural studies. The substrate perparation was the same as described in chapter III, section 3.2. All heterojunctions were prepared at 380°C and 400°C.

Annealing of CdSe/Ge(100), CdSe/Ge(110) and CdSe/Ge(111) heterojunctions was carried out in pyrex and quartz ampoules 6 to 8 cms long and 1 to 1½ cm diameter. In the case of pyrex ampoules the annealing temperature was 600°C, and in the case of quartz ampoules, 700, 800 or 900°C. The times of annealing were 2 to 3 and 10 hours with immediate cooling or slow cooling of about 8 to 12 hours. The ampoules were evacuated to 10^{-3} torr. The annealing of these heterojunctions was done in the presence of small quantity of CdSe powder in the ampoules. The annealing results ended in failure. Always the substrate surfaces were found to be pitted very badly showing a type of chemical reaction between the germanium substrates, the CdSe film and the gases like oxygen present in the ampoules. Hence it was decided to anneal at high vacuum to reduce the oxygen reaction with the substrate and the film. Annealing was done in the same vacuum system

in which the heterojunctions were prepared, and in which CdSe vapour was an important constituent of the residual gas.

For this purpose four CdSe/Ge(110) heteroepitaxial specimens were grown at 380°C. After they had been removed from the vacuum chamber, the substrate holder and the substrate heater assembly were outgassed at 900°C, before the specimens were reinserted for annealing. This was done in order to minimise contamination from the previous growth run.

Immediately the germanium sides of the specimens were thinned one after the other by electrochemical jet thinning as described in chapter III, section 3.4. A small area of the CdSe film alone suitable for transmission electron microscopy examination, was always found to be present at the bottom of the thinned dimple. Each of these specimens were inserted into one of the four depressions of the substrate holder, very carefully so that the CdSe films were not damaged.

When the pressure in the vacuum chamber was about 10^{-5} torr the specimens were annealed at 500°C for 50 minutes. The substrate heater coil was then switched off.

The specimens were removed carefully, so that they should not be damaged; from the vacuum chamber, when they had cooled to room temperature. Transmission electron microscopy studies of the specimens were carried out in Philips EM 301. These studies showed that the planar faults of the domain-form structure of CdSe (110) films were annealed out and the domain boundaries were found to be characteristic antiphase domain boundaries as will be shown below. Hence it is

thought worthwhile to consider (1) the geometry of antiphase boundaries and (2) the method of observing them (Holt 1969b and Blank et al. 1964) before proceeding to the explanation of the experimental results.

The polarity of II-VI compounds has been dealt with in chapter I, section 1.4. II-VI compounds and III-V compounds crystallise in the sphalerite and wurtzite structures. There is a polarity in the [111] direction in sphalerite and in the [0001] direction in the wurtzite structure, as can be seen from figs. 1.4 and 1.5 (chapter 1 section 1.3). That is, the sphalerite and wurtzite structures are non-centrosymmetric. Here we consider only the sphalerite structure because CdSe grew epitaxially on all the three faces of Ge with the cubic sphalerite structure.

Figure 5 shows a face centred cubic cell of the sphalerite structure, drawn with solid lines. Part of another face centred cubic interpenetrating array is shown by the dotted lines. The pairs of atoms connected by arrows are the basis of the structure. The sphalerite structure characteristic of most of the important II-VI and III-V compounds is an ordered superlattice.

It is seen in fig. 5 that each of the elements of the compound with this structure occupies the sites of an f.c.c. sublattice. Each sublattice is displaced by a quarter of a body diagonal of the f.c.c. structure cell from the sites of the other sublattice. It is possible either for A atoms of

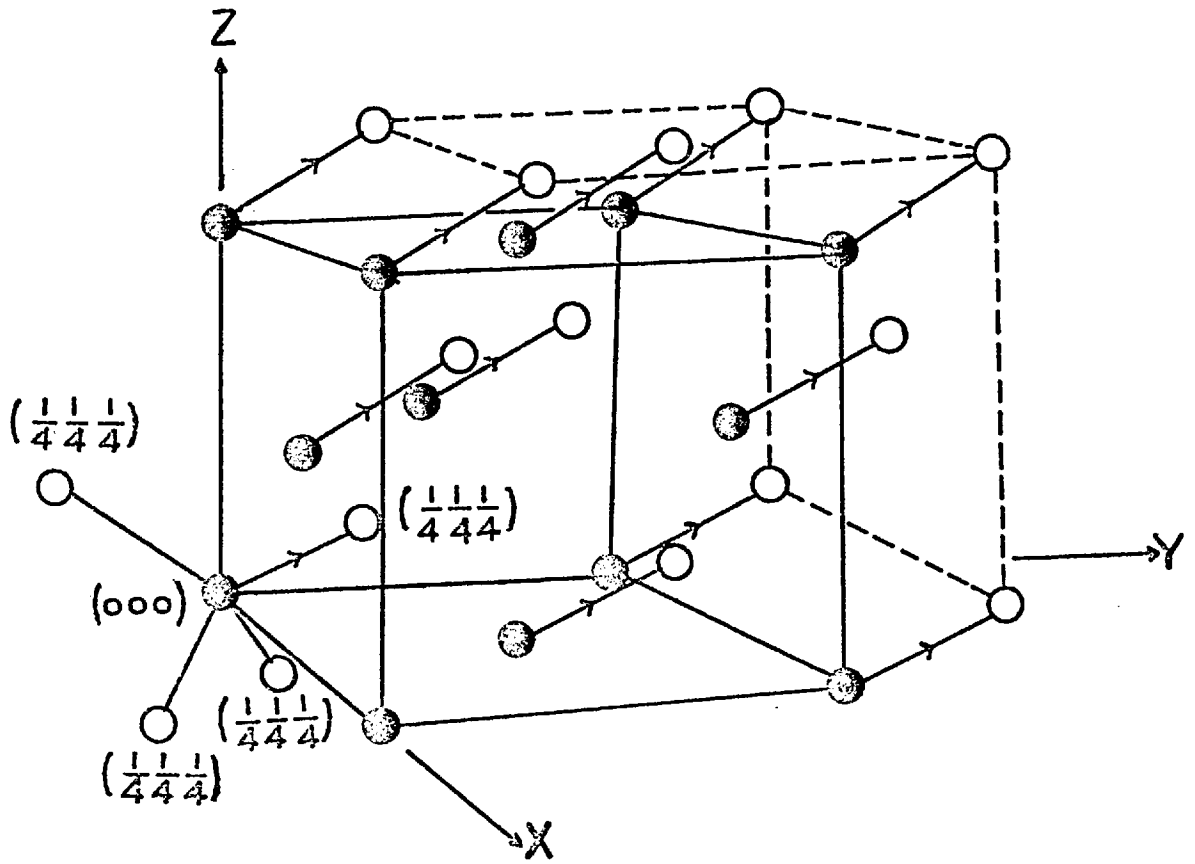


Fig. 5 A f.c.c. unit cell of the sphalerite structure is drawn with fine solid lines. Part of another face centred cubic unit cell is shown by dotted lines. The latter cell is occupied by white atoms displaced by ¼, ¼, ¼ in terms of the lattice parameter along the three crystallographic axes from the black atoms of the first unit cell. The co-ordinates are given for the four white atoms to which the black atom at the origin is bonded. The pairs of atoms connected by arrows are the basis of the structure.

the lower valence element in the compound to occur on the (000) (black atom) sites of fig. 5 and B atoms of higher valence element in the compound on the $(\frac{1}{4}\frac{1}{4}\frac{1}{4})$ (white atom) sites or for the A atoms to occupy the $(\frac{1}{4}\frac{1}{4}\frac{1}{4})$ sites and B atoms to occupy (000) sites. Changing from the one occupation scheme to the other creates antiphase domains between which polarity is reversed as shown for example in fig. 5.1. The interface between antiphase domains is an antiphase boundary (APB). In fig. 5.1 it can be seen that the nature of the top surface of the material changes across antiphase boundaries. Hence the presence of APBs changes a surface from (111) A type to $(\bar{1}\bar{1}\bar{1})$ B type. Bobb et al. (1966) and Wilson (1966) and Rozgoni and Foster (1967) showed evidence of the existence of such polarity reversal domains; i.e. antiphase domains in GaAs with the sphalerite structure, in CdS with the wurtzite structure, and in polycrystalline CdS bulk crystals and thin films respectively.

It is seen in fig. 5.1(a), (b) and (c) that one type of site is occupied by A atoms and the second type of site is occupied by B atoms (in one domain). On the other side of the boundary, the first type of site is occupied by B atoms and the second type of site by A atoms (antiphase domain). It follows that across an APB neighbouring sites are occupied by like atoms and the bonds connecting like atoms across an APB are wrong high energy bonds.

In the sphalerite and wurtzite structures there are only two sets of sublattice sites and only two ways in which

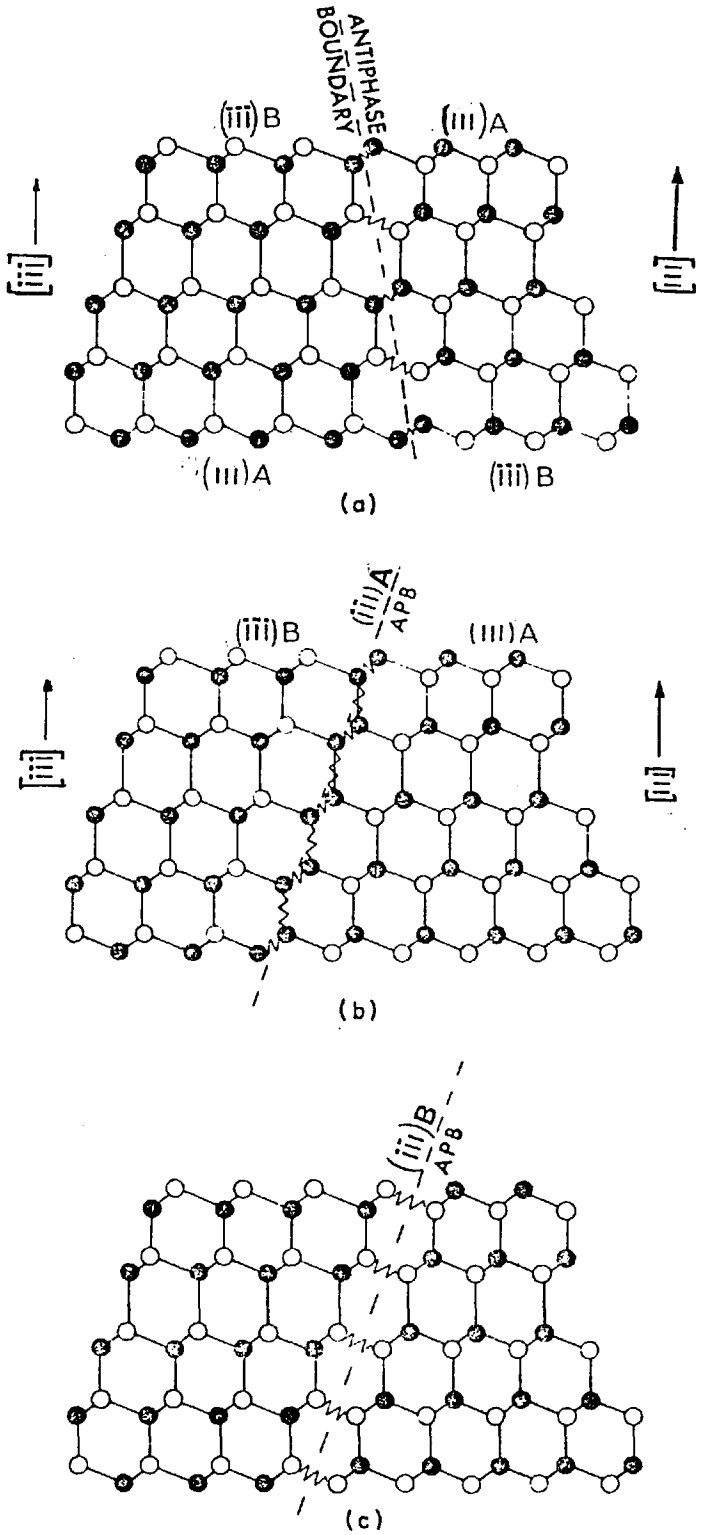


Fig. 5.1(a),(b), and (c). Antiphase boundaries in the sphalerite structure seen in projection on the $(1\bar{1}0)$ plane. In these figures zig-zag lines denote wrong bonds. (a) Shows a type I APB. (b) and (c) Illustrate type II APBS. **(Holt, 1969)**

they can be occupied. Hence APBs in this structure are incapable of forming a metastable foam structure (Flinn 1960). That is, three domains can not be in contact because there are only two ways in which the sublattice sites can be occupied. Two of the hypothetical three domains must have the same occupation and no APB separates them. It follows that three domains cannot be in contact, i.e. two APBs cannot intersect. That is APBs are closed surfaces or emerge at free surfaces of crystalline materials. Thus the domain structure in single crystals with the sphalerite structure can only take the form of a matrix of one domain type containing domains of the other type in the form of included volumes. Such structures were observed by etching GaAs and CdS by Bobb et al. (1966) and Wilson (1966) respectively as indicated above. Such a substructure is unstable and at elevated temperatures will tend to anneal out, eliminating high energy APBs. This was shown by Wilson (1966) in the case of CdS.

Holt (1969b) classified APBs into two types, APBI and APBII (by considering a translating lattice vector). Fig. 5.1(a) shows a type APBI wherein the wrong bonds connecting across an APB involve atoms of elements forming the compound in equal number. It follows that existence of an APBI type, does not affect the stoichiometry of the compound. Figs. 5.1(b) and (c) show APB of type II. Atoms and wrong bonds of one type only are involved across such an APB. In this case there are more of one kind of atoms than of the other in

the material. Hence APBII type boundaries can affect and can be affected by deviations from stoichiometry. More details on the geometry of antiphase boundaries in the sphalerite structure are given by Holt (1969b). Hence without going into these details the method of observation of APBs is given below.

The crystal structures of II-VI compounds have been dealt with in chapter I section 1.2-1.3. The face centred cubic sphalerite unit cell contains 8 atoms. The positions of the atoms in the sphalerite structure compounds may be given in terms of their co-ordinates in an f.c.c. unit cell (shown in fig. 5) as A atoms at $U_AV_AW_A$ = 000, $\frac{1}{2}\frac{1}{2}0$, $\frac{1}{2}0\frac{1}{2}$ and $0\frac{1}{2}\frac{1}{2}$ and B atoms at $U_BV_BW_B$ = $\frac{1}{4}\frac{1}{4}\frac{1}{4}$, $\frac{3}{4}\frac{3}{4}\frac{1}{4}$, $\frac{3}{4}\frac{1}{4}\frac{3}{4}$ and $\frac{1}{4}\frac{3}{4}\frac{3}{4}$. Substituting these values into the expression for the structure factor for hkl reflections

$$F_{hkl} = \sum_{UVW's} fe^{2\pi i(hU+kV+lW)} \qquad 5(1)$$

which can be simplified to the expression

$$F_{hkl} = \left[f_A + f_B\, e^{\frac{\pi}{2}i(h+k+l)}\right]\left[1 + e^{\pi i(h+k)} + e^{\pi i(h+l)} + e^{\pi i(k+l)}\right] \qquad 5(2)$$

where f_A and f_B are the atomic scattering factors for the two constituent elements of the compound. The second term in the structure factor is that for the f.c.c. space lattice

and is equal to zero when h, k and l are mixed even and odd integers and is equal to 4 when h, k and l are all even or all odd. The first term is the basis structure factor. For permitted reflections (H, k and l all even and all odd) therefore

$$F_{hkl} = 4\ f_A + f_B\ e^{\frac{i\pi}{2}(h+k+l)} \qquad 5(3)$$

which represents both the phase and the amplitude of the reflected wave. Hence there are four cases of permitted reflections in the sphalerite structure i.e. when h+k+l = 4n, 4n+1, 4n+2 and 4n+3, so that the structure factor F_{hkl} = $4(f_A+f_B)$, $4(f_A+if_B)$, $4(f_A-f_B)$ and $4(f_A-if_B)$ respectively. In the third case i.e. when h+k+l = 4n+2 and $F_{hkl} = 4(f_A-f_B)$ the type of reflection is superlattice while in the other three cases the reflections are fundamental.

The effect of interchanging the occupation of the sub-lattice sites across an APB is to interchange f_A and f_B in the structure factor. In case of H+k+l = 4n, f_A+f_B becomes, f_B+f_A. This does not involve either phase change or amplitude change and therefore no APB contrast arises in dark field electron micrographs using such reflections for imaging. In the case of h+k+l = 4n+1, f_A+if_B becomes f_B+if_A, which involves a phase change but does not change the amplitude.

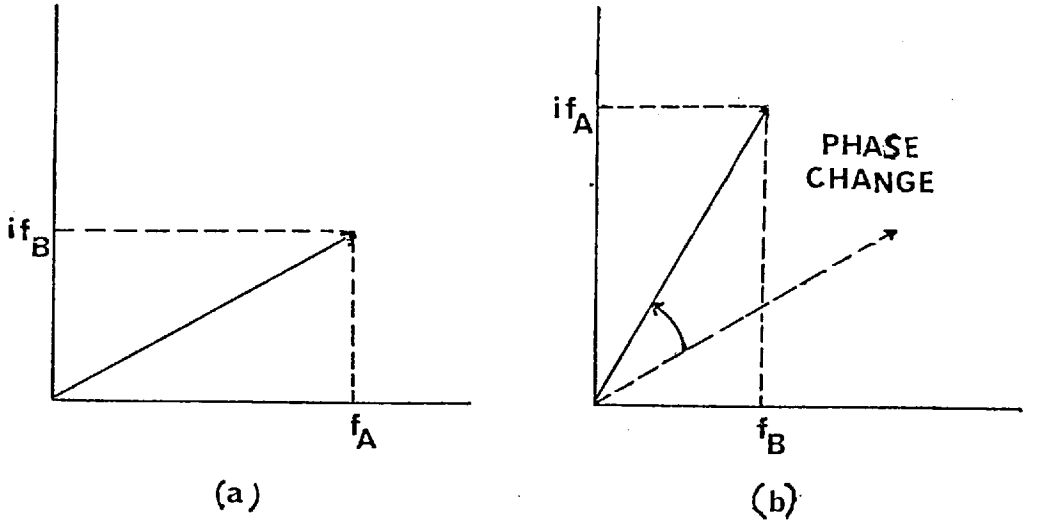


Fig. 5.2 (a) and (b) show the phase change in the case of h+k+1 = 4n + 1.

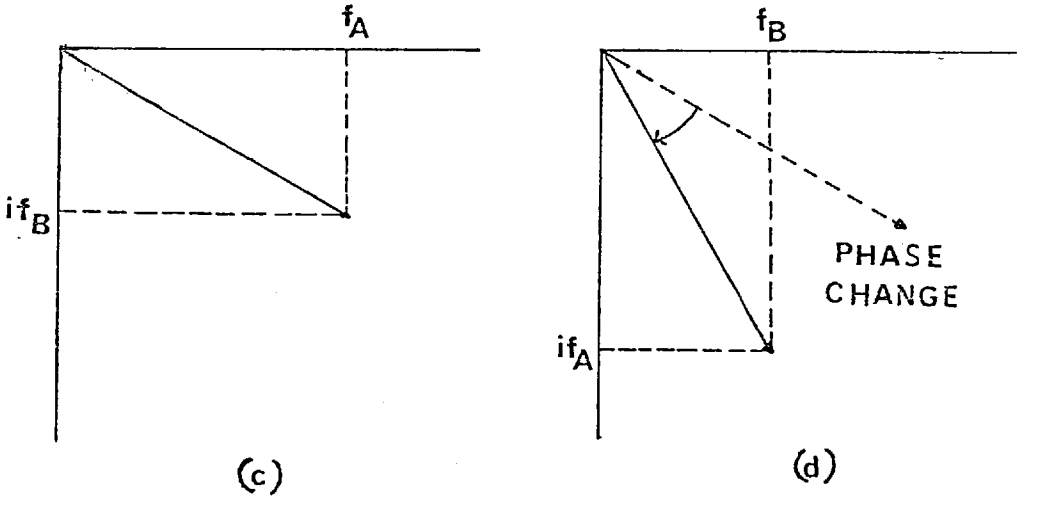


Fig. 5.2 (c) and (d) show the phase change in the case of h+k+1 = 4n + 3.

From fig. 5.2(a) and (b), the magnitude of APB phase change is given by $\tan^{-1}\frac{f_A}{f_B} - \tan^{-1}\frac{f_B}{f_A}$. This phase change depends upon the relative magnitudes of f_A and f_B and therefore varies from one compound to another. Hence APB contrast arising in dark field micrographs using such reflections for imaging varies from one compound to another. In the case of h+k+l = 4n+3, $f_A - if_B$ becomes $f_B - if_A$. This does not involve an amplitude change, but involves a phase change with the sign being reversed. From fig. 5.2(c) and (d) the magnitude of the APB phase change is given by $\tan^{-1}\frac{f_A}{f_B} - \tan^{-1}\frac{f_B}{f_A}$. In this case also APB contrast depends on the compound. In the case of h+k+l = 4n+2, $f_A - f_B$, becomes $f_B - f_A$, across an APB. In this superlattice case, the reflections undergo a phase change of π across an APB. Strong APB contrast occurs in dark field micrographs using such superlattice reflections for imaging. The reflections permitted by the sphalerite structure factor together with the reflection case for APB contrast are listed in the following table 5.1.

Diffraction contrast theory applied to the case of antiphase boundaries (APBs) in the sphalerite structure as outlined above predicts that they will be visible in dark-field transmission electron micrographs taken using superlattice reflections such as 200 and 222 and fundamental reflections such as 111, 311 and 331, but invisible in dark-field transmission electron micrographs taken using the fundamental reflections such as 220 and 400. The experimental results are presented below.

Table 5·1

Permitted Reflections hkl	h+k+l	$h^2+k^2+l^2$	Type of reflections	APB contrast
111	4n+3	3	Fundamental	D.O.C. (Depends on compound)
200	4n+2	4	Superlattice	Strong
220	4n	8	Fundamental	0
311	4n+1	11	Fundamental	D.O.C.
222	4n+2	12	Superlattice	Strong
400	4n	16	Fundamental	0
331	4n+3	19	Fundamental	D.O.C.
420	4n+2	20	Superlattice	Strong

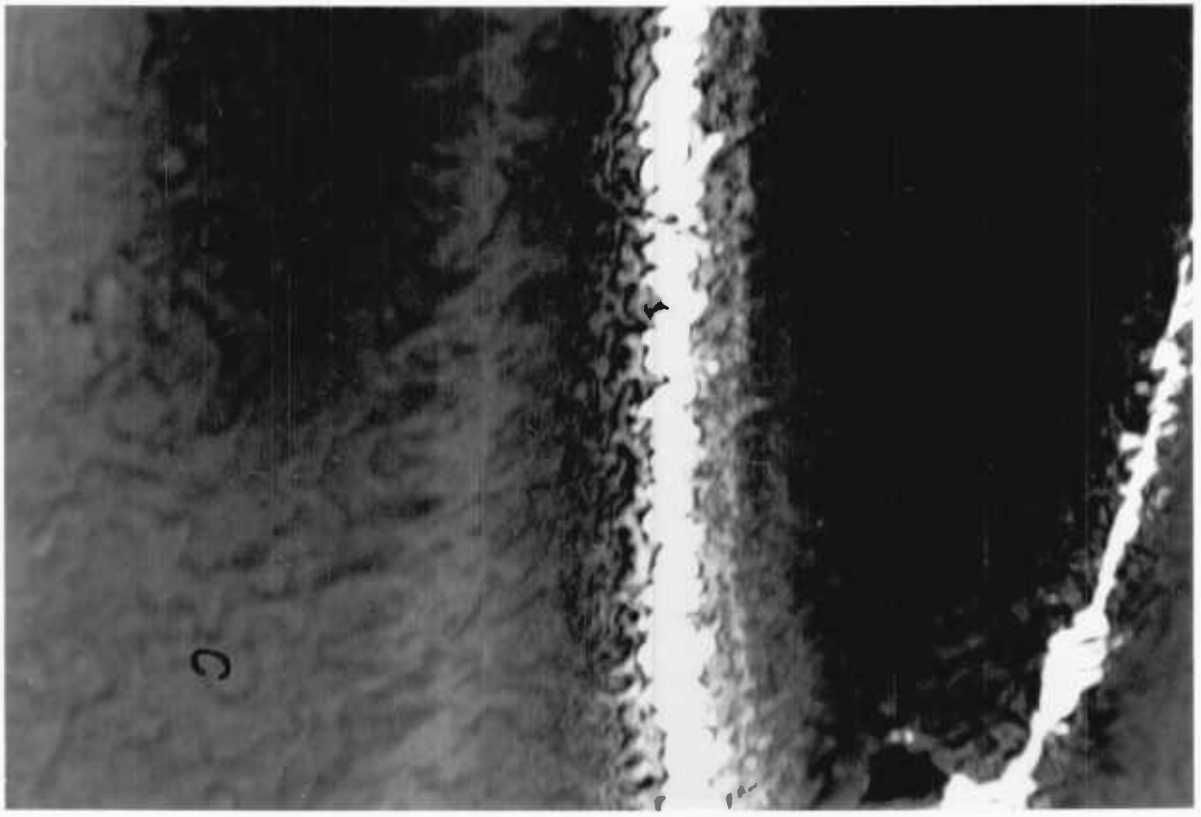


Fig. 5.3 (a) Dark field transmission electron micrograph of an area of a film of CdSe grown on (110) Ge at 380°C and annealed at 500°C for 50 minutes. This micrograph was recorded using 002 superlattice reflection for imaging. For comparison three particular domains are marked A. B. and C. The "horse with a halo" shaped domains at A should be particularly easy to recognise.

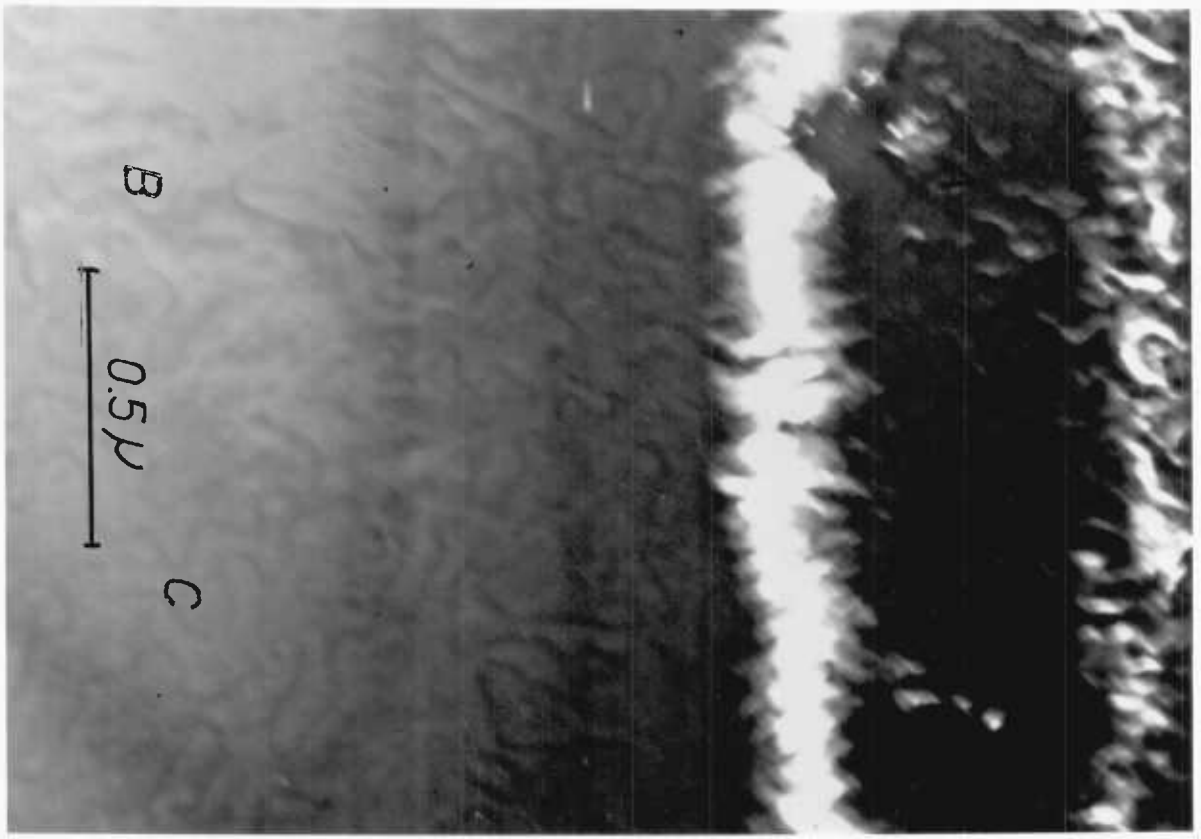


Fig. 5.3 (b) Dark field transmission electron micrograph of the same area of the CdSe film as shown in (a). This was recorded using 222 super lattice reflection for imaging. The three same particular domains marked A, B and C are visible.

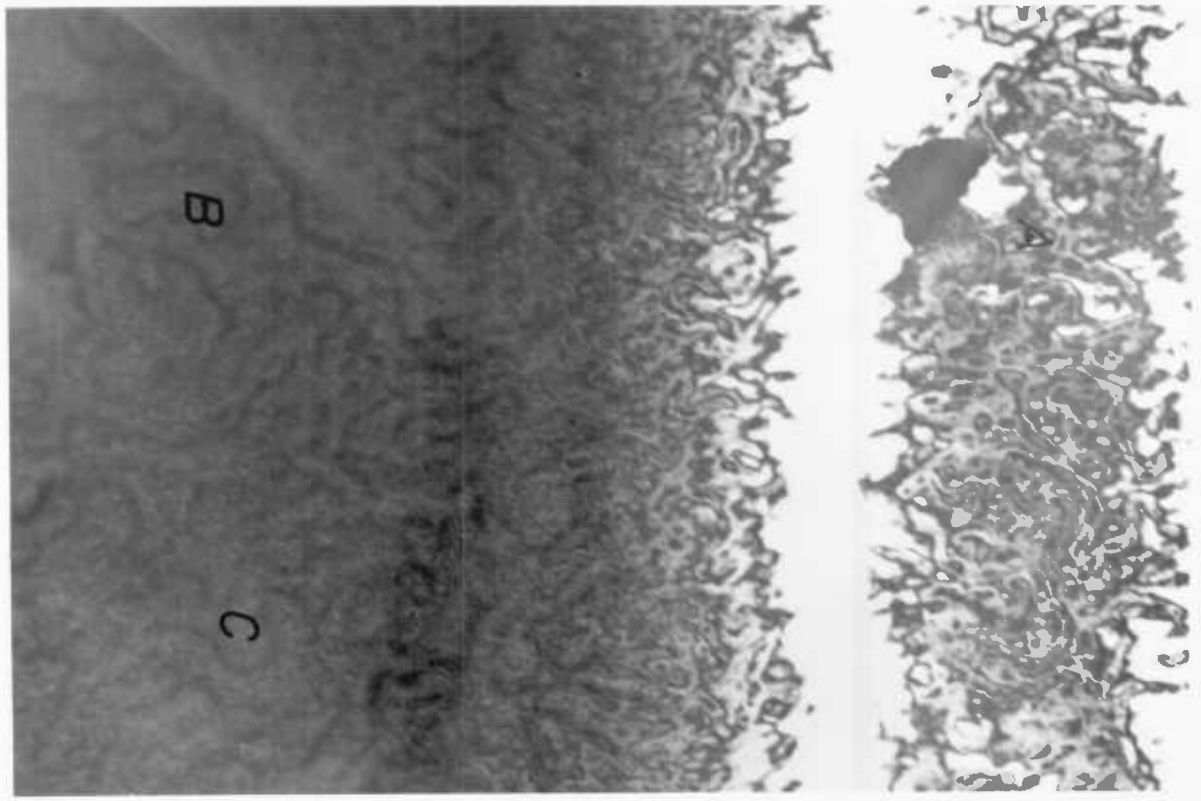


Fig. 5.3 (c) Dark field transmission electron micrograph of the same area of the same CdSe film as shown in (a). This micrograph was recorded using (111) fundamental reflection for imaging; the three same particular domains marked A, B and C are visible.

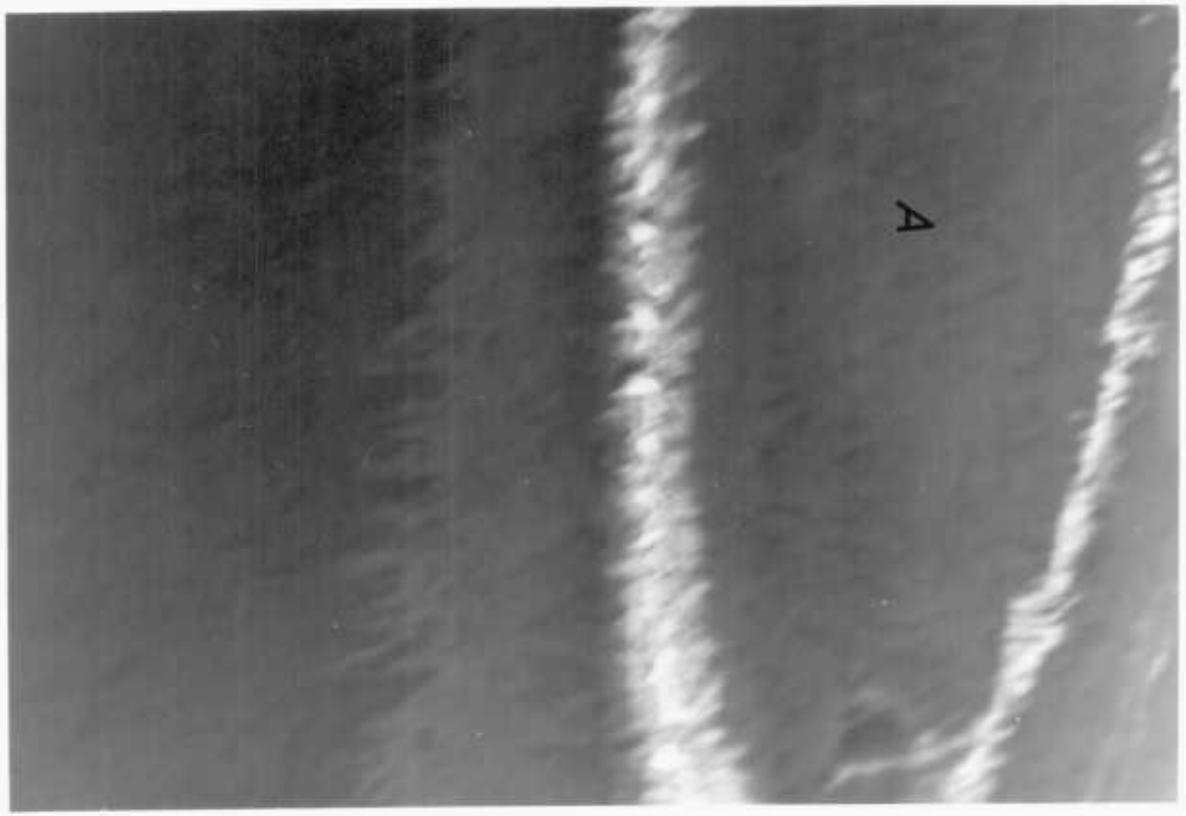


Fig. 5.3 (d) Dark field transmission electron micrograph of the same area of the same CdSe film as shown in (a). This micrograph was recorded using 004 fundamental reflection for imaging. The boundary at A is still faintly visible on one side of the 004 - $00\bar{4}$ bend extinction contour but all those in the region between B and C are completely out of contrast on the other side of the contour where the diffraction contrast conditions are well satisfied.

Fig. 5.3(a) shows the typical dark field transmission electron micrograph of an area of a film of CdSe in (110) orientation grown at 380^{o}C, and annealed at 500^{o}C. This micrograph was recorded using the 002 superlattice reflection for imaging. It is seen that the domain boundaries are in strong contrast. The "horse with a halo" shaped domains at A are particularly easy to recognise on the micrograph. For comparison three particular domains are marked A, B, and C.

Fig. 5.3(b) shows a dark field transmission electron micrograph of the same area of the same film. This was recorded using 222 superlattice reflection for imaging. It is seen that domain boundaries are in strong contrast. The three domains marked A, B and C are also seen in this micrograph.

Fig. 5.3(c) is a dark field transmission electron micrograph of the same area of the same film. This was recorded using the 111, fundamental reflection for imaging. The domain boundaries are seen in contrast. The domains marked A, B and C are also seen in these micrographs. The domain boundary contrast in these cases depends on compound.

Fig. 5.3(d) is a 400 dark field transmission electron micrograph of the same area of the same CdSe film. The domains seen in the above cases, are out of contrast. The boundary at A is still faintly visible on one side of the 400-$\bar{4}$00 bend extinction contour but all those in the region between B and C are out of contrast on the other side of the contour where the 400 diffraction contrast conditions are

well satisfied.

Thus the experimental results are in good agreement with the diffraction contrast theory of antiphase-domain boundaries in the sphalerite structure.

Some of the points on the geometry of the antiphase boundaries in the sphalerite structure discussed earlier in this chapter will now be compared with the experimental results.

Figs. 4.18 (c) and (d) are dark field micrographs of the as grown (110) CdSe film. These micrographs were recorded with the two pseudospots on either side of a 200 type reflection, when the film was tilted slightly off the (110) orientation. The two types of domains faulted on the two {111} planes are seen in dark and light contrast. This dark and light contrast is not seen in the micrographs of the annealed (110) CdSe films, shown in figs. 5.3(a) to (d).

This means that the annealing of the CdSe film at an elevated temperature e.g. at 500^{o}C after growth at 380^{o}C, eliminated the stacking faults and consequently eliminated the dark-light contrast and most of the defect content in the films. Then the domain boundaries could be observed as in fig. 5.3(a) to (d).

Comparison of the boundaries in fig. 4.18(c) and (d) and figs. 5.3(a)-(d) shows that they have the same general shape and the domains have the same average size, about 0.1μ in width, after and before annealing. Hence the effect of annealing was simply to remove the obscuring faults and dis-

locations, and not somehow to create or alter the nature of these boundaries. A feature of these boundaries that is in agreement with theory is that two domain boundaries never intersect. That is, the domain boundaries seen in figs. 4.18(c) and (d) and fig. 5.3(a) to (d) either form closed loops or run across the field of view and out of the micrographs. Therefore there are no nodes. Thus the boundaries in fig. 5.3(a) to (d) have the characteristic appearance of APBs. It is noticeable that the boundaries appear in fairly uniform contrast across their widths. The reason according to diffraction contrast theory is that APBs only appear in contrast in those beams which have relatively small values of structure factor and therefore long extinction distances so that only one interference fringe is seen (Holt 1969b).

Fig. 4.20 is a typical bright field micrograph of a CdSe/Ge (110) heterojunction (see chapter IV, section 4.3). This micrograph shows the parallel moire fringes due to the interference of beams reflected in the CdSe and the Ge overlapping crystals. The fringes run continuously across the domain boundaries with little change of direction. The crystallographic structure and the alignment of the two types of domain on the substrate was therefore approximately the same. It is also noticeable that a number of moire fringes ended at the domain boundaries. This indicates that the domain boundaries contained dislocations.

These observations were consistent with the antiphase domain hypotheses. Hence from all these agreements between

the theoretical predictions and the experimental results, there is no doubt that the boundaries of the domains of the domain-form structure in CdSe at least are APBs. Thus, this is for the first time that the APB's have been identified in the research studies of II-VI epitaxial films.

CHAPTER VI

DISCUSSION OF THE EXPERIMENTAL RESULTS

6.1 EPITAXIAL GROWTH RANGES OF SUBSTRATE TEMPERATURE

The epitaxial growth ranges of substrate temperature for the (100), (110) and (111) faces of Ge had a common upper limit of 450°C. This was the deposition cut off temperature above which CdSe films could not be deposited by evaporation in a pressure in the 10^{-5} - 10^{-6} torr range. This upper limit was attributed to the onset of some vapour phase chemical attack reaction on the Ge substrate surfaces. The evidence of the chemical attack on the Ge substrate surfaces was always observed in the form of pitting or tarnishing. Similar vapour phase chemical reaction effects were also observed in the previous investigations in this laboratory. In cases of CdS deposited on (111) Ge (Holt and Wilcox 1971) the upper cut off temperature was 550°C, CdS deposited on (100), (110) and (111) Ge (Abdalla et al. 1973) the upper cut off temperature was 500°. In CdTe deposited on the three low index planes of Ge (Abdalla and Holt 1973) it was 470°C, and CdTe deposited on to (111) Si (Holt and Abdalla 1975), it was 520°C. Thus the epitaxial upper cut off temperature varies from one deposit/substrate combination to another. Also it is clear that all these cut off temperatures are well below the sublimation temperature of Ge (about 1300°K at 10^{-5} torr, taken from RCA Vapour Pressure Chart). This suggested that

some form of chemical attack reaction sets in at the cut off temperature and hence films could not be deposited above this cut off temperature. On the other hand it has been well established by the previous and present investigations that thermal etch-pitting on the Ge substrates was never observed after the substrates had been thermally cleaned in high vacuum by heating to 600^{o}C or below 700^{o}C. Hence the cessation of II-VI films deposition in high vacuum above the upper cut off temperatures can be assumed to be due to the on set of some vapour phase chemical attack reaction on Ge and Si substrates.

It is found in general that (i) the upper cut-off temperature was well defined to within the accuracy of measurements of substrate temperatures (± 5^{o}C to ± 10^{o}C), (ii) it was unaffected by growth conditions such as contamination, rate of evaporation, substrate orientation etc. and (iii) above the cut-offs evidence of chemical attack on substrate surfaces was observed in the form of pitting.

In the case of ionic crystal substrates, the upper cut-off temperature was believed to be the sublimation temperature of the substrates. For ZnS deposited on NaCl (Woodcock 1968), CdS on ionic substrates (Wilcox and Holt 1969), Ge on NaCl (Collins and Heavens 1952) it was definitely established that the temperatures above which films could not be deposited equalled the sublimation temperature at the pressure of deposition.

The minimum epitaxial growth temperature for CdSe deposited on to (100) and (111) faces of Ge was 350°C and on to (110) face of Ge it was 300°C. This showed that the minimum epitaxial growth temperature was dependent on substrate surface orientation. Similarly in the case of CdTe deposited on the (110) and (111) surfaces of Ge the minimum epitaxial growth temperature was 200°C, whereas for CdTe on (100) Ge it was 250°C. But for CdTe/Ge the minimum epitaxial growth temperature was higher for (100) than for the other two singular surfaces, whereas for CdSe/Ge, it was lower for (110) than for the other two singular surfaces.

In the case of ZnTe deposited on (100) and (111) faces of Ge the minimum epitaxial growth temperature investigated was the same, 300°C. Similarly for CdS/Ge the minimum epitaxial growth temperature was 300°C, for all the (100), (110) and (111) faces of Ge. This showed that the minimum epitaxial growth temperature was independent of the substrate orientation for the latter II-VI materials.

Hence what determines the minimum epitaxial growth temperature is not clearly known. The minimum epitaxial growth temperatures in contrast to the upper cut-off temperatures are strongly affected by the growth conditions, such as contamination and evaporation rates. The minimum epitaxial growth temperatures are reduced as contamination from all sources is reduced (Calow et al. 1972). In the present work evaporation rate and substrate surface preparation too seem to have a significant influence, in widening epitaxial growth

ranges of temperature, or in reducing the minimum epitaxial growth temperature. It is evidenced in this work that on (110) Ge substrates epitaxy was obtained at 300^{o}C, which was 50^{o}C below 350^{o}C, the minimum temperature for the (100) and (111) surfaces of Ge. On (110) Ge surfaces the density and size of etch pits were so small that they were rarely observed by low power optical microscope after they had been chemically polished. With the same method of chemical polishing on (100) and (111) surfaces the etch pits were always found to occur on the Ge surfaces. However the minimisation of contamination in all the ways in growth techniques results in well defined and fixed minimum epitaxial growth temperatures (Holt 1974).

6.2 COMPARISON TO PREVIOUS WORK

Holt and Woodcock (1970) and Holt and Wilcox (1971) made thorough investigations on the structural properties of ZnS and CdS respectively grown on (100) ionic substrates. Since CdSe was the least studied II-VI material, epitaxial films of CdSe epitaxially grown on covalent (100) substrates were studied in detail for the first time. ZnTe and CdS grown on (100) Ge, Mufti (1972) and Abdalla (1973) respectively did not confirm experimentally the epitaxial orientation relationship. For CdTe films grown on (100) Ge substrates, Abdalla and Holt (1973) however confirmed the occurrence of the parallel epitaxial orientation relationship. In all these cases and in the present case the structure of the films

was found to be sphalerite. In the present case and the above mentioned cases the growth orientation relationship was parallel alignment. Identification of the arrangement of the {111} planar defects giving rise to pseudo-spots was made only in the (100) CdSe films grown on (100) Ge substrates and it was found to be due to random faulting, similar to the result found in ZnS and CdS films grown on (100) ionic substrates.

CdSe films grown on (110) Ge substrates were found to contain a domain-form transformed structure giving rise to pseudo-spots similar to the previously studied II-VI films. Tilting experiments showed that the faulting was random in CdTe, partly random in CdSe and more regular in CdS.

Annealing experiments showed that (110) CdS could be transformed to a lath-form transformed structure or to the domain-formed structure (Holt et al. 1976) whereas in the case of CdSe all the faults were annealed out leaving behind domain boundaries which were identified as APBs (Holt et al. 1976). This is the first time that APBs have been identified in II-VI epitaxial films.

As mentioned in the introduction, systematic investigations on the epitaxial growth and structure of II-VI compounds on ionic and elemental semiconductor substrates in this laboratory and elsewhere led to certain general rules of epitaxy. These include the general occurrence of either parallel or quasiparallel epitaxial alignment. The investigation of the epitaxial growth of CdSe on (111) Ge substrates

revealed a new phenomenon called "nearly-parallel rotation" epitaxy. This showed that the above mentioned rules of epitaxy are not of universal occurrence. Evidence indicating the probable occurrence of 60^{o} dislocations has been found in CdSe/Ge (111) heterojunctions. On this basis it was shown to be possible to account for the observed "nearly-parallel rotation" alignment. This is the first evidence of misfit dislocations in the study of the epitaxy of II-VI compounds and the first evidence for the occurrence of 60^{o} misfit dislocations in any type of epitaxy.

6.3 STRUCTURAL PERFECTION OF THE CdSe FILMS

Little systematic work on the epitaxial growth and structure of CdSe has been published. Early work by Kalinkin et al. (1962, 1963) showed that their best films were polycrystalline or contained both sphalerite and wurtzite structure material. Epitaxial films were grown on mica but their structural perfection was not determined (Brunnschwiler 1966). A study of the nucleation and growth of CdSe films evaporated onto cleavage surfaces of NaCl also provided little information on the perfection of the best films produced (Yasuda 1968). Altman et al. (1968) deposited CdSe on the (111) faces of CaF_2. Single crystal CdSe containing various microstructures was produced from $440^{o}C$ to $460^{o}C$ and above $480^{o}C$ the films had again a partial orientation. Gahsin and Simashkevich (1973) studied CdSe/ZnTe gas transport heteroepitaxy. They obtained epitaxial single crystalline CdSe films of cubic modifications

but they mainly studied the electrical properties of the heterojunctions. Ratcheva et al. (1973) grew CdSe films on (0001) surfaces of sapphire. In the substrate temperature range from 400° to 460°C, the CdSe films had the polycrystalline structure; in the range from 460°C to 530°C the films had a fine texture with a low extent of preferred orientation; in the range from 530° to 570°C the films had a fine texture with a high extent of preferred orientation; and in the narrow range from 570° to 620°C, the films had a monocrystalline structure. Sergeyeva et al. (1972) studied the epitaxial growth of CdSe on the (001) surface of mica. They found that their best CdSe films had a mixed or sphalerite structure below 400°C and the wurtzite structure for substrate temperatures from 400° to 550°C. Most of their work was to study the electrophysical properties of CdSe films.

Thus this is the first report of a systematic study of the epitaxial growth and structure of CdSe on Ge substrates. This is also the first report of single crystal CdSe films grown free of both twins and included grains of wurtzite structure material so that the films gave rise to diffraction patterns that were free of satellite or irrational spots. The absence of <111> streaks from the diffraction patterns of (111) CdSe films was the evidence that the films contained a density of planar defects below that required to produce streaks. Therefore the level of perfection of these films is similar to that of the best of other II-VI compound films (Holt 1974) and it is also similar to the best levels reported for other heteroepitaxial films (Cullis and Booker 1970, 1971).

PART II

"ELECTRICAL PROPERTIES OF CdSe/Ge HETEROJUNCTIONS"

CHAPTER VII

THEORY OF HETEROJUNCTIONS

7.1 INTRODUCTION

A heterojunction, in general, is defined as the electrical contact between two dissimilar monocrystalline semiconductor materials. Its usage in semiconductor research is normally restricted to a junction between two dissimilar materials. Such heterojunctions can be classified as abrupt or graded. This depends upon the distance during which the transition from one material to the other is completed. In the abrupt case the transition occurs within a few atomic distances ($\lesssim 1\mu m$); while in the graded case the transition takes place over distances of the order of several minority carrier diffusion lengths. Another classification often used in the literature is by the type of conductivity present on either side of the junction. If the two semiconductors forming a junction have similar types of conductivity, then the junction is called an isotype heterojunction. On the other hand if the two semiconductors forming a junction have dissimilar types of conductivity then the junction is called an anisotype heterojunction.

The important electrical parameters that change at an abrupt heterojunction are, the work function, electron affinity and energy gap. The work function depends on the doping levels of the materials whereas the electron affinity and the energy gap are intrinsic properties of the materials (that

means to a first approximation not depending upon the doping level).

The research interest in heterojunctions only developed after Kroemer (1957) suggested that anisotype heterojunctions might exhibit extremely high injection efficiencies in comparison to homojunctions. Isotype and anisotype heterojunctions were fabricated for the first time by Anderson (1960, 1962). Since then various models for different types of heterojunctions have been proposed by several workers and their validity has been verified by experiments. These heterojunction theories are dealt with in the next section 7.2.

7.2 THEORY OF HETEROJUNCTIONS

The heterojunctions considered here are abrupt anisotype heterojunctions. This is because the type of heterojunction, CdSe/Ge, studied is an anisotype abrupt heterojunction. These types of heterojunctions which include n-p and p-n heterojunctions are minority carrier devices like p-n homojunctions. Therefore existing models for anisotype heterojunctions can be essentially regarded as an extension of the conventional model for homojunctions.

A model describing the physical behaviour of a heterojunction is twofold. It consists of a diagram for the arrangement of the energy bands near the interface and a mechanism for charge-carrier conduction through this junction. Energy-band diagrams have been proposed by Anderson (1960), by

Oldham and Milnes (1964) and by Van Ruyven (1964). The Anderson model does not consider interface states or dipoles. However the Anderson model is invariably used to predict the energy band diagrams of anisotype heterojunctions.

The energy band diagram of a heterojunction is somewhat more complicated than that of a homojunction. This is because of the presence of the energy steps ΔE_C and ΔE_V. These steps arise due to the abrupt discontinuities in electron affinities and energy gaps at an interface.

Heterojunction theories have been reviewed by C. Van Opdorp (1969), Anderson (1971), Milnes and Feucht (1972) and Sharma and Purohit (1974). However a brief account of theory of anisotype abrupt heterojunctions formed between p-type narrow-gap and n-type wide-gap semiconductors is given below.

7.2.1 The Energy-Band Diagram and Diffusion Model of Anderson

A typical energy band profile of two isolated p and n-type semiconductors is shown in fig 7.1(a). χ_1, ϕ_1 and E_{g1} are the electron affinity, work function and energy gap of the p-type semiconductor. χ_2, ϕ_2 and E_{g2} are the electron affinity, work function and energy gap of the n-type semiconductor. The work function of a semiconductor is defined as that energy which is required to remove an electron from the Fermi level to a position at rest just outside the material, that is the vacuum level. The electron affinity of a given semiconductor is the energy required to transfer an electron

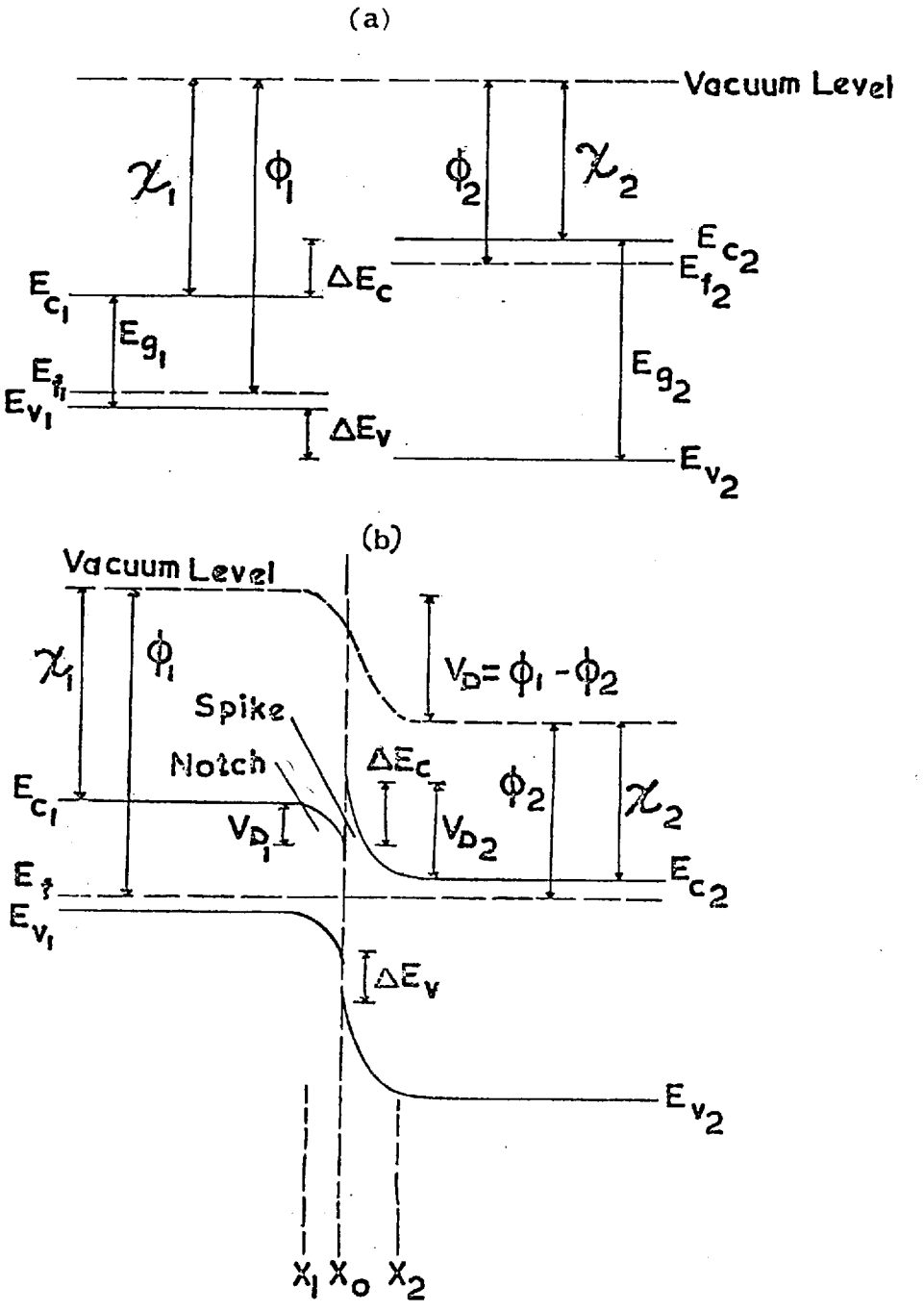


Fig. 7.1 Equilibrium energy band profile for an abrupt p-n heterojunction.
(a) before contact
(b) after contact

from the bottom of the conduction band to the vacuum level.

The equilibrium energy band profile of an abrupt p-n heterojunction formed by bringing the two materials into intimate contact is shown in Fig. 7.1(b). This energy band profile in which a "spike" and a "notch" occur in the conduction band edge at the interface is the case in which $\chi_1 > \chi_2$ and $\phi_1 > \phi_2$. The discontinuity in the conduction band edges ΔE_c is equal to the difference in electron affinities of the two semiconductors. That is $\Delta E_c = \chi_1 - \chi_2$. In this type of heterojunction a depletion layer is formed on either side of the interface. Since interface states are absent in this model, the space charges of these layers are opposite and equal in magnitude. The total built-in voltage (V_D) due to the difference in work function ($\phi_1 - \phi_2$) is equal to the sum of the built-in voltages on both sides that is $V_D = V_{D_1} + V_{D_2}$. The electrostatic potential difference between two points is represented by the vertical displacement of the vacuum level between these two points. Because of a difference in dielectric constant, the electrostatic field is discontinuous at the interface. From fig. 7.1(b) it is also evident that the valence band discontinuity

$$\Delta E_v = E_{g_2} - E_{g_1} - (\chi_1 - \chi_2) = E_{g_2} - E_{g_1} - \Delta E_c. \quad 7(1)$$

Let the co-ordinate of the interface shown in fig. 7.1(b) be denoted by X_o. Then the transition widths on either side of the interface for an abrupt p-n heterojunction

obtained by generalising the solution of the Poisson's equation for homojunctions, are given by

$$(X_0 - X_1) = \left(\frac{2\, N_{A_1}\, \varepsilon_1\, \varepsilon_2\, V_D}{q\, N_{D_2}(\varepsilon_1\, N_{A_1} + \varepsilon_2\, N_{D_2})}\right)^{\frac{1}{2}} \qquad 7(2)$$

and

$$(X_2 - X_0) = \left(\frac{2\, N_{D_2}\, \varepsilon_1\, \varepsilon_2\, V_D}{q\, N_{A_1}(\varepsilon_1\, N_{A_1} + \varepsilon_2\, N_{D_2})}\right)^{\frac{1}{2}} \qquad 7(3)$$

(Sharma and Purohit 1974)

where q is the electronic charge, ε_1 and N_{A_1} are the dielectric constant and concentration of acceptors in the p-type semiconductor, ε_2 and N_{D_2} are the dielectric constant and concentration of donors in the n-type semiconductor and $V_D = V_{D_1} + V_{D_2}$.

The relation between the built-in voltages V_{D_1} and V_{D_2} is given by $\frac{V_{D1}}{V_{D_2}} = \frac{N_{D_2}\, \varepsilon_2}{N_{A_1}\, \varepsilon_1}$ (Sharma and Purohit 1974) and the capacitance of the transition region is given by

$$C_{p_n} = \left(\frac{aq\, N_{A_1}\, N_{D_2}\, \varepsilon_1\, \varepsilon_2}{2(\varepsilon_1\, N_{A_1} + \varepsilon_2\, N_{D_2})} \cdot \frac{1}{V_D}\right)^{\frac{1}{2}} \qquad 7(4)$$

(Sharma and Purohit 1974)

where a is the junction area.

The current was assumed by Anderson to be dominated by the diffusion of injected minority carriers across the junction. The predominant current carriers will be electrons because the barrier for electrons is much smaller than that

for holes. The current voltage relation is given by (Van Opdorp 1969)

$$I = I_s \left[\exp\left(\frac{eV}{kT}\right)-1\right] \qquad 7(5)$$

$$\text{and} \quad I_s = s\, n_o\, e\left(\frac{D_n}{\tau_n}\right)^{\frac{1}{2}} \qquad 7(6)$$

Where s is the junction area, n_o is the equilibrium concentration of electrons, and D_n and τ_n are the diffusion coefficient and life time of electrons.

The energy-band diagram proposed by Anderson is generally accepted by most workers and considered to be basically right. But the experimental current values are much smaller than those predicted by the above relation. This is attributed by Anderson to the reflection of a large fraction of the charge carriers at the interface.

7.2.2 The Emission Model of Perlman and Feucht

In Anderson's model the influence of the "spike" and "notch" at the interface on the charge carrier transport mechanism is neglected, whereas in the emission model the effects due to the spike are included. It is found that in certain voltage regions the spike plays a decisive role in the current conduction mechanism. Before being injected the electrons have to pass the spike. This is assumed to take place by thermal emission over the spike in the absence of tunnelling. This thermal emission and the subsequent

diffusion in the conduction band of the narrow gap material are two processes in series. In an anisotype heterojunction for which in equilibrium the top of the spike lies below the conduction-band edge of the narrow-gap material outside the space-charge region, the current transport mechanism becomes diffusion limited (as predicted by Anderson), whereas if the top of the spike lies above the conduction-band edge of the narrow-gap material outside the space charge region, the emission over the spike becomes the dominant conduction mechanism. The current is then given by (Van Opdorp, 1969)

$$I = I_s \left[\exp\left(\frac{eV}{\eta kT}\right)-1\right] \qquad 7(7)$$

and

$$I_s = \frac{S\, n_R\, q\, v_{th}}{(6\pi)^{\frac{1}{2}}} \qquad 7(8)$$

where n_R is the equilibrium electron concentration at the top of the spike and v_{th} is the mean thermal electronic velocity and

$$\eta = 1 + \frac{\varepsilon_1 N_{D_1}}{\varepsilon_2 N_{A_2}} . \qquad 7(9)$$

Here ε_1 and ε_2 are the dielectric constants of the two materials, N_{D_1}, N_{A_2} are the donor and acceptor concentrations in the n and p-type materials. Here η can be described as the current limiting factor for the spike. Thus the Perlman and Feucht theory predicts much lower current values than does the Anderson theory in which the effect of the spike is neglected.

As the height of the spike depends upon the value of ΔE_c, it is clear that ΔE_c is an important parameter.

7.2.3 Tunnelling Model

The tunnelling mechanism to describe the current-voltage characteristics of an abrupt p-n heterojunction was first introduced by Rediker et al. (1964). They noticed that in a number of cases where the emission model of Perlman and Feucht fails either over the whole voltage range or above a certain voltage the I-V characteristics of an anisotype heterojunction could be described by an equation,

$$I = I_s(T) \exp(V/V_0) \qquad 7(10)$$

where V_0 is a constant and $I_s(T)$ is a weakly increasing function of temperature. The voltage dependence of the above equation is characteristic for tunnelling processes. This leads to a model in which tunnelling through the spike greatly exceeds thermal emission over the spike. This model does not give an expression or interpretation for the temperature dependence of the current $I_s(T)$. However Newman (1965) remarked that in all cases in which the above equation holds good, the empirical relation between I_s and T is adequately described by $I_s = I_{s_0} \exp(\frac{T}{T_0})$ where I_{s_0} is constant. Thus the above equation becomes

$$I = I_{s_0} \exp(\frac{T}{T_0}) \exp(\frac{V}{V_0}) \qquad 7(11)$$

where I_{s_0}, T_0, V_0 are constants.

7.2.4 Tunnelling-Recombination Model

The close resemblance between the tunnelling currents in anisotype heterojunctions and the current in an Esaki diode led Riben and Feucht (1966a) to propose a model based on band to band tunnelling coupled with recombination processes. The various processes involved in this model are shown in Fig. 7.2. According to this model either the electrons tunnel from the conduction band of the wide-band gap n-type material into empty interband states located in the narrow-band gap p-type material and then recombine with holes (as indicated in fig. 7.2) or holes from the p-type narrow-band gap material tunnel into occupied states in the n-type material and then recombine with electrons. If the tunnelling originates at the bottom of the conduction band or the top of the valence band, then the forward current can be expressed as

$$I = B \exp\left[-\alpha(V_D - V)\right] \qquad 7(12)$$

where B is a weak function of voltage and temperature, V_D is the diffusion voltage, V is the applied voltage and α depends on the electron effective mass in the forbidden energy gap, the dielectric constant, the equilibrium carrier concentration and the exact shape of the barrier. For the linear barrier approximation i.e. field is constant with position in the transition region and the tunnelling is mainly in the n-type material, then

$$\alpha = \frac{4}{3\hbar}\left(\frac{m_n^* \varepsilon_2}{N_{D_2}}\right)^{\frac{1}{2}} \qquad 7(13)$$

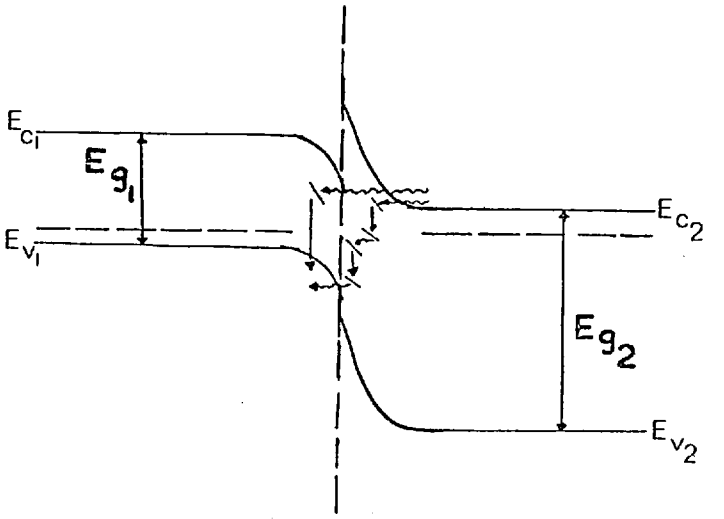


Fig. 7.2 Energy band profile for an abrupt p-n heterojunction under forward bias. The tunnelling-recombination process is indicated for both single step and multi-step processes.

where m_n^*, ε_2 and N_{D_2} are the values in the n-type material.

Because the experimental values of α are generally not in agreement with this expression, a multi-step tunnelling-recombination process was also proposed by Riben and Feucht (1966b). This process is also shown in fig. 7.2. The multistep tunnelling model has been criticised by Van Opdorp (1969) on the ground that invalid assumptions have been introduced in order to make their results fit their theory. One of these unjustified assumptions was that the height of the barrier that the electron has to surmount per tunnelling step was proportional to the square of the electric field.

Riben and Feucht also proposed a zener tunnelling model to describe the reverse current as a function of voltage and temperature. On the assumptions of a linear barrier and tunnelling predominantly in the n-type material, the reverse current was given by

$$I = C \exp\left[-A(V_D - V)^{-\frac{1}{2}}\right] \qquad 7(14)$$

where

$$A = \frac{4}{3\hbar}\left(\frac{m_n^* \varepsilon_2}{N_{D_2}}\right)^{\frac{1}{2}} E_{g_2}^{3/2} \qquad 7(15)$$

and m_n^*, ε_2, N_{D_2} and E_{g_2} refer to the n-type material. Once again as in the previous case of forward bias, a multistep process was postulated to obtain agreement between experiment and theory.

7.2.5 Emission-Recombination Model

Dolega (1963) proposed this model based on the assumptions that there exists a thin layer at the interface containing a strongly disturbed lattice. Electrons and holes reach the interface via thermal emission over their respective barriers and infinitely fast recombination of charge carriers occurs. Infinitely fast recombination implies that the electron and hole quasi-Fermi levels coincide at the interface.

Dolega's complicated expression for the forward current-voltage characteristics has been rewritten by Van Opdorp (1969) in simplified form as

$$I = I_s \left[\exp\left(\frac{qV}{\beta kT}\right) - 1\right] \qquad 7(16)$$

with

$$I_s = B \exp\left(-\frac{qV_D}{\beta kT}\right) \qquad 7(17)$$

where β is very weakly temperature-dependent. The values of β in the above two expressions are identical and depend on the ratio of the densities of imperfections in the two semiconductors.

β varies between 1 and 2. The reverse current predicted by this model, rises exponentially with voltage. This model is basically similar to the Sah, Noyce and Shockley (1957) model for homojunctions. The only difference is that in the latter model the recombination states are uniformly distributed in space and have definite ionization energies, whereas in the Dolega's model the recombination centres have

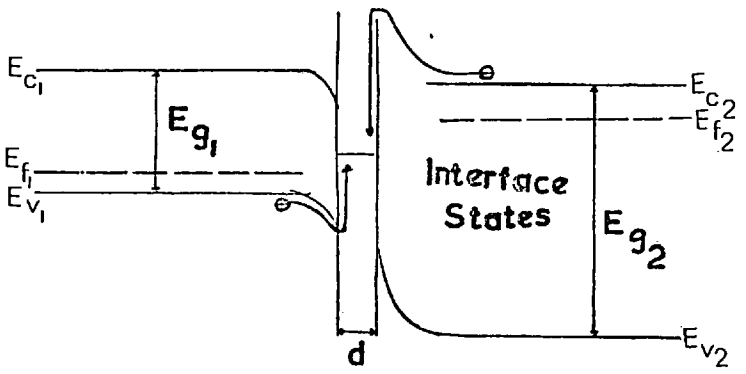


Fig. 7.3 Energy band profile showing the emission-recombination process for a p-n heterojunction.

a continuous energy distribution and are spatially restricted to a fixed plane or very narrow layer at the interface.

7.3 THE SYNTHESIS OF TRANSPORT MODELS

Donnelly and Milnes (1966) while interpreting their experimental results on anisotype heterojunctions tried to construct a synthesis of the theories for heterojunctions. Anderson (1971) while reviewing the theory of heterojunctions, surveyed the existing transport models and also tried to construct a synthesis capable of explaining the main functional behaviour of all experimentally observed current-voltage characteristics for all values of applied voltages.

According to Donnelly and Milnes the carrier transport takes place along two different groups of parallel channels simultaneously as shown in fig. 7.4. Group I mechanisms lead to minority-carrier injection into the space charge region and into the bulk of the narrow-band gap p-type material. After the injection the minority carriers disappear by a diffusion-recombination mechanism. The mechanisms of carrier injection are thermal emission over the spike and tunnelling through the spike. Their experimental observations and those of others ruled out the possibility of carrier transport by these processes.

Group II leads to the recombination at the interface of electrons and holes transported via thermal emission over or tunnelling through their respective barriers. In this case transport channels can be divided into three processes

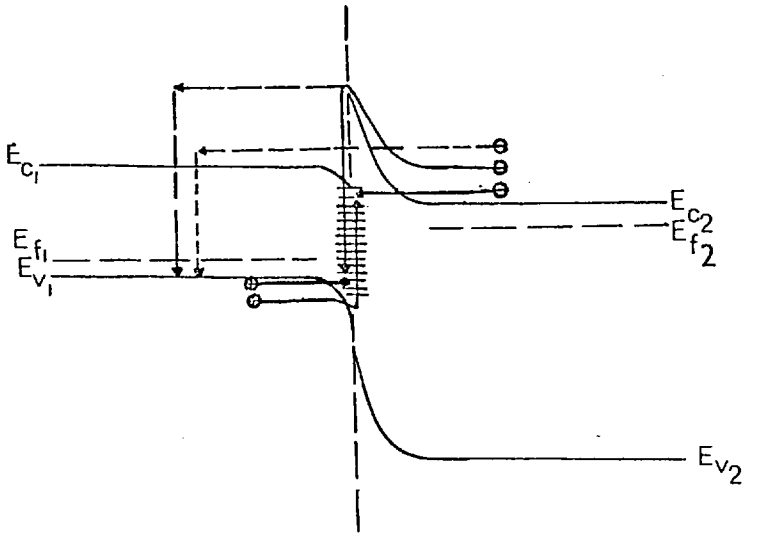


Fig. 7.4 Schematic representation of the two groups of charge transport mechanisms. Dashed line-group is 1; and solid line group is 2; proposed by Donnelly and Milens (1966).

in series: a transport mechanism of electrons to the interface, a mechanism transporting the holes to the interface and the recombination processes. The transport of electrons and holes to the interface in its turn may be by two parallel mechanisms: thermal emission over and tunnelling through the respective barriers. In a given voltage interval the I-V characteristic can be described adequately by that one of the five mechanisms described in this group which is rate-determining.

On the other hand Anderson has classified the forward currents into thermal and non-thermal currents. Thermal currents are those in which the current-carriers must surmount potential barriers to cross the junction and the general form of expression for these currents can be written as

$$I = A \exp\left(-\frac{qV_{B_o}}{kT}\right) \exp\left(\frac{qV}{\eta kT}\right) \qquad 7(18)$$

where V_{B_o} represents the barrier voltage at zero applied voltage, η is a measure of the variation of the barrier with applied voltage. It is also an indicator of the type of rate-determining process for thermal currents. A depends on the model.

The current-carriers can also tunnel through the potential barrier that is through the "spikes". In such a case if the tunnelling is mainly at higher energy, then the tunnelling currents are thermal in nature. However, if the tunnelling is predominantly at the base of the "spikes"

that is potential barriers, then the currents are non-thermal in character. These non-thermal currents often are referred to as excess currents. Therefore these are at least partly tunnelling in nature and are not strongly dependent on temperature. In practice, it is difficult to estimate the non-thermal currents quantitatively because many of the details regarding them are not well understood.

Reverse currents are also classified as thermal and non-thermal by Anderson. Thermal currents result from thermal generation in or near the transition region. Current carriers generated within the transition region are removed immediately by the electric field and contribute to the current flow. Those generated outside the region, diffuse to the high field region before they recombine and contribute to the flow of current. Again non-thermal reverse currents are predominantly tunnelling currents.

CHAPTER VIII

POSSIBLE CURRENT CONDUCTION MECHANISMS

The direct conduction of electric current through thin semiconductor layers is of interest in the thin film approach to active devices and has stimulated research on the mechanism of conduction of carriers through such layers. The conduction mechanisms in thin films have been reviewed by Jonscher (1967), Lamb (1967), Hill (1967) and Simmons (1971). A brief account of mechanisms which are of interest such as single carrier space charge limited conduction, two carrier space charge limited conduction and tunnelling effects are given below briefly.

8.1 SINGLE CARRIER SPACE CHARGE LIMITED CURRENT

If an electron injecting ohmic contact is made to a thin film of a semiconductor, electrons will travel from the metal into the conduction band of the semiconductors. This facilitates the establishment of a space charge similar to that of a vacuum diode (Mott and Gurney 1940). Thus the flow of electrons through the film under the action of an applied voltage, subsequently becomes space charge limited. In this process the current flow is due to the injected carriers of one type and it will not be influenced by the presence of carriers of the opposite type. This leads to the well known single-carrier space charge limited current flow.

The theory of the space-charge limited conduction mechanism was first given by Mott and Gurney (1940). According to the theory, for a trap-free semiconductor the current in the space-charge-limited (SCL) mode is given by

$$J = \frac{9}{8} \mu\varepsilon \frac{V^2}{S^3} \qquad 8(1)$$

where J is the current density, V is the voltage applied and μ, ε, and S are the electron mobility, dielectric permittivity or dielectric constant and the thickness of the semiconductor. The interesting feature of the theory is that the space charge limited current is proportional to V^2. The theory is in fact, based on field driven currents and cannot give an accurate description of the physical situation near the injection contact where the field will be zero and the current must be due to diffusion alone.

If now thermally generated free carriers with density n_o, are included then at low voltages where the injected carrier density is less than n_o, Ohms law will be obeyed,

$$J = e\, n_o\, \mu \frac{V}{S} \qquad 8(2)$$

where e is the electronic charge.

The transition from Ohm's law to the Mott-Gurney law occurs at the transition voltage V_{tr}, which is given by

$$e\, n_o\, \mu \frac{V_{tr}}{S} = \frac{9}{8} \varepsilon\mu \frac{V_{tr}^2}{S^3}$$

$$\therefore \quad V_{tr} = \frac{8}{9} \frac{en_o}{\varepsilon} S^2 \qquad 8(3)$$

This can be expressed as $T_{tr} = \frac{\varepsilon}{q}\tau$, where $T_{tr} = \frac{S^2}{\mu V_{tr}}$ = carrier transit time between electrodes at voltage V_{tr}. And $\tau = \frac{\varepsilon}{en_o\mu}$ = ohmic (or dielectric) relaxation time (Lamb 1967).

Lampert (1956 , 1964) and Rose (1955) have postulated a simple model which can be used to describe the trapping effects on the space charge limited currents very easily. When traps are present the current would be greatly reduced because some of the injected carriers would be captured and become immobilised. If θ is that fraction of the injected carriers which remains free, then the current will be reduced to,

$$\theta \times J_{trap\text{-}free} \quad \text{that is} \quad J_{trap} = \frac{9}{8}\varepsilon\mu\theta\frac{V^2}{S^3} \qquad 8(4)$$

The transition from Ohm's law to the V^2 law occurs for a semiconductor containing shallow traps, at the transition voltage V_{tr}, which is given by

$$en_o\,\mu\frac{V_{tr}}{S} = \frac{9}{8}\varepsilon\mu\theta\frac{V_{tr}^2}{S^3}$$

$$\text{i.e.} \qquad V_{tr} = \frac{8}{9}\frac{en_o}{\varepsilon\theta}S^2 \qquad 8(5)$$

Shallow and deep traps are defined according to whether the trap level lies above or below the Fermi level. The shallow traps above the Fermi level are empty, whereas the deep traps below the Fermi level are filled. The position of the Fermi level depends upon the injection level, that is on the applied voltage.

Therefore when the injection level increases, that is when the applied voltage increases, the shallow traps become deep and hence the Fermi level moves up and crosses the trap level. The transition voltage for deep lying traps is given by

$$V_{TFL} = \frac{8}{9} \frac{eN_t}{\varepsilon} S^2 \qquad 8(6)$$

where N_t is the density of traps, and TFL stands for trap filled limited. In the trap filled limited regime all the traps are full and the current rises rapidly to higher values than in the shallow trapping case. This is because all the injected carriers contribute to current.

8.2 TWO CARRIER SPACE CHARGE LIMITED CURRENTS

With suitable ohmic contacts it can be possible to inject electrons into the conduction band of a semiconductor at the cathode and holes into the valence band of the semiconductor at the anode. This means that the cathode is ohmic to electrons and the anode is ohmic to holes. Then the space charge limited currents of both signs of carriers can flow in the semiconductor. However, whether the resultant current will be ohmic or space-charge-limited depends on the relative magnitudes of the dielectric relaxation time and the transit times for electrons and holes, as discussed by Lampert (1962, 1964), Tredgold (1966) and Lamb (1967). The required condition for double injection to occur is that the transit time for both carriers is smaller than the dielectric

relaxation time. If the transit time of both the charge carriers is larger than the dielectric relaxation time, then the current flow will be ohmic because the injected carriers will be relaxed by the thermal carriers after a time τ, where τ is the dielectric relaxation time. However, if the transit time of only one type of carrier is smaller than τ, while the transit time of other type of carrier is larger than τ, then the current essentially will be carried by the one type of carrier. This leads to single carrier space-charge-limited current flow. The space charge due to the other carrier will be compensated after a time τ. The dielectric relaxation time τ and the transit time T_r are given by the following relations.

$$\tau = \frac{\epsilon}{en_0\mu} \qquad 8(7)$$

$$\text{and} \quad T_r = \frac{s^2}{\mu V} \qquad 8(8)$$

where n_0 is the density of the thermally generated charge carriers and V is the applied voltage. A brief account of the double injection theory is given below.

Suppose both the contacts are ohmic to a trap free semiconductor whose dielectric relaxation time is larger than the transit time. Assuming that the diffusion currents are neglegible, then the current density is given by

$$J = \frac{9}{8} \epsilon \mu_{eff} \frac{V^2}{s^3} \qquad 8(9)$$

$$\text{where} \quad \mu_{eff} = \frac{2}{3}\left[2\pi\left(\frac{\mu_n\mu_p}{\mu_0}\right)(\mu_n+\mu_p)\right]^{\frac{1}{2}} \qquad 8(10)$$

and μ_0 is the recombination mobility. It is generally very small making μ_{eff} greater than the electron and hole mobilities μ_n and μ_p respectively. This means that the two-carrier current is larger than that in either one carrier case.

On the other hand, in the case of a semiconductor containing a single set of deep lying recombination centres the following assumptions were made by Lampert (1962). The recombination centres are assumed to lie sufficiently far below the Fermi level to be completely filled with electrons in thermal equilibrium (no applied voltage). Thermal re-emission of carriers from the recombination centres and diffusion currents are neglected.

Ohmic contacts are applied at the cathode and anode. The density of thermally generated electrons (n_0) is greater than that of thermally generated holes (p_0) and the average cross-section σ_p for capture of free holes by a filled centre is greater than the average cross-section σ_n for capture of free electrons by an empty centre. ($\sigma_p >> \sigma_n$). This means that the recombination centres are of acceptor type, that is they are negatively charged when occupied by electrons.

Then at low injection levels (at low applied voltages) the hole life-time is very small because of the condition $\sigma_p >> \sigma_n$. This makes holes difficult to conduct across the solid and hence most of the injected holes will be captured by the recombination centres. Whereas the electron life-time is infinite because there are no empty centres to capture

the injected electrons. Hence the current at this low applied voltage is ohmic because the injected carrier density is smaller than n_o, and is given by

$$J = en_o \mu_n \frac{V}{S} \qquad 8(11)$$

If the applied voltage (injection level) is increased so that $n, p > n_o, p_o$, then the injected electrons can traverse the solid with a minimum probability of being captured and recombining with holes just in front of the anode. Whereas the injected holes will still be unable to penetrate the solid because the condition $\sigma_p >> \sigma_n$ continues to hold good. Hence the total current is carried by a single carrier (injected electrons) and this leads to SCL current flow i.e. to a V^2 power law.

The transition from ohmic current to SCL current occurs at the transition voltage and this is obtained by equating the electron transit time with electron life time.

$$\tau_n = \text{electron life-time} = \frac{1}{\sigma_n V_{th} N_R} \qquad 8(12)$$

where N_R is the concentration of donor centres and V_{th} is the electron thermal velocity $= \sqrt{\frac{8kT}{\pi m^*}}$ 8(13)

$$T_n = \text{electron transition time} = \frac{S^2}{\mu_n V_\Omega} \qquad 8(14)$$

where V_Ω is the transition voltage and

$$V_\Omega = \frac{S^2}{\mu_n T_n} = \frac{S^2 \sigma_n V_{th} N_R}{\mu_n} \qquad 8(15)$$

$$\therefore \quad T_n = \tau_n$$

That is beyond V_Ω the current is a single carrier-space-charge-limited and is given by

$$J = \frac{9}{8} \epsilon \mu_n \frac{V^2}{S^3} \qquad 8(16)$$

At high enough applied voltages (injection levels) the recombination centres will be filled up with holes. Then holes will transport through the semiconductor without being captured. That is the hole transit time decreases (life time increases). Therefore holes will then contribute to transporting current. The single carrier space charge regime continues until the minority carrier life time is equal to their transit time. At this point the conduction mechanism will change from a single carrier SCL regime to the two-carrier SCL regime. For further details the reader is referred to the above references.

8.3 TUNNELLING EFFECT

When the applied electric field is very high, then a new conduction process becomes predominant. That is quantum mechanical tunnelling occurs through the potential barrier. Then the applied electric field will produce an energy gradient which will be very steep so that the two points marked × in figure 8.1 are at the same energy and they are separated by a very short distance. The electron wave function ψ_x can, therefore, still have a non-zero value outside the potential barrier, and hence tunnelling can occur. The quantum

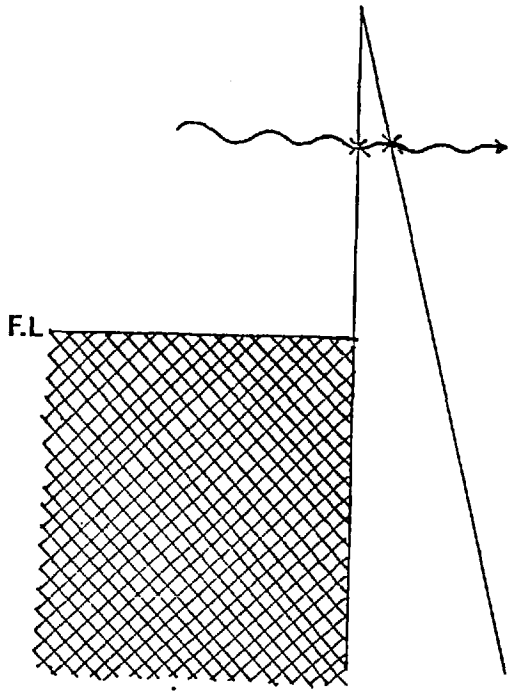


Fig. 8.1 Showing that quantum mechanical tunnelling can occur at higher electric fields.

mecahnical tunnelling effect has been discussed in detail by Hill (1967), (1971) and by Lamb (1967).

The tunnelling theories lead to current-voltage relationship of the type

$$I = A_1 F^n \exp \frac{-B_1}{F} \qquad 8(17)$$

where A_1 and B_1 are constants, F is the applied electric field and n takes values from 1 to 3.

The main characteristic of the tunnelling effect is the extreme sensitivity of current to voltage and the weak temperature dependence of the current.

CHAPTER IX

EXPERIMENTAL RESULTS AND DISCUSSION

9.1 PREPARATION OF CdSe/Ge(111) HETEROJUNCTIONS

In part 1 of this thesis epitaxial growth and structural studies of CdSe films grown on (100) (110) and (111) surfaces of Ge have been reported (Chapters III to VI, Gejii and Holt 1975 and Holt et al. 1976). All the structural studies of CdSe films was carried out on 3mm diameter germanium substrates. This restriction was to suit the transmission electron microscope specimen holder. However this restriction was not necessary for the electrical property measurements on the heterojunctions. Ge slices in (111) orientation, and 3cms in diameter were mechanically polished as described in chapter III, section 3.2. These were ultrasonically cut into 5mm diameter discs. The 5mm diameter discs were chosen one by one and chemically polished in the reagent described in chapter III, section 3.2 before being put in the recess in the substrate holder in the vacuum growth chamber. These Ge substrates were of p-type with resistivities of 0.1Ωcm to 0.25 Ωcm.

All the experimental set up and growth conditions remained the same as described in chapter III, section 3.3; CdSe films were grown on Ge (111) substrates at 400^{o}C for 20 minutes. 400^{o}C was chosen as being the centre temperature of the epitaxial growth range from 350^{o}C to 450^{o}C. No cracks were observed in the deposited films. This showed that the differential co-efficient of expansion during cooling

Fig. 9.1

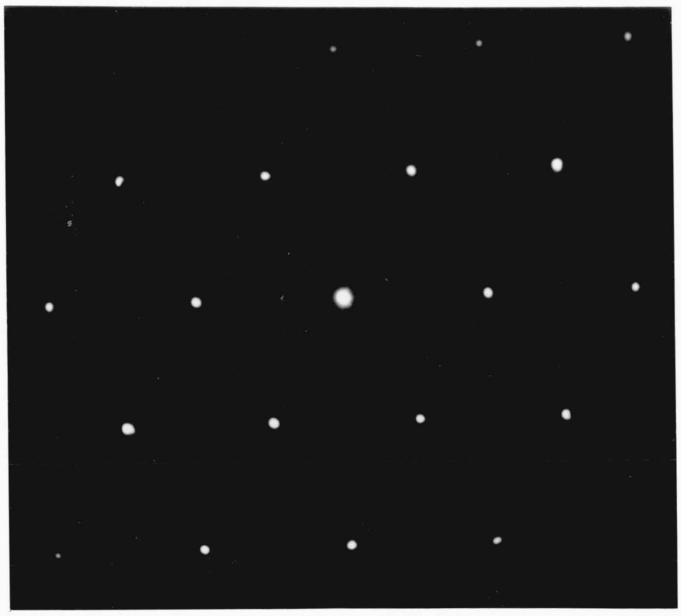


Fig. 9.2

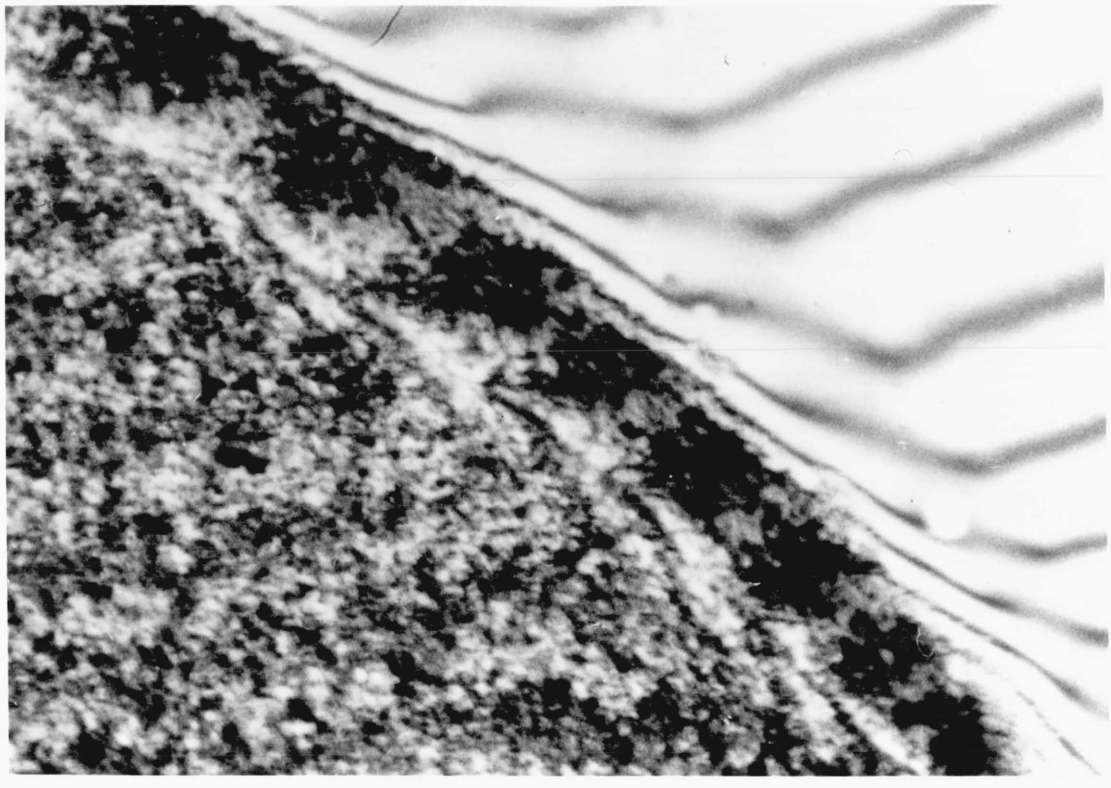


Fig. 9.1 Selected area transmission electron diffraction pattern of a CdSe film grown on (111) Ge at 400°C for 20 minutes.

Fig. 9.2 Interferogram of a CdSe/Ge heterojunction taken near the edge of the CdSe film with a Nomarsky Interferometry arrangement. The CdSe was grown on (111) Ge at 400°C for 20 minutes.

of these specimens from the growth temperature to room temperature had no fracture effect on the heterojunction system.

For transmission electron microscope examination, a few specimens were electrochemically jet-thinned from the germanium side in such a way that after thinning through the germanium the CdSe was further thinned carefully without breaking the film. Fig. 9.1 shows a selected area spot diffraction pattern of the (111) oriented cubic sphalerite structure of a CdSe film. Thus the fact that the CdSe/Ge (111) heterojunctions were formed between two single crystals was confirmed.

The thickness of the CdSe films was measured using a Nomarski interferometer on a MeF Reichert microscope as described in chapter III section 3.5. The thickness of the films was found to be about 0.8 micron. An interferogram of the Nomarski interference fringes is shown in fig. 9.2. A comparison of fig. 9.2 and fig. 3.5 clearly shows the difference in thickness of the films prepared for the structural analysis work and this work.

In order to join the heterojunction in the electrical circuit, indium was used as contact material as described in the next section 9.2.

9.2 METAL CONTACTS TO CdSe

In order to carry out electrical measurements on the heterojunctions these have to be provided with contacts and

leads. In the literature it is found that three types of metal-semiconductor contacts are distinguished (Simmons 1970, 1971, Van der Ziel 1968). These are blocking, neutral and ohmic contacts. In the present work only the ohmic contact is important in the sense that it is a low resistance contact and it does not affect or override significantly the electrical property of the heterojunction under investigation. The equilibrium energy band profile for ohmic contact to n-CdSe is shown in fig. 9.3. A brief account of these contacts is given below.

The work function of the metal (ϕ_m) and the semiconductor (ϕ_s) forming a contact are used (Blount et al. 1966) to explain these types of contacts. If the work function of a metal ϕ_m is greater than the work function ϕ_s of a n-type semiconductor then on bringing these into contact electrons should be transferred from the semiconductor into the metal to equalise the Fermi levels across the contact. This results in a space charge region of positive charge in the semiconductor (a depletion region). The depletion region has a much lower electron density than the bulk of the semiconductor. Hence its conductivity is much lower, so that it acts as a blocking barrier to electron flow at the contact-interface from semiconductor to the metal electrode. Such a contact is called a blocking contact. Such a blocking contact is an example of a Schottky barrier. When the work function of the metal is equal to the work function of the semiconductor, the Fermi levels of the metal and semiconductor are already equal prior

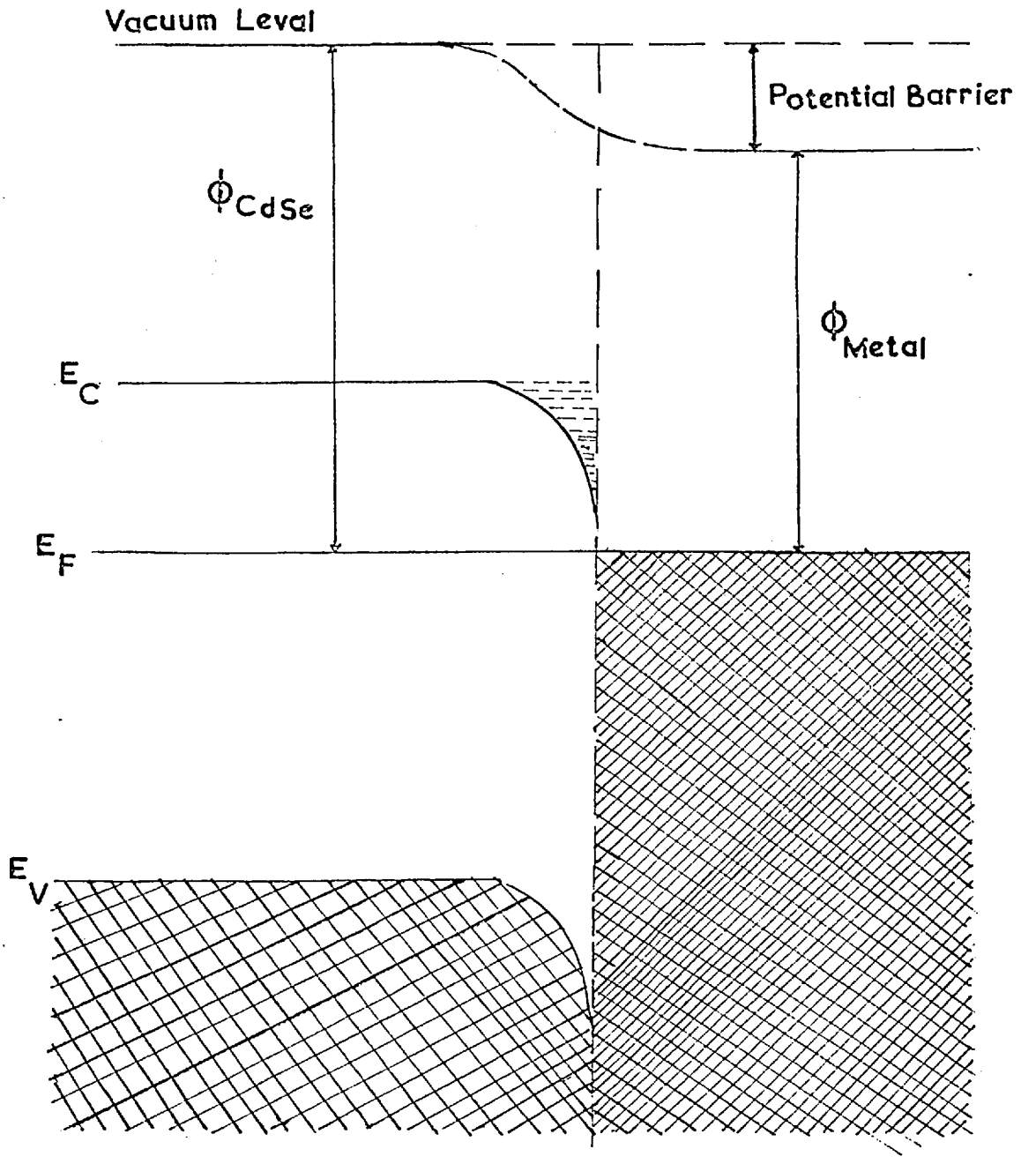


Fig. 9.3 Equilibrium energy band diagram for metal/n-CdSe contact with $\phi_{metal} < \phi_{CdSe}$.

to contact, hence no charge transfer occurs at the metal-semiconductor interface. As a result no depletion or accumulation region occurs in the semiconductor and hence no barrier to the electrons exists at the contact-interface. Such a contact is called neutral.

Finally if the work function of the metal ϕ_m is smaller than the work function ϕ_s of the semiconductor, on bringing the metal and the semiconductor into contact, in order to satisfy thermal equilibrium requirements i.e. to equalise the Fermi levels across the two materials, electrons are injected from the metal into the semiconductor. This results in a region of negative space charge in the semiconductor (an accumulation region). Such a contact acts as a reservoir of electrons in the semiconductor. The differential resistance of such a contact is very small due to the higher electron density at the interface than in the bulk of the semiconductor. This type of contact is termed an ohmic or Mott-Gurney contact.

Following the above guidelines there was no difficulty in achieving an ohmic contact to CdSe. Among the zinc chalcogenides ZnTe seems to be always p-type and among cadmium chalogenides CdTe can be of either p-type or n-type conductivity, whereas CdS and CdSe seem to be always n-type (see section 2.2).

Smith (1955) used indium as a contact material to CdS crystals. He found that (1) simple pressure contacts to the CdS had ohmic characteristics, (2) there was no apparent reaction of indium with CdS and diffusion into the CdS crystal

was not necessary for an ohmic contact. He also showed that a simple and convenient technique of applying electrodes was to evaporate an opaque layer of indium on the CdS, which gave an ohmic contact. Aven and Garwaki (1963) suggested that small size contacts have some definite resistance and hence proved to be non-ohmic. Some of these experimental guide lines were followed in the present work to achieve ohmic contact to the heterojunctions.

Indium has been shown to make ohmic contact to p-type Ge (Hunter 1956, 1962, Matsuura et al 1962, Turner 1959, Pikhtin et al 1970, Biondi 1958, Borneman et al 1955, Dale and Turner 1963).

Indium has been used as an ohmic contact electrode to CdSe by many workers. (Tubota 1963, Arnold et al 1970, Khosla and Fischer 1971, Suri and Sharma 1974.) Gold has been also used for making ohmic contact to CdSe (Nakai et al 1964, Nakai et al 1965). But Gold was found to make non-ohmic contacts to CdSe (Demey 1974).

In the present work indium was evaporated on to CdSe and Ge in high vacua of 10^{-5} torr. The evaporated indium layers on both sides were transparent. The deposited indium was 3mm in diameter on 4mm diameter films and 5mm diameter Ge substrates. This gave good ohmic contact to both Ge and CdSe.

9.3 THE EXPERIMENTAL SET UP

The specimen mounting arrangement used to carry out the electrical measurements on CdSe/Ge heterojunctions is

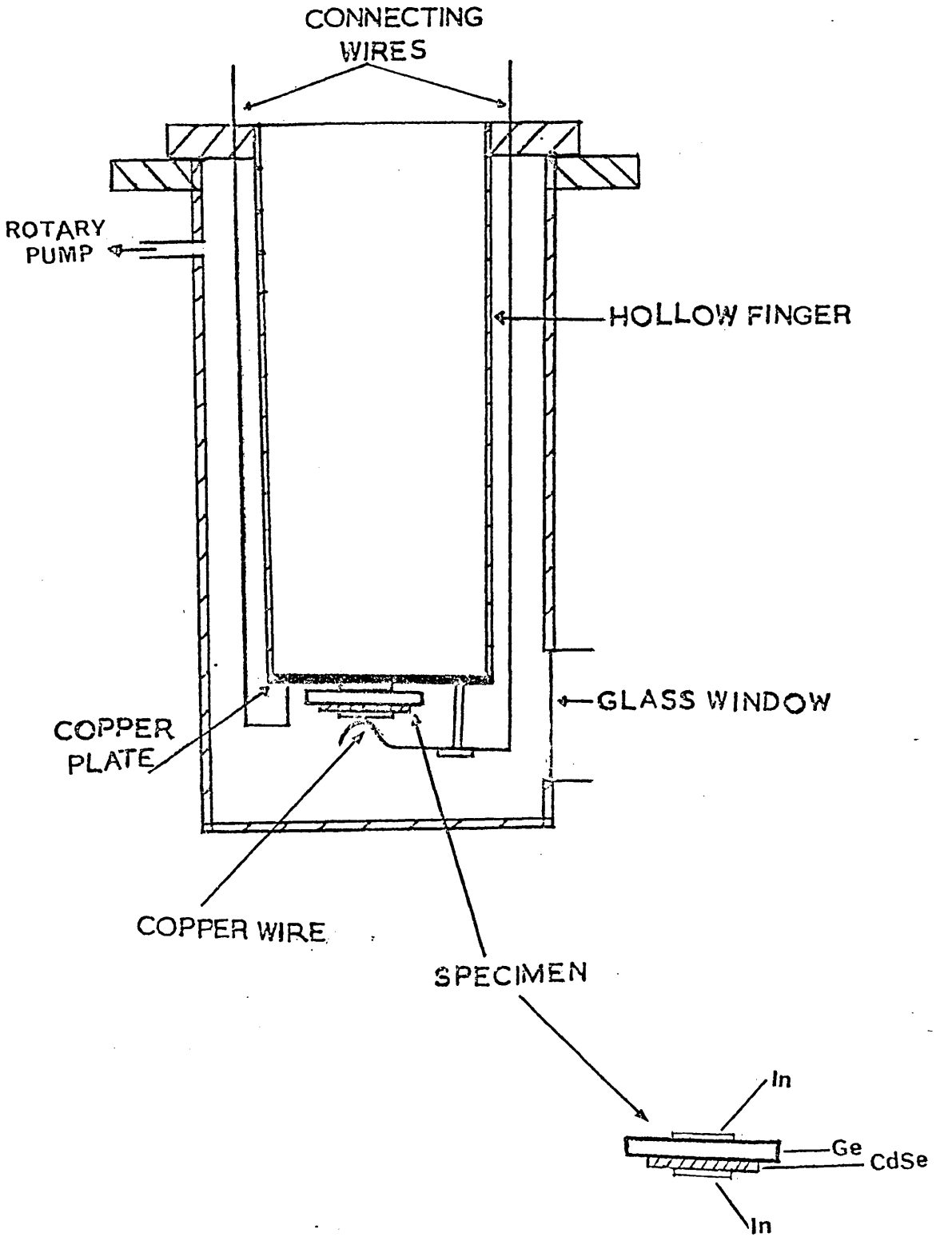


Fig. 9.4 The electrical measurements apparatus showing the specimen mounting arrangement.

shown in fig. 9.4. After the indium contact had been deposited on both the CdSe and Ge sides of a CdSe/Ge heterojunction, it was mounted on a copper plate. The Ge side indium contact was attached to the copper plate by a drop of high conductivity silver dag. The copper plate was connected to a copper lead to make connections in the circuit. A bent copper wire, as shown in the fig. 9.4 was gently pressed on the indium contact on CdSe without scratching it. A drop of high conductivity silver dag was applied to give a better contact. The copper plate was fixed to the hollow finger. This was placed in a jacket which was evacuated by rotary pump to 10^{-3} torr. The hollow finger provided the facilities to measure the I-V characteristics at different temperatures. The hollow finger was filled with water at room temperature and the I-V characteristics were measured at room temperature. Then it was filled with ice or with liquid nitrogen and the I-V characteristics were measured at the melting point of ice and at the liquid nitrogen temperature respectively. In these cases great care was taken to see that the hollow finger was full of ice or liquid nitrogen, all the time during the measurement of I-V characteristics at these temperatures. This was assured by the reproducibility of the I-V characteristics. In this preliminary I-V characteristics measurement work, the room temperature, melting point of ice and liquid nitrogen temperatures were assumed to be $293^{o}K$, $273^{o}K$ and $77^{o}K$ respectively for the purposes of the analysis of the experimental results. The I-V characteristics as shown in Fig. 9.6 were reproducibly obtained in all the CdSe/Ge(111) heterojunctions.

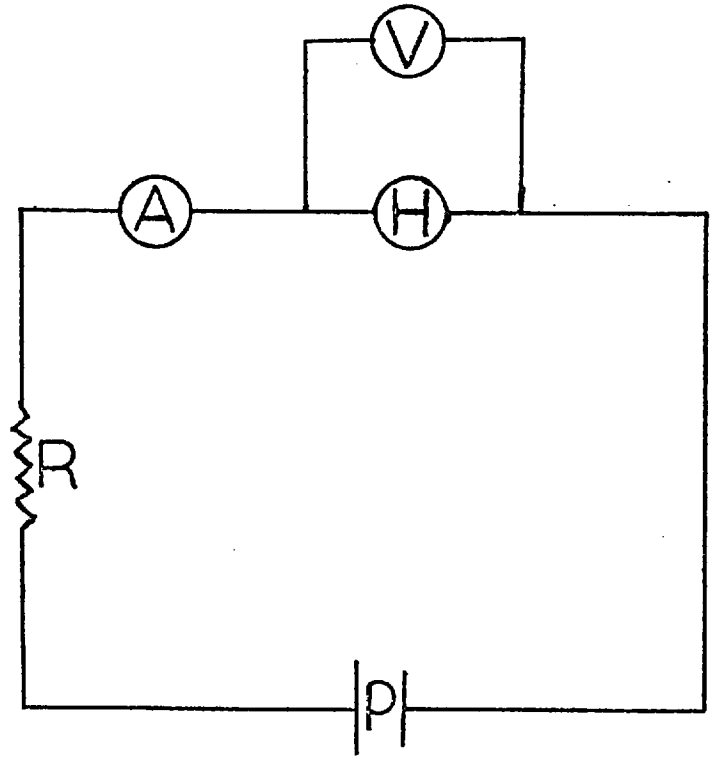


Fig. 9.5 The current-voltage characteristics measurements circuit. The various components are:

P.. Stablised DC power supply
H.. Heterojunction
V.. Voltmeter
A.. Ammeter
R.. Series Resistance

The measurements of I-V characteristics were made using the simple electrical circuit shown in fig. 9.5. The potential was provided by a stabilised D.C power source, P, which was capable of supplying up to 50 volts and 10 amps. A series resistance of 100 ohms was used in the circuit to limit the current passing through the heterojunction. The voltage drop across the heterojunction, H, and the current passing through it were measured using a voltmeter and an ammeter respectively.

9.4 EXPERIMENTAL I-V CHARACTERISTICS

Forward and reverse current-voltage characteristics of epitaxial CdSe (111)/Ge(111) heterojunctions were measured at about 293^{o}K, 273^{o}K and 77^{o}K (section 9.3). The "forward" characteristic in which the current rose rapidly with small values of applied voltage, was that with the p-type Ge positively biased and the n-type CdSe negatively biased. The "reverse" characteristic in which the current did not grow rapidly even with high values of applied voltages in comparison to the forward bias voltage values was that for which the p-type Ge and n-type CdSe were negatively and positively biased respectively. The I-V characteristics of these heterojunctions thus showed well-defined rectifying properties. Fig. 9.6 shows a typical I-V characteristics of a CdSe/Ge (111) heterojunction at these temperatures. It is evident that there is a marked difference in the form of forward and reverse bias curves. The ratio between the reverse and forward bias voltages applied for the same value

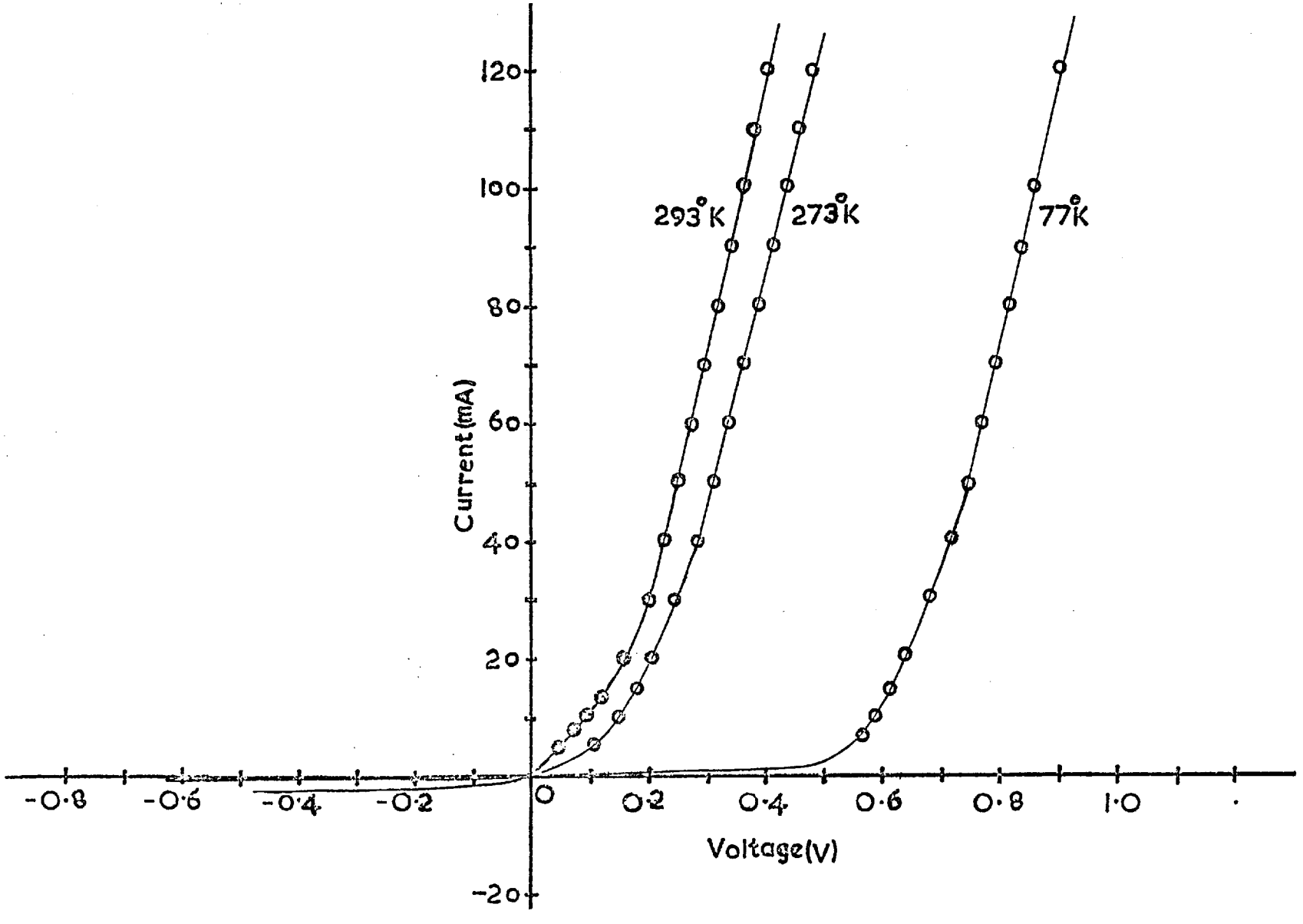


Fig. 9.6 Current-voltage characteristics of an epitaxial CdSe/Ge heterojunction.

of current was often found to exceed 10.

To understand the current transport mechanism involved in the observed I-V characteristics it is essential to compare them with the forms of behaviour predicted by the various theories of current conduction through semiconductor films and heterojunctions. The reviews of such theories (Jonscher 1967,1969, Simmons 1971 and Van Opdorp 1969) indicate that three types of plots should be tried for forward characteristics. These are log I versus V, log I versus $V^{\frac{1}{2}}$ and log I versus log V. The significance of these will now be outlined.

The energy band diagrams of Anderson (1960) of Oldham and Milnes (1964) of Van Ruyven (1964) and heterojunction conduction models such as the diffusion model of Anderson (1960), the emission model of Perlman and Feucht (1964), the tunnelling model of Rediker , Stopeck and Ward (1964), the tunnelling and recombination model of Riben and Feucht (1966) and the emission recombination model of Dolega (1963) have led to characteristics of the general form $I = I_0 \exp(BV)$, where B stands for a characteristic constant for each model. This suggested a suitable plot of I-V characteristics as log I vs. V. The theories of space charge limited currents for single and double injection of carriers (by Mott and Gurney 1940, Rose 1955, Lampert 1956, 1964) have led to relations of the form $I \propto V^2$ and higher powers. To test for the operation of such power laws a suitable plot is log I vs. log V. Field-assisted thermal ionisation or emission theories (Poole-Frenkel 1938, Schottky 1914) have led to characteristics of the form $I \propto \exp(\beta V^{\frac{1}{2}})$. This suggested plotting log I vs. $V^{\frac{1}{2}}$.

In the present preliminary work log I vs. V and log I versus log V are plotted and the details are dealt with in 9·6 and 9·7 sections. However before the analysis of the forward log I vs. V characteristics is given the equilibrium energy band profile for the p-n Ge/CdSe heterojunction is considered in the next section 9.5.

9.5 THE EQUILIBRIUM ENERGY BAND DIAGRAM FOR THE Ge/CdSe p-n HETEROJUNCTION

The construction of the energy band diagram for the CdSe/Ge heterojunction is based on the Anderson (1962) model. In order to construct this energy band diagram the values of bulk properties such as the work functions, electron affinities and energy gaps of the two materials were obtained from the literature and listed in table 9.1.

In this case the energy band diagram is of the type characterized by the following relations.

$$\chi_1 < \chi_2$$

$$\phi_1 < \phi_2$$

and $$\chi_2 < \chi_1 + Eg_1$$

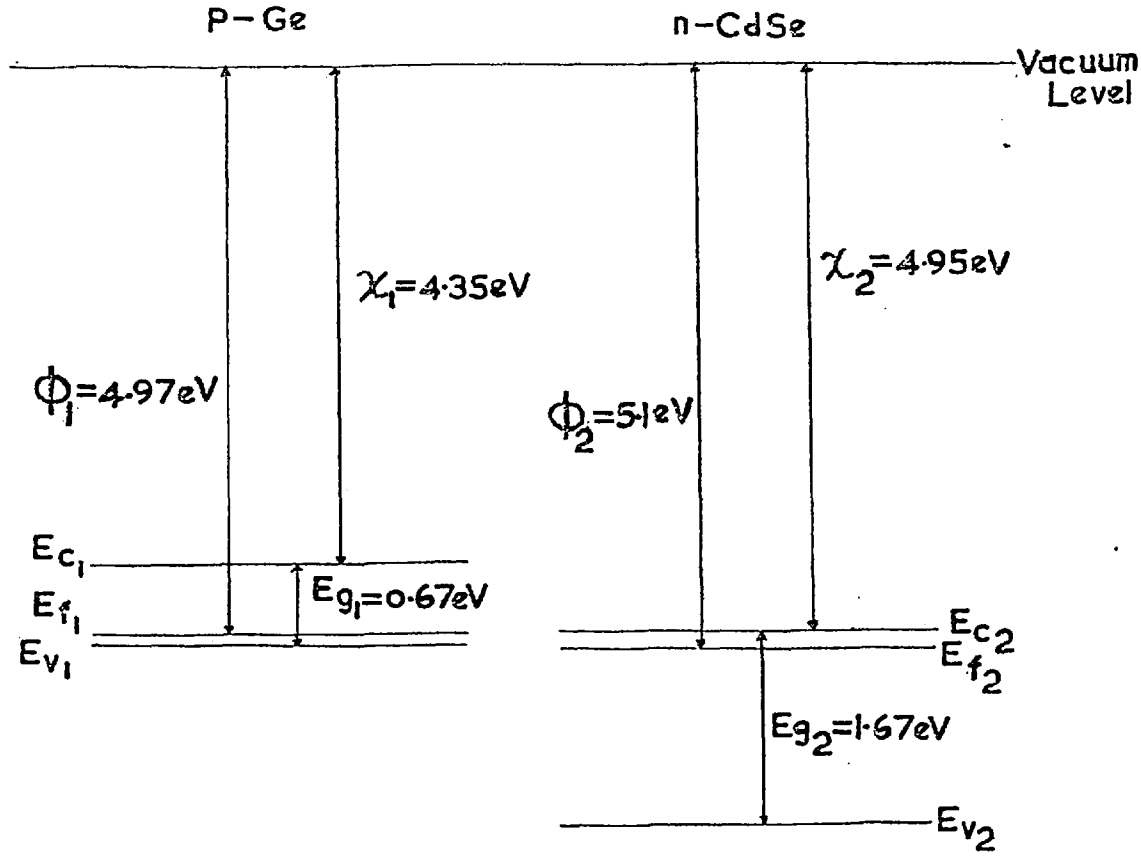
Where ψ_1 and ψ_2 are the electron affinities and ϕ_1 and ϕ_2 are the work functions of Ge and CdSe respectively and Eg_1 is the energy gap of Ge as detailed in table 9·1.

The construction of the energy band diagram proceeds from the energy diagrams for the Ge and CdSe separately. These are constructed using a common energy scale and zero: the energy of an electron at rest outside the material and known as the vacuum level. Fig. 9.7 shows the energy band

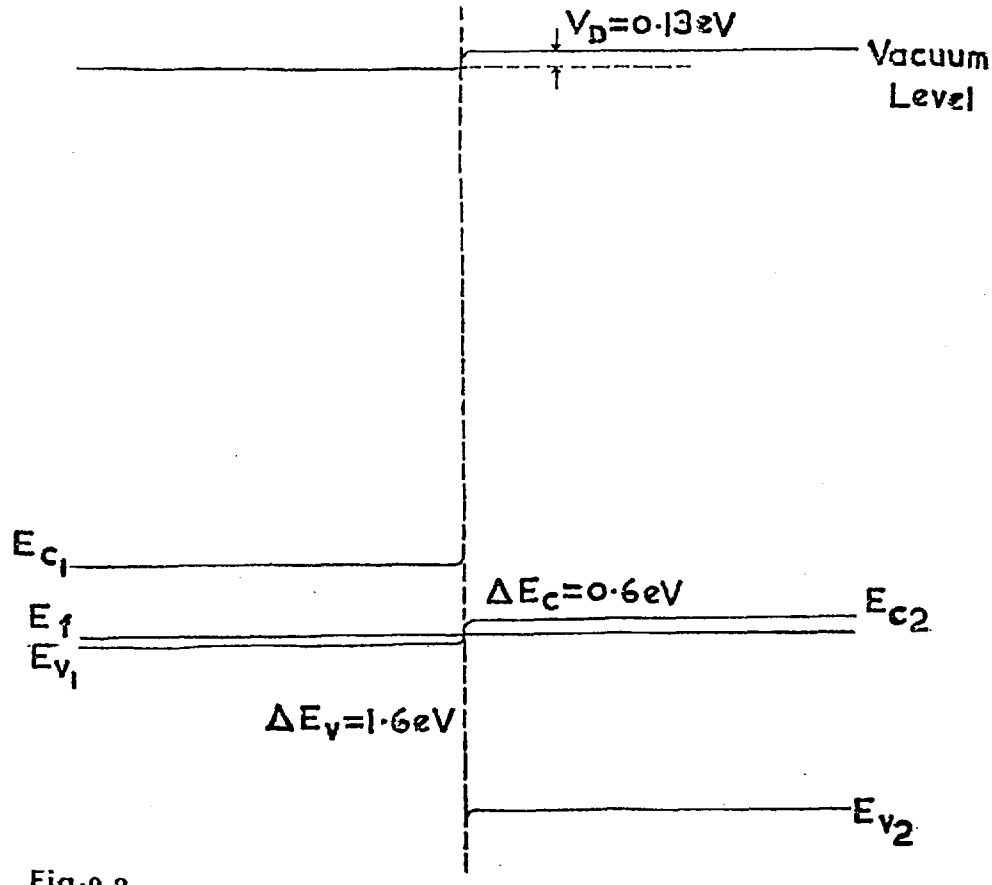
Table 9.1

Physical Properties / Semi-conductors and References	Ge	Reference	CdSe	Reference
Electron Affinity	χ_1 = 4.35eV	Haneman (1959)	χ_2 = 4.95eV	Swank (1967)
Work Function	ϕ_1 = 4.97eV	*Calcu-lated	ϕ_2 = 5.1eV	Adamchuk (1967)
Energy Gap	Eg_1 = 0.67eV	Richman (1967)	Eg_2 = 1.67eV	Delvin (1967)

*ϕ_1 = 0.67eV + 4.35eV - 0.05eV = 4.97eV



Fig·9·7
Energy Band Diagram For Two Isolated Semiconductors.



Fig·9·8
Equilibrium Energy Band Diagram of a P-n Ge/CdSe Heterojunction At Zero Bias (Based on Anderson Model(1962).

diagrams for the isolated Ge and CdSe materials. It is evident that the Fermi level in p-Ge is higher than the Fermi level in n-CdSe. When the two materials are brought into electrical contact charge transfer therefore takes place from the Ge into the CdSe to equalize the Fermi-level across the interfaces. Fig. 9.8 shows the equilibrium energy band diagram for the Ge/CdSe p-n heterojunction. The bulk properties of the two semiconductors are valid right up to the interface where there is an abrupt transition from one material to the other. Because of the transfer of electrons across the interface the conduction band edge E_{c_1} in the Ge bends up and the conduction band edge E_{c_2} in the CdSe bends down. The discontinuity of the conduction band edges at the interface ΔE_c is equal to the difference in electron affinities of the two materials; that is

$$\begin{aligned} \Delta E_c &= \chi_2 - \chi_1 \\ &= 4.95 - 4.35 \\ &= 0.6\text{eV}. \end{aligned} \qquad 9(1)$$

The discontinuity in the valence band edge at the interface is given by simple geometrical considerations as

$$\begin{aligned} \Delta E_v &= (E_{g_2} + \chi_2) - (E_{g_1} + \chi_1) \\ &= (1.67 + 4.95) - (0.67 + 4.35) \\ &= 1.60\text{eV}. \end{aligned} \qquad 9(2)$$

It is evident that from the equilibrium energy band diagram that there is an accumulation region for electrons

on the n-CdSe side of the heterojunction and an accumulation region for holes on the p-Ge side of the heterojunction. The values of the energy steps ΔE_c and ΔE_v at the conduction and valence band edges are found to be very large. Such large energy spikes may so limit electron and holes injection over the energy barriers as to allow the recombination of charge carriers at the interface to dominate the current flow. (Donnelly and Milnes 1966 and Milnes and Feucht 1972). Since the recombination current is generally a rapidly increasing function of the applied voltage, a transition from recombination-limited to tunnelling-limited conduction with forward applied voltage is possible (Donnelly and Milnes 1966). That this may be the case for the charge transport mechanism in CdSe/Ge heterojunction will be seen in more detail in the next section 9.6. The equilibrium energy diagram at the CdSe/Ge interface is such that the charge transport is strongly heterojunction-limited with consequent rectifying properties (please see fig. 9.6). This is because of the electron accumulation region on the n-CdSe side of the space charge and the electron depletion region on the p-Ge side of the space charge region. When the device is biased in the forward direction there can be easy injection of electrons and holes into the space charge region for a small value of applied voltage.

From the energy band diagram it is evident that there exists a large barrier both for electrons and for holes, when the device is biased in the reverse direction. And hence

little current flows as can be seen from the rectifying experimental I-V characteristics shown in fig. 9.6. As the reverse bias is increased there can be alignment between the valence band of p-Ge and the conduction band of CdSe resulting in the possibility of Zener tunnelling between these bands across the heterojunction. This is the main current transport mechanism in the reverse direction at higher voltages as will be shown in section 9.7.

9.6 FORWARD LOG I—V CHARACTERISTICS

The forward current-voltage characteristics of a wide variety of anisotype p-n heterojunctions have been extensively measured by many workers. It has been a common practice in all these works especially on Ge/Si (by Donnelly and Milnes 1966, Hampshire and Wright 1964, Shewchun and Wei 1964, Szekely et al 1971) and on Ge/GaAs (by Donnelly and Milnes 1966, Anderson 1962, Kurata and Hirai 1969 and Feucht 1971) to compare the observed forward bias characteristics with a current-voltage relation of the type,

$$I \propto \exp \frac{qV}{\eta kT} \qquad 9(3)$$

where η is a parameter related to the various physical properties of the heterojunction and mostly varies between 1 and 3, and the other symbols have the usual meaning.

It is interesting to see in the literature (Sharma and Purohit 1974) that the current-voltage characteristics of both p-n Ge/GaAs and n-p Ge/GaAs heterojunctions have been

extensively investigated by various workers. Inspite of the different methods used to fabricate these heterojunctions, there exists a close resemblance between their characteristics. Most of the forward bias log I-V characteristics of these heterojunctions can be divided into two distinct regions. That is a low voltage region and a high voltage region at and below room temperature.

In the low-voltage region (i.e. for voltages <0.3V at room temperature) the main contribution is due to recombination-limited current and this can be represented by expression 9(3),while in the high-voltage region the current due to tunnelling across the heterojunction dominates and it is represented by an expression of the type

$$I \propto \exp(AV) \qquad 9(4)$$

where A is a constant independent of temperature.

In the present work on CdSe/Ge heterojunctions similar effects in the forward log I-V characteristics have been observed and the analysis of these results is given below.

The basic form of the forward log I-V characteristics of n-CdSe/p-Ge heterojunctions is shown in figs. 9.9 and 9.10. It is seen that there are two different straight portions of each curve with distinct gradients. There is a transition voltage at which the slope of the curve changes.

This transition voltage at 293^{o}K is 0.13V, it is 0.18V at 273^{o}K and it is about 0.62V at 77^{o}K. This indicates that two different mechanisms are responsible for the current flow

across the heterojunction below and above the transition voltage.

Fig. 9.9 shows a typical log I-V forward characteristic measured at 293°K. It is evident from the characteristic that in the low voltage region (applied voltage <0.13V) the forward current across the heterojunction, can be represented by the law,

$$I_f \propto \exp\left(\frac{eV}{\eta kT}\right) \qquad 9(3)$$

that is

$$I_f = I_s \exp\left(\frac{eV}{\eta kT}\right) \qquad 9(5)$$

(Rediker et al 1964 and Kurata and Hirai 1968)

where I_s = saturation current

q = electron charge

k = Boltzman's constant

T = absolute temperature

V = applied voltage

and η = recombination parameter.

The above equation can be rewritten as

$$\ln I_f = \ln I_s + \frac{qV}{\eta kT} \qquad 9(6)$$

so that

$$\frac{d}{dV}(\ln I_f) = \frac{q}{\eta kT} \qquad 9(7)$$

This gives the slope of the curve for the low applied voltage.

$\frac{q}{kT}$ can be obtained from the known values of the three quantities

$$\therefore \frac{q}{kT} = \frac{1.602 \times 10^{-19}}{1.38 \times 10^{-23} \times 293}$$

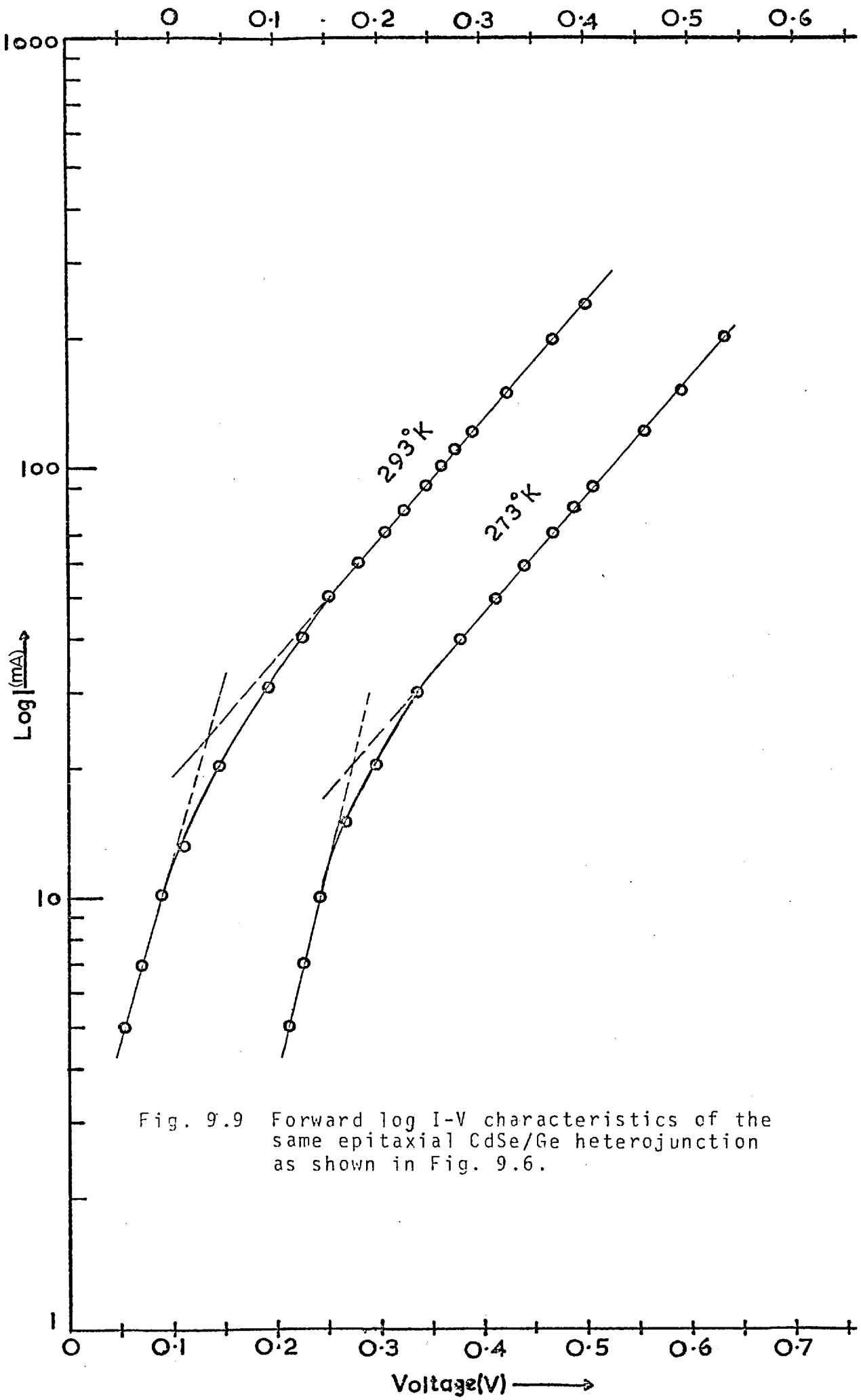


Fig. 9.9 Forward log I-V characteristics of the same epitaxial CdSe/Ge heterojunction as shown in Fig. 9.6.

$$\therefore \frac{q}{kT} = \frac{1.602}{1.38 \times 293} \times 10^4$$

$$= 39.61 \qquad 9(8)$$

The slope of the curve is calculated and tabulated in the following table 9.2 and it is given by

$$\frac{d(\ln V)}{dV} = 2.303 \frac{d}{dV}(\log V) = 19.24 \qquad 9(9)$$

Therefore from 9(7), 9(8) and 9(9)

$$\frac{39.61}{\eta} = 19.24$$

$$\therefore \quad \eta = \frac{39.61}{19.24}$$

$$\therefore \quad \underline{\eta = 2.05}$$

The experimental value of $\eta = 2.05$ indicates that at room temperature i.e. at $293^{o}K$ the conduction mechanism in the applied voltage range below 0.13 volts was predominantly by recombination of carriers in the space charge region, as predicted on the equilibrium energy band profile for the CdSe/Ge heterojunction in the section 9.5. In case of CdSe/ZnTe heterojunctions the value of η investigated by Vanyukov et al (1970) is found to be 3 at $310^{o}K$. In the case of CdSe/PbS n-p heterojunctions as reported by Suri and Sharma (1974) at room temperature it was found to be 2, while Karpinskas et al (1971) reports the variation of η between 1 and 4 in the case of CdSe/Ge and CdSe/Si heterojunctions.

In the case of heterojunctions with CdSe as one of the constituent materials, η the recombination parameter is found to vary from one pair to another.

In the high voltage region, that is above the transition voltage 0.13V, the curve changes its slope as can be seen from the fig. 9.9. In this high voltage region the current due to tunnelling can be expected to dominate across the junction. Hence in this part of the characteristic the forward current flow can be represented by the law.

$$I_f \propto \exp AV \qquad 9(4)$$

That is $$I_f = I_o \exp AV \qquad 9(10)$$

(Zeidenberg and Anderson 1967)

Where A is a constant which is practically independent of temperature, I_o is the initial current which decreases with decreasing temperature (Zeidenberg and Anderson 1967), and V is the applied voltage.

The above expression can be rewritten as

$$\ln I = \ln I_o + AV$$

so that $$\frac{d}{dV}(\ln I) = A$$

i.e. $$\frac{d}{dV}(\ln I) = 2.303 \frac{d}{dV}(\log I) = A \qquad 9(11)$$

which is the slope of the curve, in the high voltage region. In this region of the graph the slope is found to be 6.66.

That is $A = 6.66/_V$. The smallest value of A reported in the literature is A = 2.3, at 300°K, in the case of Ge-GaAs p-n heterojunctions by Kurata and Hirai (1968), whereas Laugier at al. (1970) report A = 5.75 at 77°K in the case of Ge/GaAs n-p heterojunctions.

In the case of GaP/GaAs p-n heterojunctions A is found to be 7 for V < 1.3V and 2.3 for V ≥ 1.3V by Davis et al. (1969). The rest of the reported values for A are found to be much higher than the one found in this work.

Fig. 9.9 also shows the log I-V characteristic of the same CdSe/Ge heterojunction, measured at 273°K. The overall form of the characteristic is the same as that at 293°K.

Again the characteristic shows low voltage and high voltage regions. The slope of the curve changes at the transition voltage at about 0.18V. Below this point is a low voltage region in which the charge transport mechanism across the junction is predominantly recombination-limited and the current has the form given by the expression (3)

$$\text{i.e. } I_f = I_s \exp\left(\frac{qV}{\eta kT}\right) \qquad 9(3)$$

so that the slope is given by $\frac{d}{dV}(\ln I_f) = \frac{q}{\eta kT}$.

$\frac{q}{kT}$ is again obtained from the values, i.e.

$$\frac{q}{kT} = \frac{1.602 \times 10^{-19}}{1.38 \times 10^{-23} \times 273}$$

$$= \frac{1.602}{1.38 \times 273} \times 10^{4}$$

$$= 42.51 \qquad 9(12)$$

From the characteristic in fig. 9.9 the slope calculated is

$$\frac{d}{dV}(\ln I_f) = 2.303 \frac{d}{dV}(\log I_f) \qquad 9(13)$$

$$= 20.05 \text{ (from table 9.2)}$$

$$\therefore \frac{42.91}{\eta} = 20.05$$

$$\therefore \eta = \frac{42.91}{20.05}$$

$$= 2.11$$

$$\therefore \underline{\eta = 2.11}$$

It is seen that the value of η at $273^{o}K$ is slightly higher than that at $293^{o}K$.

In the high voltage region, that is for applied voltages greater than 0.18V the current due to tunnelling dominates and is given by expression;

$$I_f = I_o \exp AV. \qquad 9(14)$$

Where A is a constant and I_o is the initial current, which is different from that for $293^{o}K$.

The slope of the high voltage region of the characteristic is given by

$$\frac{d}{dV}(\ln I_f) = 2.303 \frac{d}{dV}(\log I_f) = A.$$

The value of A calculated from this part of the characteristic was found to be 6.66 which is practically the same as at $293^{o}K$. This shows that the constant A is practically independent of temperature of the device under investigation.

Fig. 9.10 shows the log I-V characteristic of the same device, measured at $77^{o}K$. The overall form of the characteristic is basically again the same as shown in fig. 9.9 having distinct low voltage and a high voltage regions. The slope of the characteristic changes at the transition voltage of about 0.62 volt. Below this voltage the current contribution is mainly due to the recombination-limited current and the current flow obeys the law given by the expression 9(3),

Hence the slope of this low voltage region is given by

$$\frac{d}{dV}(\ln I_f) = \frac{q}{\eta kT} \qquad 9(15)$$

The slope calculated from the low voltage region of this characteristic is, $\frac{d}{dV}(\ln I_f)$ =

$$2.303 \times \frac{d}{dV}(\log I_f) = 68.04 \text{ (see table 9.2)}$$

and $$\frac{q}{kT} = \frac{1.602 \times 10^{-19}}{1.38 \times 10^{-23} \times 77}$$

$$= 150.7 \qquad 9(16)$$

$$\therefore \frac{150.7}{\eta} = 68.04$$

$$\therefore \eta = \frac{150.7}{68.4}$$

$$= 2.21$$

$$\therefore \underline{\eta = 2.21}$$

The value of η at $77^{o}K$ is found to be slightly higher than the values for η at $273^{o}K$, $293^{o}K$. This means that the

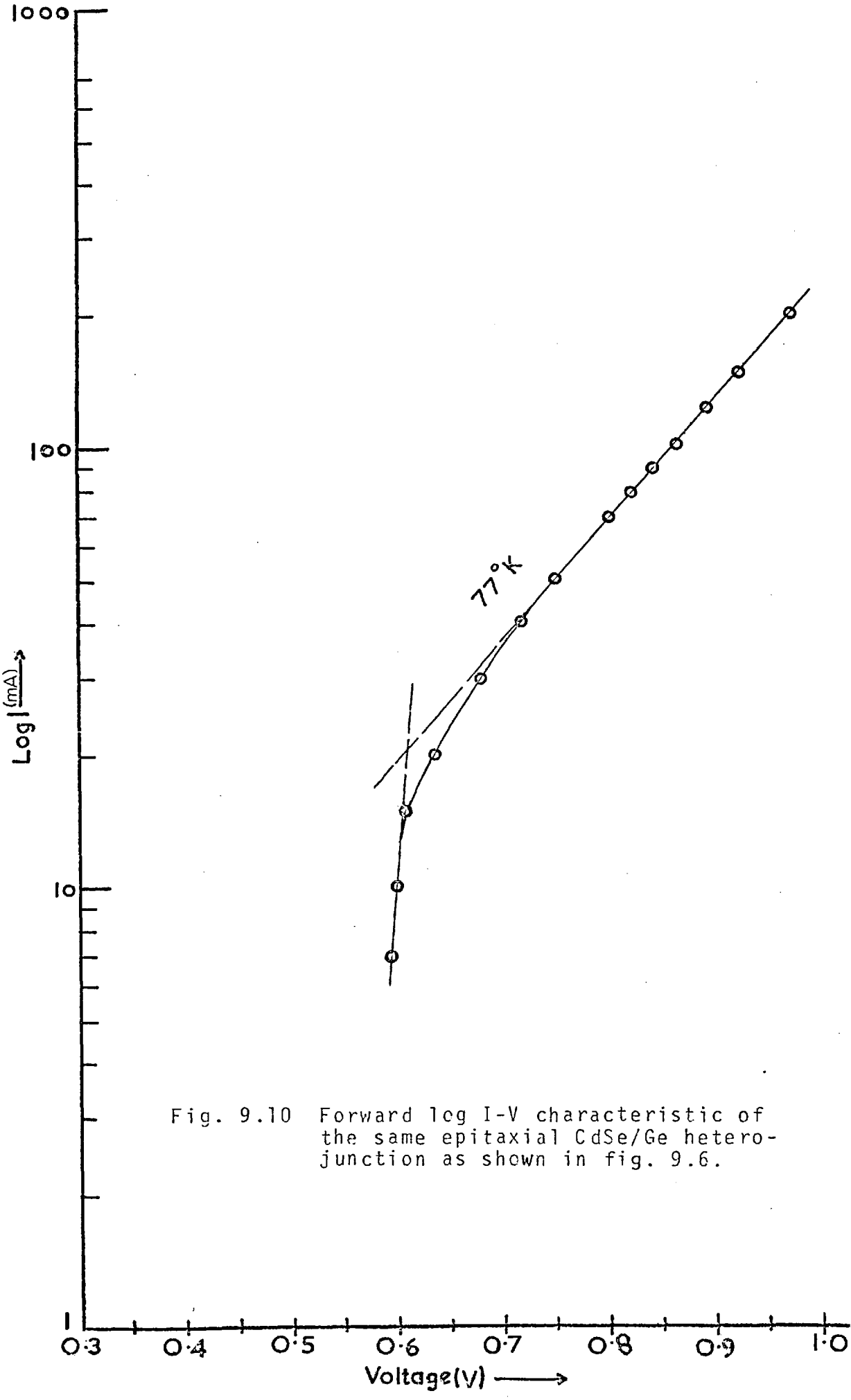


Fig. 9.10 Forward log I-V characteristic of the same epitaxial CdSe/Ge hetero-junction as shown in fig. 9.6.

value of η increases with decrease in the temperature of the CdSe/Ge heterojunction. Such a slight increase in the η values with a similar decrease in the device temperature has been observed by Donnelly and Milnes (1966) in p-n Ge/Si and by Feucht (1971) in p-n Ge/GaAs heterojunctions.

In the high voltage region that is above the transition voltage, 0.62V, the slope of the curve changes. In this high voltage region the current due to tunnelling dominates and it is given by the expression

$$I_f = I_0 \exp AV. \qquad 9(17)$$

Where A is a constant and I_0 is the initial current, which should be different from the two previous cases, because it decreases with decreasing temperature.

Hence the slope of the high voltage region is given by $\frac{d(\ln I_f)}{dV} = 2.303 \times \frac{d}{dV}(\log I_f) = A$. The value of A calculated from the high voltage region of the characteristic in fig. 9.10 is found to be A = 6.66 which is practically the same as those obtained from the characteristics at 293°K and 273°K. Again it shows that A is independent of temperature. This temperature independence of slope is indicative of tunnelling (Donnelly and Milnes 1966, Davis et al 1969). This is because any transport mechanism involving emission over a barrier is expected to give log I_f-V curves, whose slopes are very temperature sensitive. Hence the temperature independence of slope indicates that the current

Table 9.2

Temperature	Slope				Average
	1	2	3	4	
293°K	19.22	19.26	19.23	19.23	19.24
273°K	20.08	20.00	20.04	20.09	20.05
77°K	68.03	68.03	68.00	68.08	68.04

is mainly due to the temperature independent tunnelling process.

Thus from the experimental log I-V characteristics it is evident that the current conduction across the p-Ge/n-CdSe heterojunction is predominately by recombination-limited current in the low voltage region and by tunnelling in the high voltage region at and below room temperature.

These results are in agreement with the predictions of the equilibrium energy band profile at the p-n Ge/CdSe heterojunction shown in fig. 9.8.

9.7 REVERSE BIAS I-V CHARACTERISTICS

The reverse bias I-V characteristics of a n-CdSe/p-Ge heterojunction measured at about 293^{o}K, 273^{o}K and 77^{o}K are shown in fig. 9.11. It is evident from the I-V characteristics that at low reverse bias, the current is a slowly increasing function of voltage and as the reverse voltage is increased a soft breakdown is observed. At 293^{o}K a soft breakdown is observed at about 5.3 volts and the characteristics measured at 273^{o}K and 77^{o}K showed soft breakdowns at about 6.3 and 9 volts respectively.

It is evident in the literature that even though the reverse-bias I-V characteristics have generally been measured together with the forward I-V characteristics, very little attention has been paid to their analysis (Sharma and Purohit 1974). This is attributed to the fact that the soft breakdown observed in almost all the reverse characteristics is not well understood. A number of workers have however fitted

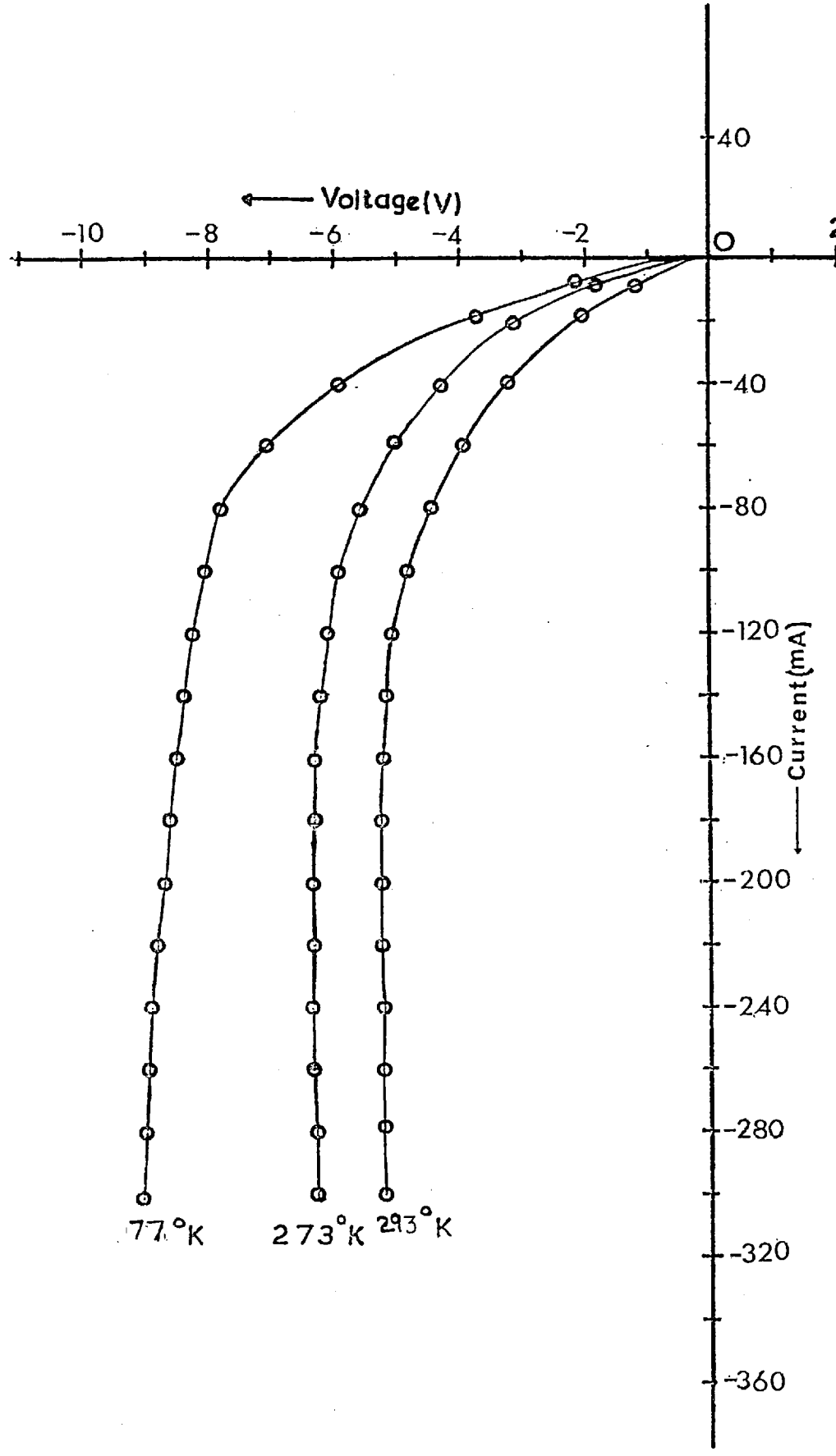


Fig. 9.11 Reverse bias I-V characteristics of an epitaxial CdSe/Ge heterojunction.

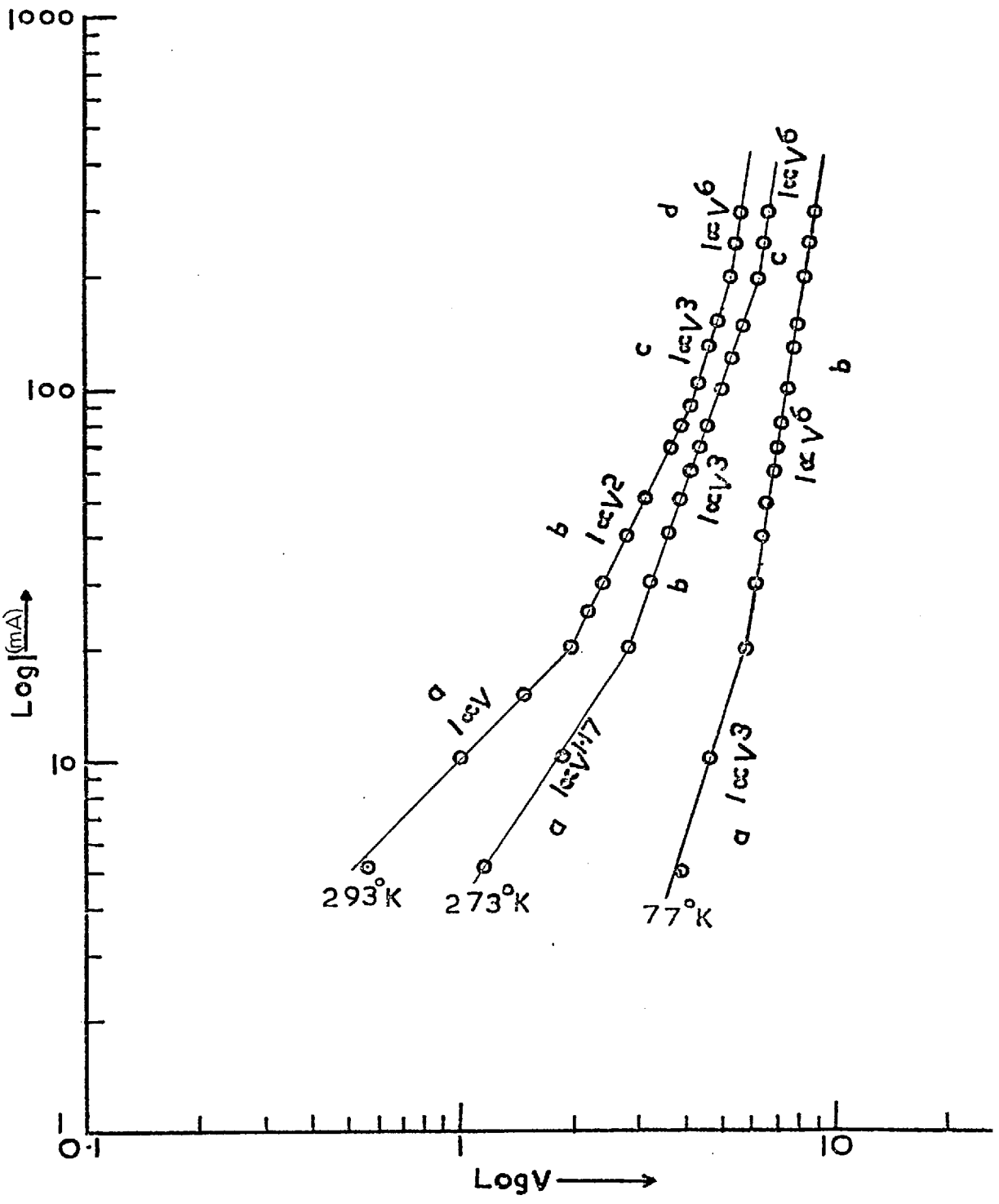


Fig. 9.12 Reverse bias log I-log V characteristics of the same CdSe/Ge heterojunction as shown in fig. 9.11.

their experimental data to a power law of the form $I_R \propto V^m$; where I_R is the reverse current, V is the reverse bias voltage and m is greater than 1 and is a function of temperature, and tried to explain their results on the basis of the tunnelling model of Riben and Feucht (1966a). Donnelly and Milnes (1966) have observed in p-Ge/n-GaAs heterodiodes a linear variation of the type $I_R \propto V$ at low reverse voltage and a power law variation of the type $I_R \propto V^m$, where m is greater than 3 for high reverse voltages. Similar behaviour has been also observed in the present work on p-n Ge/CdSe heterojunctions.

Fig. 9.12 shows the log I-log V characteristic of the same p-n Ge/CdSe heterodiode measured at about 293°K. It is seen that at low applied reverse bias, that is in region a, there is linear variation of current with voltage. That is $I \propto V^1$, showing an ohmic regime to occur at low reverse bias.

As the reverse bias voltage is increased, region b is reached in which the current $I \propto V^2$. This is a space-charge-limited regime. On further increasing the reverse bias region c is reached in which the current is proportional to V^3. Lastly, further increase of voltage gives rise to an higher power law in which the current is proportional to V^6, as shown in region d.

Fig. 9.12 also contains the logI-log V characteristic of the same device measured at 273°K. At low applied bias

an approximately linear variation of current with voltage is seen. That is, in region a, the current is found to be proportional to $V^{1.17}$. On increasing the voltage, region b, is reached in which the current is found to be proportional to V^3. On further increasing the reverse bias, the current is found to be given by $I \propto V^6$, as shown in region c.

The log I-log V characteristic of the same device measured at 77^oK, in fig. 9.12, is of V^3 form even at low bias as shown in region a. In region b the current was found to be proportional to V^6.

Thus as the temperature is decreased from 293^oK to 77^oK in the low voltage region the ohmic regime changed to a higher power regime and at higher voltages a V^6 power law was found to occur at all these temperatures. This shows that in the lower applied voltage ranges m is a function of temperature. Similar effects were also observed in the case of the n-p Ge/GaAs heterodiodes studied by Riben and Feucht (1964, and 1966a&b). They found that when the temperature of the diode was reduced from 300^oK to 77^oK, the reverse I-V characteristics showed a linear ohmic regime change into a $V^{6.5}$ power law. Abdalla (1973) observed ohm's law at low voltages followed by a V^m power law in the reverse I-V characteristics of n-CdTe/p-Ge heterojunctions, where m was found to vary between 4.5 and 6.5.

Abdalla (1973) also plotted the log $\frac{I}{V}$ versus log $V^{-\frac{1}{2}}$ characteristics and found evidence that Zener tunnelling was the principal conduction mechanism in the reverse direction

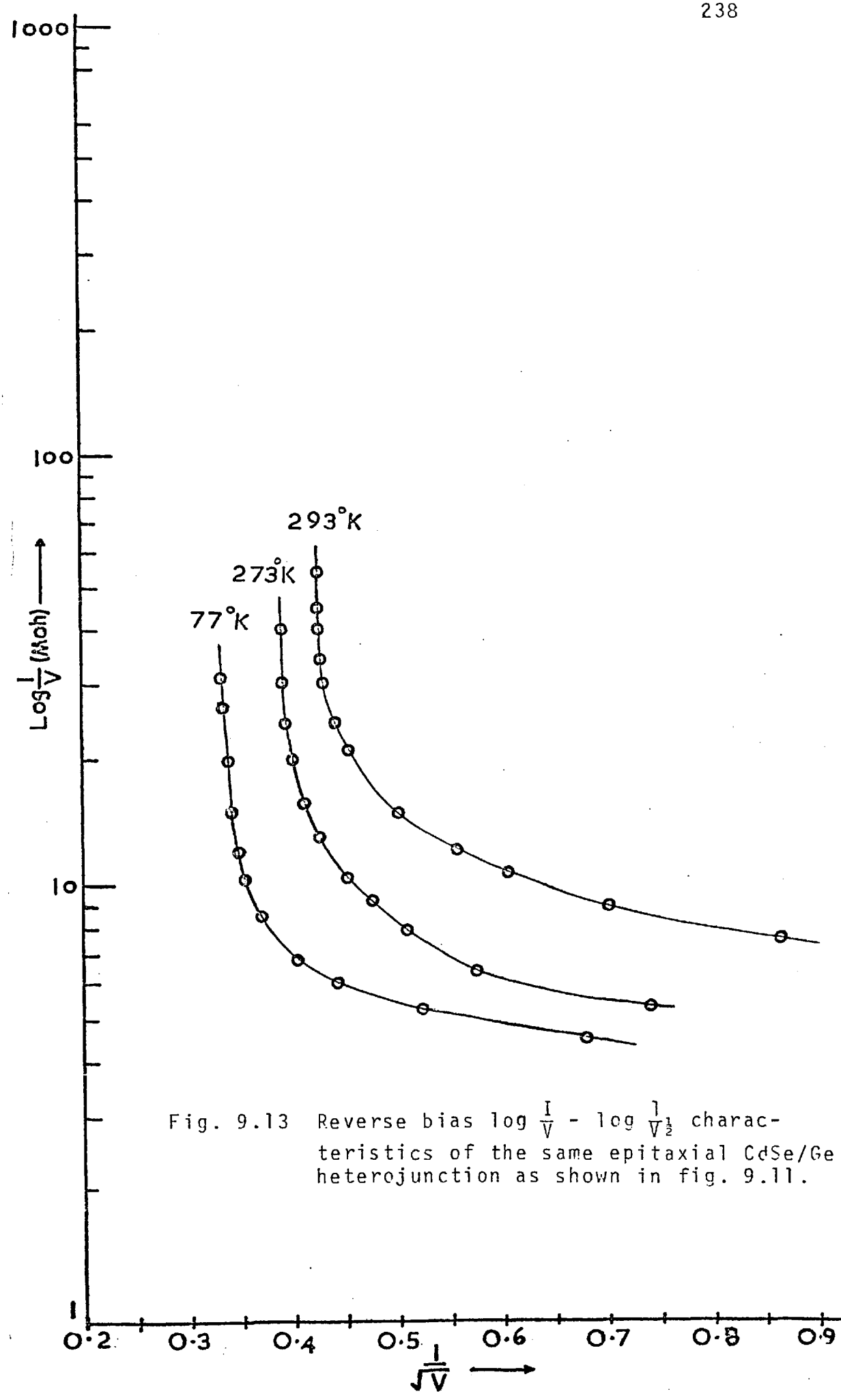


Fig. 9.13 Reverse bias log $\frac{I}{V}$ - log $\frac{1}{V^{\frac{1}{2}}}$ characteristics of the same epitaxial CdSe/Ge heterojunction as shown in fig. 9.11.

across the CdTe/Ge heterodiodes. The observation of a high power law dependence in the reverse characteristics could be due to the Ge valence band gaining enough energy to come level with the CdSe conduction band as predicted by the equilibrium energy band profile (see section 9.5) of the p-n Ge/CdSe heterojunction. If this happens Zener tunnelling is expected to be the predominant current transport mechanism (Riben and Feucht 1966b). Donnelly and Milnes (1966), Riben and Feucht (1966a, and 1966b) and Hovel and Milnes (1968) suggested that if Zener tunnelling is operating, then the current is given by the expression,

$$I = AV \exp(-BV^{-\frac{1}{2}}) \qquad 9(18)$$

where A and B are constants.

Fig. 9.13 gives the $\log \frac{I}{V}$ versus $V^{-\frac{1}{2}}$ characteristics measured at 293°K, 273°K and 77°K. From these graphs it is evident that $\log \frac{I}{V}$ is proportional to $V^{-\frac{1}{2}}$ at higher voltages and that these straight portions of the graphs are parallel with practically constant slope. This suggests that the current transport mechanism across the n-CdSe/p-Ge heterodiodes in the reverse bias direction is predominantly Zener tunnelling.

CHAPTER X

CONCLUSIONS AND PROPOSALS FOR FUTURE WORK

This research programme was started with the following purposes; (1) to grow reproducible and controllable epitaxial films of cadmium selenide on germanium for the first time with the minimum defect content; (ii) to study the growth habits and structure of the CdSe films and the CdSe/Ge heterojunctions; (iii) to identify and analyse the defects such as planar defects and domain-form transformed structures by annealing; (iv) to obtain information about the nature of the misfit dislocations at the CdSe/Ge heterojunctional interfaces; (v) to examine the experimentally observed epitaxial phenomena in CdSe/Ge devices and to compare them with existing general features of epitaxial phenomena found in the literature and (vi) lastly to study the physical properties of p-n Ge/CdSe heterojunctions.

In this thesis the results of the experimental investigations have been reported in two parts I and II.

From the results of part I of this thesis it is quite clear that the first set of objectives (I to V) were achieved to a satisfactory extent. With the study and adjustment of various growth parameters such as the substrate temperature, substrate surface perfection , vacuum conditions etc. the epitaxial ranges of CdSe on (100), (110) and (111) oriented Ge substrates were established reproducibly. The epitaxial CdSe films had always the cubic sphalerite structure. Three

dimensional defects were never observed in these CdSe films. The films of CdSe grown on (100) and (110) faces of Ge contained two dimensional planar defects in high densities but the films of CdSe grown on the (111) faces of Ge did not. Most of the work reported here was done in high vacuum ~ 10^{-6} torr and the effects of the various growth parameters were fully explored in this range. So in order to make more perfect films, and to get wider epitaxial ranges, it is suggested that the effect of ultra-high vacuum (of 10^{-8} torr and below) should be studied.

The CdSe films grown on (100) and (110) surfaces of Ge follow the general rules of epitaxy found for other II-VI compounds. That is they were found to grow in parallel alignment with the substrate. However when the CdSe was grown on (111) faces of Ge it was found that it does not follow previously observed rules for II-VI compounds. That is, it grows with a new epitaxial orientation relationship with the substrate. This was described as the "nearly-parallel rotation" epitaxial orientation. This orientation relation is the first of its kind found in the research study of II-VI epitaxy. Further investigations indicated that 60^{o} mixed misfit dislocations could account for the relative rotation of the CdSe film and Ge substrate through $2^{o}24'$ about the (111) heterojunction normal. This evidence for the possible importance of 60^{o} misfit dislocations is the first in the field of epitaxy. The spacings of the 60^{o} dislocations was obtained both from independent measurements and by

comparison with moire fringe spacings. The spacing of 60^{o} dislocations was calculated by assuming the edge components accounted for the whole of the lattice parameter misfit and that the screw components accounted for the rotation from parallel alignment. Both the theoretically calculated and experimentally observed values of the spacing was found to be about 50 Å . However transmission electron microscope determination of the Burgers vector of these misfit dislocations is still needed to establish the facts beyond any doubt. Hence it is suggested here that following the chemical thinning technique used in this work, more films of CdSe/Ge (111) should be prepared and transmission electron microscope observations should be continued to determine the Burgers vectors of these dislocations by diffraction contrast. It is also suggested that it should be very interesting to start electron microscopy studies of the nucleation and growth of CdSe on the (111) faces of Ge to explore the initial growth mechanism and of the accommodation of misfit by the nucleation of 60^{o} mixed misfit dislocations at the heterojunctional interface.

The characteristic defect structure found in films of all the II-VI compounds studied in this laboratory over many years when grown on (110) oriented ionic or semiconductor elemental substrates was of <111> planar defects in a "domain-form transformed" structure. In the present work high resolution dark field microscopy revealed the jig-saw-puzzle-piece shaped domains in these films. When these epitaxial CdSe/

Ge (110) specimens were annealed the jig-saw-puzzle-pieces disappeared leaving behind their domain boundaries. From high resolution darkfield microscopy studies of these annealed films it was concluded that these domain boundaries were in fact antiphase domain boundaries. This is the first time that antiphase domain boundaries were found in the field of epitaxial studies of II-VI compounds. It is suggested for future work that (110) CdSe/(110) Ge specimens should be annealed at higher temperatures to discover whether the antiphase domain boundaries could be also annealed out; thus improving the structural perfection of (110) II-VI films.

The present work on the (110) CdSe/(110) Ge heterojunctions has explored the structural properties of these heteroepitaxial devices, but further interesting investigations of the electrical properties of these devices remain to be made. Measurements at different temperaturesshould be carried out. This should make it possible to identify the mechanism of current transport across these devices and to correlate them with the types of defects present and their effects.

As reported in part II of this thesis studies of the I-V characteristics of CdSe/Ge (111) heterodiodes were carried out. These I-V characteristics showed the rectifying properties of p-n Ge/CdSe (111) heterojunctions. In case of the forward I-V characteristics the current transport mechanism seemed to be predominantly recombination-tunnelling and in the reverse I-V characteristics the current transport

was found to be predominantly due to Zener tunnelling at higher voltages. For future work it is suggested that capacitance-voltage measurements in the reverse direction should be carried out to determine the built-in-voltage in these heterojunctions and thus remove the only uncertainty in the construction of the equilibrium energy band diagram at these abrupt heterojunctions. CdSe is a photoconductor. Hence the study of the optical properties such as the "window effect" in the photovoltaic response of these heterojunctions is suggested as an interesting future study on these heterojunctions.

REFERENCES

Abdalla, M.I., Holt, D.B. and Wilcox, D.M. (1973), J. Mater. Sci. 8, 590.

Abdalla, M.I. and Holt, D.B. (1973), Phys. Stat. Sol. (a)17, 267.

Abdalla, M.I. (1973), Ph.D. Thesis, University of London.

Aberdam, D., Bouchet, G., Ducros, P., Daval, J. and Grunberg, G. (1969), Surface Sci. 14, 121.

Adamchuk, V.K. (1967), Opt. and Spectr. 22, 325.

Al'tman, L.V., Vorontsova, E.N., Ruban, Yu.V. and Tikhomirov, G.P. (1968), Sov. Phys. Crystallography, 12, 601.

Anderson, R.L. (1960), IBM. J. Res. Develop. 4, 283.

Anderson, R.L. (1962), Solid State Electron. 5, 351.

Anderson, R.L. (1971), Proc. Int. Conf. on the Phys. Chem. of Semicond. Heterojunctions (Ed. in chief G. Szigeti) Akademiai Kiado, Budapest, Vol. II, p. 55.

Arnold, H. Kaufmann, T. and Mach, R. (1970), Phys. Stat. Sol. (a)1, K5.

Aven, M. and Garwaki, W. (1963), J. Electrochem. Soc. 110, 401.

Barber, H.D. and Heasell, E.L. (1965), J. Phys. Chem. Solids 26, 1561.

Basset, G.A., Menter, J.W. and Pashley, D.W. (1958), Proc. Roy. Soc. London A246, 345.

Basset, G.A. (1960), Proc. Eur. Regional Conf. Electron Microsc. Delft (A.L. Houwink and B.J. Spits, eds.), Vol. 1; p.270. De Nederlandse Vereniging Voor Electronmikrosc., Delft.

Basset, G.A. (1964), Proc. Int. Symp. Condensation Evaporation Solids, E. Rutner, P. Goldfinger and J.P. Hirth eds. (Gordon and Breach New York) p.599.

Bauer, E. (1958), Z. Kristallogr. 110, 372

Biondi, F.J. (ed.) 1958, "Transistor Technology", vol. 3, p.175 (Van Nostrand-Reinhold, Princeton, New Jersey).

Blankenburgs, G. and Wheeler, M.J. (1963-64), J. Inst. Metal, 92, 337.

Blank, H., De Lavignette, P., Gevers, R. and Amelinckx, S. (1964), Phys. Stat. Sol. 7, 747.

Blount, G.H., Fisher, W.M., Marrison, R.G., Bube, R.H. (1966), J. Electrochem. Soc. 113, 690.

Bobb, L.C., Holloway, H., Maxwell, K.H. and Zimmerman, E. (1966), J. Appl. Phys. 37, 4687.

Booker, G.R. and Stickler, R. (1962a), J. Appl. Phys. 33, 3281.

Booker, G.R. and Stickler, R. (1962), Brit. J. Appl. Phys 13, 446.

Booker, G.R. and Unvala, B.A. (1965), Phil. Mag. 11, 11.

Borneman, E.H., Schwartz, R.F. and Stickler, J.J. (1955), J. Appl. Phys. 26, 1021.

Brooks, H. (1952), Metal Interfaces, Am. Soc. Metals, Cleaveland, Ohio, p.20.

Brück, L. (1936), Ann. Physik, 26, 233.

Brunnschweiler, A. (1966), Nature, 209, 493.

Bube, R.H. (1960), Photoconductivity of Solids (John Wiley and Sons, Inc: London).

Burmeister Jr., R.A. and Stevenson, D.A. (1967), Phys. Stat. Sol. 24, 683.

Calow, J.T., Owen, S.J.T. and Webb, P.W. (1968), Phys. Stat. Sol. 28, 295.

Cardona, M., Weinstein, M. and Wolff, G.A. (1965), Phys. Rev. 140, A637.

Cherns, D. and Stowell, M.J. (1973), Scripta Met. 7, 489.

Chopra, K.L. and Khan, I.H. (1967), Surface Sci. 6, 33.

Chopra, K.L. (1969), "Thin Film Phenomena" (McGraw Hill:N.Y.).

Collins, L.E. and Heavens, O. (1952), Proc. Phys. Soc. B65, 825.

Coopersmith, B., Curzon, A.E., Kimoto, K. and Lisgarten, N.D. (1966), in "Basic Problems in Thin Film Physics" (R. Niedermayer and H. Mayer, eds) p.83 Vandenhoeck and Ruprecht, Gottingen.

Cullity, B.D. (1956), Elements of X-ray Diffraction. (London: Addison Wesley)

Cullis, A.G. and Booker, G.R. (1970), Proc. Seventh Int. Cong. Electr. Microsco. Grenoble (Soc. Fronc. Micr. Elect. Paris), p.423, "Electron Microscopy and Analysis" Inst. Phys. London, 1971, p.320.

Cusano, D.A. (1967), Physics and Chemistry of II-VI Compounds, eds. Aven, M. and Prenner J.S. (North Holland: Amsterdam) p.707.

Dale, J.R. and Turner, R.G. (1963), Solid State Electron. 6, 388.

Davis, M.E., Zeidenbergs, G. and Anderson, R.L. (1969), Phys. Stat. Sol. 34, 385.

Deasley, P.J., Owen, S.J.T. and Webb, P.W. (1970), J. Mater. Sci. 5, 1054.

Delvin, S.S. (1967), Physics and Chemistry of II-VI Compounds, eds. Aven, M. and Prenner, J.S. (North Holland: Amsterdam).

Demey, G. (1974), Electrocomponent Science and Technology, 1, 39.

Dhere, N.G. and Goswami, A. (1969), Thin Solid Films, 3, 439.

Dickson, E.W. and Pashley, D.W. (1962), Phil. Mag. 7, 1315.

Dolega, U. (1963), Z. Naturf. 18a, 653.

Donnelly, J.P. and Milnes, A.G. (1966), Proc. IEE 113, 1468.

Dowell, W.C.T., Farrant, J.L. and Rees, A.L.G. (1956), Proc. 3rd Int. Conf. on Electron Microsc. London, (1954), p.279.

Dowell, W.C.T., Farrant, J.L. and Rees, A.L.G. (1957), Proc. Reg. Conf. on Electron. Microsc. Tokyo (1956), p.320.

Evans, T. and Noreika, A.J. (1966), Phil. Mag. 13, 717.

Feucht, D.L. (1971), Proc. Int. Conf. on the Phys. of Semicond. Heterojunctions (Editor in chief G. Szigeti), Akademiai Kiado, Budapest. Vol. 1, p.39.

Fischer, A.G. (1966), Luminescence of Inorganic Solids, Ed. Goldberg, P. (Academic Press New York and London).

Flinn, P.A. (1960), Trans. Metall. Soc. A.I.M.E. 218, 145.

Francombe, M.H. and Sato, H. (1964), "Single Crystal Films" (Pergamon Press:Oxford) eds.

Frank, F.C. and Van Der Merve, J.H. (1949), Proc. Roy. Soc. London, A198, 216.

Frenkel, J. (1938), J. Phys. Rev. 54, 647.

Gashin, P.A. and Simashkevich, A.V. (1973), Phys. Stat. Sol. (a)19, 379.

Gatos, H.C. and Lavine, M.C. (1965), Prog. Semicond. 9, 1.

Goldfinger, P. and Jeunehomme, M. (1963), Trans. Faraday Soc. 59, 2851.

Halpern, V. (1967), Brit. J. Appl. Phys. Ser. 2, 2, 775.

Hampshire, M.J. and Wright, G.T. (1964), Brit. J. Appl. Phys. 15, 1331.

Haneman, D. (1959), J. Phys. Chem. Solids, 11, 205.

Hashimoto, H. and Uyeda, R. (1957), Acta. Cryt. 10, 143.

Hill, R.M. (1967), Thin Solid Films, 1, 39.

Hill, R.M. (1971), Phil. Mag. 23, 59.

Hirsch, P.B., Howie, A., Nicholson, R.B., Pashley, D.W., Whelan, M.J. (1965), "Electron Microscopy of Thin Crystals (Butterworths; London).

Hirth, J.P. and Pound, G.M. (1963), "Condensation and Evaporation: Nucleation and Growth Kinetics", (Pergamon, Oxford).

Holloway, H. and Wilkes, E. (1968), J. Appl. Phys. 39, 5807.

Holt, D.B. (1966a), Brit. J. Appl. Phys. 17, 1395.

Holt, D.B. (1966b), J. Phys. Chem. Solids 27, 1053.

Holt, D.B. (1966c), J. Mater. Sci. 1, 280.

Holt, D.B. (1969a), J. Mater. Sci. 4, 935.

Holt, D.B. (1969b), J. Phys. Chem. Solids, 30, 1297.

Holt, D.B. (1974), Thin Solid Films, 24, 1.

Holt, D.B. and Woodcock, J.M. (1970), J. Mater. Sci. 5, 275.

Holt, D.B. and Wilcox, D.M. (1971), J. Cryst. Growth 9, 193.

Holt, D.B. and Abdalla, M.I. (1974), Phys. Stat. Sol. (a)26, 507.

Holt, D.B. and Abdalla, M.I. (1975), Phys. Stat. Sol. (a)29, 129.

Holt, D.B., Abdalla, M.I., Gejji, F.H. and Wilcox, D.M. (1976), To be published in Thin Solid Films.

Holt, D.B. and Wilcox, D.M. (1976), To be published in Thin Solid Films.

Hovel, H.J. and Milnes, A.G. (1968), Int. J. Electron. 25, 201.

Hunter, L.P. (1956), "Handbook of Semiconductor Electronics" (McGraw-Hill, New York), 2nd Ed. 1962.

Igarashi, O. (1971), J. Appl. Phys. 42, 4035.

Ino, S., Watanabe, D. and Ogawa, S. (1964), J. Phys. Soc. Japan, 19, 881.

Jesser, W.A. and Matthews, J.W. (1967), Phil. Mag. 15, 1097.

Jesser, W.A. and Matthews, J.W. (1968)[a], Phil. Mag. 17, 461.

Jesser, W.A. and Matthews, J.W. (1968)[b], Phil. Mag. 17, 475.

Jesser, W.A. and Matthews, J.W. (1968)[c], Phil. Mag. 17, 595.

Jesser, W.A. and Matthews, J.W. (1969), Phil. Mag. 20, 999.

Jesser, W.A. and Matthews, J.W. (1968)[d], Acta. Met. 16, 1307.

Jonscher, A.K. (1967), Thin Solid Films, 1, 213.

Jonscher, A.K. (1969), J. Electrochem. Soc. 116, 217c.

Kalinkin, I.P., Sergeeva, L.A. Aleskovskii, V.B. and Strakhov, L.P. (1962), Sov. Phys. Sol. Stat. 3, 1922.

Kalinkin, I.P., Sergeeva, L.A., Aleskovskii, V.B. and Strakhov, L.P. (1963), Sov. Phys. Sol. Stat. 5, 86.

Karpinskas, S., Smilga, A., Vaitkus, J. and Viscakas, J. (1971), Proc. Int. Conf. on the Phys. and Chem. of Semicond. Heterojunctions (Editor in Chief G. Szigeti), Budapest. Vol. II.P.355.

Khoshla, R.P. and Fischer, J.R. (1971), J. Appl. Phys. 42, 2157.

Krikorian, E. (1964), "Single Crystal Films", Eds. M.H. Francombe and H. Sato (Oxford: Pergamon Press) p.113.

Krikorian, E. and Sneed, R.J. (1966), J. Appl. Phys. 37, 3665.

Kroemer, H. (1957), Proc. IRE. 45, 1535.

Kroger, F.A. (1964), The Chemistry of Imperfect Crystals (North Holland).

Kurata, K. and Hirai, T. (1968), J. Electrochem. Soc. 115, 869.

Lamb, D.R. (1967), "Electrical Conduction Mechanisms in Thin Insulating Films (Methuen, London).

Lampert, M.A. (1956), Phys. Rev. 103, 1648.

Lampert, M.A. (1962), Phys. Rev. 125, 126.

Lampert, M.A. (1964), Rept. Progr. Physics, 27, 329.

Lewis, B. and Campbell, D.S. (1967), J. Vacuum Science and Technology, 4, 209.

Ludke, R. (1971), J. Vacuum Science and Technology, 8, 199.

Manasevit, H.M., Simpson, W.I. (1971), J. Electrochem. Soc. 118, 644.

Matthews, J.W. (1959), Phil. Mag. 4, 1017;
(1961), Phil. Mag. 6, 1347;
(1963), Phil. Mag. 8, 711;
(1964), in "Single Crystal Films", eds. M. Francombe and H. Sato (Pergamon, Oxford) p.167;
(1965), Phil. Mag. 12, 1143;
(1966), Phil. Mag. 13, 1207;
(1967), in "Physics of Thin Films", Vol. 4, eds. G. Haas and R.E. Thun (Academic Press, New York), p.137;
(1971), Phil. Mag. 23, 1405;
(1975), "Epitaxial Growth", Part A (Academic Press, New York);
(1975), "Epitaxial Growth", Part B (Academic Press, New York).

Matthews, J.W. and Grunbaum, E. (1964), Appl. Phys. Lettr. 5, 106.

Matthews, J.W. and Grunbaum, E. (1965), Phil. Mag. 11, 1233.

Matthews, J.W. and Jesser, W.A. (1967), Acta. Met. 15, 595.

Matthews, J.W., Crawford, J.L. (1970), Thin Solid Films, 5, 187.

Matsuura, E., Matsui, K. and Hasiguti, R.R. (1962), J. Appl. Phys. 33, 1610.

Menter, J.W. (1956), Proc. Roy. Soc. A236, 119;
(1957), Proc. Eur. Reg. Conf. on Electron Microsc. Stockholm, p.88;
(1958), Advan. Phys. 7, 299.

Milnes, A.G. and Feucht, D.L. (1972), "Heterojunctions and Metal-Semiconductor Junctions" (Academic Press New York).

Mitsuishi, T., Nagasaki, N. and Uyeda, R. (1951), Proc. Imp. Acad. Japan, 27, 86.

Mott, N.F. and Gurney, R.W. (1940), Electro. Process. in Solids (Oxford: Clarendon Press).

Mufti, A.R. and Holt, D.B. (1972), J. Mater. Sci. 7, 694.

Mufti, A.R. (1972), Ph.D. Thesis University of London.

Nakai, J., Mitsusada, K. and Yasuoka, A. (1964), Jap. J. Appl. Phys. 3, 490.

Nakai, J., Yashuoka, A., Okumura, T. and Kano, G. (1965), Jap. J. Appl. Phys. 4, 545.

Newbury, D.M. and Kirk, D.L. (1974), Thin Solid Films, 22, 322.

Ogden, R., Bradley, R.R. and Watts, B.E. (1974), Phys. Stat. Sol. (a)26, 135.

Oldham, W.G. and Milnes, A.G. (1964), Solid State Electron. 7, 153.

Pashley, D.W. (1956), Advan. Phys. 5, 173;
(1965), Advan. Phys. 14, 327.

Pashley, D.W., Stowell, M.J. (1962), Proc. Int. Conf. Electron Microsc; 5th, Philadelphia, Pennsylvania (S.S. Breese, ed). Paper GG-1, Academic Press: New York.

Pashley, D.W. and Stowell, M.J. (1963), Phil, Mag. 8, 1605.

Pashley, D.W., Stowell, M.J., Jacobs, M.H. and Law, T.J. (1964), Phil. Mag. 10, 127.

Pashley, D.W. and Stowell, M.J. (1966), J. Vac. Sci. Technol. 3, 156.

Pashley, D.W., Menter, J.W. and Basset, G.A. (1957), Nature, Lond. 179, 752.

Patterson, M.S. (1952), J. Appl. Phys. 23, 805.

Perlman, S.S. and Feucht, D.L. (1964), Solid State Electron. 7, 911.

Pikhtin, A.N., Popov, V.A. and Yaskov, D.A. (1970), Sov. Phys. Semicond. 3, 1383.

Ratcheva, T.M., Stambolieva, T., Yu.D. Tchistakov, Krsulin, G.A. Vanyukov, A.V. and Djolev (1973), Phys. Stat. Sol. (a) (16), 315.

Ratcheva, T.M., Stambolieva, T., Tchistyakov Yu.D., Djogev, D.H. and Bakardjieva, V.J. (1972), Phys. Stat. Sol. A10, 209.

Read, W.T. (1953), "Dislocations in Crystals", (McGraw Hill), p.157.

Rediker, R.H., Stopek, S., Ward, J.H.R. (1964), Solid State Electron. 7, 621.

Riben, A.R. and Feucht, D.L. (1966b), Int. J. Electron. 20, 583.

Riben, A.R. and Feucht, D.L. (1966a), Solid State Electron. 9, 1055.

Riben, A.R. and Feucht, D.L. (1964), IEEE. Trans. on Electron. Devices 11, 534.

Richman, D. (1967), Electronics, 40, 108.

Rose, A. (1955), Phys. Rev. 97, 1538.

Roth, R.L. (1967), Physics and Chemistry of II-VI Compounds, eds. Aven, M., Prenner, J.S. (North Holland Amsterdam) ch. 3.

Rowe, J.E. and Richard, A. Forman, (1968), J. Appl. Phys. 39, 1917.

Royer, L. (1928), Bull. Soc. Franc. Mineral, 51, 7.

Rozgonyi, G.A. and Foster, N.F. (1967), J. Appl. Phys. 38, 5172.

Sato, H., Shinozaki, S. and Cicotte, L.J. (1969), J. Vac. Sci. Technol. 6, 62.

Schalla, R.L., Tideswell, N.W. and Coffin, F.D. (1964), "Single Crystal Films", eds. M.H. Francombe and H. Sato (Oxford Pergamon Press), p.301.

Schulz, L.G. (1951a), J. Chem. Phys. 19, 504;
(1951b), Acta. Cryst. 4, 487;
(1952), Acta. Cryst. 5, 269.

Schottky, W. (1914), Z. Phys. 15, 872.

Segall, B. (1967), "Physics and Chemistry of II-VI Compounds": eds. Aven, M. and Prenner, J.S. (North Holland: Amsterdam), ch. 1.

Sella, C. and Trillat, J.J. (1964) "Single Crystal Films" eds. M.H. Francombe and H. Sato (Oxford Pergamon Press) p.201.

Sergeyeva, L.A., Kazannikova, T.P., Kharlamov, I.A. and Aleskovsky, V.B. (1972), Thin Solid Films, 11, 105.

Sharma, B.L. and Purohit, R.K. (1974), "Semiconductor Heterojunctions" (Pergamon Press: Oxford).

Shewchun, J. and Wei, L.Y. (1964), J. Electrochem. Soc. 111, 1145.

Simmons, J.G. (1970) "Hand Book of Thin Film Technology", eds. Maissel, L.I. and Glang, R. (McGraw Hill, New York) ch. 14.

Simmons, J.G. (1971), J. Phys. D.: Appl. Phys. 4, 613.

Sloope, B.W. and Tiller, C.O. (1962), J. Appl. Phys. 33, 3458.

Sloope, B.W. and Tiller, C.O. (1965), J. Appl. Phys. 36, 3174.

Smith, R.W. (1955), Phys. Rev. 97, 1525.

Somarjai, G.A. (1962), Proc. Int. Symp. on Evaporation and Condensation of Solids, Dayton.

Somarjai, G.A. and Jepsen, D.W. (1964), J. Chem. Phys. 41(2), 1389.

Somarjai, G.A. and Stemple, N.R. (1964), J. Appl. Phys. 35, 11, 3398.

Somarjai, G.A. and Lester, J.E. (1965), J. Chem. Phys. 42, 4140.

Spinnulescu-Carnaru, L., Draghici, I., Petrescu, M. (1969), Thin Solid Films, 3, 119.

Stowell, M.J. (1969), in "Molecular Processes on Solid Surfaces" (E. Drauglis, R.D. Gretz and R.I. Jaffee eds) p.461, McGraw-Hill: New York.

Stowell, M.J. (1972), Thin Solid Films, 12, 341.

Stowell, M.J. (1975), in "Epitaxial Growth" ed. J.W. Matthews (Academic Press: New York), Part B. Ch. 5. p.437.

Suito, E. and Shiojiri, M. (1963), J. Electron Microsc. Japan, 12, 134.

Suri, S.K. and Sharma B.L. (1974), Int. J. Electron. 36, 629.

Swank, R.K. (1967), Phys. Rev. 153, 844.

Szekely, C., Bertoti, I., Stubnya, G., Varga, L. and Gutai, L. (1971), Proc. Int. Conf. on the Phys. and Chem. of Semicond. Heterojunctions (Ed. in chief G. Szigeti) Akadamiai Kiado, Budapest, vol. 1, p.341.

Thomas, G., Bell, W.L. and Otte, H.M. (1965), Phys. Stat. Sol. 12, 353.

Tredgold, R.H. (1966), "Space Charge Conduction in Solids" (Elsevier, London).

Tubota, H. (1963), Jap. J. Appl. Phys. 2, 259.

Turner, D.R. (1959), J. Electrochem. Soc. 106, 786.

Unvala, B.A. (1963), Le Vide, 104, 109.

Unvala, B.A., Woodcock, J.M. and Holt, D.B. (1968), Brit. J. Appl. Phys. (J. Phys. D) Ser. 2, vol. 1, 11.

Van der Merwe, J.H. (1950), Proc. Phys. Soc. A63, 616.

Van der Merwe, J.H. (1964), "Single Crystal Films", eds. Francombe, M.H. and Sato, H. (Pergamon Oxford) p.139.

Van der Merwe, J.H. (1973), "Epitaxial Interfaces": in Treatise on Material Science and Technology (Academic Press, New York), vol. 2, p.1.

Van der Merwe, J.H. (1974), J. Microscopy, 102, 261.

Van Dijk, H. (1967), J. Phys. Chem. Solids, Supplement No. 1, 31.

Van der Ziel, A. (1968), "Solid State Electronics", (2nd ed. Prentice-Hall Englewood Cliffs, New Jersey).

Van Opdorp, C. (1969), Philips Research Reports Suppl. 1, No. 10.

Van Ruyven, L.J. (1964), Phys. Stat. Sol. 3, K109.

Vanyukov, A.V., Kireev, P.S., Figurovskii, E.N., Korovin, A.P., and Vishnyakova, Z.P. (1970), Soviet. Phys. Semicond. 3, 1297.

Vermaak, J.S. and Van der Merwe, J.H. (1964), Phil. Mag. 10, 785.

Vecht, A. (1966), Phys. Thin Films, 3, 165.

Walton, D. (1962a), J. Chem. Phys. 37, 2182.

Walton, D. (1962b), Phil. Mag. 7, 1671.

Walton, D., Rhodin, T.N. and Rollins, R.W. (1963), J. Chem. Phys. 38, 2698.

Warekois, E.P., Lavine, M.C., Mariano, A.N. and Gatos, H.C. (1962), J. Appl. Phys. 33, 690.

Weinstein, M., Wolff, G.A. and Das, B.N. (1965), Appl. Phys. Letters, 6, 73.

Weinstein, M. and Wolff, G.A. (1967), Proc. Int. Conf. on Crystal Growth: ed. Peiser, H.S. (Pergamon Press Oxford) Boston, p.537.

Whelan, M.J. and Hirsch, P.B. (1957), Phil. Mag. 2, 1127.

Wilcox, D.M. (1970), Ph.D. Thesis University of London.

Wilcox, D.M. and Holt, D.B. (1969), J. Mater. Sci. 4, 672.

Wilson, R.B. (1966), J. Appl. Phys. 37, 1932.

Woodcock, J.M. and Holt, D.B. (1969), Brit. J. Appl. Phys. (J. Phys. D) 2, 775.

Yagi, K., Kobayashi, K. and Honjo, G. (1969), J. Appl. Phys. 40, 3857.

Yagi, K. Takayanagi, K., Kobayashi, K. and Honjo, G. (1971), J. Cryst. Growth 9, 84.

Yang, L., Birchenall, G.E., Pound, G.M. and Simnad, M.T., (1954), Acta. Met. 2, 463.

Yasuda Yukio (1968), Japan J. Appl. Phys. 7, 1171.

Yim, W.M. and Stofko, E.J. (1974), J. Electrochem. Soc. 121, 965.

Zeidenbergs, G. and Anderson, R.L. (1967), Solid State Electron. 10, 113.

Calow, J.T., Kirk, D.L. and Owen, S.J.T. (1972), Thin Solid Films, 9, 409.

X-Ray Powder Diffraction Data File. No. 19-191.

Swanson and Tatge (1951) in X-ray Powder. Data File No.1-5, Page 625.

Laugier, A., Gavand M. and Mesnord, G. (1970), Solid State Electron. 13, 741.

Gejji, F.H. and Holt, D.B. (1975), J. Electrochem. Soc. 122, 535.

Newman, P.C. (1965) Electronic, Letters, 1, 265.

Pocza, J.F. (1967), Proc. Colloq. Thin Films, 2nd P.93. Hungarian Acad. of Sci., Budapest.

Sah, C., Noyce, R.W. and Shockley, W. (1957), Proc. I.R.E. 45, 1228.

Aven, M. and Prener, J.S. (1967), Physics and Chemistry of II-VI compounds (North Holland, Amsterdam).

ACKNOWLEDGEMENTS

Thanks are due to Professor J.G. Ball for the provision of research facilities and to the Science Research Council for financial support of the work.

I am highly indebted to my supervisor Dr. D.B. Holt for his constant and stimulating suggestions, discussions and encouraging guidance which he has given throughout this work.

I would like to thank the Governments of India and Karnatak for the provision of study grants.

Mr. B.H. Barter deserves my thanks for his help in the experimental setup and the members of the Holt's group for useful discussions.

I would like to thank my very old parents Sri. Hanumappa and Smt. Dyamavva for their godly blessings and my wife Smt. Hemavathi who wrote encouraging and inspiring letters every week.

Finally I thank Miss Molly Chock for the typing of this thesis.